
CDF STUDY REPORT QPPF

Assessment of a Quantum Physics Payload Platform



CDF Study Report

QPPF

Assessment of Quantum Physics Payload Platform



FRONT COVER

Quantum Physics Platform (QPPF)
Study Logo

This study is based on the ESA CDF Open Concurrent Design Tool (OCDT), which is a community software tool released under ESA licence. All rights reserved.

Further information and/or additional copies of the report can be requested from:

T. Voirin
ESA/ESTEC/SCI-FMP
Postbus 299
2200 AG Noordwijk
The Netherlands
Tel: +31-(0)71-5653419
Fax: +31-(0)71-5655985
Thomas.Voirin@esa.int

For further information on the Concurrent Design Facility please contact:

M. Bandecchi
ESA/ESTEC/TEC-SYE
Postbus 299
2200 AG Noordwijk
The Netherlands
Tel: +31-(0)71-5653701
Fax: +31-(0)71-5656024
Massimo.Bandecchi@esa.int



STUDY TEAM

This study was performed in the ESTEC Concurrent Design Facility (CDF) by the following interdisciplinary team:

TEAM LEADER			
AOCS/DFACS		PROGRAMMATICS/ AIV	
COMMUNICATIONS		CHEMICAL PROPULSION	
CONFIGURATION		ELECTRIC PROPULSION	
COST		RADIATION	
DATA HANDLING		RISK	
GS&OPS		STRUCTURES	
NANO PARTICLES		SYSTEMS	
MISSION ANALYSIS		THERMAL/CRYO	
POWER			

Under the responsibility of:

T. Voirin, SCI-FMP, Study Manager

P. Falkner, SCI-FM, Study Responsible

The editing and compilation of this report has been provided by:

A. Pickering, TEC-SYE, Technical Author

TABLE OF CONTENTS

1	INTRODUCTION.....	11
1.1	Background	11
1.2	Objective.....	11
1.3	Scope	12
1.4	Document Structure.....	12
2	EXECUTIVE SUMMARY	13
2.1	Study Flow.....	13
2.2	Requirements and Design Drivers.....	13
2.3	Baseline Design	15
2.4	Technical Conclusions.....	18
2.5	Option.....	19
3	SCIENCE OBJECTIVES	21
3.1	Mission Justification	21
3.2	Science Requirements.....	21
3.2.1	Science Objectives (Level 0)	21
3.2.2	Science Requirements (Level 1) and Justification	22
3.2.3	Science Performance Requirements (Level 2)	24
3.3	System Requirements	28
3.3.1	Thermal and Vacuum Subsystem	28
3.3.2	GNC.....	29
3.4	Payload Requirements	30
4	PAYLOAD	33
4.1	Measurement Principle.....	33
4.1.1	Particle Transportation.....	33
4.1.2	Optical Cooling.....	33
4.1.3	Evolution and Phase Grating.....	33
4.1.4	Measurement of Position of Particle	34
4.2	Requirements and Design Drivers.....	34
4.2.1	Vacuum Level.....	34
4.2.2	Thermal Environment	35
4.2.3	Thermo-Elastic Deformation of Optical Bench.....	35
4.3	Assumptions and Trade-Offs	35
4.3.1	Closed Versus Open Cavity	35
4.3.2	Temperature of Cavity	35
4.3.3	Paul Trap	35
4.4	Baseline Design	36
4.4.1	Redundancy Concept	36
4.5	Options	36
4.6	Technology	37

5	MISSION ANALYSIS.....	39
5.1	Requirements and Design Drivers.....	39
5.2	Assumptions and Trade-Offs	39
5.3	Baseline Design	41
5.3.1	Launch.....	41
5.3.2	Orbit TCMs and Station Keeping.....	41
5.3.3	Orbit Geometry	41
5.3.4	Gravity Gradient along the Orbit	42
5.3.5	Ground Station Coverage.....	43
5.4	Budgets	44
5.5	Options	45
5.5.1	Earth-Trailing Orbit	45
5.5.2	Earth-Trailing Orbit with Limited Drift	48
5.5.3	L1 and HEO	48
6	SYSTEMS.....	49
6.1	System Requirements and Design Drivers	49
6.1.1	Design Drivers.....	50
6.2	System Assumptions and Trade-Offs	50
6.2.1	Assumptions.....	50
6.2.2	Trade-Offs	51
6.3	Mission System Architecture	57
6.3.1	Mission Phases	57
6.3.2	System Modes	62
6.3.3	Payload Modes	63
6.4	System Baseline Design	64
6.4.1	Enclosed Test Bench	67
6.4.2	Budgets.....	69
6.4.3	System Options	75
6.5	Open System Points	76
6.6	Mission Options	76
7	CONFIGURATION	79
7.1	Requirements and Design Drivers.....	79
7.2	Baseline Design	79
7.3	Overall Dimensions.....	83
8	STRUCTURES.....	85
8.1	Requirements and Design Drivers.....	85
8.2	Assumptions and Trade-Offs	85
8.2.1	Assumptions.....	85
8.2.2	V-Groove Design Trade-Off	85
8.3	Baseline Design	91
8.3.1	V-Grooves.....	92
8.3.2	Sun Shield.....	93
8.3.3	Service Module Panels	93

8.3.4	Struts and Payload Adapter	97
8.4	List of Equipment.....	99
8.5	Technology Needs for V-Groove Manufacturing.....	100
8.5.1	Additive Layer Manufacturing (ALM)	101
8.5.2	Aluminium Foam Sandwich Panels (AFS)	102
8.5.3	Conclusion.....	105
9	NANO PARTICLE HANDLING.....	107
9.1	Requirements and Design Drivers.....	107
9.1.1	Functional Requirements	107
9.1.2	Review of Terrestrial Methods for Particle Loading	107
9.1.3	Design Drivers.....	108
9.2	Technologies Considered	108
9.3	Assumptions and Trade-Offs	110
9.3.1	Van der Waals Interaction	110
9.3.2	Nanoparticle Charge	111
9.3.3	Summary of Assumptions.....	111
9.4	Baseline Design	112
9.4.1	Overview.....	112
9.4.2	MEMS Array Catapults	112
9.4.3	Paul Trap.....	115
9.4.4	Summary of Baseline Design Parameters	121
9.5	List of Equipment.....	122
9.6	Technology Needs	122
10	PROPULSION	125
10.1	Requirements and Design Drivers.....	125
10.2	Assumptions and Trade-Offs	125
10.3	Baseline Design	125
10.4	List of Equipment.....	131
10.5	Options	131
10.5.1	Hydrazine Propulsion System	131
10.5.2	Earth Trailing Option – Cold Gas System	133
10.5.3	Electric Propulsion.....	134
10.6	Technology Requirements	134
11	AOCS/DFACS	137
11.1	Requirements and Design Drivers.....	137
11.2	Assumptions.....	137
11.3	Trade-Offs/Options.....	138
11.3.1	Off the Shelf Accelerometers	139
11.3.2	Lisa Pathfinder Inertial Sensor as an Accelerometer.....	140
11.3.3	Attitude Sensing/Control.....	141
11.3.4	Free-Drifting Experiment	142
11.4	Baseline Design	146
11.4.1	Science Timeline Baseline.....	146

11.4.2	Sensor Selection for Drift-Recovery AOCS	147
11.4.3	Fuel Consumption (Science)	148
11.4.4	Transfer Baseline Design	149
11.4.5	Preliminary AOCS Modes List	150
11.5	List of Equipment	150
11.5.1	Star Tracker	151
11.5.2	Gyros	152
11.5.3	Digital Sun Sensors	152
	S3 – Smart Sun Sensor	152
11.6	Technology Needs	153
11.7	Summary & Conclusions	153
12	TELECOMMUNICATIONS	155
12.1	Requirements and Design Drivers	155
12.1.1	Requirements	155
12.1.2	Design Drivers	155
12.2	Assumptions and Trade-Offs	155
12.2.1	Bandwidth Trade-Off	156
12.2.2	Antenna/Power Trade-Off	156
12.2.3	Orbit Trade-Off	156
12.3	Baseline Design	157
12.3.1	Transponder and Travelling-Wave Tube Amplifier	158
12.3.2	Radio Frequency Distribution Network (RFDN)	159
12.3.3	Low Gain Antennas (LGA)	159
12.3.4	Medium Gain Antenna (MGA)	160
12.4	List of Equipment	161
12.5	Options	162
12.5.1	Medium Gain Antenna accommodation options	162
12.5.2	Additional Low Gain Antenna option	163
12.6	Technology Needs	163
13	DATA HANDLING	165
13.1	Requirements and Design Drivers	165
13.2	Assumptions and Trade-Offs	166
13.2.1	On-Board Storage Calculation	166
13.2.2	Housekeeping Real-Time Telemetry Check	166
13.2.3	Centralised vs. Distributed Architecture Trade-Off	167
13.3	Baseline Design	167
13.3.1	Redundancy Concept	168
13.3.2	Computer Module: Single Board Computer Core	169
13.3.3	I/O System With AOCS Interface	170
13.3.4	Solid State Mass Memory	171
13.3.5	Spacecraft Data Handling Architecture	172
13.4	List of Equipment	172
13.5	Options	173
13.6	Technology Needs	174

14	POWER.....	175
14.1	Requirements and Design Drivers.....	175
14.2	Assumptions and Trade-Offs	175
14.2.1	MPPT vs S3R.....	176
14.2.2	Regulated vs Unregulated Power Bus.....	176
14.3	Baseline Design	176
14.3.1	Solar Cell	177
14.3.2	Battery	179
14.3.3	Power Conditioning and Distribution Unit	179
14.4	Simulations Results.....	180
14.5	List of the Components	181
14.5.1	Solar Array	181
14.5.2	Battery	182
14.5.3	PCDU.....	182
14.6	Options	183
14.7	Technology Needs	183
15	THERMAL AND VACUUM.....	185
15.1	Requirements and Design Drivers.....	185
15.2	Assumptions and Trade-Offs	185
15.3	Baseline Design	185
15.3.1	H2 Sorption Cooler Dimensioning	187
15.3.2	SVM Thermal Architecture.....	194
15.3.3	Vacuum Aspects	195
15.4	List of Equipment.....	197
15.5	Options	199
15.6	Technology Needs	199
16	ENVIRONMENT.....	201
16.1	Requirements and Design Drivers.....	201
16.1.1	Requirements on Scientific Payload	201
16.1.2	Requirements on S/C System	202
16.2	Assumptions.....	202
16.2.1	Plasma Environment	202
16.2.2	Radiation Environment	203
16.2.3	Micrometeoroid & Debris Environment.....	204
16.2.4	Summary	205
16.3	Trade-Offs	205
16.4	Analysis Results	206
16.4.1	Plasma Environment	206
16.4.2	Radiation Environment	208
16.4.3	Micrometeoroids	211
16.5	Summary & Recommendations	214
17	GS&OPS.....	217
17.1	Assumptions and Constraints.....	217

17.2	LEOP and Transfer Phase	217
17.3	Routine Phase Operability	218
17.3.1	HKTM Downlink Strategy Operational Approach	219
17.3.2	Orbit Determination, Ranging and Station Keeping	219
17.3.3	Data Management, Storage, Operability	220
17.4	List of Equipment.....	220
17.5	Options	221
18	PROGRAMMATICS/AIV	223
18.1	Requirements and Design Drivers.....	223
18.2	Technology Requirements	223
18.3	Model Philosophy.....	226
18.4	System Level Verification Aspects	227
18.5	Development Approach.....	227
18.6	Schedule	228
18.7	Summary and Recommendations.....	232
19	TECHNICAL RISK ASSESSMENT	233
19.1	Reliability and Fault Management Requirements	233
19.2	Risk Management Process and Scope of Risk Assessment	233
19.2.1	Approach for the Risk Identification and Risk Reduction	235
19.3	Risk Management Policy.....	237
19.3.1	Success Criteria	237
19.3.2	Severity and Likelihood Categorisations	238
19.3.3	Risk Index & Acceptance Policy.....	240
19.4	Risk Drivers.....	241
19.5	Top Risk Log (preliminary).....	242
19.5.1	Risk Log General Conclusions	252
19.6	Risk Log Specific Conclusions and Recommendations	252
20	COST	255
21	CONCLUSIONS.....	257
21.1	Satisfaction of Study Objectives.....	257
21.2	Satisfaction of Mission Requirements	257
21.3	Further Study Areas	259
21.4	Final Considerations	260
22	REFERENCES.....	261
23	ACRONYMS.....	267

1 INTRODUCTION

1.1 Background

In 2016, ESA issued an open “Call for New Science Ideas”: This was Not a Call for Missions, but intended to scan for new ideas which could lead to new interesting future missions, possibly following some maturation time.

Three topics have been selected from the received proposals and CDF studies have already been carried out for the first two:

- GAIA-NIR
- Small Planetary Platforms (small/cubesats for planetary science)
- Quantum Physics Platform

Before the Quantum Physics Platform (QPPF) CDF study, the Quantum Physics Platform (QPPF) concept has been further iterated by the science community in several workshops to derive a consolidated science case. The goals of the study are based on several ideas proposals made by the quantum physics community, with limited space-related experience to:

- Provide a *reference mission design* for Quantum-Physics experiment
- *Inform the community* of the ESA process of requirements engineering in order to enhance the chance of successful mission proposals in the future ESA Cosmic Vision calls.

Managed by the Future Missions Department (SCI-F) and funded by the General Studies Program, the QPPF study was carried out by an interdisciplinary team of experts from across the ESA sites, starting with a kick-off on the 15th May 2018 and ending with an internal final presentation on the 10th July 2018.

1.2 Objective

The main goal of the mission is to test quantum superposition principle with "massive" test bodies and to compare the results with theoretical models. This has to be done in a perturbation free environment, hence the need for a space mission.

A key CDF objective was to assess the **feasibility envelope** for a Quantum Physics Platform in terms of “*free fall time, interference resolution and test particle mass range*”

- For meeting the science requirements, the QPPF mission shall enable the measurement of the matter wave interference for particles of up to at least 10^9 amu (goal: 10^{11} amu)
- The key metric for a quantum decoherence mission is the free fall time
- Free fall time performance is driven by :
 - Maximum time without collision (e.g. with any residual gas particle)
 - Maximum time for the particle to drift outside of the experiment volume

1.3 Scope

The scope of the study was to:

- Refine and mature the payload design (especially related to the nanoparticles feeding concept)
- Provide a justified reference orbit for the mission
- Identify technology development activities
- Estimate the cost class of the mission, its development time, and the associated risks

1.4 Document Structure

The layout of this report of the study results can be seen in the Table of Contents. The Executive Summary chapter provides an overview of the study; details of each domain addressed in the study are contained in specific chapters.

Due to the different distribution requirements, only cost assumptions excluding figures are given in this report. The costing information is published in a separate document.

2 EXECUTIVE SUMMARY

2.1 Study Flow

In 2016, ESA issued an open “Call for New Science Ideas” that intended to scan for new ideas which could lead to new interesting future missions, possibly following some maturation time.

Three topics have been selected from the received proposals, and each one has been subject to a dedicated CDF study :

- GAIA-NIR
- Small Planetary Platforms (small/cubesats for planetary science)
- Quantum Physics Platform

Before the Quantum Physics Platform (QPPF) CDF study, the concept has been further iterated by the science community in several workshops to derive a consolidated science case, based on several ideas proposals made by the quantum physics community. The goals of the CDF are to :

- Provide a *reference mission design* for Quantum-Physics experiment
- *Inform the community* of the ESA process of requirements engineering in order to enhance the chance of successful mission proposals in the future ESA Cosmic Vision calls.

Managed by the Future Missions Department (SCI-F) and funded by the General Studies Program, the QPPF study was carried out by an interdisciplinary team of experts from across the ESA sites, starting with a kick-off on the 15th May 2018 and ending with an internal final presentation on the 10th July 2018.

2.2 Requirements and Design Drivers

The objectives of the study were to:

- Refine and mature the payload design (especially related to the nanoparticles feeding concept)
- Provide a justified reference orbit for the mission
- Identify technology development activities
- Estimate the cost class of the mission, its development time, and the associated risks.

The main goal of the mission is to test quantum decoherence with "massive" test particles and to compare the results with theoretical models. This has to be done in a perturbation free environment, hence the need for a space mission.

A key CDF objective was to assess the **feasibility envelope** for a Quantum Physics Platform in terms of “*free fall time, interference resolution and test particle mass range*”

- For meeting the science requirements, the QPPF mission shall allow to measure matter wave interference for particles of up to at least 10^9 amu (goal: 10^{11} amu)

- The key metric for a quantum decoherence mission is the free fall time
- Free fall time performance is driven by :
 - Maximum time without collision (e.g. with any residual gas particle)
 - Maximum time for the particle to drift outside of the experiment volume.

The following design drivers were identified :

- Low risk of collision of the test particle during free fall (less than 2 collisions during free fall time with any other type of particles) to reach the quantum decoherence regime required for science.
 - This requires to protect the particle from external particle collisions, driving the need for an enclosed payload
 - This requires to ensure a sufficiently low particle density within the optical bench, driving the need for cryogenic temperature (20K), 3 V-grooves, sorption cooler and the use of a specific coating (Non Evaporable Getter) in the optical bench to chemically capture the residual particles
- Repeatability of the experiment over several thousands of runs to reach the matter-wave interference resolution required for science.
 - This requires to minimise the influence of the spacecraft on particle position evolution during each experiment, where the test particle would be left free drifting :
 - The S/C needs to ensure mechanical stability during experiments, driving the need for avoiding any actuation (mechanisms, reaction wheels, thrusters or active mechanical cooler) during science observations.
 - The S/C needs to be properly balanced (to minimise self gravity), constraining the positioning of tanks and S/C configuration
 - This requires stable external forces acting on the spacecraft, driving the choice of the Orbit (L2 or Earth Trailing possible)
 - This requires to know the test particle position excursion with an accuracy much better than the targeted matter-wave resolution
 - The direct test particle position excursion measurement is not possible with current technology, but indirect measurement is possible
 - The “non repeatable” component of the test particle position excursion is dominated by the attitude motion of the S/C during an experiment, which is due mostly to solar radiation pressure torque. A good, calibrated SRP model could allow to predict accurately the test particle position evolution with a standard star-tracker based attitude measurement. This would place constraint on the surface properties of the Sun-facing panel to maximise the modeling accuracy.
 - An alternative is to use the payload (CMOS + interferometer) and specific test particles without the grating applied, to get regular calibration points of the test particle position. If the calibration frequency is such that the S/C drift remains below the acceptable limit between two calibrations, then the particle position excursion is known sufficiently well.

2.3 Baseline Design

QPPF – Mission description	
Launch Vehicle	Ariane 6.2
Launch date	2034 (earliest, with proper technology development programme)
Lifetime	Transfer: 0.5 years Commissioning: during Transfer Science phase: 3 years Science extension: 2 years Total nominal lifetime: 3.5 years Total extended lifetime: 5.5 years
S/C orientation	Payload side anti-Sun pointing
Maximal de-pointing angle	10 degree
Transfer Scenario	Single launch for the S/C into the escape trajectory Chemical Propulsion for transfer insertion manoeuvre (cold gas nitrogen)
Orbit	L2 orbit, with station keeping Distance to Earth: 1.8 million km
Delta-V	106 m/s with margins

Table 2-1: QPPF mission characteristics

QPPF - System Characteristics	
Mass (incl. 30 % system margin on dry mass)	Payload Module dry mass: 208.2 kg Service Module dry mass: 1144.4 kg Propellant mass: 241.9 kg Spacecraft: - Dry mass: 1352.6 kg - Wet mass: 1594.5 kg Total launch mass incl. adapter: 1684.5 kg
Payload	Optical bench on cryogenic part (20K) Particle Loading unit CMOS sensor and interferometer

QPPF - System Characteristics

Configuration

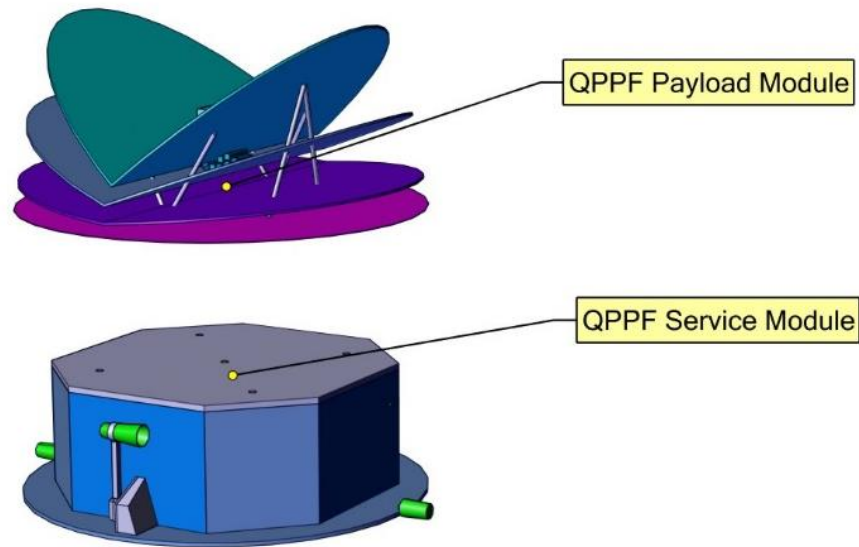


Table 2-2: QPPF system characteristics

QPPF – Payload Module Characteristics

Mass (incl. 30 % system margin on dry mass)	Payload Module dry mass: 208.2 kg including 30% payload mass margin on the instrument and particle transportation and storage equipment
Test bench	Optical bench on cryogenic part (20K) Particle Loading unit CMOS sensor and interferometer
Data Handling	Control of the sensors and actuators of the Optical bench Control of the Particle handling equipment
Thermal Control	Passive cooling with V-grooves down to 50K Active cooling with H2 sorption coolers down to 20K
Mechanisms	Opening valve on the side of the closed cover for venting

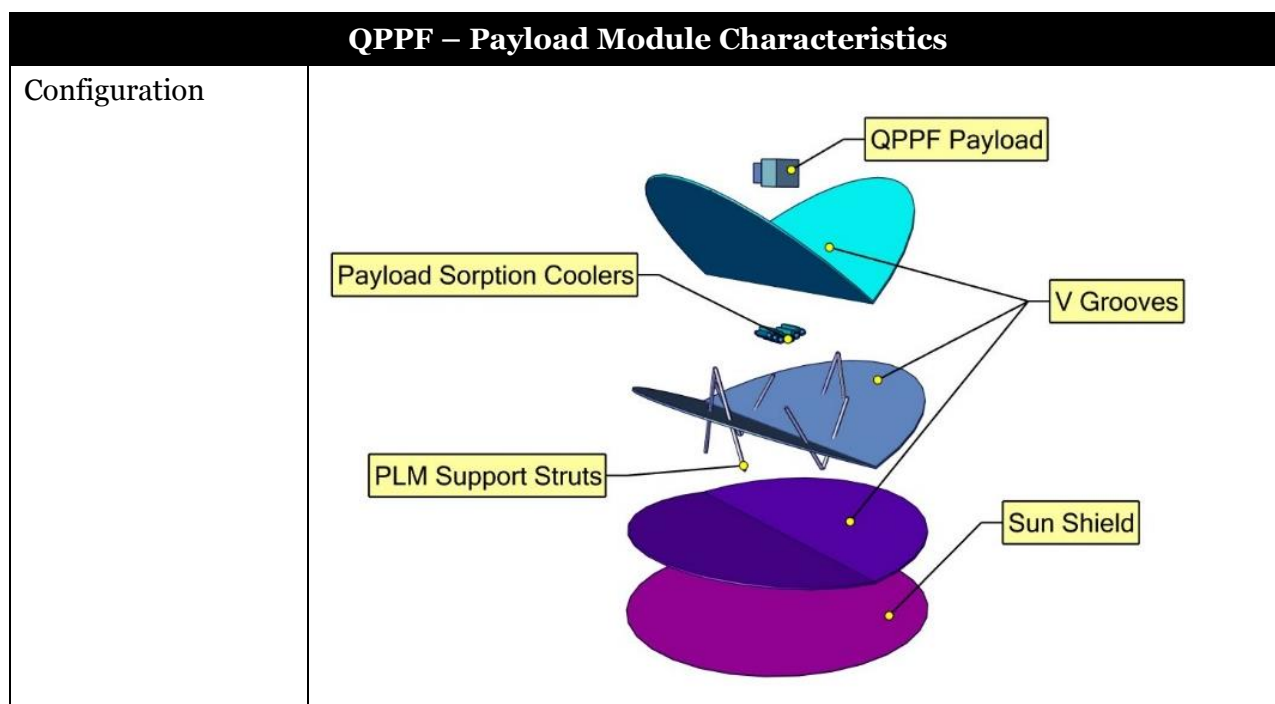


Table 2-3: Payload Module characteristics

QPPF - Service Module Characteristics	
Mass (incl. 30 % system margin on dry mass)	Service Module dry mass: 1144.4 kg Propellant mass: 241.9 kg
Data Handling	2 Tb of data storage
Power	3.4 m ² area body-fixed solar panel with 30% efficiency cells
Propulsion	One cold-gas (nitrogen) propulsion system <ul style="list-style-type: none"> High thrust with four small tanks for initial orbit insertion. Micro Newton thrusters for station keeping, repointing and disposal on main central tank
AOGNC	Two cold redundant Miniature Inertial Measurement Unit Two cold redundant Star Trackers
Communication	One Medium Gain Antenna for large data dump between batches Two (optionally three) Low Gain Antenna for daily housekeeping data X-band transponder
Thermal Control	244W of heaters in service module for safe mode (minimal equipment temperature. -30C)
Mechanisms	Medium Gain Antenna pointing and stowing mechanism
Structures	Sun shield and intermediate shield sandwich panels with aluminium honeycomb core and CFRP facesheet

QPPF - Service Module Characteristics

Configuration

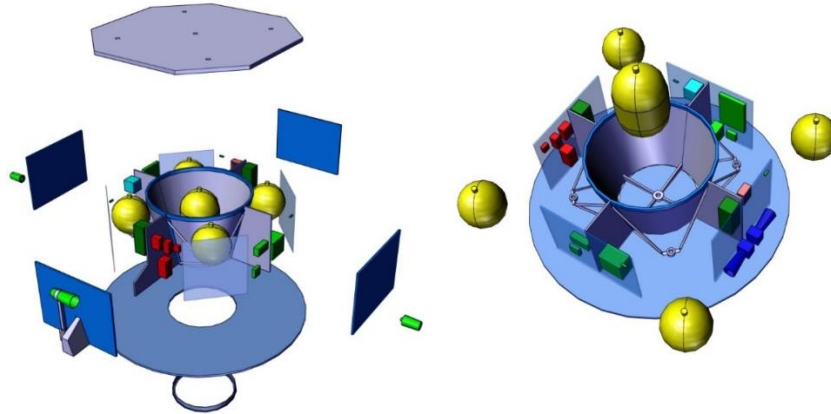


Table 2-4: QPPF service module characteristics

2.4 Technical Conclusions

The requirements of the science community have been iterated over the course of the study. These changes have been agreed with the science community and a clear reason for the change has been provided. The final iterated requirements have been agreed by the community and the CDF team.

The payload sequence has been looked into and a baseline sequence, which fits in the mission lifetime has been proposed. The nanoparticle transportation and storage concept has been investigated in detail. It became clear over the course of the study that this system has a very low TRL and required dedicated technology developments (see chapter 9 for more detailed discussion on this aspect).

A complete orbit trade-off has been performed. The L2, earth trailing and, earth leading orbits have been identified as feasible orbits. Only the L2 orbit has been studied in detail, and a feasible design solution has been identified for this orbit.

The risk, cost, and schedule have been estimated by the experts. Their results are in line with the expected/hoped for results.

The following areas for further study have been identified.

- The current baseline pressure within the optical bench is 10-11 Pa at 20K for the payload which is considered feasible and allows to meet the science requirement (testing quantum decoherence for masses of 10^9 amu). Lower pressure levels would be required to allow testing more massive particles, but further investigation would need to be done to assess the feasibility of a more extreme vacuum.
- Further investigation needs to be done on the science side regarding the acceptable probability of collision per experiment. Currently the requirement is derived by assuming that the particle can be hit less than (or equal to) twice per experiment by other molecules with a probability of more than 80%. It has to be

analysed scientifically what the impact of these hits on the experiment is, and derive a requirement and experiment duration from that.

- What is the exact temperature stability of the optical bench and can this be reached with the small peak heat loads of the instrument.
- The Non-Evaporable Getter that coats the inner wall of the optical bench may need 80°C to be activated. This can cause some problems since the optical bench should be kept at a low temperature. A solution for this problem has not been proposed in the study and should be investigated since the getter is an important contributor to the high vacuum.
- The particle storage and transportation system has to be investigated and developed. The degradation of the particles over the duration of the mission while they are in the storage container and the effect this will have on the mission will have to be investigated and any mitigation actions required flown down to the particle storage and transportation system design.
- The current baseline assumes that the CMOS detector on the payload is capable of operating at 20K. This assumption has to be investigated and a technology development might be required.
- A preliminary design of the closed optical bench design has been performed during the study. The design of the cover has to be further elaborated mainly on the material and thickness of the cover to ensure the experiment will not be degraded due to radiation. The venting path of the cover has to be investigated. No detailed analysis has been done to ensure that the cover can vent correctly to the required pressure at which point the H₂ sorption coolers can reduce the pressure even more.
- The behaviour of the spacecraft is a major driver for the science efficiency, propellant budget during science mode and the propellant budget during the safe mode. Over the course of the study it has been analysed using some optimistic assumptions. More in depth analysis is required since the science efficiency is a major driver for the mission.

The low TRL of the PLM technologies are the main driver for the QPPF schedule. In case additional efforts are made to decrease the development times of a limited number of technology developments, the mission could be compatible with a launch in 2034.

2.5 Option

One option identified during the CDF study was to perform the mission in an Earth Trailing / Earth Leading Continuous Drift Orbit.

Benefits:

- This type of orbit does not require station keeping, hence there is a reduction in the system complexity compared with L2, reducing the delta-v from 120m/s (L2) to approximately 35 m/s (ET/EL), an estimated 160 kg of mass saved.
- Without station keeping manoeuvres, there is an increase in the time dedicated to science, 12 hours with the current concept of operations.

- Earth / Sun Angle can accommodate the HGA behind the sunshield - no technology development needed.

Drawbacks:

- Additional power required in order to achieve the required data rate / larger antenna. This may possibly be the driver for the end-of-mission.
- The CDF did not assess how to achieve the compliance with 10 degrees Sun Aspect Angle to avoid light trapping within the V-grooves, one possibility was to keep the fairing attached until arrival on the Continuous Drift orbit.

3 SCIENCE OBJECTIVES

3.1 Mission Justification

QPPF will be the foundation of future space-based experiments to answer some of the most fundamental questions of modern physics: do the laws of quantum physics still hold for macroscopic objects or do yet unknown effects set a limit for massive objects? What is the fundamental relation between quantum physics and gravity?

The purpose of QPPF mission is to test quantum superposition principle with massive test bodies in an untested parameter regime where deviations from quantum theory are expected due to a quantum-to-classical transition or due to gravity. As per superposition principle, a quantum system can be in a superposition state of clearly distinct states, and quantum physics does not set a principle limit to the mass, size or complexity of systems that are in such superposition states. Realizing superposition states of increasingly massive particles has been a strong research effort in the last 80 years, culminating in the mass record of 10^4 amu obtained via matter-wave interferometry in a ground-based experiment. However, deviations from the quantum physics are predicted for much higher masses, typically higher than 10^8 amu, and can only be observed by measuring the decoherence parameter of massive particles in a “clean” environment with e.g. low temperature (20K), low residual pressure (10^{-11} Pa), low residual perturbation forces and long free fall duration (several tens of seconds), conditions, with high repetition rate (several tens of thousands of runs are required to build one interferogram), which can only be met on a space experiment.

QPPF will therefore measure in such a perturbation-free environment, the decoherence parameter for massive nanoparticles, using the matter-wave interference and diffraction measurement techniques. Comparing the measured decoherence parameter with predictions will allow to discriminate between competing theoretical models.

3.2 Science Requirements

The science requirements and their derivation into system-requirements have been performed in the frame of the CDF and are reported here.

3.2.1 Science Objectives (Level o)

Three main science objectives have been defined for this mission.

Lo-SCI-10000	The mission shall allow to test quantum physics in a parameter regime where deviations are expected, due to quantum-to-classical transition or due to gravitational effects, by measuring the decoherence parameter for large mass particles, with an accuracy such that it allows discriminating between competing quantum decoherence models (K, DP and CSL) Rationale : SO1 RD[2]
Lo-SCI-20000	The mission shall allow to quantify the parameter dependence of quantum decoherence for macroscopic superpositions high-mass test particles. Rationale : SciRD SO2 RD[2]
Lo-SCI-30000	The mission shall ensure an overlap of tested parameter regime with the

	parameter regime testable on-ground and allow to test an intermediary parameter regime. Rationale : SO3 RD[2]
--	--

3.2.2 Science Requirements (Level 1) and Justification

3.2.2.1 Decoherence regime

Science Objective SO1 requires the ability to discriminate between competing quantum decoherence models. Which experimental parameters will have to be chosen in order to be sensitive to potential deviations from quantum physics? In general, it is expected that deviations from quantum theory become larger with increasing size/mass of the test particle. In order to know which experimental parameters will present an interesting choice, the predictions for the decoherence parameter of various theoretical models predicting deviations from quantum theory can be investigated. All such models predict decoherence depending on the mass of the test body. That means decoherence parameters Λ as functions of mass for each of these models can be assigned. This is illustrated in Figure 3-1.

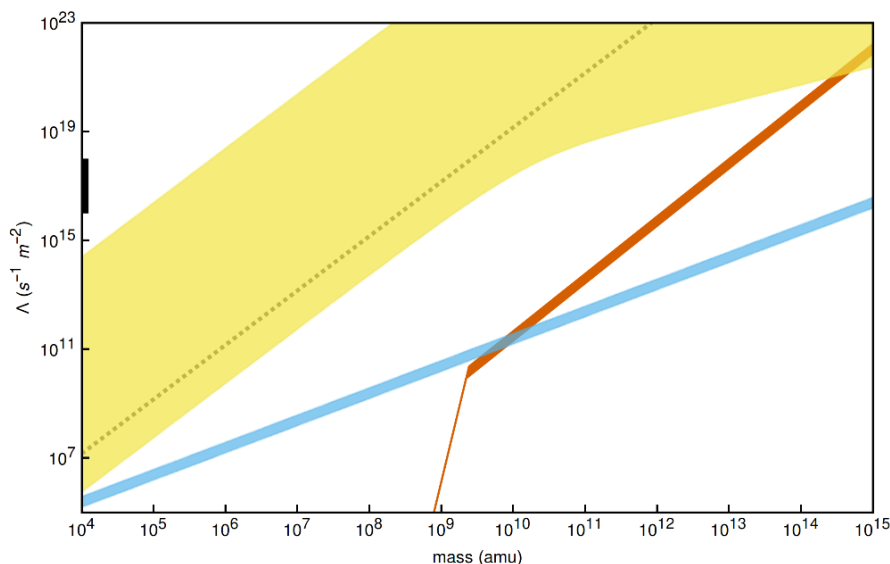


Figure 3-1: From RD[2] The plot shows ranges of predicted values Λ for various theoretical models predicting deviations from quantum theory. Larger values of Λ correspond to stronger decoherence. Yellow region: decoherence due to continuous spontaneous localization (CSL) ; Blue region: model of Diósi-Penrose for a mass density ranging from 2200 kg m⁻³ (fused silica) to 5500 kg m⁻³ (Schott SF 57HT). Red region: predictions of the model of Károlyházy for the same range of mass densities.

Below 10⁹ amu, the predicted decoherence parameter value predicted by the K-model drops abruptly, making a measurement challenging, as illustrated in Figure 3-1. This puts a lower limit of 10⁹ amu on the particle mass requirement for such an experiment.

The total amount of decoherence is the sum of standard decoherence effects (emission, scattering and absorption of black-body radiation), called Λ_{QM} , and the decoherence resulting from deviation from quantum physics called Λ_{dev} which is the one needed to be

measured. In order to clearly evidence deviations, it is necessary to have $\Lambda_{QM} < \Lambda_{dev}$ (as per RD[2]) For a particle mass range above 10^9 amu, the predicted decoherence range by the K and DP theories Λ_{dev} is greater than $10^{10} \text{ m}^{-2}\text{s}^{-1}$. This leads to the following requirement:

L1-SCI-11000	The mission shall allow to perform measurement of the decoherence parameter in a regime such as Λ_{QM} is smaller than $10^{10} \text{ m}^{-2}\text{s}^{-1}$, for test particles with masses greater than 10^9 amu
--------------	---

3.2.2.2 Measurement principle

Matter-wave interference allows a measurement of decoherence for a "low" decoherence environment regime (Λ_{dev} of $10^{10} \text{ m}^{-2}\text{s}^{-1}$), as required to discriminate between K and DP models. Diffraction measurement accuracy is limited by the mechanical oscillator frequency which lead to higher decoherence regimes (Λ_{dev} above $10^{15} \text{ m}^{-2}\text{s}^{-1}$), but is sufficient to discriminate between CSL and other models.

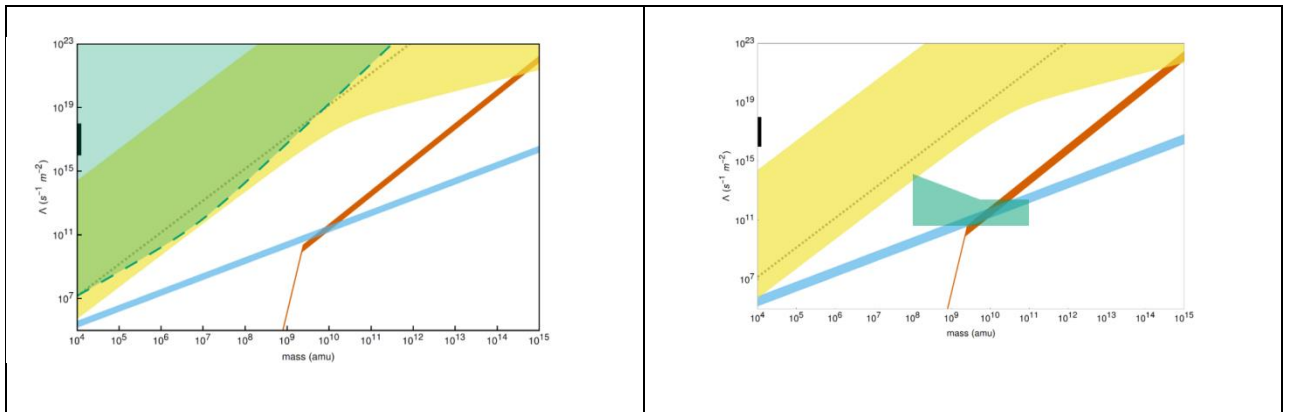


Figure 3-2 : In green-shaded, left : The regime accessible to the proposed matter-wave interferometer as per RD[2] as a function of particle mass ; right : the regime accessible to the proposed matter-wave interferometer as per RD[2] as a function of particle mass

L1-SCI-12000	L1-SCI-110000 shall be achieved via matter-wave interference measurements and comparing the fringe patterns visibility with the predictions from various decoherence models, and via observing matter-wave diffraction measurements and comparing the width of the wave function with the predictions from various decoherence models.
--------------	--

3.2.2.3 Number of measurements

The number of measurements required to build one matter-wave interferogram shall be derived based on statistical confidence expected. 10^4 is assumed as a minimum for CDF purpose, but this number shall be consolidated e.g. by statistical interpretation of representative science simulation results.

L1-SCI-130000	The tests to be performed for a given measurement run shall comprise at least 104 measurements, with an additional margin of at least 10% (TBC) to account for potential losses.
---------------	--

3.2.2.4 Derived from SO₂

The decoherence parameter shall be measured as per L1-SCI-110000 & L1-SCI-120000 for various combinations of particles masses, materials and properties to characterise the dependency of decoherence to various parameters (science objective 2), and help discriminating between theories.

L1-SCI-21000	The decoherence parameter shall be measured as per L1-SCI-110000 & L1-SCI-120000 for various combinations of particles masses, materials and properties
--------------	---

3.2.2.5 Derived from SO₃

The state of the art in testing the quantum superposition principle is the matter-wave experiment by the Arndt group, where matter-wave interferometry was demonstrated with test particles with a mass of 10^4 amu and sensitive to decoherence regime with $\Lambda \geq 10^{16}$ m-2s⁻¹. While the current mass record is at 10^4 amu, continuously improving results and technology development should lead to experiments with test masses up to 10^6 amu within the next years, and progress towards 10^7 amu or even 10^8 amu seems conceivable within the next one or two decades, e.g., by using drop towers to achieve the required free-fall times.

L1-SCI-31000	The mission shall allow to perform measurement of the decoherence parameter in a regime such as $\Lambda_{QM} \leq 10^{15}$ (TBC) m-2s ⁻¹ for test particles with masses as low as 10^8 amu
--------------	--

3.2.3 Science Performance Requirements (Level 2)

3.2.3.1 Collision rate

For the CDF study it has been assumed that the probability of having less (or equal to) 2 collisions shall be higher than 80%. Assuming a Poisson distribution, this is equivalent to having a probability of having no collision higher than 22%.

Collisions with the test particle will lead to decoherence and the corresponding measurement will be lost, leading to an outlier in the reconstructed interferogram, resulting in a blur of the interference pattern. The exact number of acceptable collisions from a scientific point of view over an entire measurement run needs to be derived accurately based on scientific considerations and translated into a requirement on the probability of collision per measurement.

To derive this requirement, the following assumptions were used :

- $\sigma \times n \times l = 1$ for an ideal gas
 σ = collision cross section (m²)
 n = density of molecules (nbr / m³)
 l = mean free path (m)
- $\sigma = \Pi(r^2 + r_g^2)$ where r is the radius of the test particle, r_g the radius of the gas molecule.
- The average gas velocity in an ideal gas is : $\langle v \rangle = \sqrt{2 \cdot k_B \cdot T / m_G}$ with m_G mass of a gas particle

- The mean free path $l = k_B T / (\sqrt{2} \cdot \Pi \cdot d^2 \cdot P)$ where P is the gas pressure and d the particle diameter.
 - $P = \rho \langle v \rangle^2 / 2 = n k_B \cdot T$
 - Time between collisions τ : $\tau \langle v \rangle = 1 / (\sigma \times n) \Rightarrow \tau = \sqrt{m_G} / (\sigma \times n \times \sqrt{2 \cdot k_B \cdot T})$
 - The collision rate is given by $\gamma = 1 / \tau$
 - Assuming Poisson distribution (γ : collision rate)
- Probability of 0 collision during t : $P_0 = \exp(-\gamma \cdot t)$
 Probability of 1 collision during t : $P_1 = \exp(-\gamma \cdot t) \cdot (\gamma \cdot t)$
 Probability of 2 collisions during t : $P_2 = \exp(-\gamma \cdot t) \cdot (\gamma \cdot t)^2 / 2!$
 Probability of 2 collisions OR less during t : $P_{012} = P_0 + P_1 + P_2$

For example, for a radius of 100nm and a mass for the gas particle of 4 amu (Helium, or alpha particle), at temperature 20K, and a gas pressure of $\sim 1e^{-13}$ Pa then the collision rate is ~ 1 every 300s. This corresponds, assuming a Poisson distribution, to a $\sim 70\%$ chance of having 0 collision in 100s, or 99.6% chance of having 2 collisions or less in 100s.

These equations can be used, for a given pressure and a given density of the nanoparticle, to derive the requirement in terms of free fall time as a function of the test particle mass for a given test particle material.

L2-SCI-111000	For each measurement test, the probability of collision of the nanosphere under test with any particle shall be smaller than 22% (TBC) during the measurement duration	L1-SCI-110000 L1-SCI-130000
---------------	--	--------------------------------

3.2.3.2 Black-body radiation

The black body radiation on the test particle, including scattering, emission and absorption of blackbody photons and thermal emission shall remain such that the contribution to the overall decoherence parameter remains much smaller than $10^{10} \text{ m}^{-2} \text{ s}^{-1}$.

L2-SCI-112000	For each measurement test, the black body radiation toward the test particle shall be such that the associated decoherence remains smaller than $10^{10} \text{ m}^{-2} \text{ s}^{-1}$	L1-SCI-110000
---------------	---	---------------

3.2.3.3 Free fall time

The Talbot time is defined in RD[2] and varies between a few seconds on the lower end of the mass range, and more than 1000s for the upper end. The Talbot time gives the time scale needed to ensure sufficient expansion of the matter-wave function, giving a lower bound for the free fall time.

<i>TP mass [amu]</i>	<i>Talbot Time [s]</i>
<i>1.00E+08</i>	<i>2.52E+00</i>
<i>5.00E+08</i>	<i>1.26E+01</i>
<i>1.00E+09</i>	<i>2.52E+01</i>

<i>TP mass</i> <i>[amu]</i>	<i>Talbot Time</i> <i>[s]</i>
<i>5.00E+09</i>	<i>1.26E+02</i>
<i>1.00E+10</i>	<i>2.52E+02</i>
<i>1.00E+11</i>	<i>2.52E+03</i>

L2-SCI-113000	For each particle matter wave interference or diffraction measurement, it shall be possible to have a free fall duration greater than the associated Talbot time	L1-SCI-110000
---------------	--	---------------

3.2.3.4 Interference Observability Requirement

Contrary to optical interferences, the matter-wave interference pattern is constructed based on the succession of N measurements of the particle Centre Of Mass position obtained with N identical nanospheres. The detection area is divided in bins, and the interference pattern is reconstructed based on the histogram of the recorded positions in each bin. If the position excursion of the particle over N measurements is much smaller (or known better) than the detector bin width, this is not an issue as the datapoints will be well localized and interferogram can be reconstructed.

For test masses of 10^8 amu, $5 \cdot 10^8$ amu, 10^9 amu, $5 \cdot 10^9$ amu, 10^{10} amu and 10^{11} amu the resolution should be 500nm, 60nm, 13nm, 2nm, 1nm and 0.5nm, respectively, for a 100s free fall time. At the Talbot time (which depends on the mass), the requirement becomes ~20 nm whatever the test mass.

The requirement could in principle be achieved either by ensuring a good stability of the platform AND/OR by accurate measurement of the spacecraft versus test-mass position drift during the measurement (e.g. thanks to integration of differential acceleration measurements)

L2-SCI-121000	Over the duration of a given interference measurement run, composed of N measurements, the drift of the particle position excursion (defined as the relative position change of the test particle wrt spacecraft in S/C frame during measurement duration Tmeas) shall be known better than 20 nm, along the sensitive axis	L1-SCI-120000
---------------	---	---------------

The science requirement L2-SCI-121000 on repeatability has been broken down into lower system-level requirements

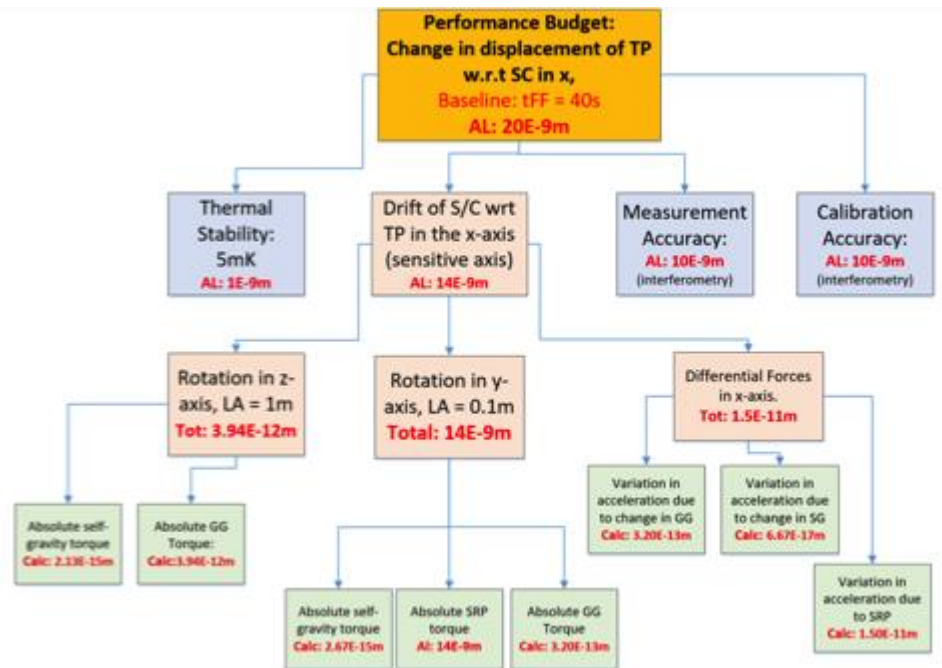


Figure 3-3: Science repeatability requirements breakdown

- L3-MIS-121100 Thermal stability of the testbench – which affect the interference pattern. 1 nm requirement has been derived, corresponding to 5 mK stability over 1 measurement
- L3-MIS-121300 Particle CoM position measurement accuracy: the CoM position of the test particle is measured by an interferometer. A 10 nm requirement has been derived for this measurement accuracy L3-MIS-121300 Regular calibration of the Particle excursion (the excursion being defined as the trajectory followed by the particle in S/C frame during the measurement duration) is required : there is therefore a requirement on the calibration performance. Since the calibration relies on Centre of Mass measurement as well, a requirement of 10 nm is allocated for that as well.

L3-MIS-121200 Finally, the last requirement is on the actual drift of the Particle excursion between two calibrations (driven mostly by change in S/C angular rate between two calibrations, the S/C being free-drifting) : a requirement of 14 nm has been derived for this contributor.

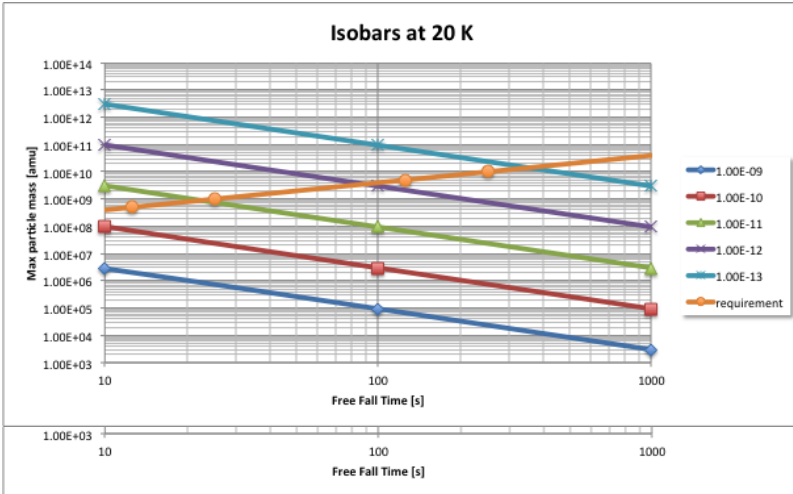
The drift of the spacecraft with respect to the test particle in the x-axis is driven mainly by rotation in the y-axis due to contributors such as solar radiation pressure, self-gravity and the gravity gradient torques. As there is a difference between the centre of pressure of the spacecraft and the centre of mass, any forces acting upon the spacecraft will cause a rotation. As the spacecraft rotates during free fall time and over the whole batch period, the detected position of the test particle on the detector will vary. This variation can be predicted using sophisticated solar radiation pressure models along with calibration runs.

A calibration experiment, which involves running the same experiment on the test particle of same mass without the optical grating, is run between measurements of a given number of experiments (depending on free fall time). Together with a

calibration run and a solar radiation pressure model, one can predict the trajectory of the Test particle and rotation of the spacecraft, hence being able to correct the detected position during data processing on ground.

3.3 System Requirements

3.3.1 Thermal and Vacuum Subsystem

L3-MIS-111100	<p>The required pressure during each measurement run, around the test particle, shall be smaller than 10^{-11} Pa.</p> <p><i>Rationale : 10^{-11} Pa is currently the lowest pressure which can be reached with existing technology, and which can be accurately tested on-ground. For the intended experimental set-up, requiring transparency of the test particles in the 1064 nm wavelength, this puts an upper limit on the achievable mass of the test particle, which is $5 \cdot 10^9$ amu assuming the densest transparent material (Hafnium dioxide), a probability of 2 or less collisions of 80% (L2-SCI-111000), a temperature of 20K (L2-SCI-112000), which is compatible with the required free fall time (L2-SCI-113000) for the required mass range requirement (L2-SCI-114000)</i></p> <p><i>Case 1 : fused silica particles (density 2200 kg/m³)</i></p>  <p><i>Case 2 ; hafnium dioxide particles (density 9600 kg/m³)</i></p>	L2-SCI-111000 L2-SCI-112000 L2-SCI-113000 L2-SCI-114000
L3-MIS-112100	The temperature within the optical testbench during a measurement shall remain at 20K during the measurement duration	L2-SCI-112000 L3-MIS-211100

	<i>Rationale : direct derivation of L2-SCI-112000</i>	
L3-MIS-121100	<p>The stability of the testbench temperature shall be better than 5 mK over the whole duration of a measurement run (composed of N measurements)</p> <p><i>Rationale : Breakdown of L2-SCI-121000 requirement ("20 nm"). 1 nm apportioned to thermal stability of the optical bench. Thermal expansion effect on grating shall be \ll wavelength to avoid excessive smearing of interference fringes. We want : $d(\lambda/a \cdot D) = \lambda D/a^2 da \ll X$ nm. Assuming 1 nm acceptable leads to $da/a \ll X \cdot (100e-9)/200e-9/D$; $da/a = a \cdot dT$ where a is the thermal expansion coefficient. leads to $dT < 0.5 \cdot X/D/a$. Assuming $a = 1e-6 \text{ K}^{-1}$ and $D = 0.1 \text{ m}$ leads to $dT < 0.5/0.1/1e-6 \cdot X = 5e6 \cdot X$. Assuming $X = 1 \text{ nm}$ (1/100 of wavelength) lead to $dT < 5 \text{ mK}$ over a time horizon of $N \cdot T_{\text{meas}}$ (2 weeks TBC).</i></p>	L2-SCI-121000

3.3.2 GNC

L3-MIS-115100	<p>The S/C motion during each measurement run shall be such that the particle remains within 1mm (TBC) of the nominal detection area, with a confidence level of 99.7% (TBC) (with the ensemble interpretation)</p> <p><i>Rationale : 1 mm corresponds to the radius of the detection area ; if particle goes outside, its position CoM can not be measured and the experiment is lost. The motion of the S/C during the measurement is composed of a linear acceleration (due to differential forces) and a rotation (due to absolute torques acting on the S/C + residual angular rate)</i></p>	L2-SCI-115000 L2-SCI-113000
L3-MIS-121200	<p>The Spacecraft to Test-Particle Excursion Drift Error (PDE) shall not drift by more than 14 nm between 2 calibrations, with a 99.7% confidence assuming the ensemble interpretation.</p> <p><i>Rationale :</i> <i>During each free fall experiment, the relative position of the optical bench with respect to the test mass will change due to the actions of external forces. This can be calibrated by measuring the position excursion for a reference test particle, without the grating applied.</i> <i>In-between calibrations, the drift results of the integration of the differential effects affecting the S/C (at its Centre Of Mass) and the test particle (external forces and torques on the S/C, gravity gradient, internal forces e.g. self-gravity, and inertial forces) during each</i></p>	L2-SCI-121000

	<p><i>experiment duration.</i></p> <p><i>If the position excursion between 2 calibrations is much smaller or known better than the detector bin width, this is not an issue as the datapoints will be well localised and interferogram can be reconstructed. This leads to a requirement on " position excursion drift error" between 2 calibrations. The interval between 2 calibrations depends on the behaviour and properties of the S/C (Surface properties, e.g. absorption coefficient, Moments of Inertia): e.g. a poorly reflective surface exposed to the Sun coupled with low inertia would lead to more frequent calibrations than a highly reflective surface coupled with high s/c inertia.</i></p> <p><i>This requirement ensures repeatability of the particles position measurements within scientifically acceptable limits to build an interferogram.</i></p>	
--	--	--

3.4 Payload Requirements

L2-MIS-115200	<p>The laser system used for the interferometer shall operate at a wavelength of 1064 nm or 1550 nm</p> <p><i>Rationale : typical wavelengths for quantum optomechanics, and which should also be available in a space-based setting. The tested particle radius between are 30nm and 220nm which remain smaller than 1/5th of the laser wavelength. If the particle size becomes comparable to the optical wavelength, one can only achieve reasonable coupling if the particle size hits a Mie resonance</i></p>	L2-SCI-115000
L3-MIS-121300	<p>The particle detection system shall have a measurement noise smaller than 10 nm</p> <p><i>Rationale : Breakdown of L2-SCI-121000 requirement ("20 nm"). 10 nm apportioned to CMOS + interferometer detection system noise which contributes to the interference reconstruction performance.</i></p>	L2-SCI-121000
L3-MIS-121400	<p>The payload shall allow the use of test particles for calibration runs</p> <p><i>Rationale : A calibration run shall allow to calibrate a particle position excursion during a given time by measuring its position evolution on the CMOS detector. This implies that such particles are not subject to matter-waves interferences.</i></p>	L2-SCI-121000
L3-MIS-211100	<p>Each particles set as per L2-SCI-211000 shall be stored in a dedicated reservoir. There shall therefore be 15 different</p>	<p>L2-SCI-211000</p> <p>L2-SCI-114000</p>

	<p>reservoirs for the mission with the following characteristics :</p> <ul style="list-style-type: none"> - Reservoir i : N particles of material i, mass m_i <p><i>Rationale: Direct derivation of L2-SCI-211000 requirement</i></p>	
L3-MIS-211200	<p>The particles within each reservoir as per L3-MIS-211100, shall have physical properties identical within 1% (TBC) in terms of mass, diameter, optical properties, and these properties shall not be altered by more than 1% between BOL and EOL</p> <p><i>Rationale : statistical uncertainty shall be much smaller than the deviations we want to evidence. A 1% uncertainty is targeted in RD[2], which is translated into an accuracy requirement on nanoparticles properties</i></p>	L2-SCI-211000

This Page Intentionally Blank

4 PAYLOAD

4.1 Measurement Principle

QPPF aims at detecting deviations from ‘classical’ Quantum Mechanics which are expected (according to some theories) above a certain mass. Two types of experiments are foreseen: matter-wave diffraction and matter-wave interference.

In order to test which theory describes deviations from quantum mechanics best (and to establish the deviation per se) particles (within a certain mass range) are:

- Moved to an optical bench
- Optically cooled (“quantum state”)
- The particle wave packet can evolve for a time t_1
- An optional phase grating is applied
- The particle wave packet can evolve further for a time t_2
- The position of the particles is measured (“collapse of wave packet”).

The phase grating is only applied for the matter-wave interference experiment. All the measured positions of a ‘batch’ of identical particles ($\sim 10,000$) are used to construct a distribution of measured positions. This can be seen as the interference pattern of the particle(s) in case of the matter-wave interference experiment.

The steps above are detailed in the following subsections.

4.1.1 Particle Transportation

Particles composed of different material and masses (in the range from 10^8 - $2 \cdot 10^9$ amu) are stored in a container (or multiple containers). Currently 15 different combinations of masses and materials are foreseen. These stored nano-particles are moved from their storage location by means of a magnetic field and their movement is halted by a Paul trap. A detailed description of the storage and transportation system is provided in Section 9.4.1. After this the optical cooling takes over.

4.1.2 Optical Cooling

Particles are cooled using a 1064 nm laser, i.e. their centre-of-mass (CoM) motion is reduced to small values which brings the particles into a quantum state. Two TEM_{00} modes with orthogonal polarization are used for trapping and for side-band cooling of the CoM motion along the cavity axis. A TEM_{01} and a TEM_{10} mode are to be used to cool the transverse motion of the trapped particle. These four modes can be combined in a few-mode fibre using a few-mode spatial multiplexer,

4.1.3 Evolution and Phase Grating

The particle is allowed to evolve freely with no (or minimal) interaction with the environment. This free evolution phase places stringent requirements on the level of the vacuum and the temperature of the environment (to minimise interaction with the blackbody radiation resulting from the environment). Optionally, for the matter-wave interference experiment, somewhere within the evolution time (the details depend, in a

complex way, on the mass of the particle, the applied phase grating, and the expected decoherence parameter) an optical phase grating will be applied. This phase grating is applied by an UV-laser of ~ 400 nm, which is doubled in frequency using β -BaB₂O₄. This results in a grating period of ~ 100 nm.

4.1.4 Measurement of Position of Particle

After the quantum-mechanical evolution, the position of the particle is measured (i.e. the waveform collapses). This measurement is done in a two-fold process. The position is in principle determined by interferometric means using the 1064 nm IR laser. This exploits the interference of scattered/diffracted light by the particle with the coherent light of the laser itself. This will lead to a difference in intensity depending on where the particle is located. This intensity is measured by a photo-diode in the laser beam. This interferometric measurement however contains an ambiguity equal to the wavelength of the laser (1064 nm). This ambiguity is resolved by measuring the position of the particle, using scattered light, with a detector. This detector has to be sensitive in the near IR. Currently a H2Rg1 detector is baselined. This detector is a HgCdTe detector which features 1024x1024 18 μ m pixels and has high sensitivity ($\sim 70\%$) at this wavelength. Since the optical bench is cold (20 K) and this detector (and many others) does not operate at these temperatures (due to freezing out of the carrier electrons) the detector is located outside the cavity and the light needs to pass through a window (e.g. sapphire). Outside the cavity the temperature is around 50 K. It is foreseen that a modest optical magnification is used. Since the area which needs to be imaged is $\sim 2 \times 2$ mm and the size of the detector is $\sim 18 \times 18$ mm this magnification cannot exceed 9, and is foreseen to be 5-8 to allow some margin. Since the detector is only aimed to resolve the wavelength ambiguity, the position (i.e. centroid of scattered light) needs to be determined with an accuracy of 1 μ m. This seems within reach using an out-focus image (in order to spread the light over more pixels and obtain a better estimate of the centroid) and the expected number of scattered photons. Additionally, this imposes a stringent requirement on the lateral motion of the detector between measurement (or between beginning and end when a reference image using markers is obtained) of around 2-5 μ m (dependent on the magnification and the allocation between centroiding error and thermo-elastic displacement error). Two scattered light images are foreseen: one before the free-fall time, which can possibly be used to correct for any motion on the free-fall time by imaging possible reference markers within the image area; two images are foreseen in the data budget.

4.2 Requirements and Design Drivers

4.2.1 Vacuum Level

The evolving particle can only tolerate up to 2 hits (with 80% probability) of moving gas molecules. This leads to a strict requirement on the vacuum level, which is also dependent on the free-fall time. The required vacuum level is 10^{-11} Pa which could be reachable using non-evaporable getters (see Section 15.3 and Section 3.3.1 for the requirement derivation).

4.2.2 Thermal Environment

In order to minimise interaction with background thermal black-body photons, a stringent requirement is placed on the surrounding environment of 20 K. At this temperature the interaction with blackbody radiation induces a decoherence which is (much) lower than the decoherence parameter which is measured. Two main factors drive the requirement for the ambient temperature: i) the cross-section of the test particles, and ii) the low absorption of blackbody photons in the material of the test particle. It is noted here that the requirement for 20K was derived for masses of 10^{-11} amu, for which the required free-fall times are out of reach for the spacecraft. However, the low temperature is extremely beneficial in two ways: i) it allows to reach lower vacuum levels (cryo-pumping), and ii) it slows gas molecules down and hence decreases the probability of interaction with the test particle.

4.2.3 Thermo-Elastic Deformation of Optical Bench

Thermo-elastic deformation of the optical bench (SiC) will spoil the accuracy of the measurement. This leads to a requirement on the temperature stability of 5mK over the measurement time of a complete interference pattern (assumed to be 3 weeks).

4.3 Assumptions and Trade-Offs

4.3.1 Closed Versus Open Cavity

In the original mission proposed by the scientific community an open cavity was foreseen for the payload to achieve the extremely high vacuum conditions. However, based on the expected achievable vacuum in the near vicinity of a contaminating spacecraft (which was not analysed in detail), but mainly the quick (within seconds) charging of the test particle by swarming solar electrons (which can make it around the sun shield) and the difficulty to validate such an environment on ground, it was considered too risky and decided to use a closed cavity for the payload.

4.3.2 Temperature of Cavity

A lower temperature of the cavity is beneficial for the requirement on the vacuum pressure level: a lower temperature slows gas molecules down and decreases the chance of interaction with the test particle. During the study, temperatures of 4K and 20K were assessed. For 4K an active mechanical cooler was needed, which introduces mechanical vibrations, which might lead to non repeatable test particles position measurements. On the other hand, a vacuum level of 10^{-11} Pa can more easily be reached (and verified) at 4K. In order to balance between vacuum and mechanical issues (due to vibration damping requirements) it was decided to opt for a 20K environment.

4.3.3 Paul Trap

The Paul trap is the interface between the particle transportation system and the optical bench. The Paul trap is, while operating, powered by a relatively high voltage. When the Paul trap is not operated it is assumed that the residual electro-magnetic field of the trap is negligible. In the future this assumption should be translated into a requirement on the residual electro-magnetic field of the trap.

Since the Paul trap is located on the optical bench, it is also a necessity that the trap does not interfere with the working of the lasers (e.g. by blocking part of the beam). Furthermore, a low contribution to scattering of photons (i.e. low background) is beneficial to the coarse measurement using the imaging detector.

4.4 Baseline Design

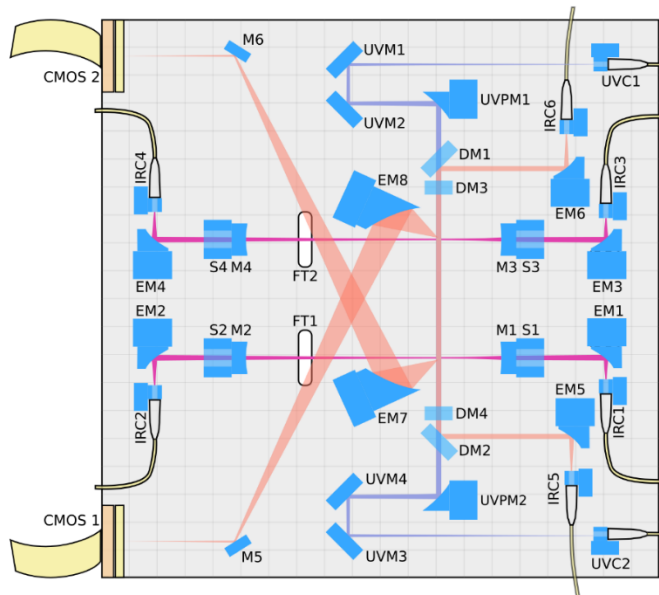


Figure 4-1: The layout of the optical bench. Note the presence of the detectors which are foreseen to be outside the cavity

4.4.1 Redundancy Concept

The payload as presented has a fully redundant design (two IR lasers, two UV lasers, two detectors, two feed-through holes etc.). However, during the CDF it was identified that a strong driver is the offset between the particle position and the CoM. Therefore, the redundant part of the optical bench (FT2) will have a poorer performance, since it will have a larger offset (if the offset of FT1 is minimised). A redundant system with the same performance can be reached when the nominal and redundant IR cross at one feed-through hole, preferably at a small angle (or alternatively at 90 degrees with appropriate moving of the UV laser). The only component which is then not redundant is the feed-through hole itself; however, this is only a mechanical hole. Additionally, the Paul trap (which is considered part of the particle storage and transportation system) needs to be redundant in place, i.e. by doubling the electrodes.

4.5 Options

The detection of the IR scattered light can in principle be done with any detector having a sufficient Quantum Efficiency at 1064 nm, small enough pixels, and a sufficient number of pixels to image to the area. A suitable alternative for the H2RG1 detector is the European ALFA detector which has 2048x2048 15 μm pixels which is currently in development. The Saphira HgCdTe avalanche photo diode has sufficient sensitivity (1

photon rms), 24 μm pixels, but only 320x256 pixels which is too small for the foreseen magnification factor.

4.6 Technology

Please note that the table below does not include technology needs for the particle storage and transportation system, which are described elsewhere.

Technology Needs						
*	Equipment Name & Text Reference	Technology	Supplier (Country)	TRL	Funded by	Additional Information
*	High-finesse cavities			4		TRL 4-5 foreseen at end of the year.
*	Interferometric position of test-particle			3		
*	Baseplate optical bench (SiC)			5		
*	GHz EOMs			4		
*	AOMs		Oerlikon (CH)	6		LPF heritage
*	NIR laser		Tesat (DE)	5		LPF heritage, performance tbc
*	DUV laser			4		
*	DUV phase grating			4		M. Arndt group (University of Vienna)
*	Cooling test particles			4		University of Vienna
*	Cooling with multiple cavity modes			2		
*	Spatial mode multiplexers			4		
*	Temperature tunable narrow-band fiber Bragg filters			3-4		Aspelmeyer group (University of Vienna)
*	Low-noise fiber amplifiers			4		LISA developments on-going
*	Homodyne detection			4		Limited by ultra-low noise photo diodes, heritage

						from LPF?
*	Cavity Housing incl particle disposal			4		
*	Cavity Venting opening mechanism			4		
*	H2RG1 detector		Teledyne (US)	9		European alternative: ALFA, currently TRL 4

From the table above, it is clear that significant technology development is needed to mature the payload (also the particle storage and transportation concept, see Section 4.1.1). This technology development is not limited to a single item of the payload, but more-or-less equally distributed over the payload. Except for the optical bench (including mounting of the component with strict thermo-elastic/mechanical and low-outgassing requirements) the main development is related to the lasers, including high-finesse cavities, detection system, and associated equipment.

An item which was not addressed in detail during the CDF was the disposal of the test particles: based on physical considerations (i.e. the strength of the van der Waals attraction) it is assumed that disposed test particles will stick to the walls of the cavity. This, however, should also be verified experimentally.

5 MISSION ANALYSIS

5.1 Requirements and Design Drivers

The mission design is driven by the requirement to place the spacecraft into a quiet and stable environment. In particular, the photon flux on the payload shall be minimised, i.e. it is advantageous if the Sun shield could also be used to block photons from other radiating bodies like the Earth. Moreover, the environment shall be characterised by a low particle density ($<500/\text{cm}^3$) and gravity gradient.

5.2 Assumptions and Trade-Offs

Assumptions	
1	The mission is launched using a direct injection by a suitable launcher like Ariane 62 from Kourou.
2	A launch in 2030 is assumed, however the analysis in this section is not strongly dependent on the launch year.
3	The duration of the mission is 3.5 years (3 years science phase) with a possible extension to 5.5 years.
4	The large manoeuvres are executed with a cold gas propulsion system with 1N thrust.
5	The station keeping manoeuvres are executed with a cold gas system with 1 mN of thrust.
6	The initial spacecraft mass is 1000 kg.

The following orbit options were discussed during the study:

1. Sun-Earth libration point L2
2. Earth-trailing/leading orbit (ETO/ELO)
3. Sun-Earth libration point L1
4. HEO

The list is ordered by preference, although the L2 option and the ETO/ELO options are of similar preference. Figure 5-1 and Figure 5-2 show examples for each of the orbit options in the Sun-Earth rotating frame defined as follows:

- X-axis along the Sun-Earth line
- Z-Axis along the Earth angular momentum vector
- Y-Axis completing the right-handed system

The L2 option was selected as a baseline for the study.

Orbit	Pros	Cons
L2	<ul style="list-style-type: none"> • Communications distance $< 1.8\text{e6 km}$ • Sun and Earth are always in the same direction as seen 	<ul style="list-style-type: none"> • Station keeping required

Orbit	Pros	Cons
	<ul style="list-style-type: none"> from the spacecraft. Can be designed eclipse-free 	
ETO/ELO	<ul style="list-style-type: none"> Can have rather constant Sun-Earth geometry Operationally and system-wise by far the simplest option No station keeping required No transfer phase, no manoeuvres, no propulsion system required Eclipse-free 	<ul style="list-style-type: none"> Earth range grows up to 50e6 km in 3.5 years and will continue increasing if the mission is extended.
L1	<ul style="list-style-type: none"> Communications distance < 1.8e6 km Eclipse-free 	<ul style="list-style-type: none"> Sun and Earth are on opposite sides of the spacecraft. Station keeping required
HEO	<ul style="list-style-type: none"> Can be designed eclipse-free 	<ul style="list-style-type: none"> High gravity gradient Strong variation of gravity gradient and photon flux from Earth. Perigee must be high enough to avoid radiation belts → large manoeuvre needed.

Table 5-1: Pros and Cons for the various orbit options

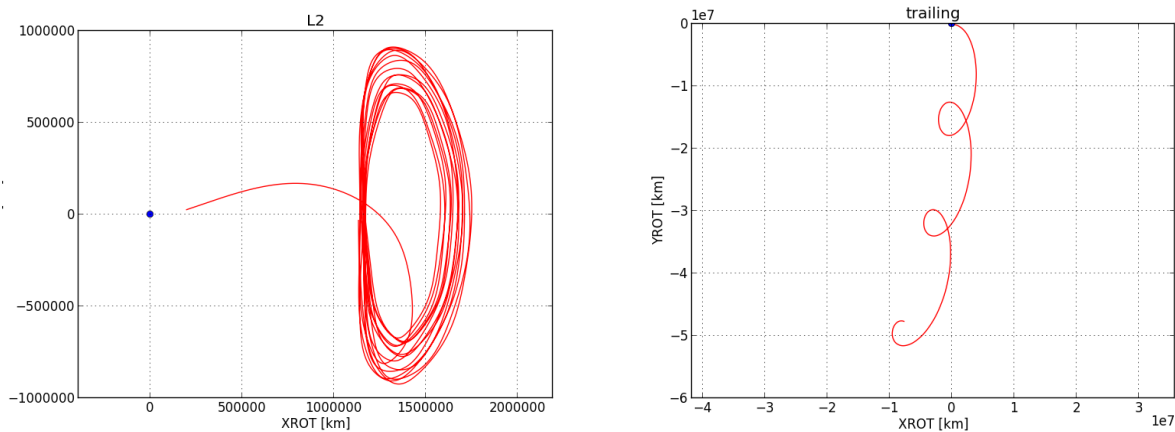


Figure 5-1: Examples of an orbit around Sun-Earth L2 (left) and an Earth-trailing orbit (right) in the Sun-Earth rotating frame

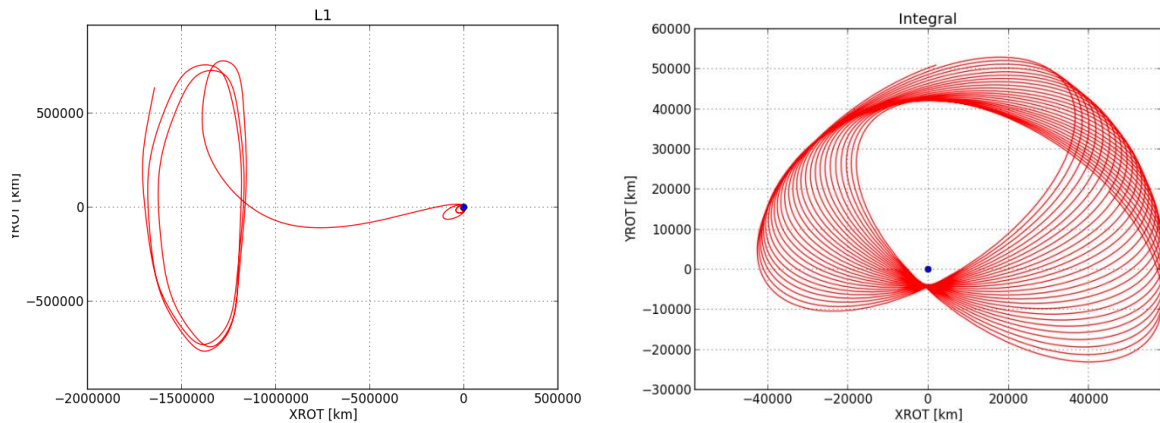


Figure 5-2: Examples of an orbit around Sun-Earth L1 (left) and a HEO (right) in the Sun-Earth rotating frame

5.3 Baseline Design

5.3.1 Launch

No analysis of the launch has been done during the CDF. For the purpose of this study, it was assumed that the mission would use a direct injection by Ariane 62 from Kourou with an expected delivery mass of 3000 kg to L2.

5.3.2 Orbit TCMs and Station Keeping

After launch, the spacecraft trajectory needs to be determined by ground-based Range and Doppler measurements. These are then used on ground to compute the TCMs needed to guide the spacecraft to the nominal trajectory. The first TCM is assumed to take place 24 hours after separation. Two smaller follow-up manoeuvres are then needed to reach the required orbit injection accuracy. Due to the similarity of the mission, all delta-V estimates are based on computations given in RD[3]. The compiled delta-V budget can be found in section 5.4.

5.3.3 Orbit Geometry

Figure 5-3 shows the L2 orbit geometry w.r.t. Earth and Sun. After the initial transfer of about 30 days, the Earth range oscillates about a distance of 1.5 million kilometres giving rather stable communications link to Earth. The Earth-Sun-spacecraft angle has a maximum value of about 35 deg. It means that the Sun shield will also be suitable for blocking photons coming from the Earth.

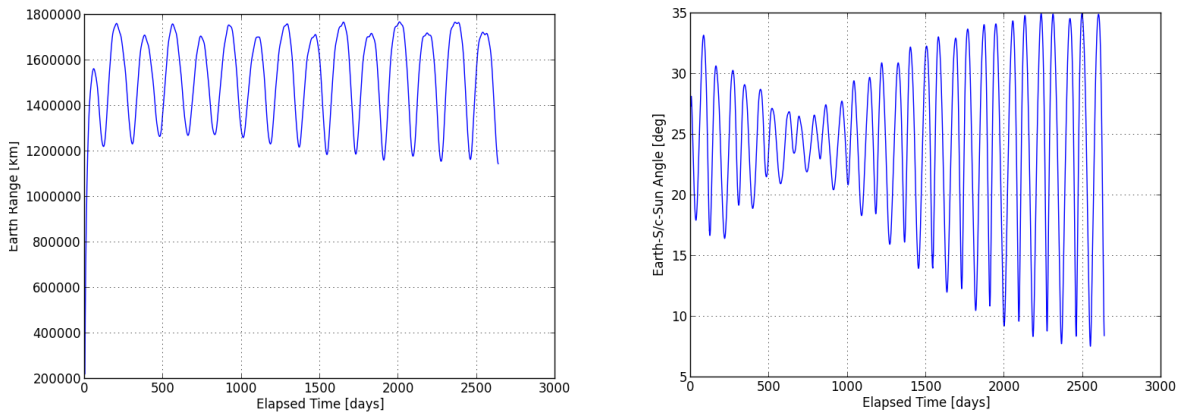


Figure 5-3: Earth range evolution and Earth-Sun-s/c angle for the baseline L2 orbit

5.3.4 Gravity Gradient along the Orbit

For the instrument design, the gravity gradient and its rate of variation are of interest. This is shown in Figure 5-4. The maximum gravity gradient (for a 1 m offset) encountered along the orbit is about $6 \cdot 10^{-13} \text{ 1/s}^2$. The maximum rate is about $2 \cdot 10^{-19} \text{ 1/s}^3$. These numbers are also resolved in components along and perpendicular to the Sun direction and shown in Figure 5-5 and Figure 5-6. The gravity gradient component in the Sun direction is dominant by about a factor of 5. The component perpendicular to the Sun direction is caused by the Earth gravity and the out-of-ecliptic excursions by the spacecraft.

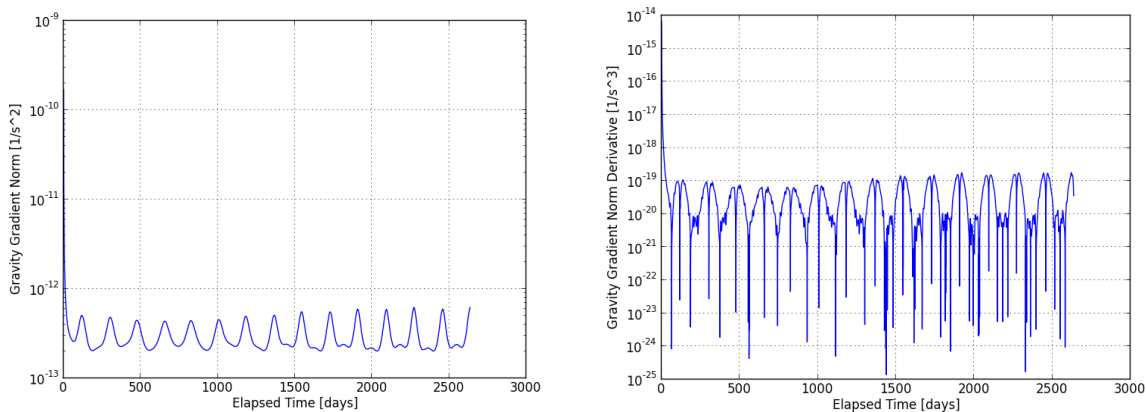


Figure 5-4: Total gravity gradient (left) and gravity gradient rate (right) for the baseline L2 orbit

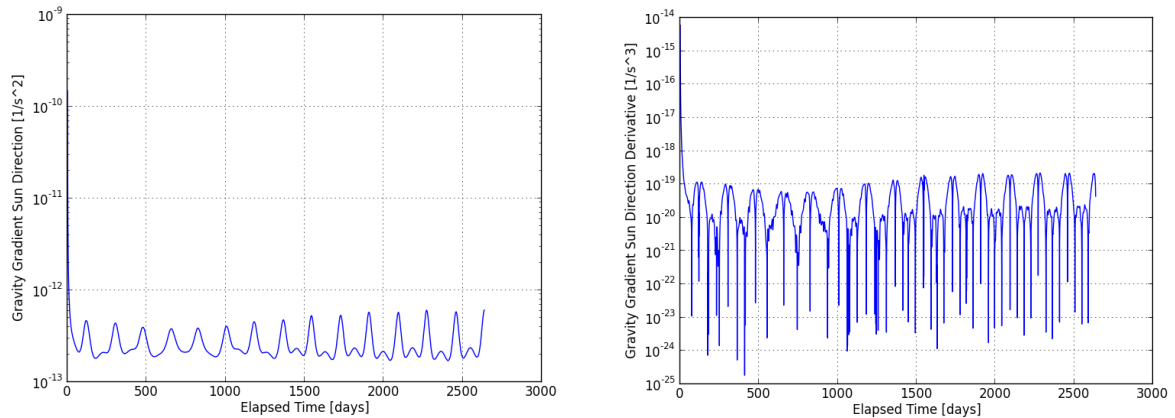


Figure 5-5: Gravity gradient (left) and gravity gradient rate (right) components in the Sun direction for the baseline L2 orbit

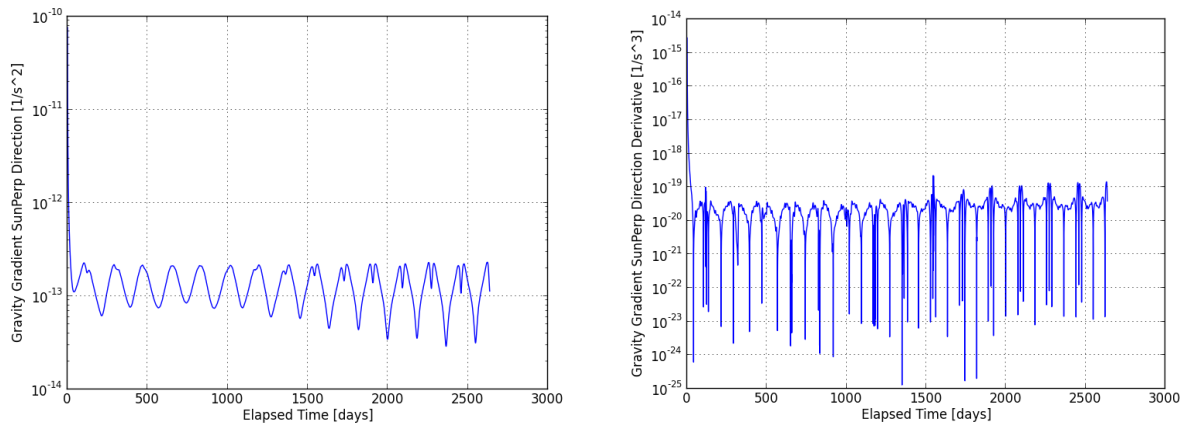


Figure 5-6: Gravity gradient (left) and gravity gradient rate (right) components perpendicular to the Sun direction for the baseline L2 orbit

5.3.5 Ground Station Coverage

In order to dump the science data and telemetry, command the spacecraft and do orbit determination which is required for the station keeping a good ground station visibility is needed. Figure 5-7 shows the daily coverage hours by the three ESA Deep Space Antennas. The minimum and maximum pass durations are summarised in Table 5-2. Please note that the short minimum pass durations for Cebreros and Malargue are caused by Moon occultations which happen very rarely. Typically, a minimum pass duration of around 7 hours can be assumed.

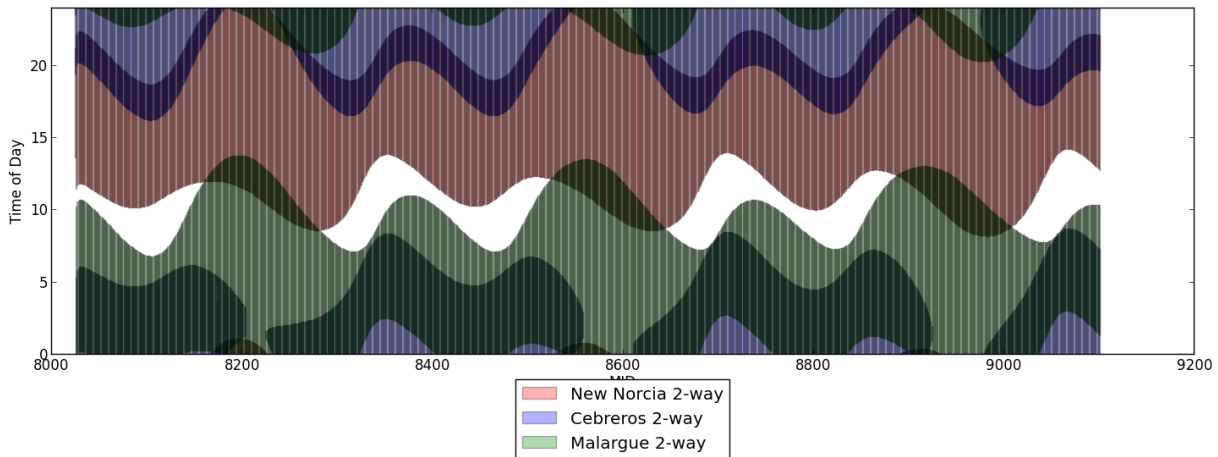


Figure 5-7: DSN ground station coverage for the baseline L2 orbit

Station	Min. pass [hours]	Max. pass [hours]
New Norcia	6.6	14.3
Cebreros	0.5	14.3
Malargue	5.6	15.2

Table 5-2: Minimum and maximum pass durations for the baseline L2 orbit

5.4 Budgets

Table 5-3 summarises the delta-V budget for the baseline mission.

Manoeuvre	Type	Delta-V [m/s]	Margin [%]
TCM1 part 1	Stochastic	32.8	0 %
TCM1 part 2	Deterministic	13.8	0
TCM2	Stochastic	1.7	0 %
TCM3	Stochastic	0.7	0 %
TCM delay allocation	Deterministic	13.4	10 m/s
Station keeping for 3.5 years	Stochastic	11.2	50 %**
TOTAL		73.6 m/s (w/o margin)	89.2 m/s (w/ margin)**

Table 5-3: Delta-V budget for the baseline L2 orbit

** Values differ from Table 6-13: QPPF Delta-v budget due to the assumed margin.

5.5 Options

5.5.1 Earth-Trailing Orbit

The main design parameter for the ETO/ELO is the launch RAAN. It determines in which direction w.r.t. the Sun the spacecraft escapes and thus determines the evolution of the orbit geometry. Figure 5-8 and Figure 5-9 shows the range of possible evolution scenarios for the Earth range, the Earth-spacecraft-Sun angle, the gravity gradient and the gravity gradient rate. This is assuming a standard direct escape launch from Kourou with 0.5 km/s escape velocity and a launch date on 21. March 2030. No manoeuvres are executed after separation.

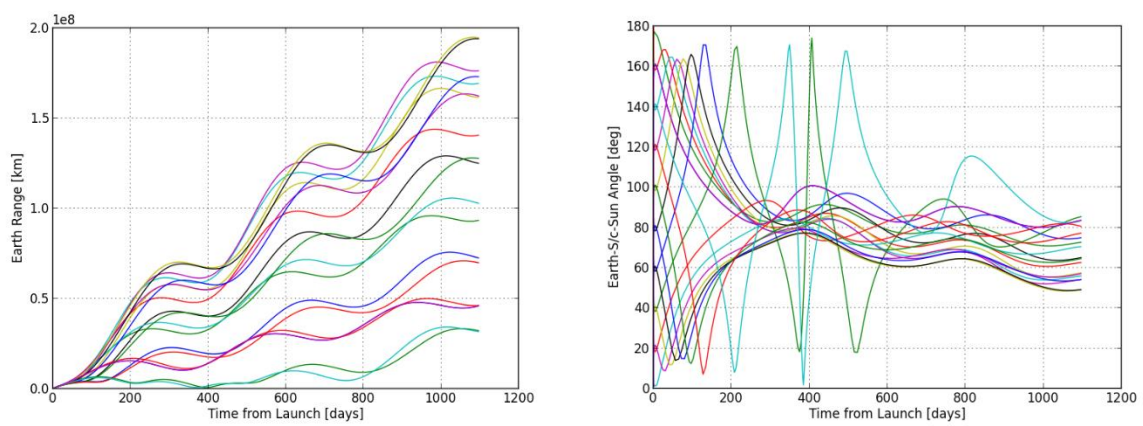


Figure 5-8: Evolution of Earth range (left) and Earth-S/c-Sun angle (right) for a number of launch RAANs between 0 deg and 360 deg.

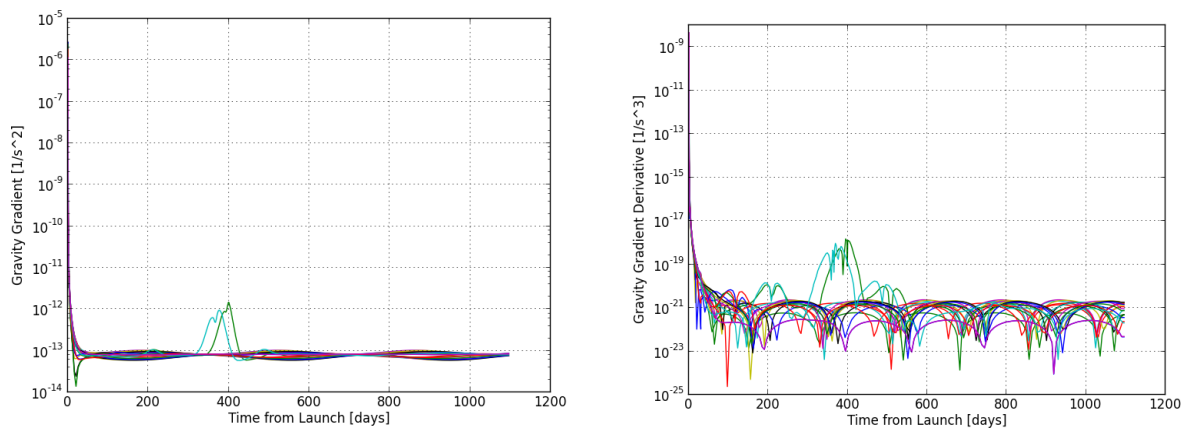


Figure 5-9: Evolution of gravity gradient (left) and gravity gradient rate (right) for number of launch RAANs between 0 deg and 360 deg.

Figure 5-10 and Figure 5-11 show the maximum values for Earth range and gravity gradient (rate) during the mission as a function of the launch RAAN. Note the regions around 170 deg and 350 deg launch RAAN, where the behaviour of all these quantities is quite sensitive to the initial condition. This is because for these values of the launch RAAN the spacecraft comes close to the Earth again which causes a rather chaotic behaviour. For a robust mission design, it is recommended to avoid these regions, but

still choose a launch RAAN which minimises the maximum Earth range and the gravity gradient (rate). A suitable choice would be RAAN = 180 deg.

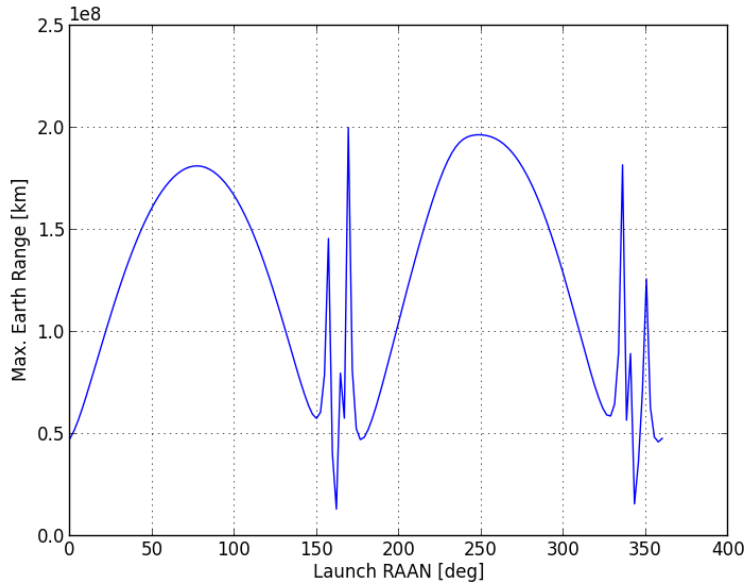


Figure 5-10: Maximum Earth range during 3.5 years mission duration as function of the launch RAAN for an ETO

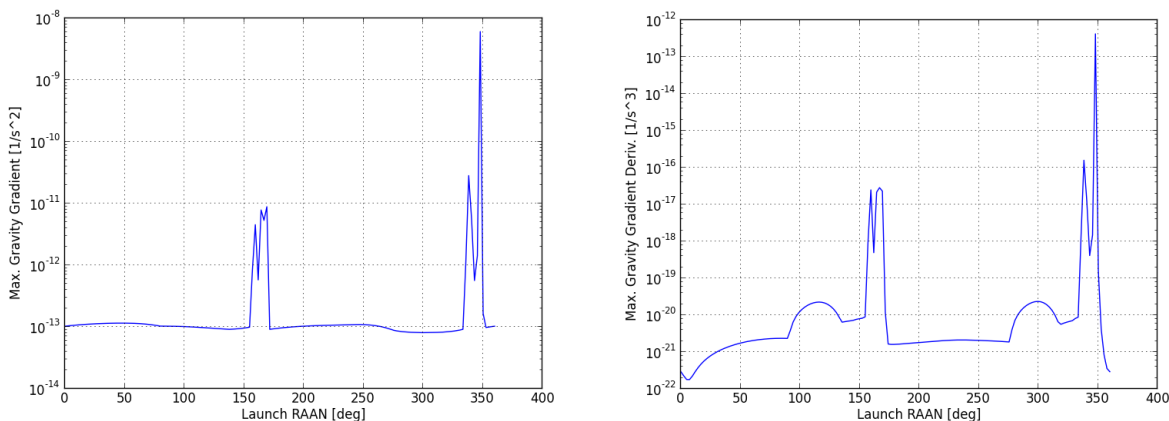


Figure 5-11: Maximum gravity gradient (left) and gravity gradient rate (right) during 3.5. years mission duration as function of the launch RAAN for an ETO

Figure 5-12 shows the evolution of the Sun Earth geometry for such an ETO. The Earth distance is gradually increasing up to a distance of about 50 million km. Note that a rather stable Earth-S/c-Sun angle is only reached after an initial phase of about 180 days.

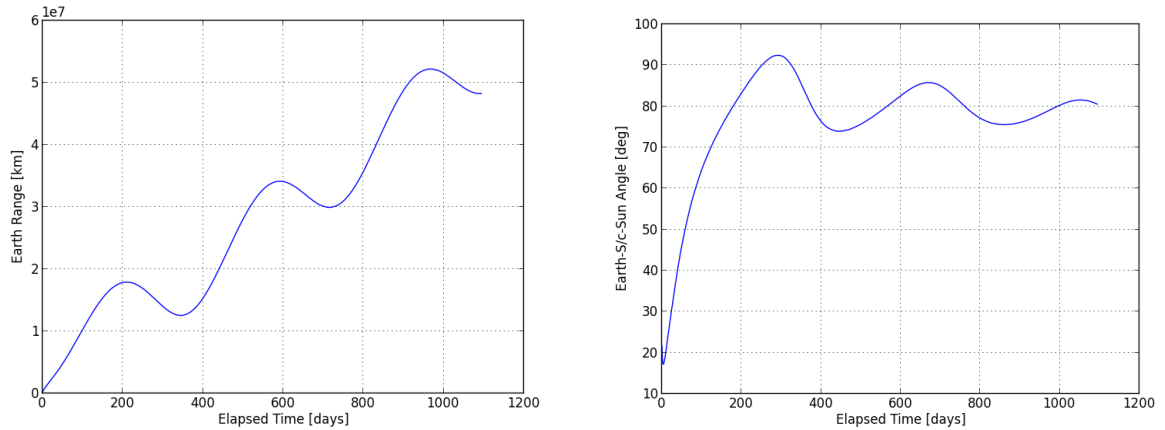


Figure 5-12: Evolution of Earth range (left) and Earth-s/c-Sun angle for the ETO option

The evolution of the gravity gradient is shown in Figure 5-13. Note that the maximum value is smaller than for the L2 case. Here the component perpendicular to the Sun direction is virtually zero due to the distance to Earth.

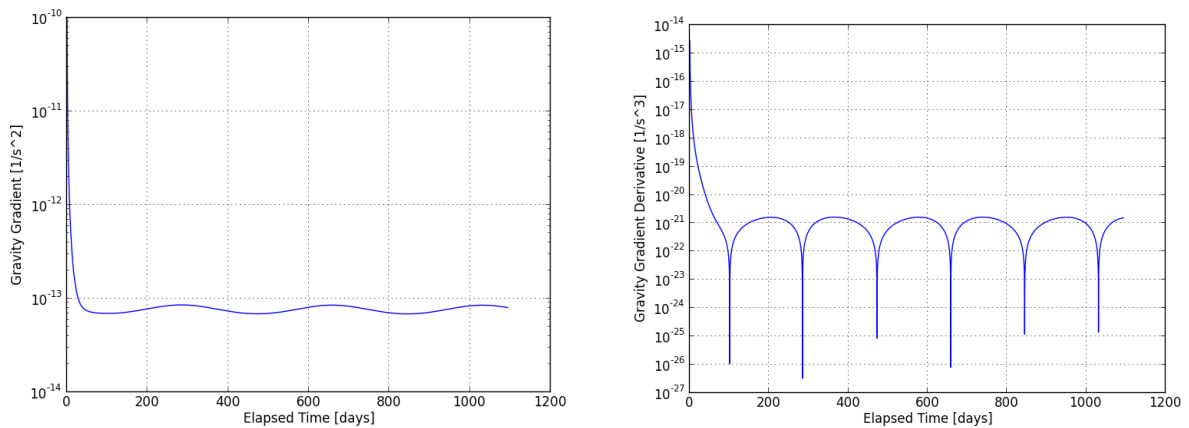


Figure 5-13: Evolution of the gravity gradient (left) and gravity gradient rate (right) for the ETO option

Figure 5-14 and Table 5-4 summarise the DSN coverage for the ETO option. Almost continuous coverage can be assumed.

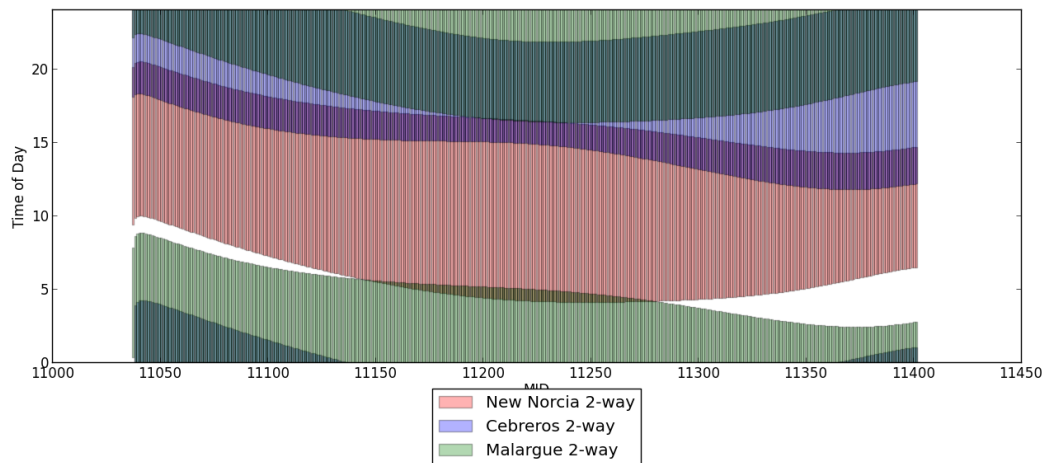


Figure 5-14: DSN coverage for the ETO option

Station	Min. pass [hours]	Max. pass [hours]
New Norcia	8.2	12.3
Cebreros	6.9	12.9
Malargue	7.6	12.6

Table 5-4: Minimum and maximum pass durations for the ETO option.

5.5.2 Earth-Trailing Orbit with Limited Drift

The main drawback of the Earth-trailing orbit, as described in the previous section, is the drift w.r.t. Earth as time passes by. The increase of the Earth distance puts stronger requirements on the communications subsystem. One possibility to mitigate this is to implement a manoeuvre either 6 or 12 months after launch. This manoeuvre would place the spacecraft into an orbit with the same semi-major axis as the Earth's orbit, eliminating the drift, at least for a short amount of time. The perturbation of the Earth's gravity however, will change the spacecraft semi-major axis and causing it to drift again, at a slower rate though. The estimated delta-V for this kind of "stop manoeuvre" will be at the order of the chosen escape velocity from Earth, i.e. 0.5 km/s in the described case. The downside of this scenario is that it complicates the system design significantly since a much larger propulsion system is needed on the spacecraft to execute the manoeuvre. It has to be traded against the larger communications system in the scenario without the manoeuvre.

5.5.3 L1 and HEO

These options have been discussed briefly during the CDF, but were discarded early on due to unfavourable Sun-Earth geometry (L1) and/or strong variation in the environmental conditions (HEO). The trade-off is described in Table 5-1.

6 SYSTEMS

6.1 System Requirements and Design Drivers

A set of mission requirement has been derived taking into account initial set of requirement from RD[5]. The requirements that have been updated are listed below.

Mission Requirements		
Req. ID	Statement	Parent ID
MIS-010	The total mission duration shall not exceed 3.5 years (TBC) including Transfer and Commissioning phases.	L3-MIS-000100
MIS-020	The mission shall support a minimum of 15 batches of measurements, consisting of 12500 particles in each batch, with a free fall duration tFF of 40s TBC, consisting of test particle with masses within the following range: 1e8 amu - 2e9 amu (goal : up to 1e11 amu)	L3-MIS-211200
MIS-030	The mission shall provide a science availability of at least 50% (goal : 75%) over nominal science mission duration.	L4-MIS-000110
MIS-040	The pressure in the optical bench shall be below 10-11 Pa (goal : 1e-13 Pa)	L3-MIS-111100
MIS-050	The temperature within the optical bench during a measurement shall remain below 20K during the measurement duration.	L3-MIS-112100
MIS-060	The temperature stability of the test bench shall not deviate more than 5 mK from the beginning of the batch over the whole duration of the batch.	L3-121100
MIS-070	The S/C motion during each measurement run shall be such that the particle remains within 1 mm (TBC) of the nominal detection area, with a confidence level of 99.7% (TBC)	L3-MIS-115100
MIS-080	The Spacecraft to Test-Particle Relative Position Drift Error (PDE) during a measurement shall be smaller OR known better than 14 nm, with a 99.7% confidence assuming the ensemble interpretation.	L3-MIS-121200
MIS-300	The orbit for the mission shall offer an environment stable enough such that all science requirements can be reached with no active control (drag-free type) of the S/C during each measurement duration <i>Rationale : as soon as the orbit allows to meet the performance requirements in particular in terms of gravity gradient stability. L1, L2 or Earth-trailing / heading orbits are compatible with a free-drifting concept up to free fall times of typically 150s.</i>	
MIS-400	The mission shall be launched by either VEGA-C or ARIANE 62 from Kourou	

6.1.1 Design Drivers

In order to observe the decoherence parameter at a sufficient resolution, the test particle must be left in a free-fall state without perturbation in order to enable the wave function to evolve to become less localised. The longer this unperturbed state is, the larger the separation between the different peaks of the interference pattern for a particle with a quantum behavior. The disturbances / perturbations can namely be changes in energy or state due to a collision between the:

1. Test particles and other particles
2. Test particle and the satellite elements

Therefore, during the free fall phase, there must be a low risk of collision.

Other particles can be classified as those in the residual atmosphere of the spacecraft (e.g. Hydrogen) and those that are external to spacecraft due to the space environment (e.g. GCR's, background plasma). This imposes a number of design constraints, such as:

- Enclosing optical bench to avoid influence from background plasma
- Cooling the optical bench to reduce the energy in the residual particles
- Maintaining a stable temperature of the optical bench to maintain a stable collision risk.

The particle should stay within the detection area, posing constraints on the satellite in terms of:

- Self-gravity and CoM alignment
- Mechanical stability
- Acceleration of spacecraft due to solar radiation pressure.

With the differential acceleration between the spacecraft and particle, as a result of influence of the solar radiation pressure, there is a constraint on the axis of the Sun to the Sun shield posing additional constraints on the concept of operations in terms of communication windows, and hence data rates and on-board storage.

6.2 System Assumptions and Trade-Offs

6.2.1 Assumptions

In the frame of the QPPF CDF Study, the following system level assumptions were considered:

- Launch in 2030
- 60 s test particle preparation duration
- Active Cooling
- Orientation of the optical bench with respect to the rest of the spacecraft
- Based on analysis by the AOCS expert the maximum Sun de-pointing angle is 10 degrees.

6.2.2 Trade-Offs

In the frame of the QPPF CDF Study, the following system level trade-offs were conducted and reported hereafter:

- Orbit (L1 vs. L2 vs. ET/EL Continuous Drift vs. ET/EL No Drift)
- Test Bench: Exposed vs. Enclosed
- Particle Storage and Transportation Device
- Propulsion: Chemical vs. Electric vs. Cold Gas
- Attitude Control: Active vs. Passive
- Thermal Control: Active vs. Passive
- Active vs Passive cooling
- Location of Medium Gain Antenna.

6.2.2.1 Orbit Trade-Off

A system level trade-off identified the feasible orbits, and the outputs used to select the orbit for the purpose of the CDF study. The driving requirements on the orbit were to:

- Minimise the gravity gradient and the gravity gradient rate
- To minimise the thermal gradient rate (eclipse free, Sun-Earth angle in terms of radiation).

With the criteria above, four orbits were identified, namely:

- L1
- L2
- Earth Trailing/Earth Leading Continuous Drift
- Earth trailing/Earth leading with a burn at the beginning-of-life to avoid drift.

The technical content gathered to perform the trade-off is presented in Table 6-1.

	Trade-Off Criteria	L1	L1 Score	L2	L2 Score	ET/EL Continuous Drift	ET/EL CD Score	ET/EL No Drift	ET/EL ND Score
Payload Performance	Gravity Gradient [1/s ²]	1E-12	3	1E-12	3	1E-13	3	1E-13	3
	Gravity Gradient Rate [1/s ³]	1E-19	3	1E-19	3	1E-21	3	1E-21	3
	Eclipse	Eclipse Free	3	Eclipse Free	3	Eclipse Free	3	Eclipse Free	3
	Sun-Earth Angle	160 (Sun-Earth always in opposite Directions)	1	35 (Sun-Earth always in same direction)	2	85 (20 deg change)	3	85 (less constant)	3
Spacecraft	Orbit Insertion	Ariane 6.2 Class 1	3	Ariane 6.2 Class 1	3	Ariane 6.2 Class 1 + 10	2	Ariane 6.2 Class 1 + 10	2
	Orbit Insertion delta-V	Launcher Dispersion + Orbit Insertion Manoeuvre (55m/s)	2	Launcher Dispersion + Orbit Insertion Manoeuvre (55m/s)	2	None	3	200 - 300 m/s (after 6 months of drift)	1
	Station Keeping	1 - 7 m/s/y	2	1 - 7 m/s/y	2	None (minimal flight dynamics support)	3	None (minimal flight dynamics support)	3
	Ground Station	8 hours per day (ESA Deep Space Antennas)	3	8 hours per day (ESA Deep Space Antennas)	3	8 hours per day (ESA Deep Space Antennas)	3	8 hours per day (ESA Deep Space Antennas)	3
	Communications	1 Day of of Science is 0.07 of a 3 hour pass (0.3m HGA, 5Mb/s)	1	1 Day of of Science is 0.07 of a 3 hour pass assuming 0.3m HGA, 5Mb/s dynamics due to solar radiation pressure acting on antenna	3	1 Day of of Science requires 3.52 of a 3 hour pass at EOL after 3.5 year drift (or 1.37 at BOL) assuming 0.6m HGA, 100kb/s	1	1 Day of of Science requires 1.37 3 hour passes at EOL assuming 0.6m HGA, 256kb/s	2
		< 1.8e6 km 6s		< 1.8e6 km 6s		< 50e6 km (after 3.5 years) 3 mins		30e6 km 1.5m	
		pointing mechanism required		pointing mechanism required		pointing mechanism required		pointing mechanism required	
	Mission Extension	requires additional delta-v	2	requires additional delta-v	2	due to drift, to achieve link budget additional power / increase in antenna size required	1	requires additional delta-v	3

Table 6-1: Inputs for Orbital Trade-Off

For performing the trade-off, the weighting factors on the criteria were identified through a comparison ranking.

Trade-Off Comparison Overview		
1 left is more important	0 even	-1 top is more important

Trade-Off Criteria Comparison Ranking										
	Gravity Gradient [1/s ²]	Gravity Gradient Rate [1/s ³]	Eclipse	Earth Flux	Orbit Insertion Cost	Orbit Insertion Delta-V	Station Keeping	Ground Station Contact Time	Communications	Lifetime Margin
Gravity Gradient [1/s ²]		-1	1	1	1	1	1	1	1	1
Gravity Gradient Rate [1/s ³]	1		1	1	1	1	1	1	1	1
Eclipse	-1	-1		1	1	1	1	1	1	0
Sun-Earth Angle	-1	-1	-1		1	1	0	1	1	1
Orbit Insertion cost	-1	-1	-1	-1		-1	-1	-1	-1	1
Orbit Insertion delta-V	-1	-1	-1	-1	1		-1	1	1	-1
Station Keeping	-1	-1	-1	0	1	1		1	1	1
Ground Station Contact Time	-1	-1	-1	-1	1	-1	-1		0	1
Communications	-1	-1	-1	-1	1	-1	-1	0		1
Lifetime Margin	-1	-1	0	-1	-1	1	-1	-1	-1	

Table 6-2: Criteria Ranking

	Weighting Factor	L1	L1 Weighted	L2	L2 Weighted	ET/EL CD	ET/EL CD Weighted	ET/EL ND	ET/EL ND Weighted
Gravity Gradient [1/s ²]	4.47	3	13.4	3	13.4	3	13.4	3	13.4
Gravity Gradient Rate [1/s ³]	5.00	3	15.0	3	15.0	3	15.0	3	15.0
Eclipse	3.68	3	11.1	3	11.1	3	11.1	3	11.1
Sun-Earth Angle	3.16	0	0	2	6.3	3	9.5	3	9.5
Orbit Insertion cost	0.79	3	2.4	3	2.4	2	1.6	2	1.6
Orbit Insertion delta-V	1.84	2	3.7	2	3.7	3	5.5	0	0.0
Station Keeping	3.16	2	6.3	2	6.3	3	9.5	3	9.5
Ground Station	1.58	3	4.7	3	4.7	3	4.7	3	4.7
Communications	1.58	1	1.6	3	4.7	1	1.6	2	3.2
Mission Extension	1.05	2	2.1	2	2.1	1	1.1	3	3.2
Trade-Off Summary Weighted		0		67.63		71.84		0	

Table 6-3: Trade-Off Scoring

It was decided to eliminate both the L1 and Earth Trailing/Earth Leading No-Drift orbits from the trade-off due to showstoppers that were identified during the trade-off. For L1, the Sun-Earth angle of approximately 160 degrees would pose significant configuration constraints on the design of the satellite in order to avoid the thermal flux from two opposite directions. It was estimated that the Earth Trailing/Earth Leading with drift option required an approximate delta-v of 250 m/s at beginning of life, to achieve this, a separate propulsion module may be needed.

The study team identified no showstoppers for the L2 or Earth Trailing / Earth Leading Continuous Drift orbits. The L2 orbit option was adopted as baseline due to the familiarity of ESA operating spacecraft in this orbit and

the potential to extend the mission beyond nominal lifetime. However, as the Earth Trailing / Earth Leading Continuous Drift orbit is a valid option with some advantages in terms of a simplified configuration (no station keeping), some initial estimates were made to highlight the potential differences required for the system to operate in this orbit, see section [5.5.1] for more information.

6.2.2.2 Open vs. Enclosed Test Bench

It was unclear at the beginning of the study if the equipment needed to be protected from, or exposed to, the space environment. As a driving requirement, the test particle should be protected from collisions with other particles, so a trade-off was performed based on the identification of the risk of collision for these two options.

Exposed Test Bench:

Benefits

- Beneficial with passive cooling to reach low temperature

Drawbacks

- Exposed to particles from spacecraft (outgassing, thruster particles)
- Risk of stray light
- Difficult to protect from radiation
- Complex to test/validate on ground
- Independent of the orientation with respect to the sun, there will be a high electron flux if the test bench is exposed. If there is a sunshield between the test bench and the sun, the highly energetic electron flux will ‘swarm’ around the sunshield resulting in the same density at the surface of the sunshield on both sides Figure 6-1. Therefore, the risk of collision with these particles and the test particle is very high, resulting in a failure of the test particle to achieve the required free fall time without disturbance. This is the main driver for enclosing the test bench.

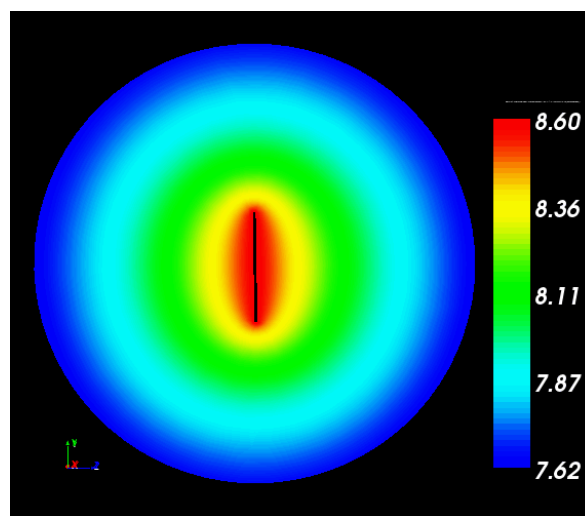


Figure 6-1: Electron Flux with Respect to the Sunshield

For more information on the electron flux, please refer to Chapter 16 Environment.

Enclosed Test Bench:

Benefits

- Ensures protection from electron flux, reducing the risk of collision with these particles.

Drawbacks

- The shielding provides some protection from radiation.
- Challenging design to support the depressurisation during launch and outgassing once on-orbit.

For more information on the Enclosed Test Bench design, please see Chapter 9 Nano particle Handling.

6.2.2.3 Propulsion: Chemical vs. Electric vs. Cold Gas

The cold gas propulsion was selected as it can provide two different levels of thrust while allowing the balancing of the propellant throughout the spacecraft and avoiding tank sloshing, as the experiment is very sensitive to variations in spacecraft attitude evolution as well as self-gravity.

The possibility of using electric propulsion was discarded as the power requirement for the initial orbit insertion would have oversized the solar panel in comparison to the need of the rest of the mission. Moreover, the gravity losses caused by the lower thrust would have accounted to a non-negligible level.

The chemical propulsion option was not selected as the estimated sloshing from residual propellant would result in a reduced overall efficiency (long tranquillisation times) and possibly shorter free fall times.

6.2.2.4 Attitude Control: Active vs. Passive

While the test particle is in free-fall, the main factor that can trouble the position measurement is the angular acceleration caused by the Solar Radiation Pressure (SRP) on the spacecraft. Regarding the Attitude Control, there are two competing strategies to remediate, active and passive. The first one would have allowed for very long free-fall durations, while the second has no correction during a period, and then the science is stopped in order for the spacecraft to get back to acceptable test conditions. However, free fall time being de facto limited by the achievable pressure level, there is no real justification system-wise for going for such long free-fall times.

An active attitude control would have consisted in a similar set-up as implemented in Lisa PF, in the form of a Drag-Free Attitude Control System (DFACS). This set-up would require for its input either an extremely precise accelerometer, which does not currently exist anywhere on the TRL scale, or the ability to measure a test mass, similar to the test particle. The latter possibility poses different issues, namely regarding the representativity of the reference particle compared to the test particle if it is in a different position in the spacecraft (and different conditions of vacuum). An active measurement on the test bench would create a heat load in an already constrained cryogenic area, and has a non-zero probability of affecting the test particle. If the reference particle is put at a different position, a supplementary analysis would indeed be required to guarantee the representativity.

The passive attitude control (“free drifting concept”) was selected for its relative simplicity. The main difficulty of the design is the prediction of the effect of the SRP torque, due to the shape of the surface under the sun-shield. Ideally it would be a planar surface and it is what has been assumed for the simulations. The faster the SRP torque varies, the more often calibration runs of the test particles will need to be run to ensure the drift between two calibrations remain well below the acceptable limit (driven by the matter-wave interferogram resolution).

6.2.2.5 Thermal control: Active vs Passive

In order to achieve the vacuum requirement, the temperature of the test bench and the surroundings of the test particle must be cooled to 20K. As a passive cooling can only bring the temperature of the payload to 50K, an active cooling system is necessary to achieve this further step in cryogenic temperatures.

6.2.2.6 Location of Medium Gain Antenna (MGA)

Due to the Sun-Earth angle, the MGA needs to be located in the Sun-facing direction. By doing this, the dynamics on the spacecraft as a result of solar radiation pressure will change, which is one of the driving constraints for the free-fall time. Therefore, it is best to avoid having non-necessary appendages Sun-facing during free-fall.

Three feasible options were identified:

1. Place the MGA on the Surface of the Sunshield
2. Place the MGA behind the Sunshield surface
3. Use a deployable boom to move the MGA as required by the different mission Phases

Place the MGA on the Surface of the Sunshield:

- Enables the use of COTS equipment
- **Will impact the free-fall time (likely to reduce) and/or frequency of calibration runs and/or frequency of attitude correction manoeuvres (hence overall science efficiency and propellant) ; requires a detailed analysis / characterisation of the effects of SRP on the spacecraft**

Place the MGA behind the Sunshield Surface:

The design would consist of the antenna recessed behind the surface of the Sun shield. Therefore, the surface would be required to reflect solar radiation but enable the antenna radiation to pass through.

- Avoids complex perturbations due to the SRP acting on the antenna
- COTS equipment for the MGA and pointing mechanism, which need to be integrated within a box/structure that can be mounted inside the Sun-shield. This may need to be the responsibility of the antenna manufacturer, which will also complicate the procurement process.
- The resulting deformation of the antenna radiation pattern due to reflections within the container need to be characterised. This distortion will also be different after TVAC testing due to the difference in properties of the materials.

- A dedicated technology development may be required to determine the optimal surface that have the desired optical properties whilst minimising the distortion of the antenna radiation pattern.

Robotic Boom with MGA & Pointing Mechanism at End-Effector:

Functionally the robotic boom would be capable of providing 1 DOF allowing the MGA to be deployed and retracted as needed.

- Avoids SRP disturbance torques during science operations
- Could use a similar technology to Solar Orbiter or Bepicolombo
- Risk of significant mission degradation if the robotic boom fails to operate
- Thermal flux on v-grooves needs to be assessed
- Need for additional DOF (pointing mechanism) needs to be assessed.

The third option, robotic boom, was considered as baseline for the reasons highlighted above. This option was considered due to the minimal impact on the solar radiation pressure. Option 1 would require more analysis of the spacecraft behaviour which is thought to be more challenging but feasible with a payload in the loop system.

6.3 Mission System Architecture

6.3.1 Mission Phases

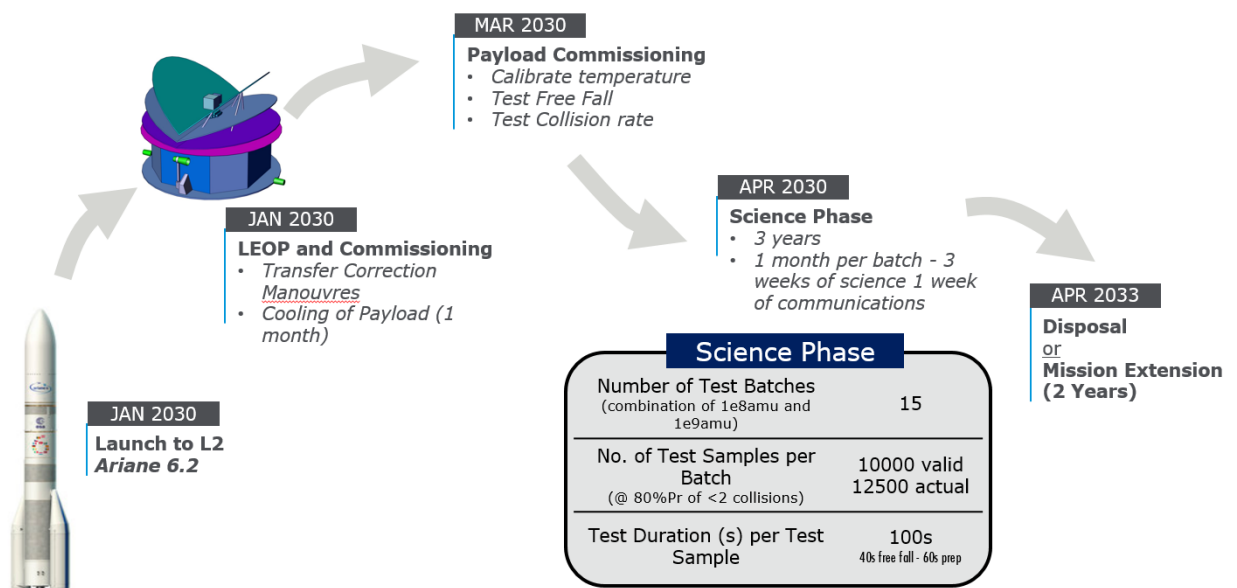


Figure 6-2: QPPF Mission Phases

6.3.1.1 Test Particle Transportation Sequence

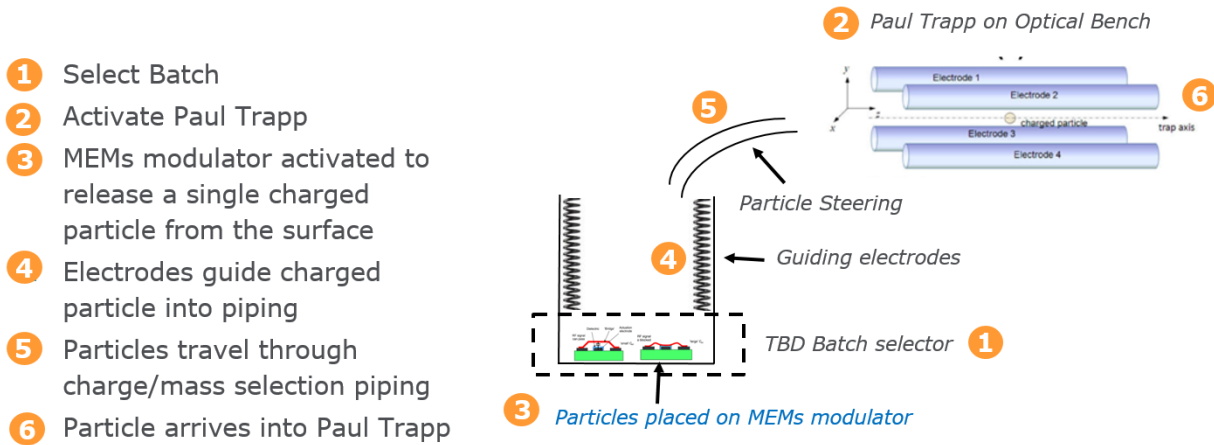


Figure 6-3 provides an overview of the process used to transfer the test particle from the storage device to the optical test bench.

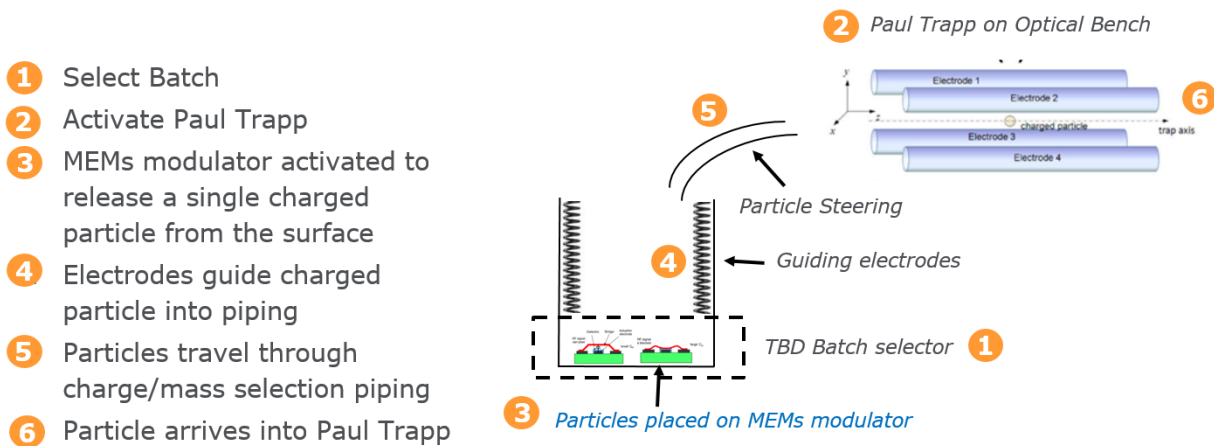
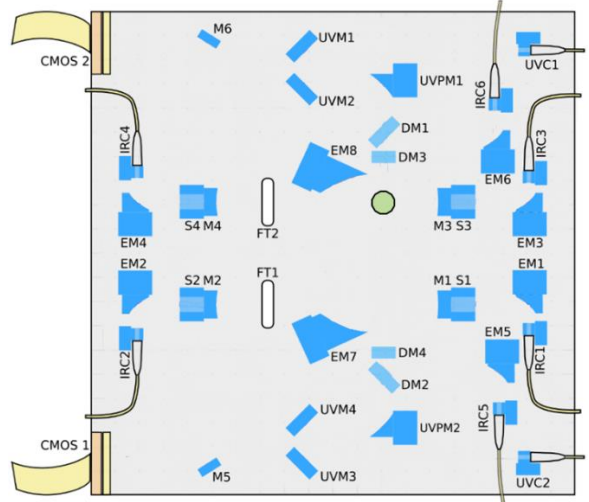
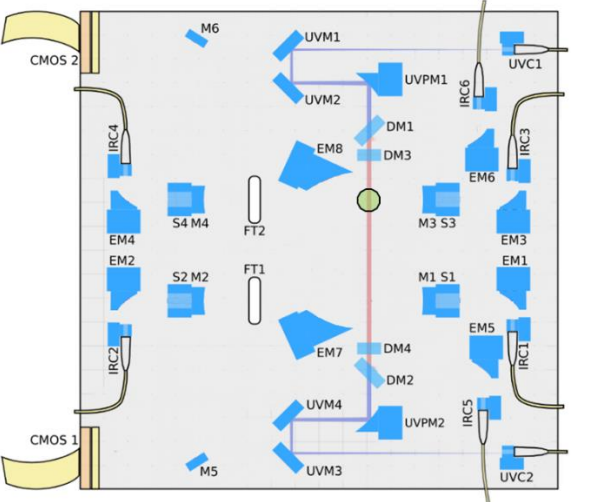
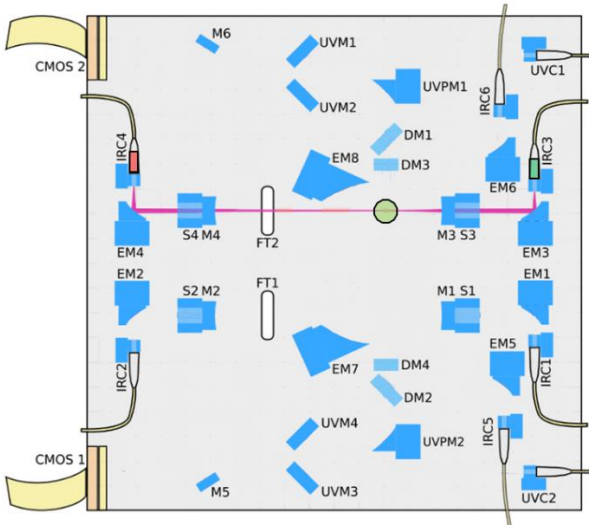
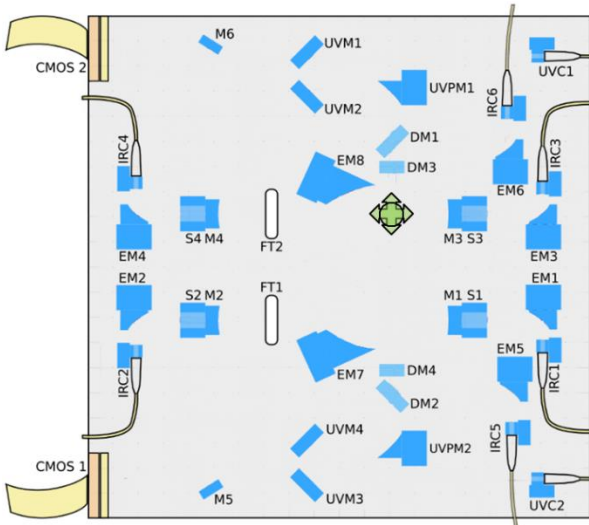
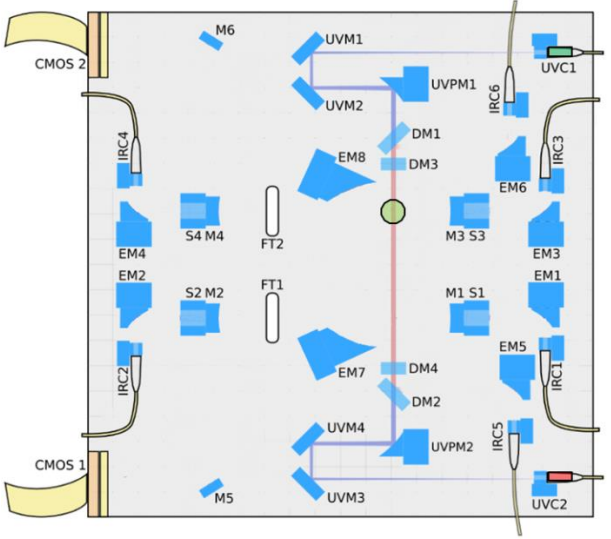
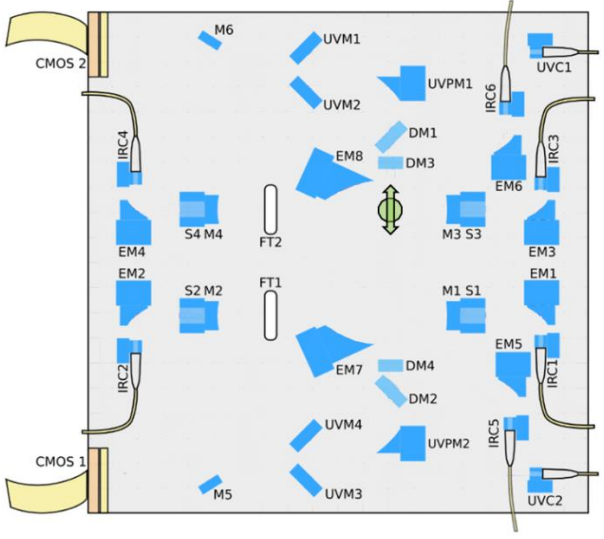
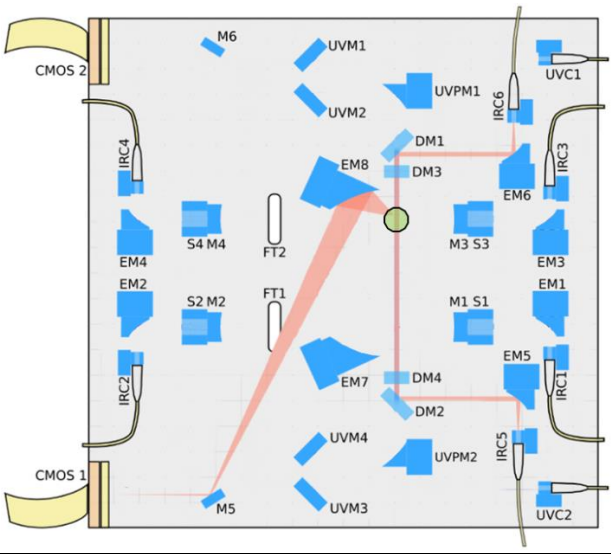
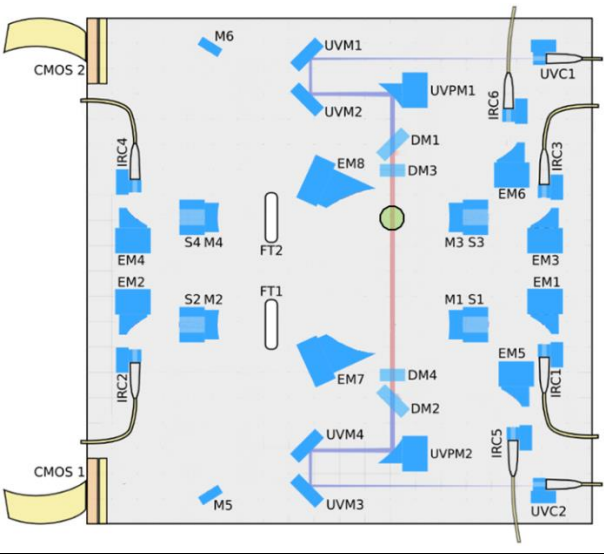


Figure 6-3: Test Particle Transportation Sequence

After the particle arrives into the Paul Trapp, the particle is also trapped due to the IR lasers on the test bench.

6.3.1.2 Payload Sequence

Step 1: Initial State Preparation 1	Step 2: Initial State Preparation 2
	
<p>Particle loaded on bench via particle handling (Paul Trap)</p> <p>Particle negatively charged</p> <p>Eventual use of CMOS detector to verify position of particle</p> <p>Assumption for preparation time: 60s</p>	<p>Discharging of particle via UV light</p> <p>Final particle charge neutral within [TBD] accuracy</p> <p>Eventual use of CMOS detector to verify position of particle</p>
Step 3: Cooling	Step 4: Free Fall 1
	
<p>Particle in optical trap</p> <p>Motion is cooled down</p> <p>Duration 0.1 s</p>	<p>Wait for particle to evolve</p> <p>Duration t1 depending on particle size</p> <p>Assumption 20 s (half of 40 s)</p>

<p>IRC3 on IRC4 off (collecting light from high finesse cavity)</p>	
<p>Step 5: Grating</p>	<p>Step 6: Free Fall 2</p>
	
<p>Phase grating of the particle with UV light Duration 10 microseconds UVC1 on UVC2 off (sensor)</p>	<p>Wait for particle to evolve Duration t2 (smaller or equal to t1) Assumed 20 s (half of 40s)</p>
<p>Step 7: Measurement</p>	<p>Step 8: Particle Disposal</p>
	
<p>Observation of position of the particle along the grating axis IRC6 on for 1 microsecond</p>	<p>Positive charging of particle with UV light and disposal to one of the walls Duration TBD (part of experiment)</p>

IRC5 off (sensor)	preparation duration)
CMOS 1 on for integration time 1 s	UVC1 on
	UVC2 off (sensor)

6.3.1.3 Science Phase

Provided in Figure 6-4 is an overview of the nominal cycle that occurs for each particle batch which consists of 12,500 test particles.

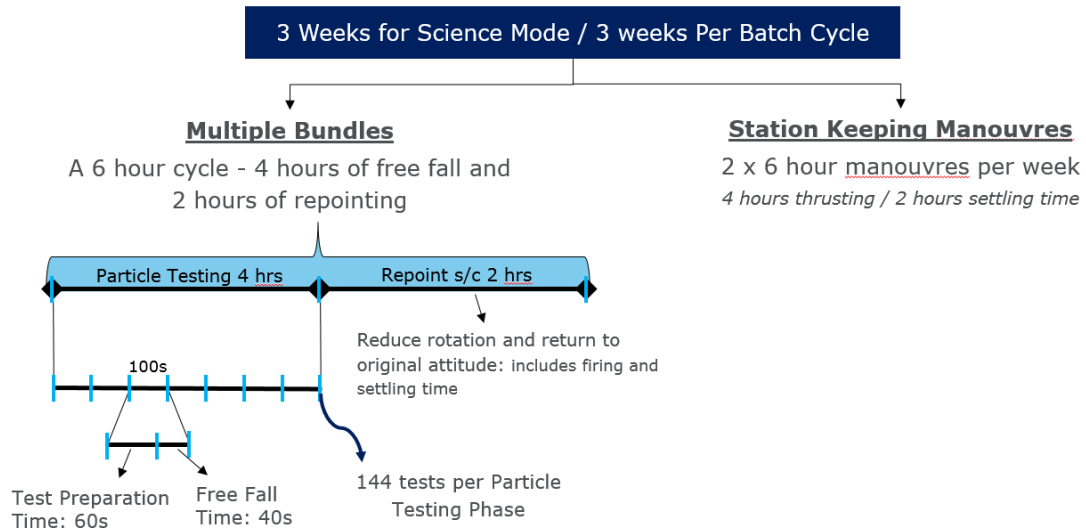


Figure 6-4 Nominal Science Phase Overview

With the above science sequence, a timeline was derived for nominal science duration. Note that the CDF study team assumed three years of science operations, and 15 batches with a limit on the free fall duration of 40 seconds. Therefore, the total time for required for science is 1.3 years. It is expected that the science community would optimise the number of batches / test particles for the three year period outside of the CDF, but some considerations for a total science operations phase of 3 years are highlighted below the table.

	Batches	Comment
Particle Size	1e8amu - 2e9amu	
Number of Test Particles	12500	based on 80% Pr < 2 collisions, requirement for 10,000 valid tests
Free Fall Duration [s]	40	
Particle Preparation [s]	60	A detailed understanding of the functions / duration is required
Bundle Free Fall Duration [s]	14400	4 hours of testing / free fall time
Test Particles per Bundle	144	
Bundles per Batch	87	
Repositioning Time per Bundle [s]	7200	2 hours to reposit
Total Test Time per Batch [days]	22	
Station Keeping Manoeuvres [days]	1.5	2 x 6 hour manoeuvres per week
Time Inbetween Batches [days]	7	Could reduce depending on time required to downlink data
Number of Test Batches	15	To be optimised by scientists
Days	453	
Months	15	
Total Time [Years]	1.26	

Table 6-4: Science Operations Time

With current assumptions for Science Timeline and mission duration of 3 years, there are approximately 1.7 years available for additional science. In order to increase the science output for this timeframe, the system could be designed to:

- Double the number of batches (different materials / temperature ranges)
- Increase the number of particles per batch – 15 batches with ≈ 30000 tests.

However, it is necessary to derive a more detailed understanding of the test preparation time, as this may increase / decrease and will have significant impact on the above timeline.

6.3.2 System Modes

Launch Mode

- Life off to separation, all equipment off except essential ones (OBC and PCDU).

Transfer Mode

- Perform detumbling and sun acquisition
- Service module equipment ON (exception: MGA)
- Gyro ON
- Payload Mode: Standby Mode (Active Cooling).

Commissioning Mode

- Commissioning remaining Service module equipment (e.g. MGA)
- Communication via LGA
- Gyro Standby

- Payload Mode: Standby Mode (Active Cooling).

Science Mode

- Service module equipment ON
- Communication via LGA
- Payload Mode: Science Mode Cycle (Test Preparation Mode, Free Fall Mode, Observation Mode).

Communications Mode

- Service module equipment ON
- MGA ON
- Payload Mode: Standby Mode (Active Cooling).

Safe Mode

- Startracker OFF
- Gyro ON
- TM OFF
- Payload Mode: Off.

Payload Safe Mode

- Service module equipment ON
- Communication via LGAPayload Mode: Standby Mode (Active Cooling).

6.3.3 Payload Modes

Off

- All items on payload bench are OFF
- Active Cooling OFF.

Test Preparation Mode

- Active Cooling ON
- Previous particle disposal
- Test bench sensors are ON (e.g. thermal)
- Particle released mechanism ON
- Particle Transportation Device is ON
- Paul Trapp ON
- Particle is discharged
- IR lasers ON
- Test bench maintained within 5mK, environment sensors ON.

Free-Fall Mode

- Active Cooling ON
- Test bench maintained at 20K within 5mK, environment sensors ON
- UV Grating firing.

Observation Mode

- Active Cooling ON
- CMOS Detector + interferometer ON
- Test bench maintained within 5mK, environment sensors ON.

Stand-by mode

- Active Cooling ON.

6.4 System Baseline Design

QPPF – Mission description	
Launch Vehicle	Ariane 6.2
Launch date	2034 (earliest, with proper technology development programme)
Lifetime	Transfer: 0.5 years Commissioning: during Transfer Science phase: 3 years Science extension: 2 years Total nominal lifetime: 3.5 years Total extended lifetime: 5.5 years
S/C orientation	Payload side anti-Sun pointing
Maximal de-pointing angle	10 degree
Transfer Scenario	Single launch for the S/C into the escape trajectory Chemical Propulsion for transfer insertion manoeuvre (cold gas nitrogen)
Orbit	L2 orbit, with station keeping Distance to Earth: 1.8 million km
Delta-V	140 m/s with margins

Table 6-5: QPPF mission characteristics

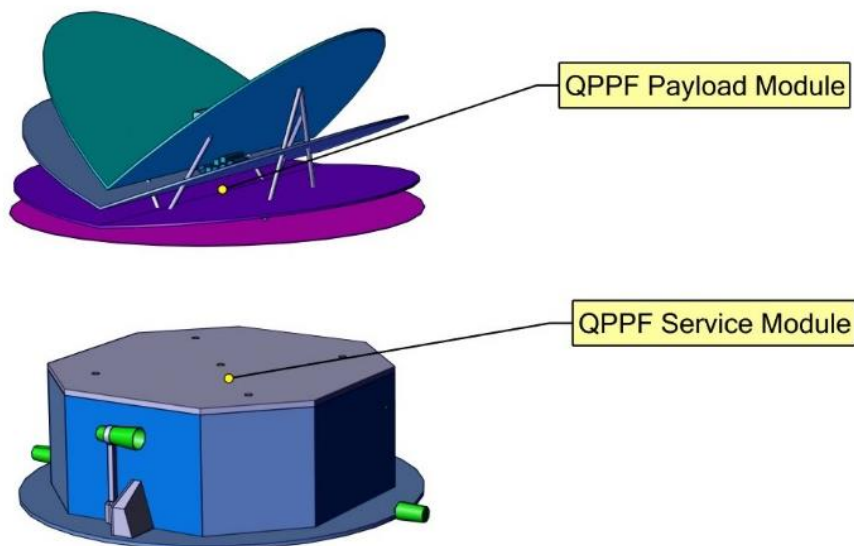
QPPF - System Characteristics	
Mass (incl. 30 % system margin on dry mass)	Payload Module dry mass: 208.2 kg Service Module dry mass: 1144.4 kg Propellant mass: 241.9 kg Spacecraft: <ul style="list-style-type: none"> - Dry mass: 1352.6 kg - Wet mass: 1594.5 kg Total launch mass incl. adapter: 1684.5 kg
Payload	Test bench on cryogenic part (20K) Particle Loading unit CMOS sensor
Configuration	

Table 6-6: QPPF system characteristics

QPPF – Payload Module Characteristics	
Mass (incl. 30 % system margin on dry mass)	Payload Module dry mass: 208.2 kg including 30% payload mass margin on the instrument and particle transportation and storage equipment
Test bench	Optical bench on cryogenic part (20K) Particle Loading unit CMOS sensor
Data Handling	Control of the sensors and actuators of the Optical bench Control of the Particle handling equipment

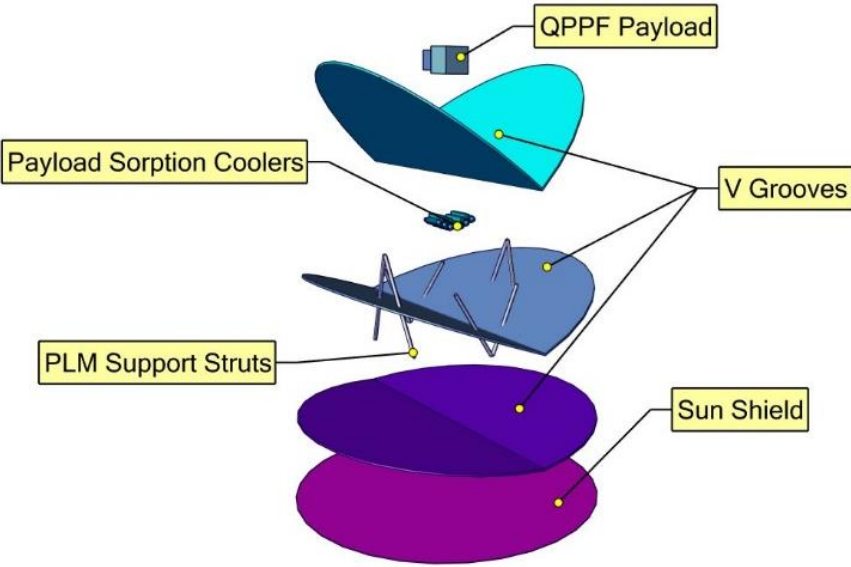
QPPF – Payload Module Characteristics	
Thermal Control	Passive cooling with V-grooves down to 50K Active cooling with H ₂ sorption coolers down to 20K
Mechanisms	Opening valve on the side of the closed cover for venting
Configuration	 <p>The diagram illustrates the configuration of the QPPF Payload Module. It shows a central blue cylindrical module (QPPF Payload) mounted on a purple cylindrical base (Sun Shield). The module is supported by PLM Support Struts. A blue rectangular panel (Payload Sorption Coolers) is attached to the side of the module. V Grooves are indicated on the side of the module. A yellow box labeled 'QPPF Payload' points to the central module. A yellow box labeled 'Payload Sorption Coolers' points to the blue panel. A yellow box labeled 'PLM Support Struts' points to the support structure. A yellow box labeled 'V Grooves' points to the side of the module. A yellow box labeled 'Sun Shield' points to the purple base.</p>

Table 6-7: Payload Module characteristics

QPPF - Service Module Characteristics	
Mass (incl. 30 % system margin on dry mass)	Service Module dry mass: 1144.4 kg Propellant mass: 241.9 kg
Data Handling	2 Tb of data storage
Power	3.4 m ² area body-fixed solar panel with 30% efficiency cells
Propulsion	One cold-gas (nitrogen) propulsion system <ul style="list-style-type: none"> • High thrust with four small tanks for initial orbit insertion. • Micro Newton thrusters for station keeping, repointing and disposal on main central tank
AOGNC	Two cold redundant Miniature Inertial Measurement Unit Two cold redundant Star Trackers
Communication	One Medium Gain Antenna for large data dump between batches Two (optionally three) Low Gain Antenna for daily housekeeping data X-band transponder
Thermal Control	244W of heaters in service module for safe mode (minimal equipment temperature. -30C)

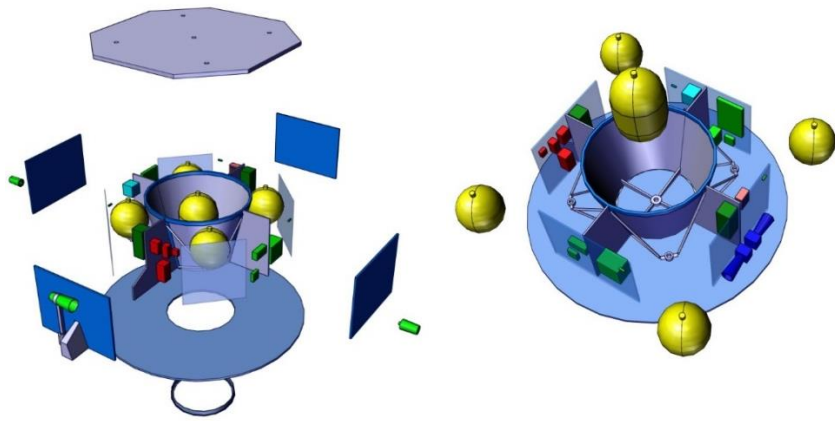
QPPF - Service Module Characteristics	
Mechanisms	Medium Gain Antenna pointing and stowing mechanism
Structures	Sun shield and intermediate shield sandwich panels with aluminium honeycomb core and CFRP facesheet
Configuration	

Table 6-8: QPPF service module characteristics

6.4.1 Enclosed Test Bench

The need for enclosing the test bench comes from the paramount need to shield the experiment from any perturbations and to have a precise control on its environment. More precisely, two kinds of requirements can be distinguished:

External constraints: The design shall shield the experiment from external perturbations coming from solar radiations, cosmic rays background, the interstellar plasma or any outgassing from external elements.

Internal constraints: The design shall have a well-controlled management of the pressure and temperature surrounding the experiment. Indeed, one requirement is to achieve a pressure of about 10^{-11} Pa (using sorption, cryo-condensation and cryo-trapping).

To achieve those requirements, the current baseline for the design of the closed cover is the following:

- The cover is a box of (30x30x30) cm³ ($V=2.7 \cdot 10^{-2}$ m³), of mass $M=12$ kg. It must be recovered with a layer of aluminum, for this study the thickness was assumed as $t=1$ mm. This allows the shielding from external elements apart from cosmic rays. The inside must be recovered with a layer of non-evaporable getter for the need of the experiment (capture escaping test particles). With an increase in thickness, the risk of secondary particles from GCRs increases.
- A side of the cover must be equipped with an active opening mechanism of about an area of $A= 5 \text{ cm}^2 / 10 \text{ cm}^2$, but **this will need to be accurately sized through further analysis**. This is a necessary part for the management of pressure and venting during the mission.

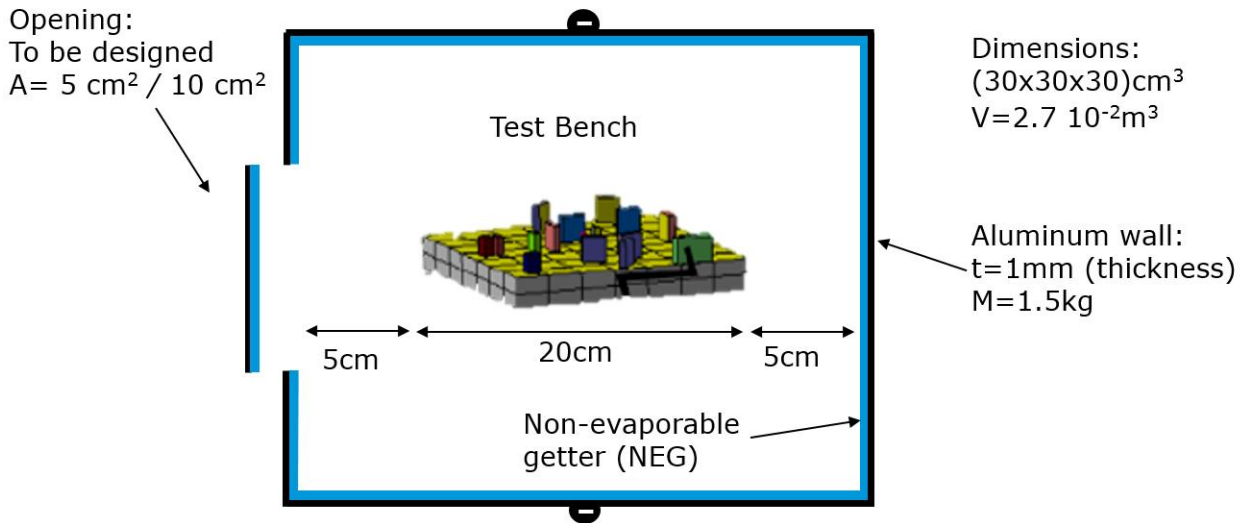


Figure 6-5: Enclosed Test Bench Design

The closed cover must include only the test bench where the experiments are performed. All detection devices, transportation or storage devices must be outside the cover. The main reason is again to minimise any potential perturbations of the experiments by those apparatuses.

The opening valve is used to achieve the very low-pressure requirements, particularly to support the venting when the gas is in a free molecular flow regime. The cover, which is pre-vacuum and fully closed during take-off, must be widely opening during the venting and active cooling phase before beginning the science phase.

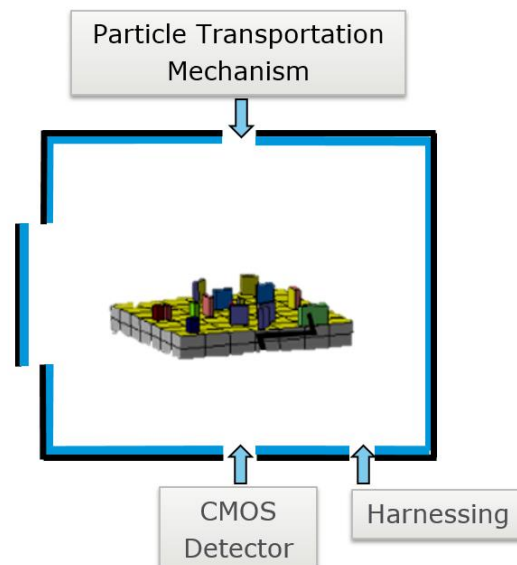


Figure 6-6: Enclosed Test Bench Interfaces

Different options for the design can still be considered, depending in the evolution of other parts of the payload. Indeed, it could be possible to include external elements inside the cover. The main trade-off here to consider is the advantage of including the

element inside the cover (less interfaces for temperature and pressure management, size) versus how it can affect and perturb the experiment (decoherence). This can only be decided by a good understanding of the physical properties of the element (electric/magnetic fields, thermal properties) and how they may induce decoherence of the experimental system.

Another design constraint is to place the detectors outside of the cover design, this may require a section of the wall to be transparent so the light can pass through.

The main technological development to be addressed is on the design of the opening mechanism. Apart from the qualitative fact that it must be a wide opening, its actual size must be justified on quantitative grounds. Moreover, the kind of opening is still an open question (door like, valve, mechanical constraints, temperature and pressure constraints).

6.4.2 Budgets

6.4.2.1 Mass budget

A margin of 30% was taken on the payload and system margin on request from the customer.

In Table 6-9, the mass budget of the Payload Module is decomposed. The instruments comprise the optical bench, where the experiment will take place, the detector and laser units, as well as their control electronics. The Particle Transportation is the Particle Handling Unit, as presented in RD[4], without the harness, which is taken into account at the payload module level.

PLM Mass Budget		Mass [kg]
Instruments		49.02
Particle transportation		36.40
Dry Mass w/o Payload Margin		85.42
Payload Margin	30%	25.63
Thermal Control		10.04
Particle transportation Data Handling		12.53
System Engineering		12.00
Harness	10%	14.56
Dry Mass w/ Payload Margin		160.18

Table 6-9: Payload Module mass budget

The mass breakdown of the Service Module is shown in Table 6-10. The mass of the Vgrooves is accounted for in the Thermal Control domain.

SM Mass Budget		Mass [kg]
Attitude, Orbit, Guidance, Navigation Control		26.24
Communications		35.04

Chemical Propulsion	208.58
Data-Handling	11.99
Power	39.25
Structures	342.18
System Engineering	20.00
Thermal Control	155.14
Harness	5% 41.92
Dry Mass w/o System Margin	880.34

Table 6-10: Service Module mass budget

The total wet and dry masses of the spacecraft are shown in Table 6-11. The launch adapter considered is the Ariane 6 PAF1194C, which has an interface diameter of 1194 mm.

S/C Mass Budget	Mass [kg]
Dry Mass PLM	160.18
Dry Mass SM	880.34
System Margin 30%	312.16
Dry Mass incl. System Margin	1352.68
Cold gas mass TCM	159.13
Cold gas mass SK and SCI	44.46
Cold gas mass DECOM	21.31
Total Wet Mass	1577.58
Launcher Adapter	90.00
Wet Mass + Adapter	1667.58

Table 6-11: QPPF spacecraft mass budget

	Unit Mass (kg)	Mass margin (%)	Unit Mass incl. margin (kg)	Units	Total Mass
PLM (Payload Module)	94.88	26.47			119.99
DH	10.77	16.31			12.53
Backplane_cPCI	0.20	20	0.24	1	0.24
Box	2.70	10	2.97	1	2.97
Instrument_data_processing_board	0.80	20	0.96	2	1.92
Particle_guiding_electr_board	0.50	20	0.60	2	1.20
Particle_release_electr_board	0.50	20	0.60	2	1.20
Paul_trap_electr_board	0.80	20	0.96	2	1.92
Payload_data_handling_board	0.64	10	0.70	2	1.40
Power_board	0.70	20	0.84	2	1.68
INS	37.71	30			49.02
Det_CMOS (Detectors CMOS)	1.90	30	2.47	1	2.47
Det_EB (Detection Electronics)	3.21	30	4.17	1	4.17
Las_EB (Laser Electronics)	1.20	30	1.56	1	1.56
Las_U (Laser unit)	7.40	30	9.62	1	9.62
Mod_Gen_EB (Mode Generation	4.80	30	6.24	1	6.24

	Unit Mass (kg)	Mass margin (%)	Unit Mass incl. margin (kg)	Units	Total Mass
Electronics)					
Mod_Gen_U (Mode-Generation Unit)	15.20	30	19.76	1	19.76
OB_struct (Optical Bench Structure)	4.00	30	5.20	1	5.20
OPT	28.00	30			36.40
PHU (Particle Handling Unit)	28.00	30	36.40	1	36.40
SYE	10.00	20			12.00
OB_Cover (Optical Bench Closed Cover)	10.00	20	12.00	1	12.00
TC	8.40	19.52			10.04
CDE_SORPH2 (Drive_Electronics_SorptionH2)	2.00	20	2.40	1	2.40
Cernox (CryogenicTemperatureSensors)	0.00	0	0.00	20	0.00
CryoHT (CryogenicHeaters)	0.02	10	0.02	20	0.44
SORP_H2 (Sorption_H2_cryocooler)	6.00	20	7.20	1	7.20
SM (Service Module)	724.73	15.69			838.42
AOGNC	24.99	5			26.24
DSS (Digital Sun Sensor)	0.33	5	0.35	3	1.04
MIMU (Honeywell Miniature Inertial Measurement Unit)	6.00	5	6.30	2	12.60
STR (Star Tracker)	6.00	5	6.30	2	12.60
COM	31.00	13.03			35.04
DIP (Diplexer)	0.40	10	0.44	2	0.88
HPA_TWTA (High Power Amplifier (TWTA))	2.30	5	2.42	2	4.83
LGA (Low Gain Antenna)	1.00	10	1.10	2	2.20
MGA (Medium Gain Antenna)	2.00	10	2.20	1	2.20
MGAPM (Medium Gain Antenna Pointing Mechanism)	10.00	20	12.00	1	12.00
RFDN (Radio Frequency Distribution Network)	5.00	20	6.00	1	6.00
XPND (Transponder)	3.30	5	3.47	2	6.93
CPROP	188.60	10.59			208.58
Cold_HP_Filter (Coldgas_HP_Filter)	0.11	5	0.12	1	0.12
Cold_HP_FVV (Coldgas_HP_FillVent_Valve)	0.25	5	0.26	1	0.26
Cold_HP_T (Coldgas_High_Pressure_Transducer)	0.23	5	0.24	2	0.48
Cold_HPLV (Coldgas_Latch_Valve_HP)	0.40	5	0.42	4	1.68
Cold_LP_Filter (Coldgas_LP_Filter)	0.18	5	0.19	4	0.76
Cold_LP_FVV (Coldgas_LP_FillVent_Valve)	0.25	5	0.26	4	1.05
Cold_LP_T (Coldgas_Low_Pressure_Transducer)	0.23	5	0.24	4	0.97
Cold_LPLV (Coldgas_Latch_Valve_LP)	0.34	5	0.36	2	0.71
Cold_Pipes (Coldgas_Pipes)	15.00	20	18.00	1	18.00
Cold_PR (Coldgas_Pressure_Regulator)	1.13	5	1.19	4	4.75
HT_CGT (HighThrust_Coldgas_Thruster)	0.12	5	0.12	16	1.93
LT_CGT (LowThrust_Coldgas_Thruster)	0.40	5	0.42	16	6.72
NO_PV (NO_Pyro_Valve)	0.16	20	0.19	2	0.37
Prop_Tank (Central_Propellant Tank)	55.00	20	66.00	1	66.00
TCM_Prop_Tank (TCM Propellant Tank)	24.95	5	26.19	4	104.78
DH	10.90	10			11.99
SMU_RUAG_next (Spacecraft Management Unit)	10.90	10	11.99	1	11.99
PWR	32.85	13.84			39.25
BAT (Battery_Module)	3.02	20	3.63	1	3.63
PCDU	14.17	5	14.88	1	14.88

	Unit Mass (kg)	Mass margin (%)	Unit Mass incl. margin (kg)	Units	Total Mass
(Power_Conditioning_Distribution_Unit)					
SA (Solar_Array_Module)	17.29	20	20.75	1	20.75
STR	285.15	20			342.18
Int_Shield (Intermediate Shield)	35.42	20	42.50	1	42.50
SM_STR (Service Module Structure)	197.89	20	237.47	1	237.47
Sun_Shield (Sun Shield)	51.84	20	62.21	1	62.21
SYE	20.00	0			20.00
Bal_mass (Balancing Mass)	20.00	0	20.00	1	20.00
TC	129.61	19.70			155.14
HT (Heaters)	0.05	5	0.05	40	2.10
RAD (Radiator)	16.00	20	19.20	1	19.20
Therms (Thermistors)	0.01	5	0.01	60	0.63
VG (VGrooves)	111.01	20	133.21	1	133.21

Table 6-12: QPPF equipment list

6.4.2.2 Delta-v budget

Delta-v Budget	Manoeuvre type	L2	Unit
Transfer Correction Manoeuvre 1 Part 1	stochastic	32.8	m/s
Transfer Correction Manoeuvre 1 Part 2	deterministic	13.8	m/s
Transfer Correction Manoeuvre 2	stochastic	1.7	m/s
Transfer Correction Manoeuvre 3	stochastic	0.7	m/s
Transfer Correction Manoeuvre delay allocation	deterministic	13.4	m/s
Margin on stochastic delta-v		0	%
Margin on deterministic delta-v		10	m/s
Total det. and stoch. Manoeuvres including margin		72.4	m/s
Objective lifetime		3.5	yrs
Orbit maintenance delta-v per year		3.2	m/s/yr
Orbit maintenance delta-v (stochastic)		11.2	m/s
Margin on orbit maintenance delta-v		0	%
Total orbit maintenance delta-v		11.2	m/s
AOCS delta-v		12.5	m/s
Margin on AOCS delta-v		0	%
Total AOCS delta-v		12.5	m/s
Disposal manoeuvre	deterministic	10	m/s
Margin on disposal manoeuvre		0	%
Total disposal manoeuvre		10	m/s
Total delta-v without margin		96.1	m/s
Total delta-v including margin		106.1	m/s
Extended lifetime		2	yrs
Orbit maintenance for extension		6.4	m/s
AOCS delta-v for extension with margin		7.1	m/s

Total extension delta-v	13.5	m/s
Total delta-v after extension without margin	109.6	
Total delta-v after extension including margin	119.6	m/s
Achievable lifetime	2.2	yr
Orbit maintenance	7.0	m/s
AOCS	7.9	m/s
Total achievable delta-v science phase	14.9	m/s
Total achievable delta-v without margin	87.3	m/s
Total achievable delta-v including margin	97.3	m/s

Table 6-13: QPPF Delta-v budget

6.4.2.3 Data budget

The raw data budget has been created with the assumption that the total test duration would be 100s (40s free fall and 60s test preparation). As the main driver in the data generation are the CMOS images taken twice per test, the variation of the test duration can have a significant impact on the datarate.

Measurement	Bit per channel	Channel count	Number of values per test (100s)	Effective sample rate [Hz]	Bit rate [bps]	Ratio over payload generation on bit rate	Comment
CMOS images	1.20E+07	1	2	0.02	240000	99.95%	CMOS images - assume 2 images, 12Mb each for each data point (1 Mega pixel, 12 bits per pixel) - one datapoint every 100s -> 0.12Mb/s
representative noise values for particle peaks over time	12	1	400	4	48	0.02%	Mechanical frequencies of the particle - 20 values for each peak -> 40 in total per measurement time for 10 times, 400 values in total
charge over time	12	2	120	1.2	28.8	0.01%	4 Hz during half of test preparation (charge over time tags)
power slope for cavity switching	12	1	120	1.2	14.4	0.01%	4 Hz during half of test preparation
representative noise values for mode peaks	12	1	80	0.8	9.6	<0.01%	20 values for each peak -> 80 in total
representative noise values for particle peaks	12	1	40	0.4	4.8	<0.01%	20 values for each peak -> 40 in total
power noise level at several frequencies	12	1	10	0.1	1.2	<0.01%	About 10 values
cavity linewidth	12	1	8	0.08	0.96	<0.01%	
height, width and area for particle peaks (blue and red detuned) -> 6 values	12	1	6	0.06	0.72	<0.01%	
powers reflected and transmitted for all four modes	12	1	3	0.03	0.36	<0.01%	
mode frequencies for cooling modes (TEM00, TEM01 and TEM10)	12	1	3	0.03	0.36	<0.01%	
height and width of	12	1	3	0.03	0.36	<0.01%	

peaks for the various frequencies (two TEM00 modes, TEM01 and TEM10 modes)							
AOM voltages (2 times, or TEM01 and TEM10 modes)	12	1	2	0.02	0.24	<0.01%	
laser temperature	12	1	1	0.01	0.12	<0.01%	
laser frequency	12	1	1	0.01	0.12	<0.01%	
PZT mean volage value	12	1	1	0.01	0.12	<0.01%	
EOM voltage	12	1	1	0.01	0.12	<0.01%	
transfer momentum	12	1	1	0.01	0.12	<0.01%	
transfer start time tag	12	1	1	0.01	0.12	<0.01%	
expected transfer end time tag	12	1	1	0.01	0.12	<0.01%	
cavity input power	12	1	1	0.01	0.12	<0.01%	
mass	12	1	1	0.01	0.12	<0.01%	
charge	12	1	1	0.01	0.12	<0.01%	
polarizability	12	1	1	0.01	0.12	<0.01%	
mass density	12	1	1	0.01	0.12	<0.01%	
radius	12	1	1	0.01	0.12	<0.01%	
start time tag	12	1	1	0.01	0.12	<0.01%	
velocity	12	1	1	0.01	0.12	<0.01%	
arrival time tag	12	1	1	0.01	0.12	<0.01%	
boolean - discharge successful	1	1	1	0.01	0.01	<0.01%	
boolean - loading initialization successful	1	1	1	0.01	0.01	<0.01%	
boolean: particle acceptable	1	1	1	0.01	0.01	<0.01%	
boolean - transport successful	1	1	1	0.01	0.01	<0.01%	
boolean - trapping successful	1	1	1	0.01	0.01	<0.01%	
					246'111.8	bps	

Table 6-14: QPPF payload raw data generation rate

Measurement	Raw Datarate [bps]	Duty cycle	Effective datarate [bps]	Effective datarate [kbps]
Payload data	246111.8	66.67%	160074.5	160.1
Spacecraft Housekeeping data	6000	100%	6000	6
			166074.5	166.1

Table 6-15: QPPF total raw data generation rate

Science mode total raw data	
166.1	kbps
14348.8	Mb/day
14.3	Gb/day
22	days/ batch
304.3	Gb/ batch
Including housekeeping	

6000 bps
518.4 Mb/day
0.5 Gb/day

Table 6-16: QPPF data generation in science mode

6.4.2.4 Power budget

	LM	TM	SM	SAFE	PSM	COMMIS	COM
Service Module without heaters	57	151	167	135	167	172	256
Payload Module	0	60	188	0	60	60	60
Heaters	0	178	163	194	163	158	0
Losses and PCDU	1	47	54	40	47	46	39
Total without margin	57	436	571	369	436	435	355
Margin 30%	17	131	171	111	131	131	107
Total w/ Margin	74	567	742	480	567	566	462

Table 6-17: QPPF power budget

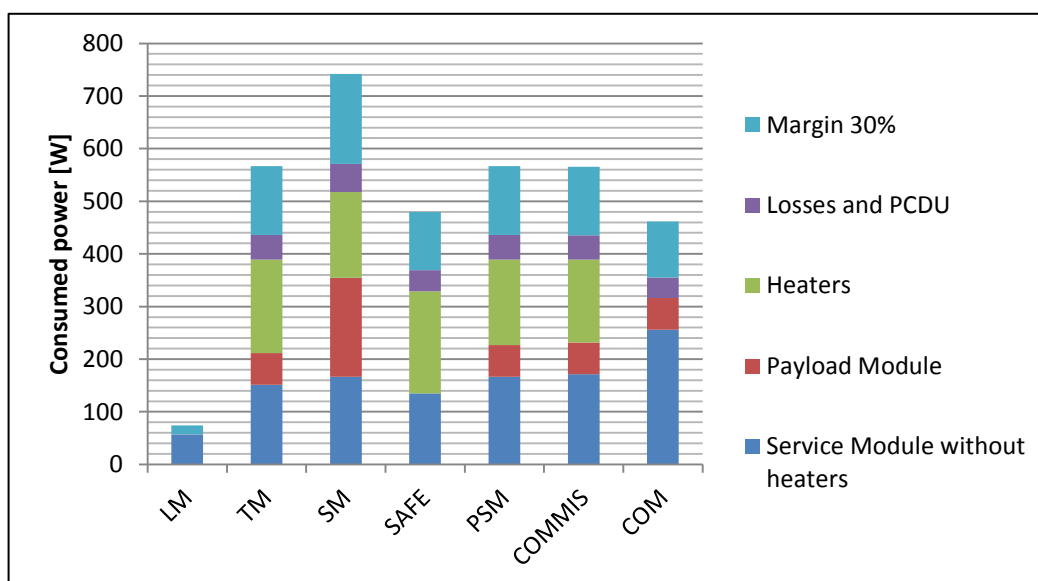


Figure 6-7: QPPF Power Budget

Please note that after the IFP, the power consumptions of the on-board computer has been updated. As it consisted of a decrease of 3.4 W in the “On” state and a decrease of 4W in the standby state, the power budget was not iterated and this was considered as an added margin.

6.4.3 System Options

Mission extension of two years

- Main system design can accommodate extended operations (power, comms, memory)
- Propellant mass scales linearly with time – additional tanks required – new configuration change of self-gravity and CoM position, additional firing of thrusters to be checked
- Degradation on V-Grooves to be assessed
- Payload design:
 - Storage device would need to accommodate additional test particles
 - number of tests would significantly increase
 - Change of requirements for technology developments
 - TBD degradation of particles during storage.

6.5 Open System Points

The following were **not** addressed during the CDF:

- The **disposal** of the particles from the optical bench, it is currently assumed they will stick to the wall and therefore no dedicated equipment is contained for this purpose.
- A system concept to provide **1000 seconds** of free fall.
- **Integration** of the particle storage and transportation device.
- **Test preparation duration** of 60s will need to be verified together with the technology development for the transportation device and optical bench.
- The current assumption of 12,500 test particles required assumes a $P_r > 80\%$ of less than 2 collisions, which means of the 10,000 valid test results, a number of these particles will have 1 collision. **The impact of 1 collision on test particle, and the associated results of the decoherence parameter are unclear and needs to be assessed at scientific level.**

6.6 Mission Options

Earth Trailing / Earth Leading Continuous Drift Orbit

- No station keeping, insertion or orbit correction manoeuvres required, therefore:
 - Reduction in propellant mass and propulsion system complexity
 - From 120 m/s (L2) to approx. 35 m/s (ET/EL),
 - approx. 160kg of propellant
 - reduction in propulsion subsystem mass
 - Reduced operations / increase in time dedicated to science
 - additional 12 hours per week
- Earth / Sun Angle can accommodate the HGA behind the sunshield - no technology development needed.
- Additional power required in order to achieve the required data rate / larger antenna.

- Given that the launch trajectory for an Earth leading/trailing orbit may require the upperstage to thrust perpendicular to the s/c- Sun direction, further investigations are necessary in order to fulfill the requirement that the cold part of the spacecraft should be kept behind the sunshield at all times.
 - A possible solution is to delay the opening of the fairing, at the expense of launcher performances.

This Page Intentionally Blank

7 CONFIGURATION

7.1 Requirements and Design Drivers

The following requirements apply to the configuration of the QPPF spacecraft.

SubSystem Requirements		
Req. ID	Statement	Parent ID
CONF -010	The configuration shall fit within the constraints of the launcher fairing of an Ariane 6.2 launcher.	
CONF -020	The interface to the launcher shall be compatible with a 1194 standard launcher adapter.	
CONF -030	The configuration shall accommodate all Payload and Equipment required for the mission objectives and requirements.	
CONF -040	The configuration shall consist of two main sub-systems, a Service Module and a Payload Module.	
CONF -050	The Configuration shall provide an unobstructed field of view for all instruments and equipment.	
CONF -060	The Configuration shall provide unobstructed position for the thrusters to fulfil the mission requirements without contamination of relevant parts of the spacecraft.	
CONF -070	The Configuration shall take into account constraints and limitations due to AIV requirements.	
CONF -080	The sub-systems distribution over the spacecraft shall result in a tightly controlled Centre of Mass compatible with the science requirements of the mission.	

7.2 Baseline Design

Figure 7-1 shows the configuration of the QPPF spacecraft in an Ariane 6-2 launcher fairing.

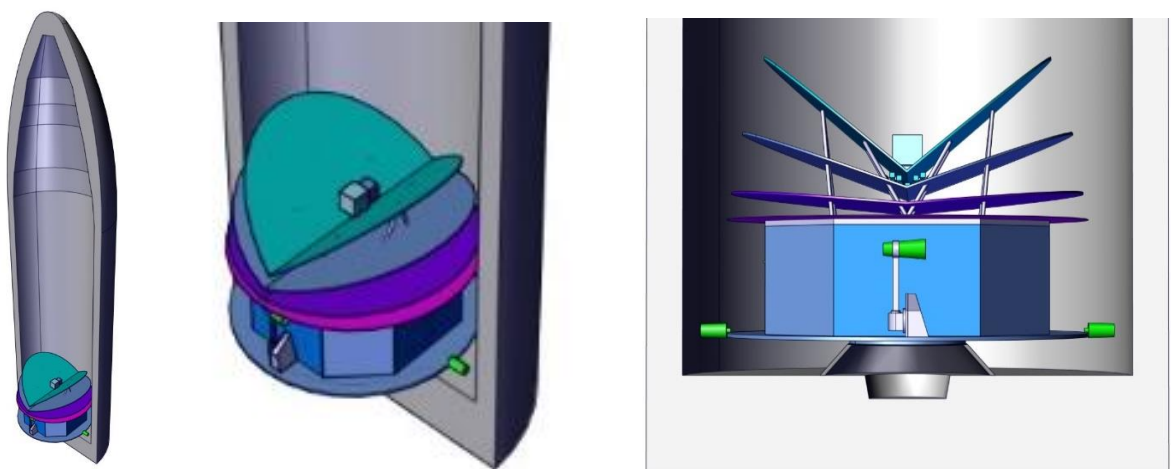


Figure 7-1: QPPF in an Ariane 6-2 launcher fairing

A side view of the spacecraft is shown in Figure 7-2, which clearly shows the V-Groove system that is used for controlling the thermal environment.

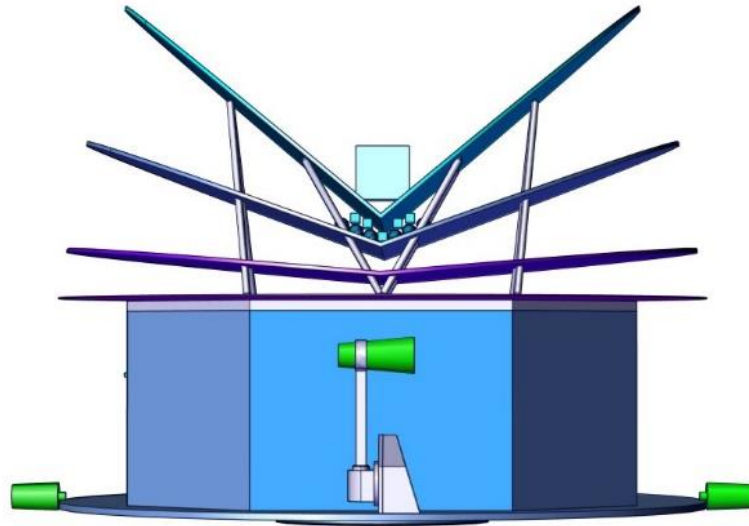


Figure 7-2: QPPF spacecraft in launch configuration

The configuration is designed to be as symmetrical as possible. The only deploying device is the Medium Gain Antenna [MGA]. The MGA will be deployed for communication, but stowed again for science operations. The stowed and deployed configurations are shown in Figure 7-3: .

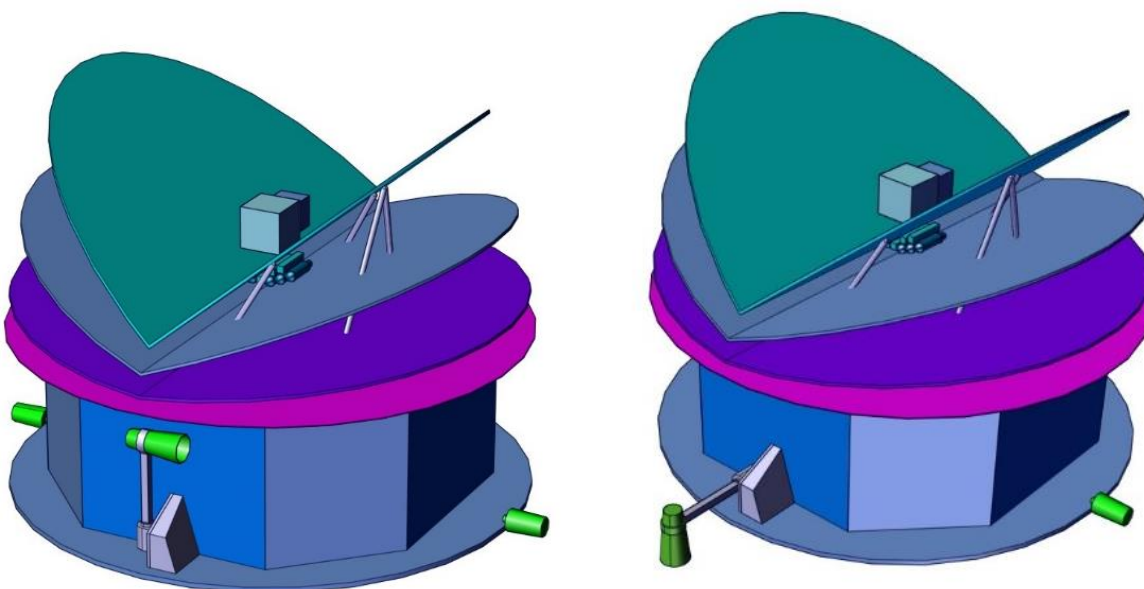


Figure 7-3: QPPF MGA when used for communication

The spacecraft has been divided into two main sub-systems, the Payload Module [PLM] and the Service Module [SVM]. Figure 7-4 shows these two main elements.

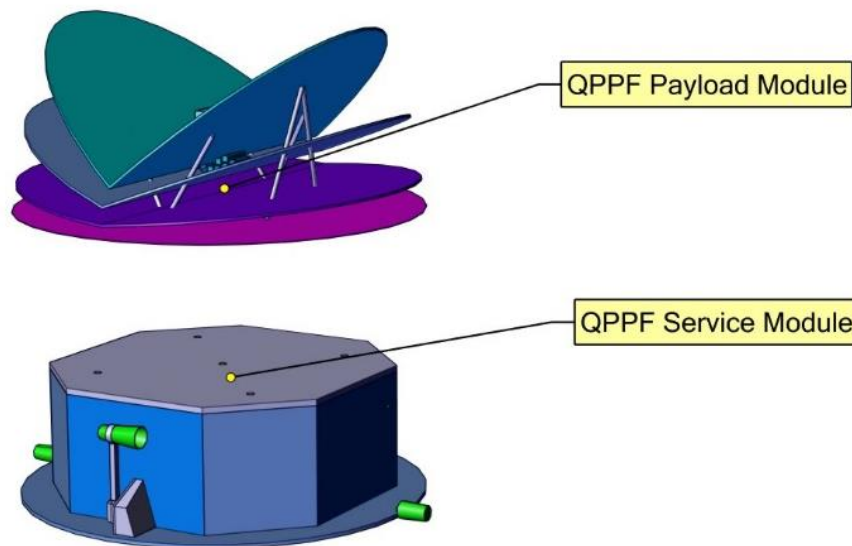


Figure 7-4: The two main elements of the QPPF spacecraft

The PLM contains the Instrument and various other sub-systems in support of the instrument. Clearly visible in Figure 7-5 are the Sun shield and V-Grooves controlling the thermal environment around the instrument, as well as the Sorption Coolers. The design of the interface (struts) are still very preliminary since the Instrument and the interface to the instrument are not clearly defined yet. For the main PLM support struts a quasi-static design is pursued which will also support the Thermal control sub-systems.

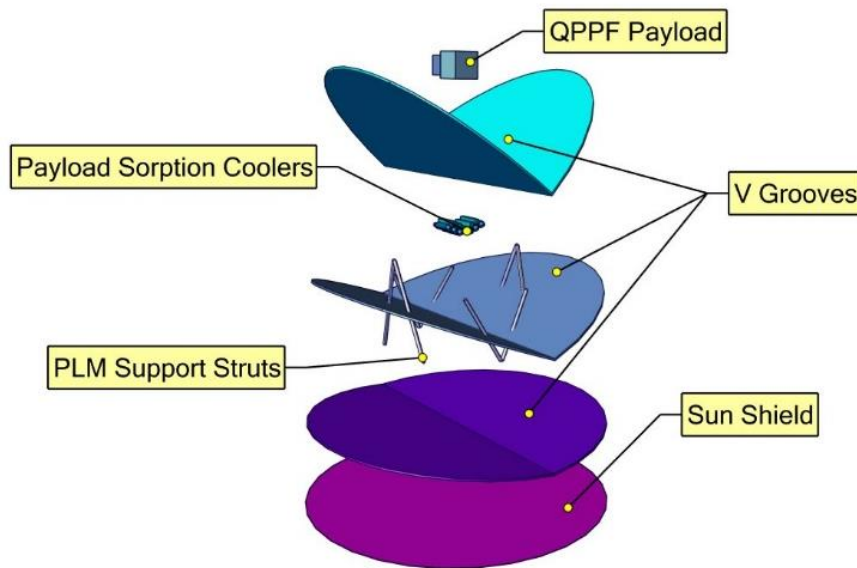


Figure 7-5: SVM in exploded view

The overall detail of the Instrument are still work in progress. An initial design is shown in Figure 7-6, specifically the Instrument Optical Bench and the required Optical Bench Cover. Further details for the interface of the Instrument with the support structure shall be studied and designed in work following the CDF.

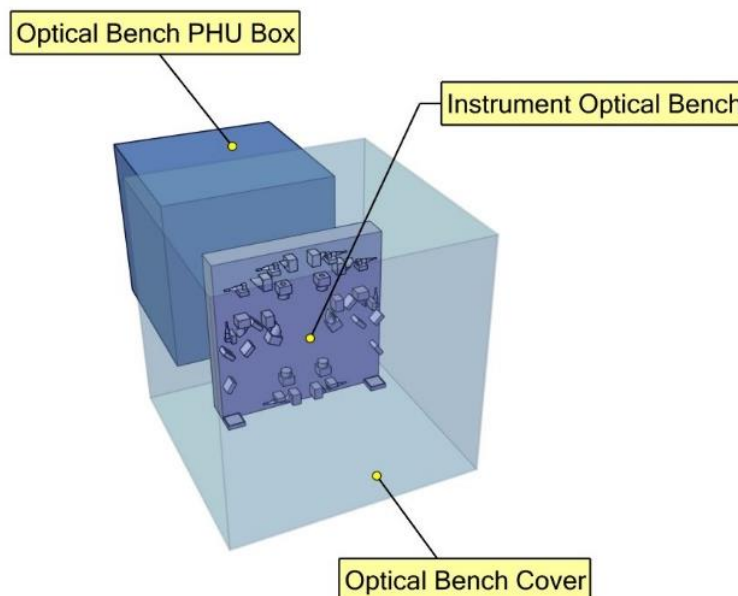


Figure 7-6: Initial Instrument layout with Optical Bench cover

The SVM contains all the relevant sub-systems for the mission such as Propulsion, Data Handling, Communication and Attitude Control. The Structure sub-system is described in the Structures chapter, however Figure 7-7 shows the central cone with shear panels and closer panes for bottom, top and outer locations.

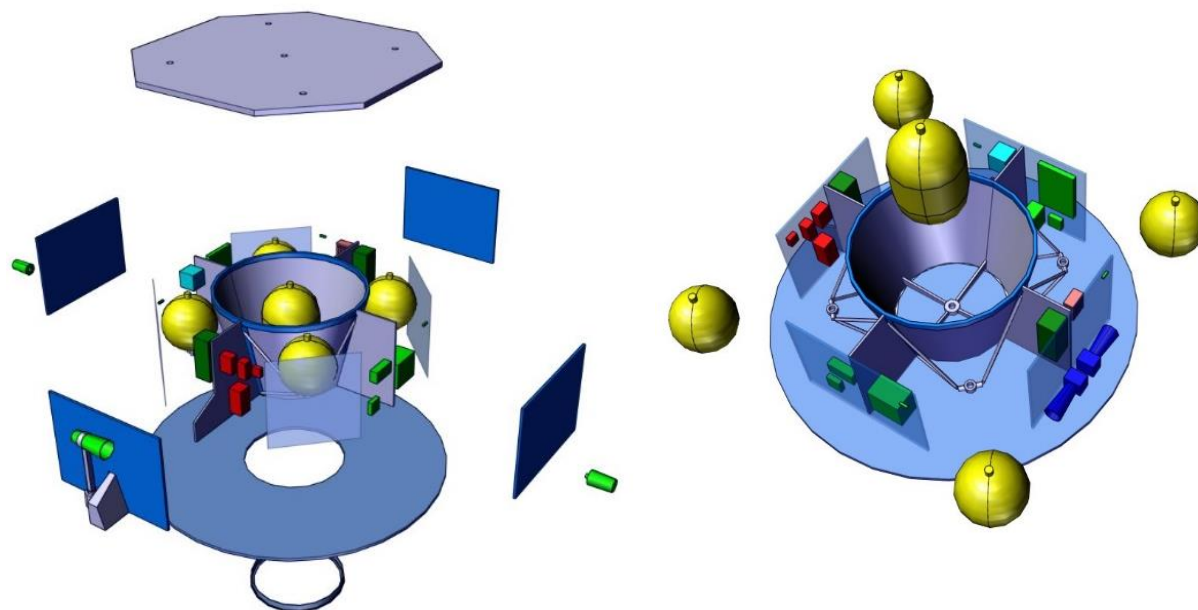


Figure 7-7: SVM in exploded view

7.3 Overall Dimensions

The dimensions of the spacecraft inside the Fairing is shown in Figure 7-8.

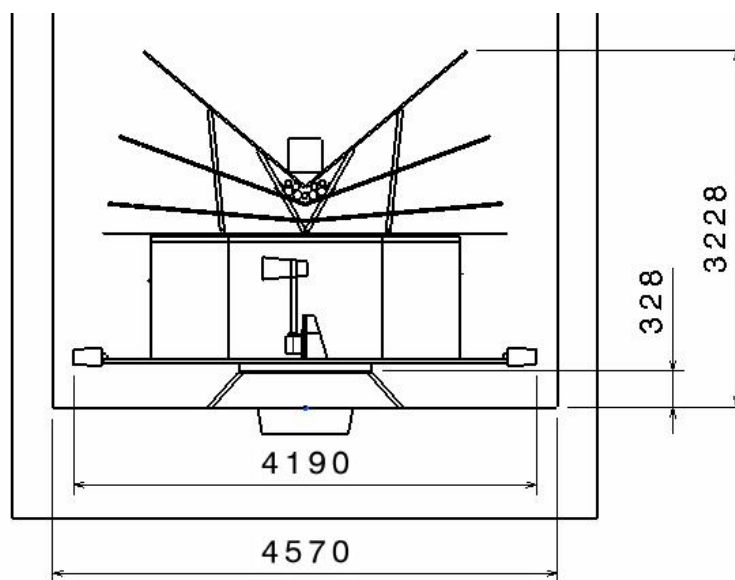


Figure 7-8: Spacecraft inside the fairing

The main dimensions of the spacecraft are shown in Figure 7-9 and Figure 7-10.

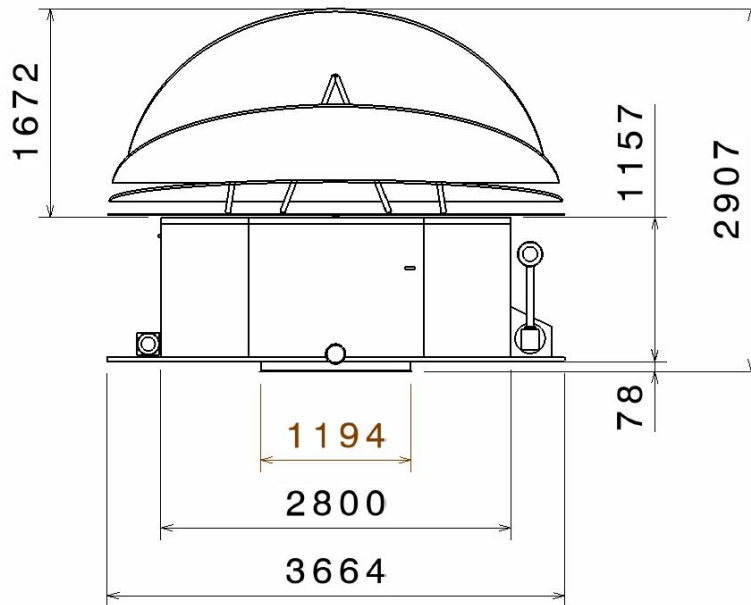


Figure 7-9: Main spacecraft dimensions view 1

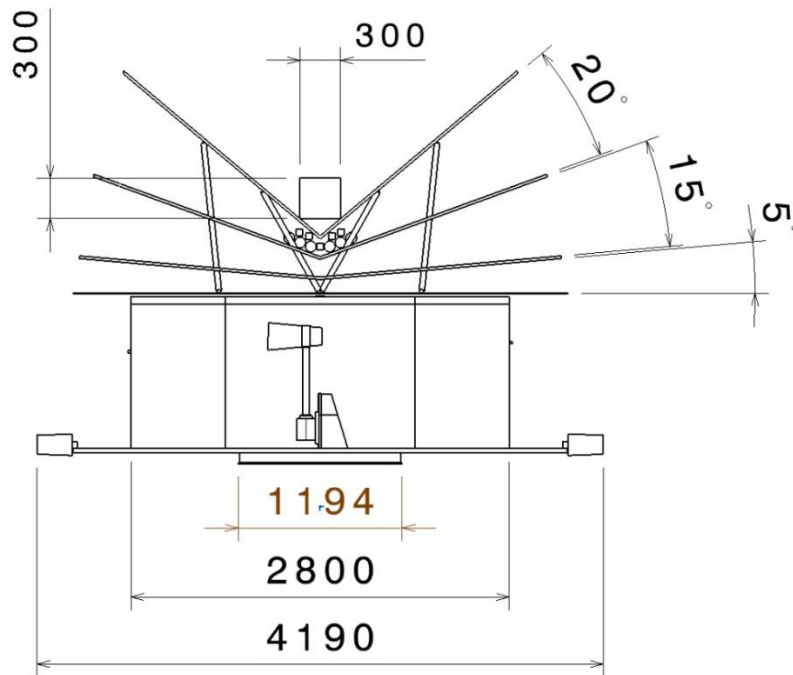


Figure 7-10: Main spacecraft dimensions view 2

8 STRUCTURES

8.1 Requirements and Design Drivers

SubSystem Requirements		
Req. ID	Statement	Parent ID
STR-010	First eigenfrequency at 30 Hz for the grooves	

Requirement STR-010 has been taken from the Planck spacecraft qualification campaign, see RD[7].

8.2 Assumptions and Trade-Offs

8.2.1 Assumptions

Assumptions	
1	“Parts within the optical bench and V-Groove structural materials are compatible with vacuum firing and extensive bake-out procedures, with outgassing values sufficiently low to ensure 10^{-11} Pa, or 10^{-13} mbar” Thermal Chapter, Assumption 1
2	For thermal conductance, the V-groove structure shall be made from aluminium or similarly conductive materials. For the radiation of heat from in between the V-grooves to space:
3	<ul style="list-style-type: none"> • Some surfaces (VG1, VG2) need to be polished • Rib-stiffening of the V-grooves may only be oriented radially • Other deviations from flat panels shall be minimised
4	No limitations on material selection for the Sun shield, Intermediate shield and spacecraft bus are assumed
5	The V-Grooves are assumed to be supported at six positions on a circle of Ø 1660 mm (derived sort of from one of the Ariane PLA sizes)

8.2.2 V-Groove Design Trade-Off

For the mechanical design, the V-grooves of the payload module pose the largest challenge, as several restrictions pertain to them. The V-grooves are three separate panels, folded along one line (or alternatively cone-shaped), see Figure 8-1 below.

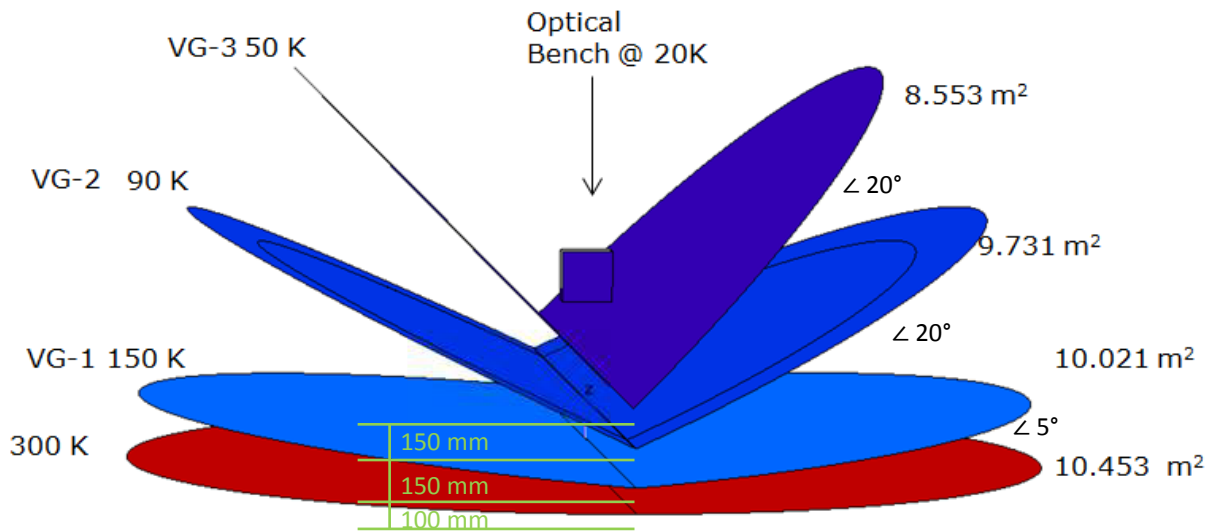


Figure 8-1: V-Groove overall geometry and dimensions

8.2.2.1 Constraints on material selection

Due to the outgassing requirements given in Assumption 1 of the thermal section of this report, organic materials are ruled out, completely eliminating carbon fibre reinforced polymer (CFRP), at least due to their thermoplastic or thermoset (epoxy) matrix materials, maybe even the fibre material itself would not fulfil the outgassing assumption.

Furthermore, this assumption also rules out sandwiches made from aluminium honeycomb cores with aluminium face-sheets, as these are usually bonded together using organic glues.

However, on the other hand, the necessary thermal conduction within the V-Groove rules out all materials with thermal conductivity less than that of aluminium, including e.g. titanium (more on this in section 8.5 below).

8.2.2.2 Constraints on the panel geometry

Due to sandwich structures being ruled out, rib stiffened aluminium panels would be the next natural choice. But there are also limitations pertaining to the orientation of the ribs, which is best illustrated by Figure 8-2 and Figure 8-3 below: In order for the cooling to work as described in section 15.3 of the thermal chapter, the infrared radiation in between the V-groove panels shall not be reflected back to the central part of the V-grooves. But circumferentially oriented ribs on the panels do just that, as exemplified in Figure 8-3. Thus, only strictly radial rib stiffening can be applied.

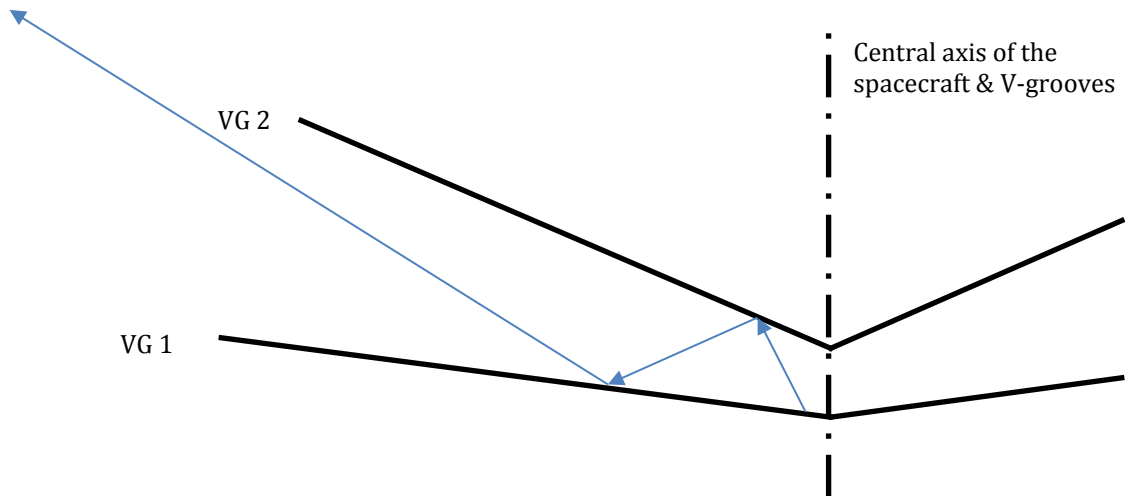


Figure 8-2: Uninhibited reflection of infrared radiation exiting the V-grooves

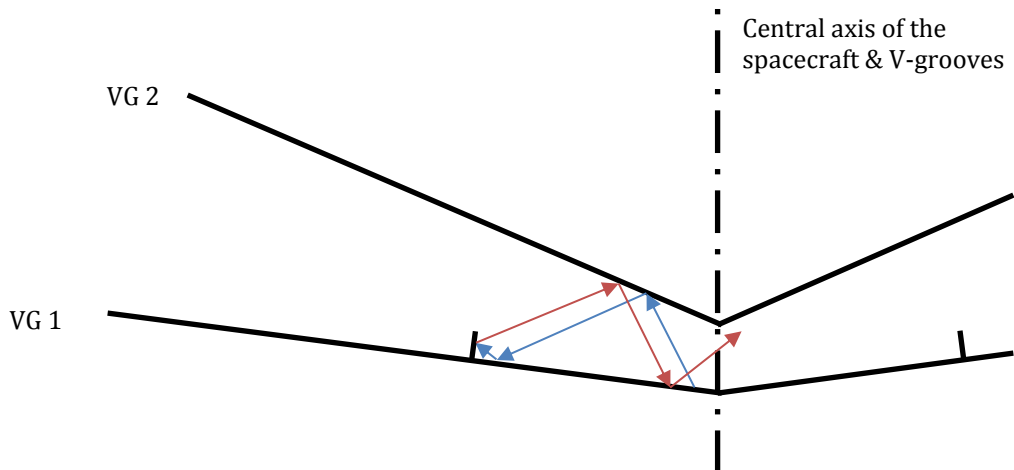


Figure 8-3: Circumferentially oriented ribs reflect infrared radiation back into the centre area of the V-grooves

Other deviations from flat panel shape also have to be minimised.

8.2.2.3 Constraints on the panel surfaces

For optimum heat dissipation from the V-grooves, the infrared radiation bouncing in between the surfaces has to be reflected as much as possible. Thus, the surfaces of V-grooves 1 and 2 need to be polished. Whatever material they are made of, they would need to have a polishable metallic coating, e.g. by vacuum deposition or any other suitable process, which again favours aluminium for these surfaces.

8.2.2.4 V-groove material selection

Due to all the constraints described above, the probably only suitable material for the V-groove panels is aluminium. In a first iteration, it is assumed that the panels are milled from 2 inch sheet material and subsequent welding of the two panel halves. For non-flat half-panels age creep, forming after milling but before welding and polishing, is assumed.

8.2.2.5 Panel design trade-off

The panels are designed toward a first eigenfrequency of 30 Hz, which has been the Planck thermal shield panels first eigenfrequency during protoflight model dynamic testing, RD[7].

The trade-off has been performed on an exemplary flat panel of 3400 mm diameter, which is supported at 6 equidistant points on a circle with 1660 mm diameter, assuming the struts supporting the V-grooves, see left image of Figure 8-4.

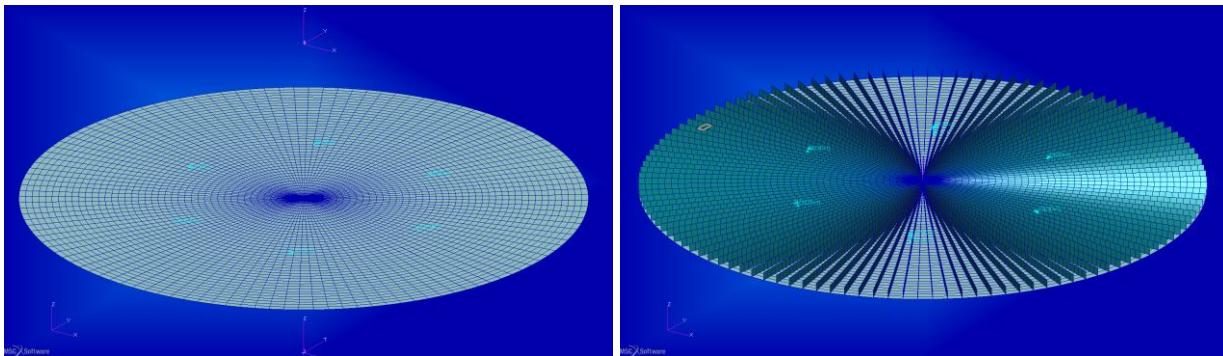


Figure 8-4: Sandwich panel as a benchmark (left) and radially rib stiffened panel (right)

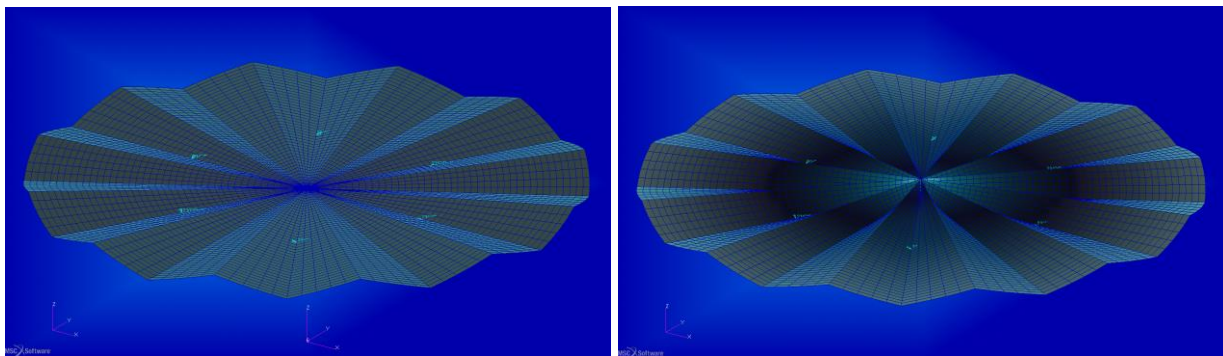


Figure 8-5: Flower petal shaped panels

As a benchmark, even though not compatible with the requirements outlined above, a standard sandwich panel composed of aluminium facesheets and honeycomb core glued together has been analysed. In the third iteration, this design's first eigenfrequency has surpassed 30 Hz with 35 mm honeycomb core height and 0.5 mm thick face sheets and a total mass of 35.6 kg, see Table 8-1, which—as a figure of merit—translates to .117 kg/Hz.

The radially rib stiffened panel has been iterated as well, but the required eigenfrequency was not achieved and the best figure of merit achieved was 11.2 kg/Hz, about ten times higher than for the benchmark design. The shape of the first eigenfrequency of the radially rib stiffened panel had a saddle-shape, see Figure 8-6 below, indicating that the stiffness at the rim is too low.

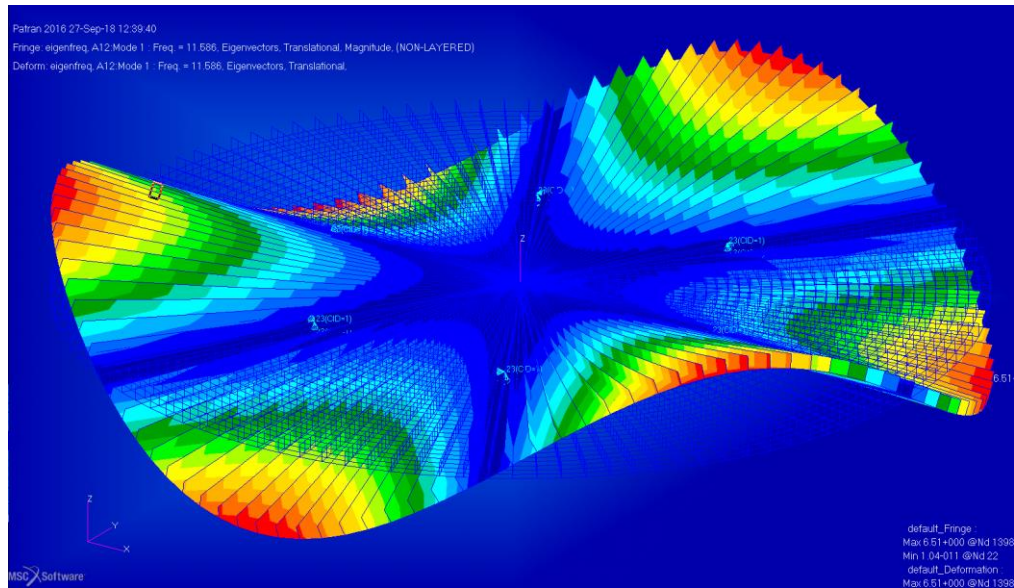


Figure 8-6: Radially rib stiffened panel (3rd run): shape of first eigenfrequency

Thus a new design was tested, in which the panel's outer rim was flower petal shaped, see left image of Figure 8-5. The difference in height of the outer rim was 100 mm, every 15 ° circumference it would rise and fall for the subsequent 15 ° circumferential length. This would stiffen the outer rim and as a positive side-effect got rid of the rib-stiffening. In the centre, the panel converges into one single point. This turned out to be its major weakness, the shape of the first eigenfrequency was an (inverted) bowl shape, see Figure 8-7, clearly highlighting the lack of stiffness in the centre region.

The second flower petal shape panel folded the slopes of the outer rim into one central connecting axis, the vertical distance between the ridges and valleys would be 100 mm not only at the outer rim of the panel, but all the way until they all connect in the centre axis of the panel, see right image in Figure 8-5. The shape corresponding to the first eigenfrequency is depicted in Figure 8-8. It exhibits no particular weakness, the shape is an overlay of—sort of—a lateral rigid body motion and saddle-shape. The highest eigenfrequency was 18.6 Hz with a figure of merit of 7.74 kg/Hz, the last run had 14.1 Hz, but with a better figure of merit of 6.17 kg/Hz.

Concluding, any alternative design would be five times heavier than the sandwich panel benchmark. With ~35 kg per sandwich panel the benchmark V-grooves would weigh about 100 kg, while the flower petal shape V-grooves would weigh about 500 kg. And thermally would not be as efficient.

Just to check whether the conclusion holds also for non-flat panels, a blunt cone shape with 85 degree half angle and radial ribs and skin thickness same as the radially ribbed flat panel (which is the right image in Figure 8-4) was analysed showing that eigenfrequencies are not impacted. Thus, for flat and conical panels any design other than sandwich panel has to be discarded.

Type	Angle [deg]	t_surf [mm]	t_str or t_core [mm]	Mass [kg]	1 st EF [Hz]	kg/Hz
Sandwich	0	1 (2x)	30	59	28.4	2.08
Sandwich (2 nd run)	0	0.5 (2x)	30	34	26.6	1.28
Sandwich (3 rd run)	0	0.5 (2x)	35	35.6	30.4	1.17
Stringered cone	5	3	3	162	13.3	12.2
Stringered	0	3	3	162	13.4	12.1
Stringered (2 nd run)	0	2	5	194	13.0	14.9
Stringered (3 rd run)	0	4	1	130	11.6	11.2
Petal	0	5	n.a.	132	5.3	24.9
Petal 2	0	5	n.a.	144	18.6	7.74
Petal 2 (2 nd run)	0	3	n.a.	87	14.1	6.17

Table 8-1: V-Groove panel design iterations

8.2.2.6 Conclusion

- All designs other than the sandwich panel exhibit eigenfrequencies way below the 30 Hz requirement.
- The figure of merit of dividing the panel mass by achieved eigenfrequency provides a measure for which design may succeed to reach 30 Hz and at which mass.
- Even the best non-sandwich design has a factor 5 higher mass-per-Hz ratio, the set of 3 V-grooves would have a prohibitive weight of about 500 kg (instead of ~100 kg for the sandwich panels).

Thus, some sort of aluminium sandwich panel is required with some aluminium honeycomb like core and without any use of organic glues. Alternative manufacturing technologies for these need to be evaluated, which is performed in section 8.5 of this report.

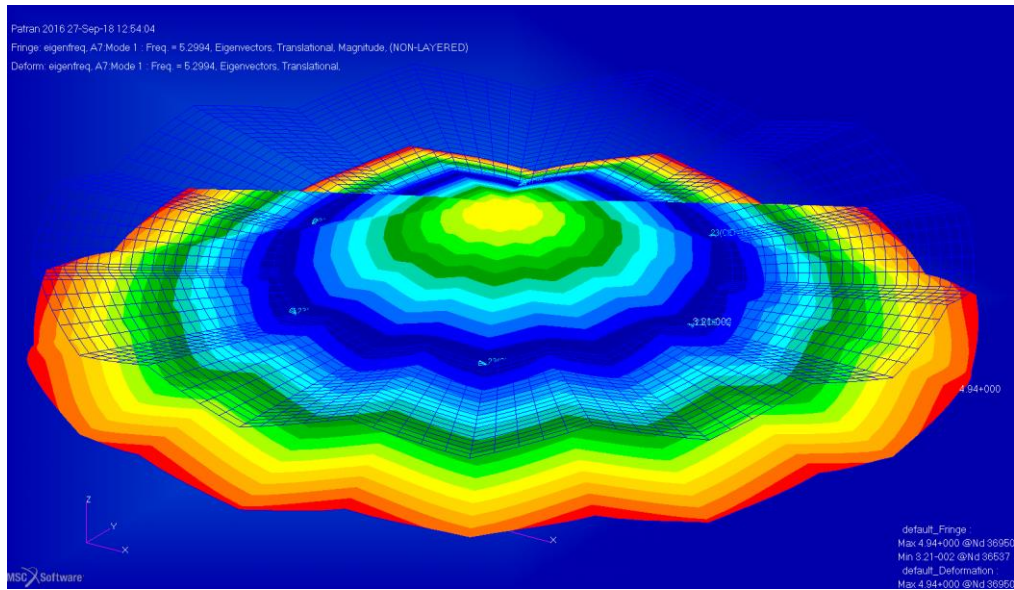


Figure 8-7: Flower petal shaped panel: shape of first eigenfrequency

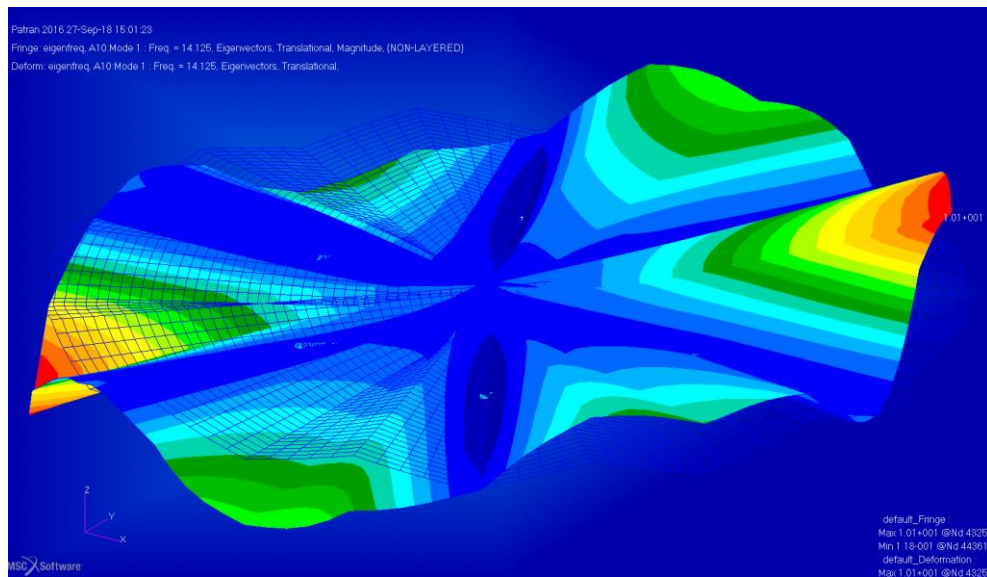


Figure 8-8: 2nd flower petal shape panel: shape of first eigenfrequency

8.3 Baseline Design

The structural components of the QPPF subdivides into two major assemblies, the payload part and the service module, see Figure 8-9. The payload part consists of the V-grooves, Sun shield, supporting struts and of course the payload itself, see Figure 8-10. However, in the mass budget, all but the actual payload and its direct support systems within the V-grooves is counted into the service module. Thus, all structural elements discussed within this chapter are part of the service module mass budget.

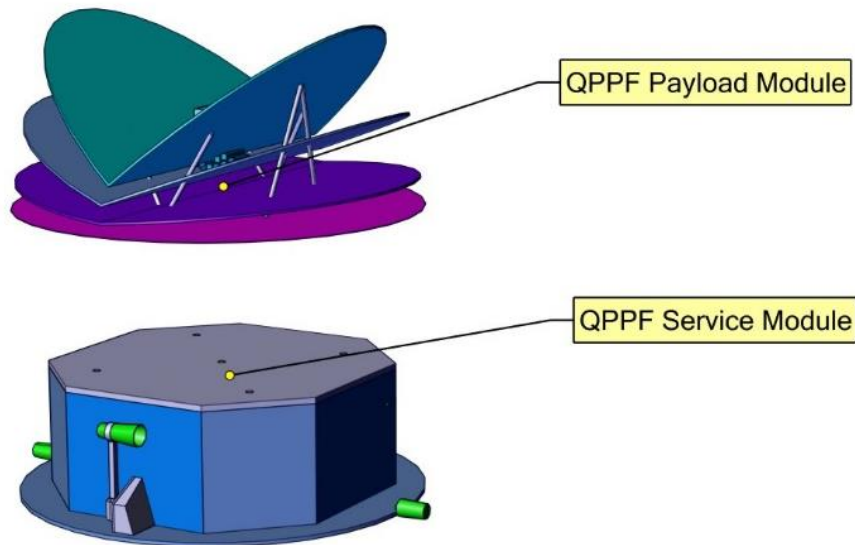


Figure 8-9: QPPF main structural assemblies

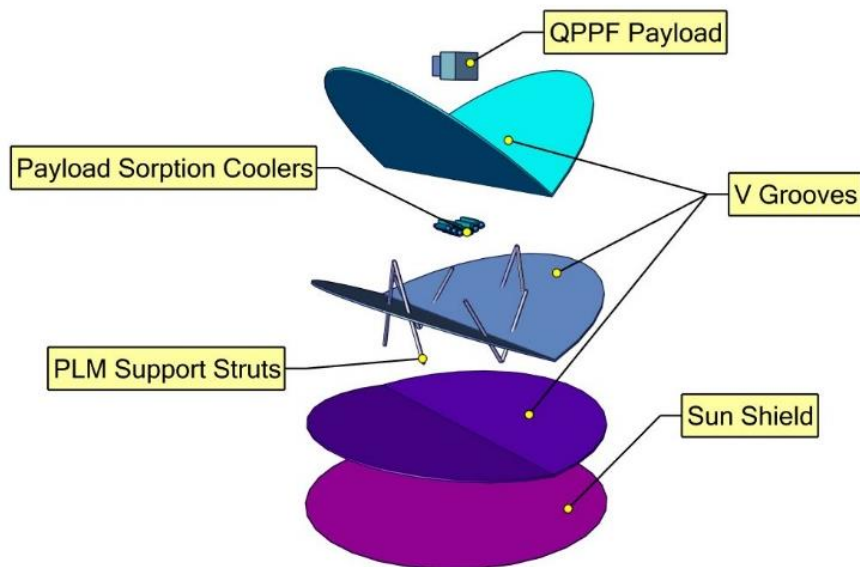


Figure 8-10: QPPF payload part sub-elements

8.3.1 V-Grooves

The V-groove and Sun shield surface areas are given in Figure 8-1 above. With the trade-off result, the mass estimate for the V-grooves found in Table 8-2 is based on the mass calculation of a sandwich panel with 0.5 mm face sheets and an aluminium honeycomb core of 35 mm height, without consideration of any glue mass, as these would need to be produced without organic glues.

<u>V-Groove 3</u>	
Surface area	8.56 [m ²]
Mass	33.564 [kg]
<u>V-Groove 2</u>	
Surface area	9.73 [m ²]
Mass	38.152 [kg]
<u>V-Groove 1</u>	
Radius	1.786 [m]
Surface area	10.021 [m ²]
Mass	39.293 [kg]
<u>Total</u>	111.01 [kg]

Table 8-2: V-groove mass summary

8.3.2 Sun Shield

Current assumption is, that Sun shield does not necessarily need to be manufactured from purely metallic materials. CFRP face sheets glued to an aluminium honeycomb core are therefore assumed. The mass calculation of the Sun shield is performed together with the service module CFRP panels in the following section.

8.3.3 Service Module Panels

The service module structure is shown as an exploded view in Figure 8-11, showing also the element's main dimensions, Figure 8-12 shows the same exploded view, but with the element's surface areas. The small strut and panel elements in the centre part of the PLM structure are shown in Figure 8-13.

The main carrying structure of the service module is the (capped conical) frustum that is equipped with the payload adapter at its bottom and supports the V-groove struts at its top end. A system of reinforcements and struts branching off the frustum supports the main service module subsystem masses, i.e. the propellant tanks at their respective lower polar mounting point. The top plate supports the tanks other polar mount in lateral directions, axial loads are only reacted by the strut system. The service module body is of octagonal shape, but due to balancing the solar wind pressure, the bottom plate is circular. It is divided in a centre plate and an annular disk by the payload adapter. Branching off from the frustum are four shear walls, which are also connected to the top and bottom plates. The outer eight panels forming the octagon likewise connect to the top and bottom panels as well as the shear panels.

The smaller panels are best seen in Figure 8-13, the four in the middle support the central propellant tank at its lower polar mounting, the outer four reinforce the central frustum. The sixteen struts support the four lower polar mounting of the outer four propellant tanks.

All panels are assumed to be made of CFRP face sheets with aluminium honeycomb core bonded together with epoxy glue. The assumed core material has a density of only 32 kg/m³, local reinforcements will be necessary but their determination is way out of scope of this report but instead assumed covered by the 20% mass margin on subsystem level. The face sheet stacking is selected based on their respective contribution to the main load path:

- The frustum is assumed to be tape placed with four CFRP layers per face sheet,
- The frustum auxiliary panels and shear walls contribute greatly to the overall service module stiffness and thus are assumed to have 6 layers per face sheet,
- The central tank support panels carry high loads and in terms of stiffness are the weakest link of the central tank mounting. They have thus been assumed with 12 layers per face sheet.
- The top panel and the outer panels forming the octagon have to react to equipment loads, but not in the main axial load path, and thus are assumed with four layers per face sheet.
- The Sun shield as well as the bottom plate carry only minor equipments—antennae and solar cells for the bottom plate and just MLI for the Sun shield—and thus are assumed to be sufficiently resilient with only two CFRP layers per face sheet.

No surface covering is included in the mass calculations below, neither the solar cells nor the MLI. The panel mass calculation given in Table 8-3 considers not only the above discussed face sheet and core masses, but also second order mass contributors summarised in Table 8-4. For calculation of the strut masses and payload adapter, please refer to section 8.3.4.

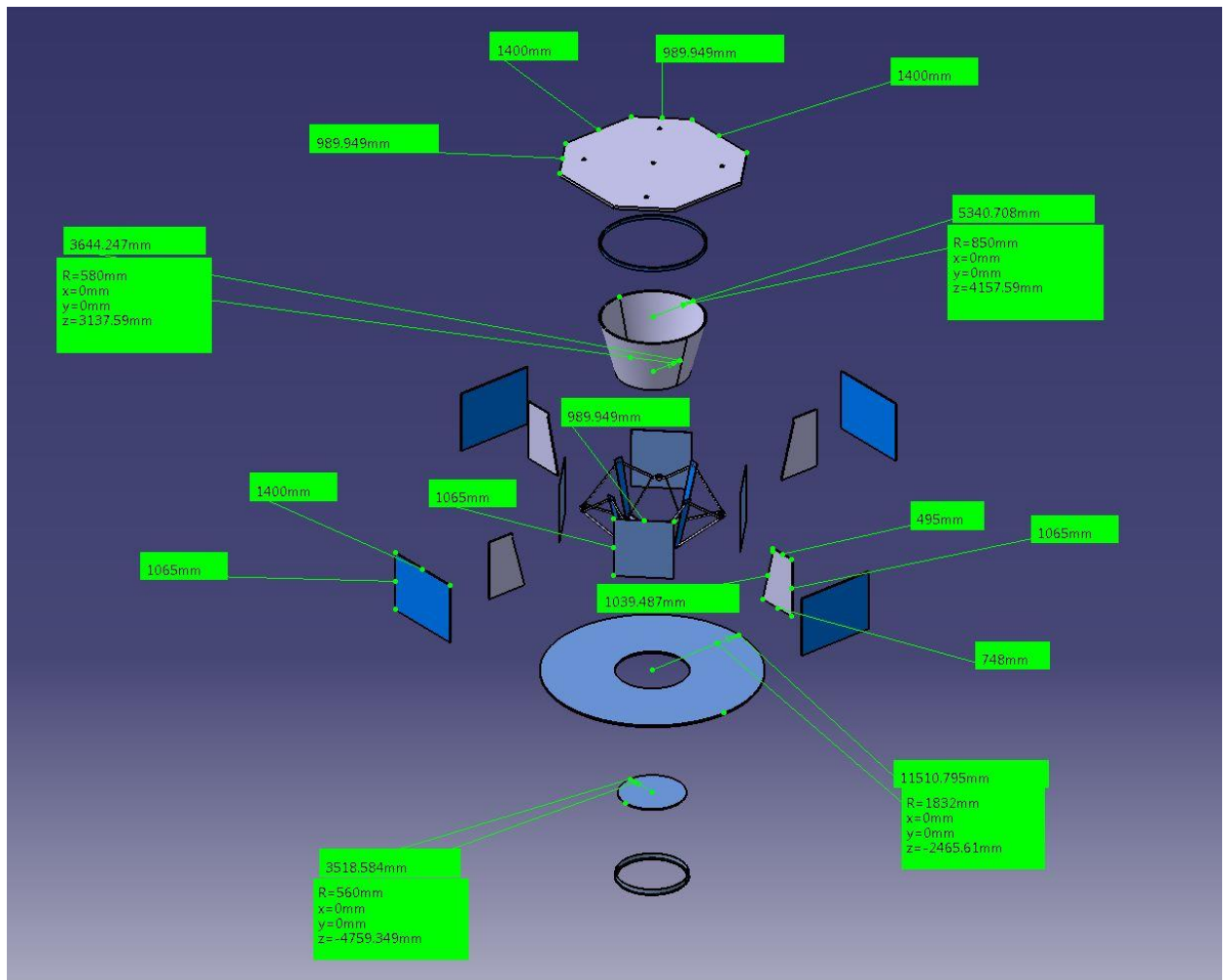


Figure 8-11: Service module structure exploded view including primary elements dimensions

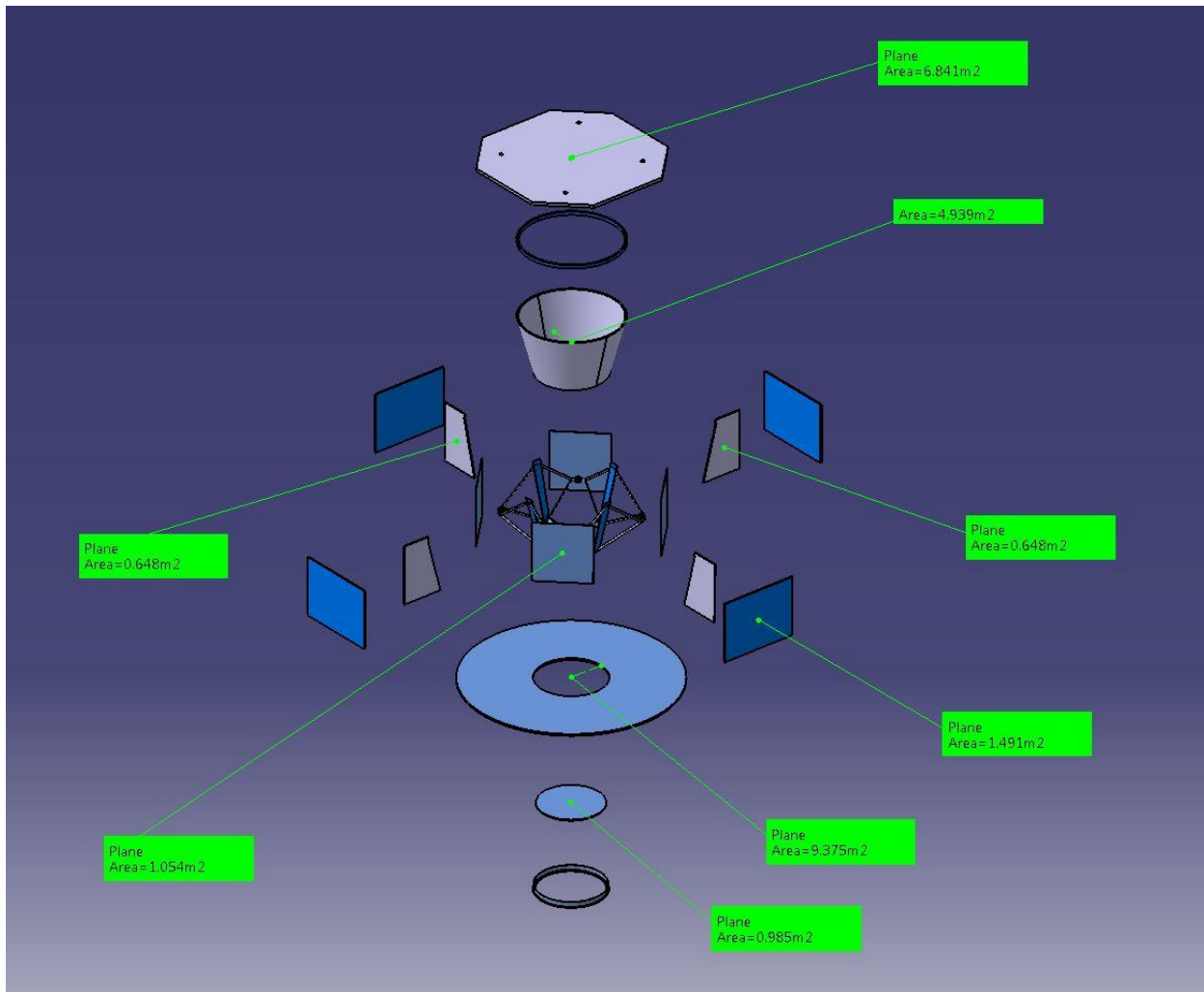


Figure 8-12: Service module structure exploded view including primary elements surface areas

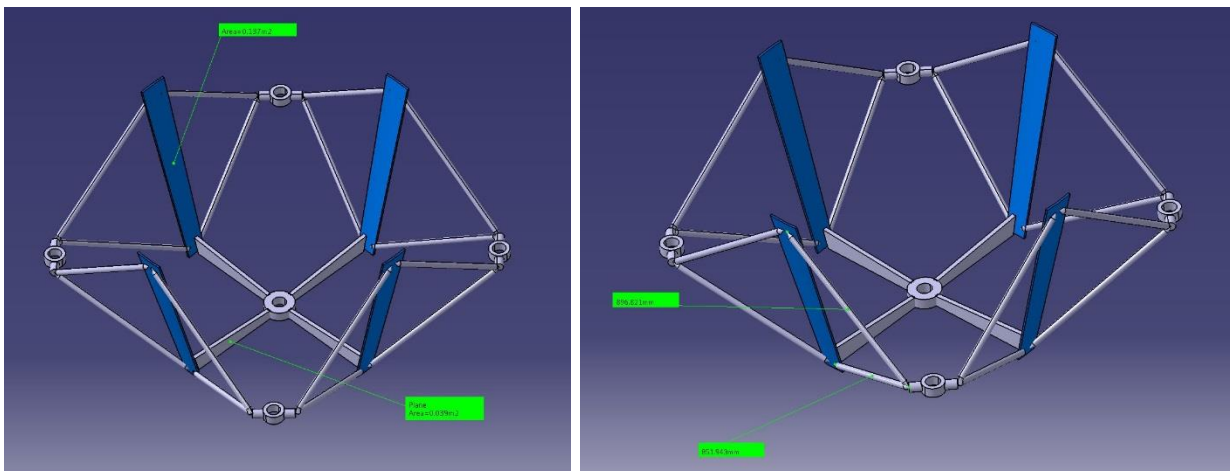


Figure 8-13: Service module supporting struts and panel elements

Part	Geometry		Facesheets			
	Shape	Area	Type/Lay-up	Density	Thickness	Mass
		[m ²]		[kg/m ³]	[mm]	[kg]
Sun Shield (between V-Grooves and S/C bus)	circular	10.534	CFRP [45,-45]	1654	0.25	8.712
Top Panel	octagonal	6.841	CFRP [0,45,-45,90]	1654	0.5	11.315
Central Frustum	conical frustum	4.939	CFRP [0,45,-45,90]	1654	0.5	8.169
Shear Walls	trapezium	0.648	CFRP [0,60,-60]s	1654	0.75	1.608
Outer Panels Type 1	rectangle	1.491	CFRP [0,45,-45,90]	1654	0.5	2.466
Outer Panels Type 2	rectangle	1.054	CFRP [0,45,-45,90]	1654	0.5	1.744
Frustum auxiliary panels	rectangle	0.137	CFRP [0,60,-60]s	1654	0.75	0.340
Central Tank Support	trapezium	0.039	CFRP [[0,60,-60]s]s	1654	1.5	0.194
Bottom Plate (below S/C bus, outside of P/L adaptor)	annular disc	9.375	CFRP [45,-45]	1654	0.25	7.753
Bottom Plate (below S/C bus, within P/L adaptor)	circular	0.985	CFRP [45,-45]	1654	0.25	0.815

Underlined column titles indicate columns for input values.

Part	Material	Core			Glue	Inserts & Cleats		Total	
		Density	Thickness	Mass		Edge Length	Mass	Units	Mass per Unit
		[kg/m ³]	[mm]	[kg]	[kg]	[m]	[kg]	[-]	[kg]
Sun Shield (between V-Grooves and S/C bus)	3/16-5056-0007	32.04	45	15.188	3.687	5.341	2.492	1	35.419
Top Panel	3/16-5056-0007	32.04	20	4.384	2.394	14.901	6.954	1	39.947
Central Frustum	3/16-5056-0007	32.04	20	3.165	1.729	13.380	6.244	1	32.686
Shear Walls	3/16-5056-0007	32.04	20	0.415	0.227	3.403	1.588	4	7.240
Outer Panels Type 1	3/16-5056-0007	32.04	20	0.955	0.522	4.930	2.301	4	11.174
Outer Panels Type 2	3/16-5056-0007	32.04	20	0.676	0.369	4.110	1.918	4	8.816
Frustum auxiliary panels	3/16-5056-0007	32.04	20	0.088	0.048	1.099	0.513	1	2.087
Central Tank Support	3/16-5056-0007	32.04	20	0.025	0.014	0.058	0.027	1	0.317
Bottom Plate (below S/C bus, outside of P/L adaptor)	3/16-5056-0007	32.04	45	13.517	3.281	13.204	6.162	1	43.917
Bottom Plate (below S/C bus, within P/L adaptor)	3/16-5056-0007	32.04	45	1.420	0.345	3.644	1.701	1	7.925
Sum									271.222

Underlined column titles indicate columns for input values.

Table 8-3: CFRP panels mass calculation

Glue density	0.35 [kg/m ²]
Border insert pitch	0.075 [m]
Insert mass	0.01 [kg]
Cleat mass	0.025 [kg]

Table 8-4: Secondary mass contributors to CFRP panels

8.3.4 Struts and Payload Adapter

The V-grooves (and of course the payload) need to be supported, but as unobtrusively as possible, in order not to introduce thermal conduction between the panels beyond the strictly necessary and also to not obstruct infrared radiation. This support is a set of struts, same as assumed in the trade-off in section 8.2.2 above,.

The strut lengths are given in Figure 8-14 below. Likewise, they are assumed to be fully metallic, aluminium hollow tubes of 0.5 mm wall thickness with steel end fittings, the mass calculation can be seen in Table 8-5.

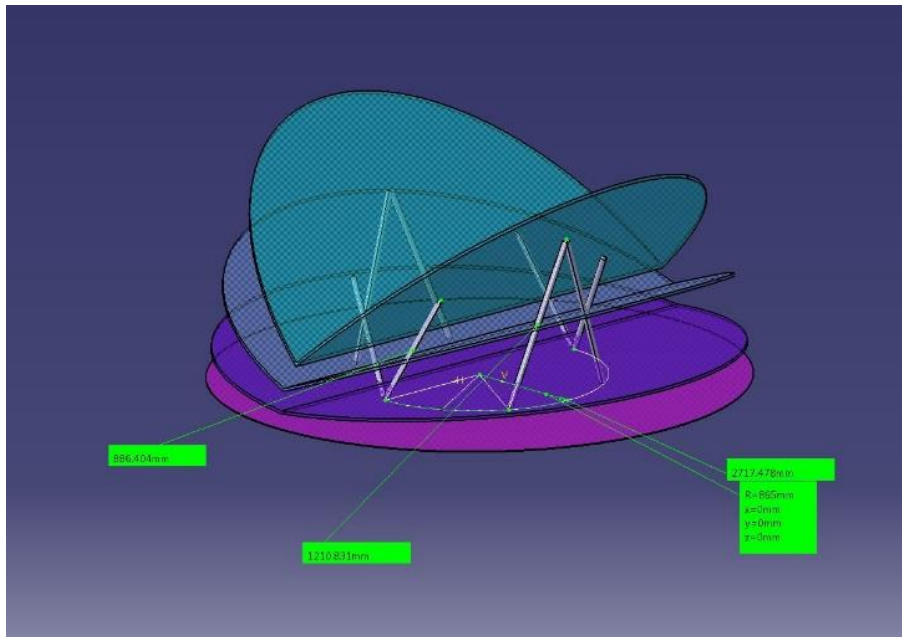


Figure 8-14: V-groove and payload related strut lengths

STRUT DESIGN 3							
Material	3.4364.T7351 (0.5 mm)						
Density	2800 [kg/m ³]	Wall thickness	0.5 [mm]				
Diameter	20 [mm]						
Length	886 [mm]	End fittings material	STEEL				
Tube mass	0.071 [kg]						
End fittings mass	0.400 [kg]	Volume:	0.000278 [m ³]				
Total mass	0.471 [kg]	Volumic density:	1690.384 [kg/m ³]				
STRUT DESIGN 4							
Material	3.4364.T7351 (0.5 mm)						
Density	2800 [kg/m ³]	Wall thickness	0.5 [mm]				
Diameter	20 [mm]						
Length	1211 [mm]	End fittings material	STEEL				
Tube mass	0.099 [kg]						
End fittings mass	0.400 [kg]	Volume:	0.00038 [m ³]				
Total mass	0.499 [kg]	Volumic density:	1311.874 [kg/m ³]				

Table 8-5: V-groove and payload supporting struts mass calculation
(mass per strut)

The service module struts are assumed to be CFRP hollow tubes, their lay-out and lengths can be seen in Figure 8-13 above, their mass calculation is performed in Table 8-6 below.

STRUT DESIGN 1							
Material	CFRP [0,60,-60]s - 0.75 mm						
Density	1654 [kg/m3]			Wall thickness	0.75 [mm]		
Diameter	20 [mm]						
Length	852 [mm]			End fittings material	ALUMINUM		
Tube mass	0.060						
End fittings mass	0.139 [kg]			Volume:	0.000268 [m3]		
Total mass	0.199 [kg]			Volumic density:	744.992 [kg/m3]		

STRUT DESIGN 2							
Material	CFRP [0,60,-60]s - 0.75 mm						
Density	1654 [kg/m3]			Wall thickness	0.75 [mm]		
Diameter	20 [mm]						
Length	897 [mm]			End fittings material	STEEL		
Tube mass	0.064 [kg]						
End fittings mass	0.400 [kg]			Volume:	0.000282 [m3]		
Total mass	0.463 [kg]			Volumic density:	1644.033 [kg/m3]		

Table 8-6: Service module struts (mass per strut)

The payload adapter ring (PLA) had been dimensioned in a past study and the result has been carried over into this study with the PLA mass assumed to weigh 5 kg.

8.4 List of Equipment

	mass (kg)	mass margin (%)	mass incl. margin (kg)
Sun_Shield (Sun Shield)	51.84	20.00	62.21
SM_STR (Service Module Structure)	197.89	20.00	237.47
Int_Shield (Intermediate Shield)	35.42	20.00	42.50
Grand Total	285.15	20.00	342.18

Table 8-7: Structure domain equipment list

8.5 Technology Needs for V-Groove Manufacturing

With the need for stiffness on par with honeycomb core sandwich panels, but strictly made from metallic material only, limits the usable manufacturing processes to just a few technologies:

- Superplastic Forming and Diffusion Bonding (SPF/DB), see RD[8] to RD[11]
- Additive Layer Manufacturing (ALM), see RD[12]
- Aluminium Foam Sandwich Panels (AFS), see RD[13] and RD[14]

Large turbojet fan blades are made using superplastic diffusion bonding, Figure 8-15 below shows “a six-step breakdown of wide-chord fan blade production for the Trent engines using the DB-SPF technique. The fan blades for the Trent engines are manufactured from three sheets of titanium (1). The two outer sheets will form the aerodynamic surfaces of the blade and the thicker root section. The middle, thinner, sheet will form the ‘Warren–Girder’ structure internally, providing the blade stiffness and impact resistance required. Once the pack of three plates has been formed a masking pattern is painted onto the internal faces of the outer plates (2). The plates are then re-stacked, with a small tube attached to the end, welded together around the edge, evacuated and heated above 950 °C (3). At this temperature diffusion occurs across the metallic surfaces in intimate contact within the pack and at its edges. Thus, after heat treatment the three plates are now a single unit. The pack is then shaped into its approximate aerofoil morphology (4), before it is inflated (5). To enable inflation the component is re-heated above 900 °C and argon gas is injected, at pressure, through the tube. After inflation the aerofoil cross section seen in images 5 and 6 is created. The girder configuration is developed because diffusion bonding is unable to occur across the ‘masked’ regions, and these unbonded areas are expanded during argon injection.” Cited from RD[8]

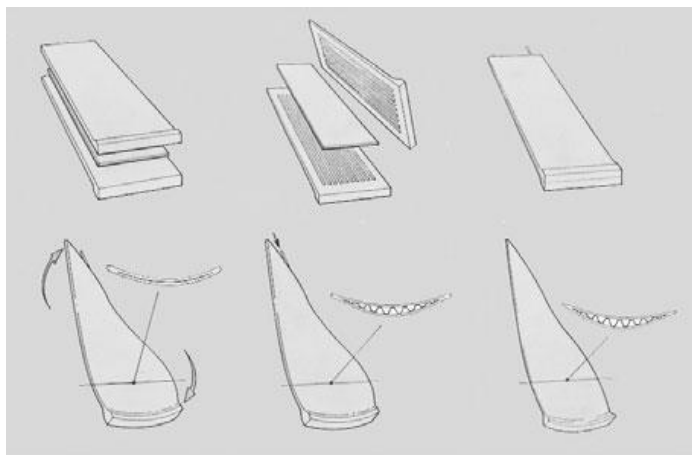


Figure 8-15: Rolls Royce Trent fan blade production, see RD[8]

Sandwich panels formed by SPF/DB have been an active topic for decades, see e.g. NASA patent US4292375A from 1981 RD[9], see also image excerpt in or Boeing patent US6820796B2 RD[10].

In the NASA patent, the middle layers have a complex layout of venting holes and masking patterns such that the inflation step (step 5 in Figure 8-15) reaches all the cells of the core allowing to inflate a complex core structure as shown in Figure 8-16.

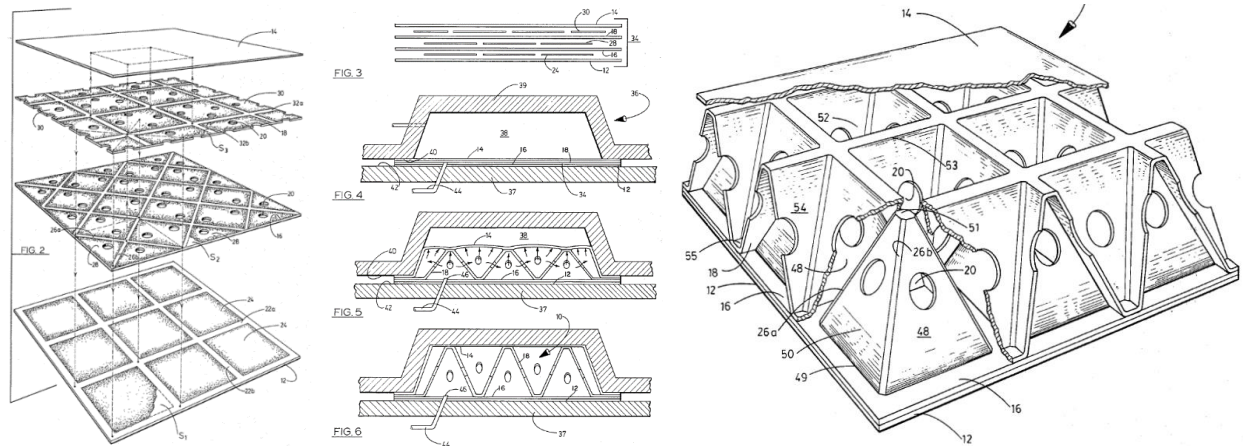


Figure 8-16: Stacking, inflation procedure and resulting geometry of honeycomb core sandwich panel, all from RD[9]

However, while this technology is in large scale application, in particular for the hollow titanium blades for jet engines, *“aluminium and many of its alloys can be formed superplastically but they have an extremely tenacious surface oxide that prevents diffusion bonding”* RD[11]. Diffusion bonding of aluminium has been an active area of research, see e.g. the patent RD[11].

However, as of today, no diffusion bonded aluminium aircraft components are operational.

8.5.1 Additive Layer Manufacturing (ALM)

It is comparatively easy to imagine additive layer manufacturing, in particular laser sintering of metallic materials, for any shape that seems too complex for other manufacturing processes. This has led to ALM being proposed everywhere and for everything.

One can easily imagine aluminium sandwich panels of 35mm height with some sort of core structure being produced by laser sintering, the core doesn't necessarily need to be of honeycomb structure, but may be a three-dimensional grid structure, which would ease cleaning procedures to remove excess metallic powder from the panel core.

However, *“with a building volume of 400 x 400 x 400 mm, EOS M 400 allows the production of large metal parts on an industrial scale – directly from CAD data and with no need for tools.”* RD[12], see also Figure 8-17 below. This is the largest machine the currently worldwide leading company for laser sintering has to offer.



Figure 8-17: EOS M 400, largest metallic powder laser sintering machine currently available, from RD[12]

Thus, the panels would need to be assembled from pieces; for which only welding processes qualify in order to remain purely metallic. Fortunately, three welding technologies are available:

Tungsten inert gas welding (TIG)

This process is limited to some aluminium alloys from the 2000, 6000 and 7000 series, but it is in wide use. It would need to be tested and qualified for ALM aluminium material, it is difficult to a priori estimate the chance of succeeding with this welding process.

Electron beam welding (EB)

For aluminium, this has to be performed in vacuum. The oxide layer would need to be scraped off before welding and in order to avoid re-establishment of the oxide layer needs to be placed in a vacuum chamber. TIG welding avoids this by surrounding the welding torch with inert gas. Vacuum welding chambers of sufficient size for a full V-groove panel are rare but exist in Europe. It would need to be tested and qualified for ALM aluminium material, chances of success cannot be determined a priori.

Friction stir welding (FSW)

FSW can basically weld anything, same as for the other processes the working window needs to be determined by testing, qualification for ALM material needs to be performed, chances of success are very high. Due to the high process forces it needs very sturdy clamping tools but only flat welds need to be made, limiting cost and complexity.

It is safe to assume that at least one of these will work for ALM aluminium panels.

8.5.2 Aluminium Foam Sandwich Panels (AFS)

During the last two decades several processes have been developed. Common to all these processes is that they start off with cover sheets and an aluminium and blowing agent (typically TiH_2) mixture for the core. In the production process a container is built from the cover layer material, filled with the powder and sealed and subsequently compacted, whereas the powder mixture in the inner reaches a density just a few percent below the theoretical density of solid material. This precursor sheet can be processed like conventional aluminium sheet material, it can be rolled to achieve

thinner sheets and deep drawing or pressing can be applied. In the subsequent foaming process the metal sheet is heated up to a temperature range where the core layer turns liquid but the cover layers still stay solid. It is evident that this restriction has to be taken into account by adequate material selection. However, the gas propellant mentioned above is adjusted that way that it starts to release gas (hydrogen in the case of TiH_2) while the core material is in its liquid phase. Thus the core starts to foam and to develop the porous structure shown in Figure 8-18. On subsequent cooling, this structure is frozen.

Complex shapes can be made, see e.g. the bicycle crank arm shown in Figure 8-19. The technology is in small scale serial production for the support structure of a telescopic lifting arm. This unit is mounted to a van sized vehicle and can carry people up to 25 m height and 11 m outreach. The largest parts currently produced are plates of 2000 mm x 1000 mm, see RD[14].

In the early 2000s, a technology demonstration activity was performed to replace the panels of the Ariane 5 payload adaptors with AFS panels. At that time the Ariane 5 payload adaptors were assembled using conical sandwich panels with aluminium face sheets and aluminium honeycomb core material. The objective was to replace these by a cheaper and easier to handle AFS-based version. This was met by welding together 12 curved AFS (1.3 mm alloy 6060 face sheets, AlSi6Cu6 foam core, i.e. C-type) segments by manual TIG welding, see Figure 8-20. The resulting cone is almost 4 m wide at the base.

Like ALM, it also requires an assembly of the segments to the full panel size, but while the ALM sandwich elements today would be 400 mm x 400 mm, the AFS elements would be up to 2000 mm x 1000 mm. Compatibility with TIG welding has been demonstrated in the Ariane 5 PLA activity RD[13].

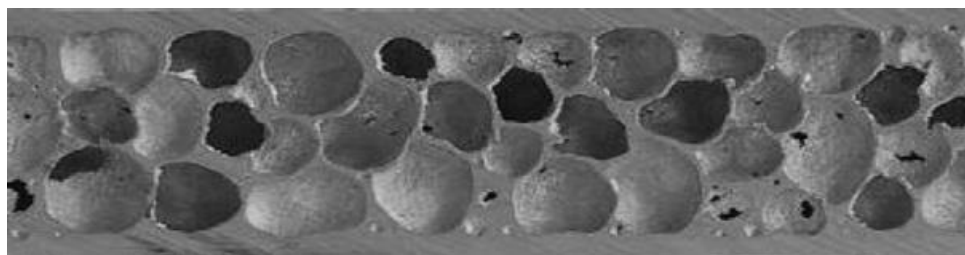


Figure 8-18: Cross-section through AFS showing two external aluminium sheet layers and an aluminium foam core in between, from RD[13]



Figure 8-19: Bicycle crank arm, forged AFS parts and section (top image), tomogram of interior (bottom image), from RD[14]

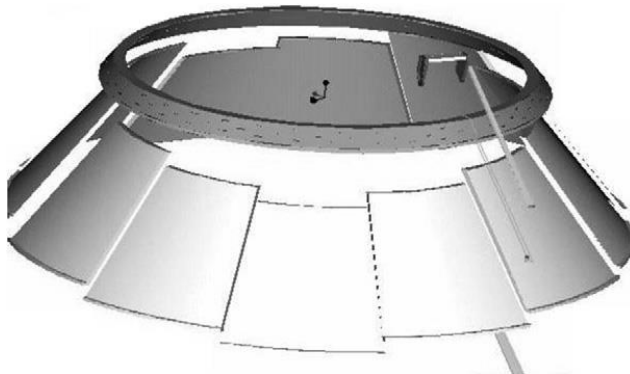


Figure 8-20: Ariane 5 payload adapter assembly with AFS panels, from RD[13]



Figure 8-21: Payload adapter cone after assembly, from RD[13]

8.5.3 Conclusion

For the V-groove panel manufacturing, three possible manufacturing technologies have been identified, all of which should deliver similarly low mass as conventional aluminium face sheet sandwich panels. The lowest risk appears to be with the aluminium foam sandwich technology, as it today provides the largest panel elements and its compatibility with TIG welding has been demonstrated. Thus, in Table 8-8, AFS along with TIG welding has been selected as baseline.

Technology Needs						
base-line	Equipment Name & Text Reference	Technology	Supplier (Country)	TRL	Funded by	Additional Information
	Section 8.5	SPF/DP	NASA (USA), Boeing (USA)	3	NASA	
	Section 8.5.1	ALM	EOS GmbH (D)	6	n.a.	
*	Section 8.5.2	AFS	Alm GmbH (D)	6	DLR, CNES	
*	Section 8.5.1 Section 8.5.2	TIG welding	MT Aerospace (D), Air Liquide (F)	9	ESA, DLR	
	Section 8.5.1	EB welding	MT Aerospace (D)	9	ESA, DLR	
	Section 8.5.1	FSW	MT Aerospace (D)	7	ESA, DLR	

Table 8-8: Technology candidates for V-groove panel manufacturing.

This Page Intentionally Blank

9 NANO PARTICLE HANDLING

9.1 Requirements and Design Drivers

9.1.1 Functional Requirements

Functional Requirements		
Req. ID	Statement	Parent ID
NPH-010	The nanoparticle handling system includes a storage means for the nanoparticles, which is sufficiently robust to withstand the launch environment, and sufficiently stable to last for the duration of the mission	
NPH-020	The nanoparticle handling system provides the means for on-demand release of the nanoparticle	
NPH-030	The nanoparticle handling system includes the means to transfer the nanoparticles once released to the optical cavity located on the optical bench	
NPH-040	<p>The nanoparticle handling system includes the capture of the nanoparticles in the optical cavity, and the pre-conditioning of the nanoparticle such that it can be further manipulated with the elements of the optical bench payload. This may include;</p> <ul style="list-style-type: none"> • Cooling of the nanoparticle (i.e. reduction of velocity) • Precisely measuring the charge of the nanoparticle • Discharging the nanoparticle 	

9.1.2 Review of Terrestrial Methods for Particle Loading

The investigation of quantum mechanical properties of optically levitated and cooled nanoparticles is a very active area of research. However, the delivery of nanoparticles into the experiment systems ubiquitously relies on nanoparticles being initially dispersed in a liquid, which is a convenient means of preventing agglomeration. Then the nanoparticles are extracted using either electrospray ionisation (ESI) or a nebulizer. ESI is a technique developed for use in mass spectrometry, where a high voltage is applied to a capillary tube as the liquid solution is forced through and expanded into vacuum RD[15]. This results in charged particles. Another means involves a nebulizer, which delivers neutral particles that can be further manipulated with an optical tweezers RD[16].

Either method faces challenges in delivering particles into a vacuum environment. One approach is to generate the aerosol, trap the desired particle in the optical cavity, and then pump the vacuum. However this unavoidably causes significant contamination to nearby optics, including the cavity mirrors and therefore reducing the cavity finesse. Such an approach is not applicable for a space based experiment, which must operate autonomously and be repeated ~200 000 times.

One potential solution involves the use of photonic crystal hollow core fibres, used as an 'optical conveyor belt' for levitated nanoparticles which can withstand a significant pressure differential across the two ends. This was demonstrated in RD[17] over several

cm and a pressure difference from 100 mbar to 0.2 mbar. This concept could be of interest in this study to achieve a pressure differential, however the problem of delivering the nanoparticles into the high-pressure end of the fibre remains.

Another approach is the load-lock as described in RD[18], where a single particle is first loaded into an optical trap in a first chamber, the vacuum is pumped, then the system is physically translated into a second chamber at high vacuum and the particle is transferred into a high-finesse optical cavity. This approach is also considered unfeasible for satellite operation since it would require; complex mechanisms, lengthy load time, and a high number of repeat cycles.

9.1.3 Design Drivers

The methods used for terrestrial experiments to store nanoparticles in a liquid are considered not compatible with a space mission, due to the inevitable contamination associated with the loading process. Therefore, the main design drivers for this sub-system are derived as follows;

- The nanoparticles should be stored by adsorption to a surface, and
- The means of releasing the nanoparticles should not generate other gaseous particles which may compromise the vacuum, or contaminate the optics.

9.2 Technologies Considered

There was a wide variety of technologies considered for the various functions of the nanoparticle handling system. A summary of the options, their function with a brief description and the justification for/against selection is presented in Table 9-1.

Option	Function	Disposition
MEMs array – “catapults” with single nanoparticle pre-loaded on ground	<i>Storage, desorption (& charging?), transport</i> A specifically developed MEMs device to store particles in precise locations, then can individually trigger release of a specific particle	Incorporated in baseline <ul style="list-style-type: none"> • Elegant solution • Can do some preliminary estimation of design parameters and seems feasible
Optical desorption	<i>Desorption, charging</i> Using UV light to both <u>desorb</u> nanoparticles from a surface, and to provide charge to them via photoelectric effect (illumination directly on nanoparticles, or on nearby electrodes)	Not selected <ul style="list-style-type: none"> • Simple solution • Not possible to assess without investigation into feasibility of optically desorbing nanoparticles
Electron gun	<i>Desorption, charging</i> For charging nanoparticles, and potentially also assisting with desorption Heritage of electron guns from ion thrusters	Not incorporated, but retained for investigation <ul style="list-style-type: none"> • Compared to other options, technologically more advanced • Requires investigation – robustness of particles to not break when bombarded, and how much

Option	Function	Disposition
		charge do they retain?
Surface Acoustic Wave device	<i>Storage, desorption (& charging?)</i> Particles are initially adsorbed on a SAW device, which is then activated to trigger release	Not selected. Some investigations already performed, and not clear if particles can be ejected from the surface this way (mostly moving around on the surface). Potential candidate for further technology developments.
Surface functionalization of nanospheres	<i>Storage, desorption (& charging?)</i> Attachment of the nanoparticles to the surface is engineered, and a bond can be broken with e.g. particular wavelength light	Not incorporated, but would be highly interesting for technology development. Could also be combined with the MEMS option.
Matrix-assisted laser desorption/ionization (MALDI)	<i>Desorption (& charging)</i> Based on ablation - high-power laser incident on an absorbing matrix upon which particles are embedded (or are a part of the material itself and are broken off by the laser as per RD[19]). Target particles along with parts of matrix are released.	Not incorporated Questionable to develop a controlled process that would deliver quality nanoparticles Very high laser power necessary
Hollow-core fibre Or Hollow-core planar waveguide	<i>Storage, transport</i> Although existing investigations in this direction usually are for the purpose of stepping-down in pressure, this is considered here as a potential storage 'container' where nanoparticles are adsorbed on the side walls of the core	Not incorporated Significant development would be needed, and this is probably better focused on the MEMs or functionalization activities which would offer individual particle addressing.
Dipole/quadrupole static magnets	<i>Transport</i> For transport from storage container to optical bench, and for trapping within the optical cavity	Incorporated pending outcome of technology developments for storage/desorption means Particles will likely be charged whatever mechanism is used for desorption, and this is one obvious solution to steer/guide the particles, and potentially also reduce their velocity if necessary.
RF electromagnetic trap (Segmented linear Paul trap)	<i>Capture and pre-cooling, charge measurement</i> Well established means for trapping charged particles	Incorporated in baseline <ul style="list-style-type: none"> • Particles will likely be charged after desorption, therefore this is a logical means to trap and pre-condition • Can be overlaid with the optical cavity • Can additionally provide means to cool using electrical feedback, and also to measure the charge of the nanoparticle

Option	Function	Disposition
UV illumination on optical bench	<i>Discharging</i> Assuming neutral nanoparticles are required for experiment	Incorporated in baseline <ul style="list-style-type: none"> Is anyway a part of the payload as a part of the physics experiment Imposes condition that nanoparticles should be negatively charged initially, such that photoelectric effect can be used to discharge

Table 9-1: Overview of technology solutions considered for achieving the various functions of the nanoparticle handling system

9.3 Assumptions and Trade-Offs

The design choice to have nanoparticle storage based on adsorption to a surface implies that the one key parameter to estimate is the force of adhesion between the particles and a substrate. This is dominated by the van der Waals (vdW) interaction.

In this section, the parameter estimation for the vdW interaction will first be presented, followed by the assumption regarding the particle's average charge when they are removed from a surface.

In the below estimations, the geometry and size of the particles is a key parameter. It is the intention for the experiments to use a range of sizes, and potentially materials. Assuming a density of fused silica (2.203 g/cm³), and a mass ranging from 1×10⁸ to 5×10⁹ au, the range of particle sizes varies from a radius of 26 nm to 97 nm. The calculations below are to be taken as order of magnitude estimates only, where the particle radius used may not always be the same, but will be within the foreseen range.

9.3.1 Van der Waals Interaction

The force due to the vdW interaction for a sphere-plane geometry is (see for example, Ref. RD[20]);

$$F = -\frac{AR}{6D^2}$$

Where the parameter values used for this estimation are;

$A = 6.5 \times 10^{-20}$ J Hamaker constant (interaction constant)

$R = 50 \times 10^{-9}$ m particle radius

$D = 0.25 \times 10^{-9}$ m distance from sphere to surface (estimate)

This results in $F = -9$ nN.

It is worthwhile to note the linear dependence of the force on the particle radius R . Compare this to the force of gravity or to kinetic energy, which depends on the mass (i.e. R^3), it becomes clear that the vdW force can be easily overcome at macroscopic scales. However at small dimensions, typically <1 μm, it becomes much more significant RD[21]. In fact, for particles larger than ~1 μm, removal from a surface can be achieved with relative ease by mechanical shaking (i.e. providing kinetic energy to overcome the vdW force). The above force of 9 nN is very difficult to overcome.

However there are some means of reducing the vdW force, mostly by modifying the surface properties. For instance introducing surface roughness can reduce the adhesion by some orders of magnitude RD[22]RD[23]RD[24]. Also it is known that the environmental temperature plays a role in the vdW force, where reducing temperatures could also reduce the force RD[25].

One of the key assumptions here that further calculations will be based on, is that the above calculated vdW force can be reduced (e.g. by surface treatments, or temperature control) by 2 orders of magnitude. This topic of surface adhesion for the particles of interest (and methods to engineer it to be in a desirable range) should be addressed in early stages of technology development, since the result is a fundamental aspect of the entire nanoparticle handling approach.

9.3.2 Nanoparticle Charge

The design choice here for storage of a nanoparticle via adhesion to a surface has very little analogy with the methods used in this research field. Therefore, it is difficult to estimate what the inherent charge of the particle will be as a result of simple mechanical removal from a surface. However, it will be beneficial for the particle to be significantly charged, since it can then be manipulated more easily with electrodynamic forces.

To give some quantitative values for charged silica nanoparticles, some measurement values can be found from literature (where Q denotes the fundamental unit of charge; $1.6 \times 10^{-19} \text{ C}$);

- Silica nanoparticles, 10-20 nm diameter; charging via ESI in the range 0.4-148 Q (RD[26])
- Silica nanoparticles, 200nm diameter, trapped in a Paul trap, typically 1-3 Q (RD[27])

More generally, RD[28] notes that materials such as aluminium oxide (Al_2O_3) can hold 10^4 to 10^6 Q per μm radius, and that the charge scales proportionally to the radius squared. It is noted that the high values can be achieved via electron bombardment or corona discharge.

Since it is considered advantageous in this application to have a relatively high level of charging, the large value of 10^6 Q for 1 μm radius is taken and scaled to a 100 nm radius, resulting in 10^4 Q . This is an assumption that would require investigation in conjunction with the desorption methodology. Ideally the charging could be achieved in the same process as the desorption, however if necessary it may be considered to include additional infrastructure (for example an electron gun) to provide this charging. Interestingly RD[28] also notes that a particle can hold more positive charge than negative.

9.3.3 Summary of Assumptions

Assumptions	
1	The force of attraction between the nanoparticle and the surface to which it is adsorbed for storage is assumed to be on the order of 0.1 nN
2	The approximate charge on a 5×10^9 <i>au</i> silica nanoparticle (~100 nm radius) is $\sim 10^4$ Q , with a scaling proportional to the square of the particle radius.

9.4 Baseline Design

9.4.1 Overview

The baseline design for the system assumes that there is a MEMS array of micro-scale ‘catapults’, and each element has one nanoparticle adsorbed to the middle of the surface. An individual nanoparticle is then ejected by activating its catapult, and becomes free flying with a certain velocity, charge, and direction towards the optical bench.

A means to control the delivery and steering to the optical bench is not yet incorporated in the baseline until there is a better understanding of the MEMS array feasibility and capability (including validating assumption 1 above). However, a means based on magnetic steering or electrostatics is envisioned.

Finally the nanoparticles arrive at the optical bench, and are captured by a Paul trap (i.e. radiofrequency electromagnetic trap) which is overlaid with the optical cavity. The nanoparticles are charged (assumption 2 above) which makes this trapping possible.

The feasibility along with some parameter estimations are presented in the following sections.

9.4.2 MEMS Array Catapults

In this solution the nano-particle is mechanically accelerated to the required direction such as to overcome the adhesion forces of the particle to the underlying mechanical structure (eg. beam, membrane, plate). As each particle has a dedicated catapult, a large array of catapults loaded with a nanoparticle is necessary. At this stage there are two major challenges to be solved. Those are the catapult function (1) for releasing the particle and the fact that one nanoparticle needs to be well positioned on each catapult (2). The catapult can only be functional if the mechanical force experienced by the particle is larger than the adhesion force of the particle to the catapult. Such a catapult could be based for instance on a suspended beam, as seen in Figure 9-1 and Figure 9-2, a deformable membrane or cantilever beam. The catapults need to be manufactured in a large array where they can be actuated individually. A possible actuation approach is to bring the catapult with the particle in to resonance with a low actuation force (e.g. electrostatic) and then to gradually increase the actuation force until the particle is released (expected timescale less than milliseconds). This avoids a too large acceleration which could lead to a too high particle speed for subsequent trapping. As an option, the particle presence on the catapult could be monitored such as to sense the successful particle release.

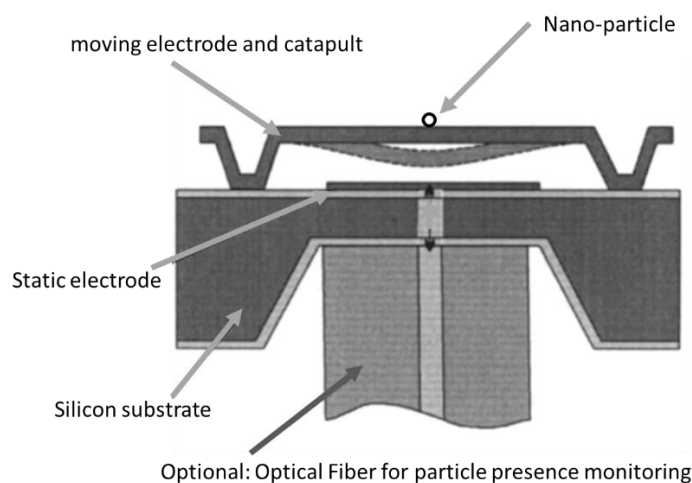


Figure 9-1: drawing of a particle launch element based on MEMS technologies. The upper membrane is pulled by electrostatic forces and serves as launch pad for a particle placed in the middle (figure based on Fig. 3 from Ref. RD[29])

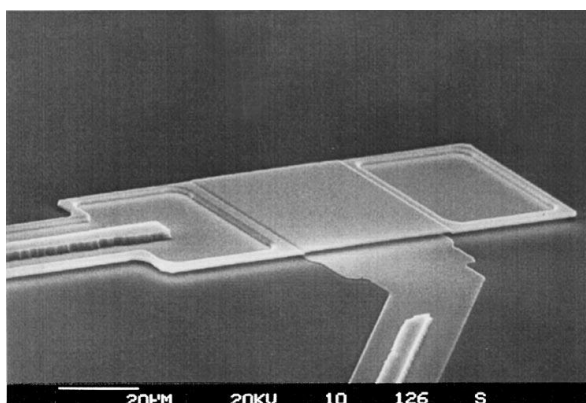


Figure 9-2: Realization of a micromechanical modulator which could serve as a particle catapult RD[29]

9.4.2.1 Parameter estimation

Based on the concept shown in Figure 9-1, Figure 9-2 RD[29], a bridge type suspended polysilicon beam (ends fixed), following catapult design parameters have been calculated (based on a particle mass in the middle of the range, $\sim 7 \times 10^8$ a.u.):

Mass of the particle to be released:	1.2×10^{-18} kg
Beam width:	40 μm
Beam length:	40 μm
Beam thickness:	1 μm
Nominal gap between electrodes	1.5 μm
Assumed full stroke without pull-in :	473 nm
Static full stroke with pull-in	1.5 μm
Surface stress at full stroke:	0.6×10^9 Pa

Surface stress in case of pull-in	1.9×10^9 Pa, above yield (1.2×10^9 Pa)
Force on beam at full stroke RD[30]:	1.5 mN
Resonance frequency:	2.1 MHz
Acceleration of the catapult surface:	2.15×10^8 m/s ²
Acceleration force on particle:	2.63×10^{-10} N
Static actuation voltage:	505 V

The catapult is in this baseline design actuated electrostatically between the moving launch platform and the static electrode underneath. As the actuation voltage increases, the gap decreases until an unstable or collapse condition is reached. For this type of plate actuators the critical pull-in gap distance is at two third of the full nominal distance. This means that only one third ($0.5 \mu\text{m}$) of the nominal gap ($1.5 \mu\text{m}$) between the launch platform and the electrode can be used for stable actuation. The calculation results shown above are based on a static actuation where 505 V are required to pull the launch platform down by 473 nm. In vacuum and working in a dynamic actuation mode, at or close to the resonance frequency, much lower voltages (<50 V) would be needed to reach the required stroke. It must be noted that the surface stress of the platform made of polysilicon once it snaps in, meaning that the platform collapses and enters in contact with the static electrode, increases to values above the yield stress. This means that the design must be modified (e.g. blockers, different design, different materials) in order to be safe. The force reached of the particle, by being accelerated by the platform, is 0.26 nN.

Therefore considering assumption 1 (that the vdW attraction can be reduced to 0.1 nN), it should be possible to launch the nanoparticles from the MEMS catapult.

Figure 9-1 shows a possible particle launch, “catapult”, with an optional single mode fibre connected to it. The fibre would allow illumination of the particle from underneath in order to know its presence or absence. However, this would require significant effort to multiplex the optical addressing of all the particles. Particle presence detection might be done also by resonance frequency shift detection, as this is done with AFMs for detecting molecules attached to the sensing tip.

The MEMS catapult would need to be arranged in a large matrix. Assumed is a $100 \mu\text{m}$ by $100 \mu\text{m}$ surface allocation for each catapult, with $\sim 15\,000$ particles for each of 15 batches (which gives some margin from the 12 500 particles per batch required). 225000 catapults/particles would require approximately $50 \text{ mm} \times 50 \text{ mm}$ chip surface, which could also be separated into segments if needed.

The positioning of each nanoparticle into the centre of each catapult is the second major challenge for this part of the study. It is assumed that via catapult surface functionalization (e.g. make them spatially hydrophobic/hydrophilic) the particles would self – organize departing from a fluid containing the particles. If this turned out to be not feasible the particles could in a clean but moist environment and at ambient temperature be picked and placed on to the catapults one by one. Then the catapult array with the particles would be put into vacuum in order to make sure the particles adhere by particle to platform Van der Waals forces, as it will be the case in space in vacuum. The adhesion forces of the particles to the platform are so large that they can be considered as shock resistant. (important during launch)

9.4.2.2 Ejection velocity of nanoparticles

Having established that it is feasible to have a MEMS catapult for selective release of the nanoparticles, it is necessary to try to estimate the resulting particle velocities, and consider if it is commensurate with the trapping capability on the optical bench.

The MEMS device offers the flexibility that the driving amplitude can be continuously increased until just overcoming the adsorption force. Then in the worst case, consider that the full energy is converted into the particle's kinetic energy (KE). For this calculation, the key input parameter is therefore the acceleration of the particle as it exits the catapult, which is estimated as $2.15 \times 10^8 \text{ m/s}^2$.

Mass (a.u.)	Acceleration (m/s ²)	KE (J)	V_{max} (m/s)
1×10^8	2.15×10^8	1.3×10^{-9}	120 000
5×10^9			17 000

Table 9-2: estimated upper bound of energy and velocity of particles as they are catapulted

Obviously this is a very rough estimation, and requires some proof of concept testing to more accurately define the exit velocity of the nanoparticles, as well as their direction. It is likely that the process is not purely elastic and thus the estimation above is considered to be the worst case.

9.4.3 Paul Trap

9.4.3.1 Trap geometry and design

A 'Paul trap', so named in honour of Wolfgang Paul who invented the device and was awarded the Nobel prize in 1989 for this work, uses dynamic electric fields to trap charged particles. They are also referred to as quadrupole ion traps, or radio frequency traps. The concept is ingeniously simple – a charged particle experiences a force from an electric field, however it is not possible to confine a charged particle using a purely static electric field (Earnshaw's theorem). Even if a potential is confining in one direction, it will be anti-confining in another. The trick is to vary the fields in time, so that on *average* the force is confining. The reason why a Paul trap is also known as a radio frequency trap is because the field-switching often happens at radio frequencies. An elegant mechanical analogy to this type of trapping potential is a ball on a saddle (see Figure 9-3). When static, it is an unstable equilibrium where the ball will simply roll off the side if perturbed. However if the entire saddle is rotated then the ball becomes trapped in the middle because the rotation occurs faster than the ball can roll out.

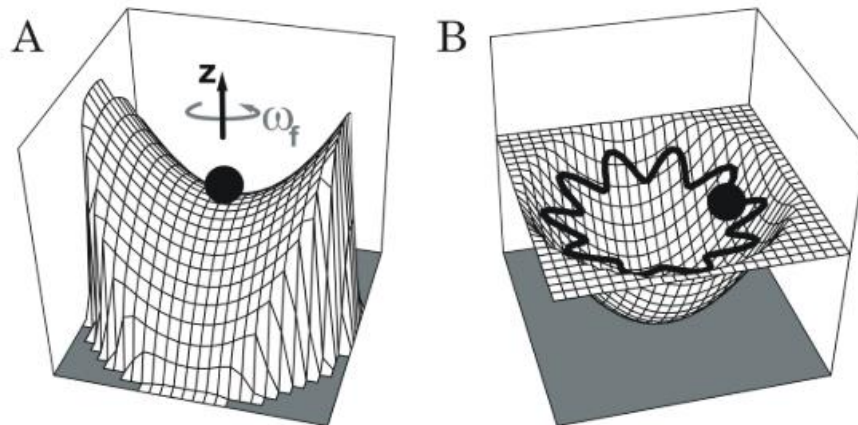
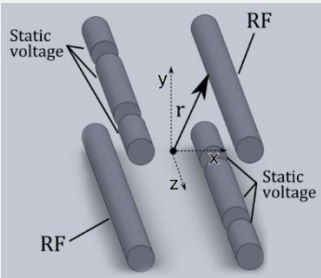


Figure 9-3: mechanical analogy for a Paul trap - a ball on a rotating saddle surface

The Paul trap has become an invaluable tool in ion-trapping research and mass spectroscopy, and there have been a plethora of geometries imagined to achieve the trapping potential, each having advantages and disadvantages depending on particular applications. With the current level of development for the nanoparticle handling in this study, a simple segmented linear Paul trap layout has been selected, which has a very large trapping volume and thus puts the least constraints on the spatial precision with which the nanoparticles need to be loaded into the trap. A summary of some other considered geometries is presented in Table 9-3.

In addition to initially capturing and holding the nanoparticles, the functionality that should be possible to implement in any trap geometry include;

- Precise measurement of the charge of the particle in the trap RD[31]
 - This measurement is necessary in order to have close to neutral particles prior to performing the experiment
- Cooling via feedback through the electrodes RD[28]
 - May be faster than optical cooling for initial temperature reduction.

Trap description	Comments for this application
<p><i>Segmented linear Paul trap</i></p>  <p>Fig 1(b) from Ref. RD[29]</p> <p>Linear Paul trap is so-called because the potential minimum is along a line, i.e. the charged particles are strongly confined only in 2 dimensions. However the</p>	<p>+ Large spatial region where particles can be trapped – injection can be less precise</p> <p>+ Open sides for integration with optical cavity</p> <p>- Larger voltages required because typically electrodes will be further apart (compared to the planar trap for instance)</p>

segmented electrodes allow for DC voltages to provide a confinement also along the z-axis. Actual implementations may look like this 4-rod arrangement, or can be more complicated shaped electrode designs as shown below;

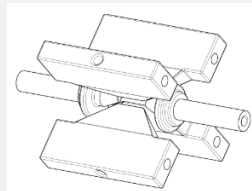


Fig 1 from Ref. RD[33]

Fig 3.1 from Ref. RD[34]

Planar Paul trap

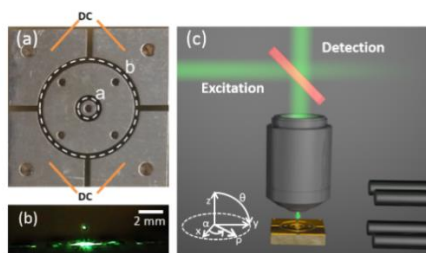


Fig 1 from Ref. RD[35] It is also possible to create a Paul trap with all electrodes in a plane. This offers advantages in terms of manufacturability and miniaturization. The potential energy minimum in this case is located at a point slightly above the plane (out of the page and above point (a) in the above figure).

- + Voltages required are lower due to compact nature
- + Clearance from 5 sides for other access, and allows injection through an aperture directly into the bottom of the potential well
- Region of potential well is small, therefore more precision needed for overlap with cavity optical mode, and UV optical mode

Round electrode configuration

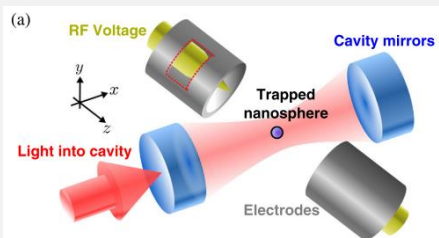


Fig 1 from Ref. RD[27]

This configuration was used to trap and cool ~200nm diameter silica nanoparticles, with 1-3 elementary charges. The electrodes are separated by 1mm (yellow in figure) and are enclosed by grounded cylindrical shields (grey in figure). Trapping is achieved with RF voltages in the range of 300-900 V amplitude, and 1.5 kHz frequency.

- + Demonstrated in an application very similar to this proposal
- + Easily integrated with an optical cavity
- Spatial region of potential well is smaller, therefore more precise loading needed

Quadrupole Paul trap

- + 3-dimensional trapping field allows more precise control over position
- difficult to incorporate with an optical cavity and other optical axis access also.

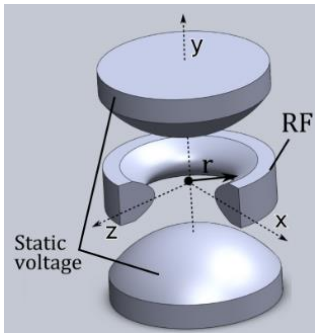


Fig 1(a) from Ref. RD[32]

This design is based on a ring electrode and end caps, usually with hyperbolic surfaces. In this configuration there is a strong confinement in 3 directions.

Table 9-3: Summary of Paul trap geometries considered for this application

The baseline design for the Paul trap is selected as the segmented linear geometry, however this could easily be changed at a later design phase once the nanoparticle loading process is better defined. The Paul trap will necessarily be located on the optical bench, in close proximity to the nanoparticles, and will require significant RF power to drive the trap (typically kV range, with frequencies 100 Hz to 1 MHz). Therefore to minimise the heat load at this critical location, it is considered necessary to use superconducting electrodes and wires.

Ion traps with superconducting electrodes are also used in terrestrial experiments, because in small trap structures the high currents can cause thermal fluctuations or in the extreme breakdown of the trap. Most examples of ion traps made with superconducting electrodes are planar geometries for this reason (see for example RD[36]–RD[38]), however it is considered feasible with current materials and technology to make a macroscopic trap also with superconducting electrodes. This is also a topic foreseen for future development, however it is an engineering challenge to be solved after the nanoparticle storage and release device is developed and its performance understood.

9.4.3.2 Parameter estimation

This section considers the geometrical constraints on the Paul trap design, and then determines the driving RF that can be applied.

It is envisaged initially that the segmented linear Paul trap is oriented with the axis parallel to the axis of the high finesse optical cavity. This is considered advantageous because the motion of the nanoparticles along this axis can then be controlled, and the injection point where the particles are introduced into the trap can be spatially separated from the region where the UV beam overlaps with the cavity mode (which could be used to discharge the particles).

The spacing between the 4 electrodes of the Paul trap should be minimised to achieve strong electric fields with as low voltage levels as possible, and also the RF frequency that can be applied will be lower if the electrodes are further apart. However the electrodes should be placed as far away as possible from the cavity optical mode,

because if there is any clipping of the mode it will reduce the cavity finesse. Moreover, having these electrodes nearby the nanoparticle experiment will be a source of stray light. Therefore a reasonable compromise between these parameters has to be found.

The input parameters for the optical cavity are as follows;

Cavity length	L	97.5 mm
Radius of curvature of mirror 1	R_1	75 mm
Radius of curvature of mirror 2	R_2	30 mm
Wavelength	λ	1064 nm

Table 9-4: Optical cavity parameters

These parameters can be used to calculate the following properties for the lowest-order spatial mode of the cavity (Gaussian TEM₀₀ mode);

Beam waist at minimum	ω_0	63 μm
Location of the beam waist		L/4 from mirror 2 (24.4 mm) 3L/4 from mirror 1
Beam waist at mirror 1	ω_{R1}	398 μm
Beam waist at mirror 2	ω_{R2}	145 μm

Table 9-5: Calculated optical mode properties for TEM₀₀ cavity mode

The Paul trap needs to be overlapping with the waist of the optical cavity, since this is location where the UV beam overlaps with the cavity mode, and it is intended that this UV light could be used for discharging the particles. Aside from simply delivering the charged nanoparticles to this location, the Paul trap electrodes are also providing a means for monitoring the particle's charge while it is being neutralised. Therefore the length of the electrodes is assumed to be ~ 44 mm, and centred around the beam waist. This gives a few mm clearance to the mirror 2, but in principle this is not a critical parameter and the electrodes could easily be extended in the opposite direction if necessary.

The smallest acceptable distance between the electrodes and the axis of the cavity is taken to be $4 \times \omega_{R2}$, or 0.54 mm. To give some additional margin to reduce the risk of stray light affecting the measurement SNR, this radial distance from cavity axis to electrodes is set at 1.5 mm, meaning that the spacing between electrodes of the same phase (i.e. the two RF electrodes) is taken as 3.0 mm.

Having established the basic geometrical features of the Paul trap, the driving voltages necessary to trap the nanoparticles is estimated. The dynamics of the Paul trap are determined by solving the equations of motion for the charged particle in a quadrupole potential in the x - y plane, and a DC potential along the z -axis (a form of Mathieu's differential equation). There are many good references with detailed derivations (for instance, see RD[39]), and therefore only the basic equations and simplified solutions

will be presented here. The solution for the motion of the particle in the trap along the x -dimension (which is analogous to the y -axis) can be written in the form;

$$x = x_0 \cos A\tau \{1 + B \cos 2\tau\} \quad \#(1)$$

where $\tau = \Omega t/2$, Ω is the angular frequency of the RF voltage and t is time. The motion can be considered in two parts; a 'slow' or 'secular' part, characterised in frequency by the constant A , and a faster oscillating term, the 'micromotion' with amplitude scaling with B . An approximate solution for these values gives;

$$\begin{aligned} A &= -\frac{q}{\sqrt{2}} \\ B &= -\frac{q}{2} \\ \text{where } q &= \frac{2KV_{RF}}{\Omega^2 M r_0^2} \cdot \#(2) \end{aligned}$$

Here K is the net charge of the particle, V_{RF} is the amplitude of the applied RF voltage, M is the mass of the particle, and r_o is the distance between the RF electrode pair. Note this solution has ignored the confinement along the z -axis, but the DC voltages applied to achieve this weak confinement are not affecting the solution significantly. Also in practice, field imperfections (i.e. deviations from an ideal quadrupole field due to non hyperbolic shaped electrodes, misalignment, external potentials etc.) lead to the existence of nonlinear resonances. Therefore the values derived here can be taken as rough estimates, to be refined once the detailed electrode geometry is better defined.

The condition for a stable motion (i.e. closed orbits within the trap) is to have $q \leq 0.9$. In practice there are a number of general factors to be considered RD[34];

- It is favourable to choose $q < 0.5$ to avoid nonlinear resonances
- Achieving high RF frequencies becomes difficult as the electrode separation becomes larger. Separation in this application should be large so as to minimise stray light, therefore solutions with $\Omega < 1\text{MHz}$ should be sought.
- Strong axial confinement would require high end-cap voltages, or small distance between the end DC electrodes. For this application the confinement provided by the Paul trap along the z -axis is considered to be weak, since the optical cavity mode could be used for additional control along this axis.

The above conditions can be used to determine the selected driving frequency for the trap. Then the next question to answer is - how energetic can the nanoparticles be upon injection into the trap. To determine the potential energy of the nanoparticle in the trap, it is necessary to consider the secular part of the motion from equation (1), and substitute for τ to obtain the angular frequency of the harmonic motion undergone by the particle ω ;

$$\omega = \frac{q\Omega}{2\sqrt{2}} = \frac{KV_{RF}}{\sqrt{2}\Omega M r_0^2}$$

This is again assuming the radial motion (in x - y plane) is much more energetic than that along the z -axis. The maximum amplitude of the motion is given by the electrode spacing, therefore the potential energy depth of the trap U_0 is given by;

$$U_0 = \frac{1}{2} M \omega^2 r_0^2$$

In Table 9-6, the trap stability parameter q , potential depth of the trap, and the maximum kinetic energy of the particle to be captured by the trap V_{max} , are calculated assuming an RF driving frequency of;

$$V_{RF} = 1000 \text{ V}$$

$$\Omega = 2\pi \times 500 \text{ Hz}$$

Mass (a.u.)	Charge (Q)	q	U_0 (J)	V_{max} (m/s)
1×10^8	1×10^4	0.22	$4.4 \times 10^{-14} \text{ J}$	720
5×10^9	1.4×10^5	0.06	$1.7 \times 10^{-13} \text{ J}$	202

Table 9-6: parameters of the trap as experienced by different families of particles (i.e. mass and charge variation)

9.4.4 Summary of Baseline Design Parameters

The key properties of the elements in the baseline design can be summarised as follows;

MEMS catapult array

- Nanoparticles are pre-loaded on ground such that there is one particle at the centre of the MEMS catapult element
- The MEMS catapult area is $40 \mu\text{m} \times 40 \mu\text{m}$, and with surrounding infrastructure assumed to have a total footprint of $100 \mu\text{m} \times 100 \mu\text{m}$
- It seems feasible to design such a device based on polysilicon structures
- The particle can be accelerated to $2.15 \times 10^8 \text{ m/s}^2$, which is sufficient to overcome an adhesion force of 0.26 nN for a nanoparticle in the middle of the range foreseen for the experiment batches
- Maximum velocities of the particles exiting the catapult if all energy is converted into motion is in the range $17\,000 - 120\,000 \text{ m/s}$ (energy 1.3 nJ)

Transport to optical bench

- No elements planned for currently, until storage and release is better understood
- However if current estimations are accurate, the energies of the nanoparticles after desorption (1.3 nJ) are too large to be caught in the Paul trap (potential depth of trap $\sim 0.0002 \text{ nJ}$), and some means of slowing the particles would be necessary.

Paul trap on optical bench

- Design geometry selected is a segmented linear Paul trap

- Spacing between the RF electrodes (diagonal distance in the 4-electrode arrangement) is 3 *mm*
- Driving voltage applied to RF electrodes:
 - Amplitude ~1 kV
 - Frequency ~ 500 Hz
- Trap electrodes are used for initial electronic-feedback cooling, and also for measurement of charge while particle is being neutralised.

9.5 List of Equipment

Due to the novel nature of the proposed baseline solution, the list of equipment for this sub-system, in Table 9-7, requires further definition. The mass of the payload assumed for the study has been extracted from the Table 18 of RD[2]. Power, mass and size estimate for the internal loading unit have also been extracted from RD[2], with the removal of the particle characterization unit.

Equipment	Mass [kg]	Mass margin [%]	Mass including margin [kg]
PHU (Particle Handling Unit)	28.00	30.00	36.40
LED_Assembly (UV LED Assembly for Particle Desorption and Charging)			
Particle_Select_Wheel (Particle Selection Wheel)			
Particle_Steering (Particle Beam Steering)			
Particle_Storage (Particle Storage Container) [15 units]			
Paul_Trap (Paul Trap Electrodes)			
Grand Total	28.00	30.00	36.40

Table 9-7: Equipment list

9.6 Technology Needs

Technology Needs						
*	Equipment Name & Text Reference	Technology	Supplier (Country)	TRL	Funded by	Additional Information
1	MEMS based nanoparticle storage and release system	MEMS Means for loading particles onto device (AFM for pick & place, or bulk self-assembly) EGSE for measuring release		2		First priority development for this system, to evaluate feasibility and define perimeter for further developments

		direction, charge state etc. of nanoparticles				
2	Paul Trap for trapping and state preparation of nanoparticles	Superconducting electrodes		3		Follow-on after activity 1
3	Transportation of nanoparticles to optical bench	Electromagnets, or permanent magnets Electrostatic plates		3		Follow-on after activity 1

* Tick if technology is baselined

This Page Intentionally Blank

10 PROPULSION

10.1 Requirements and Design Drivers

SubSystem Requirements		
Req. ID	Statement	Parent ID
PROP-010	The propulsion subsystem shall include no moving fluids impacting the scientific payload	
PROP -020	The propulsion subsystem shall have sufficient propellant mass onboard to fulfil the Δv demands including the stationkeeping	
PROP -030	The propulsion subsystem shall provide the propellant mass for a lifetime of 3 years	
PROP -040	The propulsion subsystem shall provide the deorbiting function of the spacecraft	
PROP -050	The propulsion subsystem shall provide the measurement systems to maintain the functionality and to investigate the system state during the mission	
PROP-060	The propulsion subsystem shall include the measurement system to analyse the propellant mass left inside the tank during the mission	
PROP-070	The propulsion subsystem shall provide a minimum thrust of 1 N for the main Δv manoeuvres at begin of life	
PROP-080	The propulsion subsystem shall provide a maximum of 1 mN throughout the operational mission phase	
PROP-090	The propulsion subsystem shall ensure that no leakage of the 1 N branch throughout the mission operational phase can occur	
PROP-100	The propulsion subsystem shall include the safety measures for on-ground testing and launch	
PROP-110	The propulsion subsystem shall be one fault tolerant	

10.2 Assumptions and Trade-Offs

Assumptions	
1	The firing efficiency of the thrusters is assumed to be 95%
2	The residual of the propulsion system for EoL is assumed to be 10bar
3	The propulsion system for the main Δv manoeuvres can be built in a symmetric configuration

10.3 Baseline Design

The baseline design for the spacecraft consists of a cold gas system used for the main Δv manoeuvres as well as for the station keeping and the science mode. Due to the Δv demands in relation to the thrust, different sets of thrusters are used for the Δv 's and the station keeping/science mode manoeuvres. Due to the requirement PROP-090, the

thruster branch for the 1 N thrusters are closed with normally open pyrovalves after the main Δv manoeuvres. The current schematic of the propulsion system is shown in Figure 10-1.

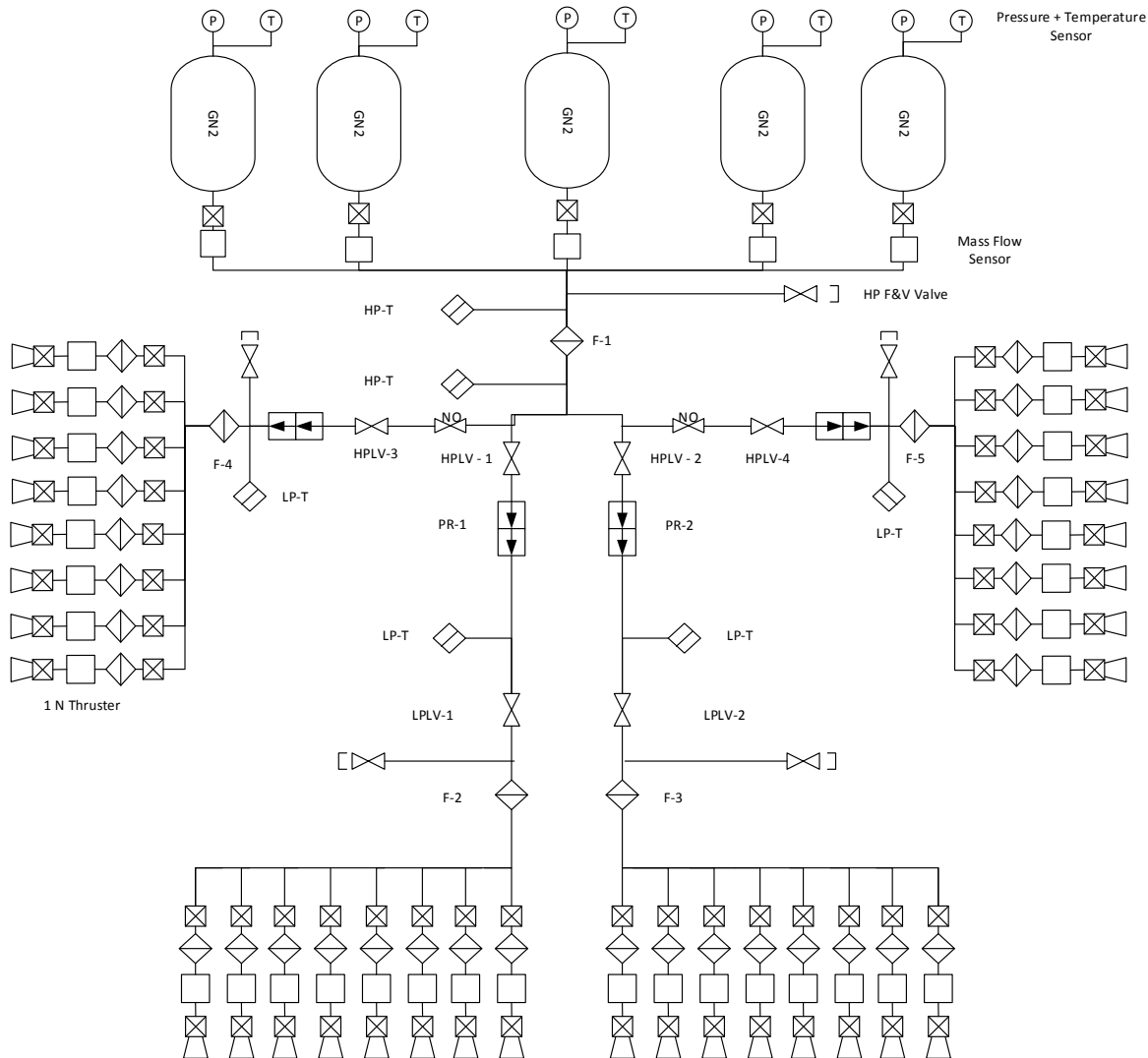


Figure 10-1: Propulsion subsystem schematic

The system was implemented in this way to have one central tank and four tanks surrounding the central core. According to this, the way it is planned to be used is to drain the tanks which are positioned outside the central core and then to use the central core for the last remaining Δv manoeuvres and the station keeping/science mode during the operational mode. The idea behind is that due to the usage of the central core and therefore only one tank during the operational phase, any kind of fluidic movement is reduced to a minimum to avoid disturbances of the science objective.

Due to the different requirements in terms of thrust, two different sets of thrusters are used. For the main Δv manoeuvres, the 1 N thruster of MOOG are used, see RD[40]. The details of the thruster are provided here:

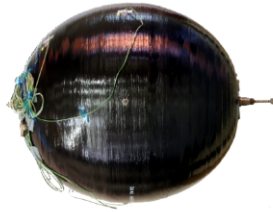
Parameter	Capability or Description
Materials of Construction	Stainless Steel, Vespel
MEOP / Proof / Burst Pressure	2700 / 4050 / 6750 psia (186 / 279 / 465 bar)
Thrust (near vacuum)	1.3 N at 1300 psia (90 bar) Xe, 21°C 0.9 N at 1300 psia (90 bar) GN2 and GAr inlet, 21°C
Isp	21 s at 21°C and 1300 psia (90 bar) Xe inlet 70 s at 21°C and 1300 psia (90 bar) GN2 inlet 54 s at 21°C and 1300 psia (90 bar) GAr inlet
Nozzle Expansion Ratio	>100:1
Internal Leakage	< 1.0 x 10 ⁻⁴ sccs GHe at MEOP
External Leakage	< 1.0 x 10 ⁻⁶ sccs GHe at MEOP
Coil Resistance	74.5 Ω nominal at 21°C
Voltage	28 Vdc nominal, 10 Vdc hold
Response	< 10 ms opening and closing
Pull In Voltage	< 20 Vdc at 2700 psia (186 bar)
Drop Out Voltage	>1.25 Vdc at 50 psia (3.4 bar)
Environmental Temperature Range	-70 to 90°C (-94 to 194°F) non-operating -70 to 60°C (-94 to 140°F) operating
Power	10.5 W nominal at 28 Vdc at 21°C, 1.3 W at 10 Vdc holding voltage
Random Vibration	19.2 grms in plane, 24.7 grms out of plane
Pyro Shock	6,000 g / 4,000 Hz in-plane (with Moog provided bracket)
Cycle Life	>100,000
Filtration	25 micron absolute
Mass	115 g maximum (not including mounting bracket)

Table 10-1: MOOG 58E163A thruster characteristics

The second set of thrusters consist of the widely used Leonardo Finmeccanica thruster (LISA, GAIA, EUCLID).

The 5 propellant tanks come in two sizes. Due to the configuration, the inner core consists of a single 300 l tank currently in development by MT-Aerospace. Around the circumferential, four tanks from ARDE are chosen to accommodate the propellant mass.

M-XTA / 120-300l Family
Xenon Tank



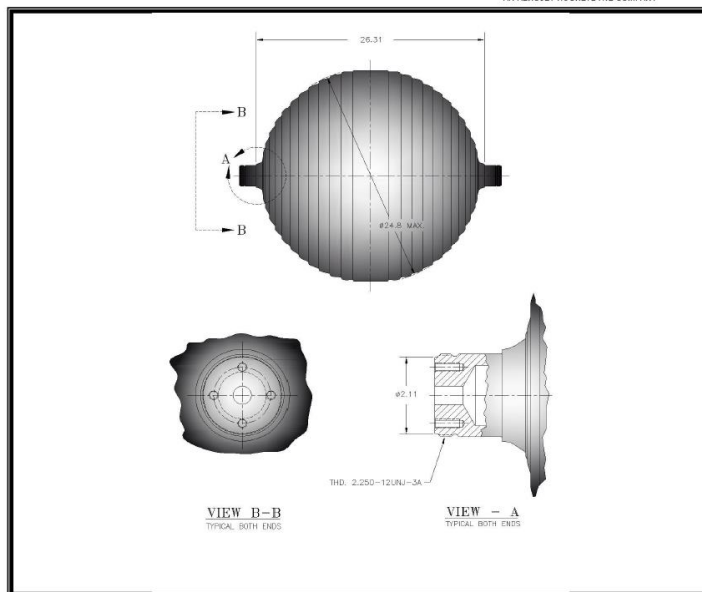
Under
Development

Heritage		
Fluids		Xenon
Materials	Shell	Ti-6Al-4V
	Tube	Ti-3Al-2.5V
Mounting Interface		polar

Total Volume	120 – 300 l	7.323 – 18.307 in ³
Temperature Range	°C	°F
Tank Dry Mass	kg	lbs
Diameter	660 mm	25.98 in
Length	mm	in
MEOP*	300 bar	4351 psi
Proof pressure (x 1.5)	450 bar	6527 psi
Burst pressure (x 3.0)	900 bar	13,053 psi
Burst pressure tested	bar	psi

* Maximum Expected Operating Pressure

Figure 10-2: MT-A 300l tank RD[41]



ARDE Part Number 4293			
Volume (cubic inches)	7300	Material of Construction	
Operating Pressure (psig)	4000	Liner	Cryoformed CRES 301
Proof Factor	1.25	Porting Interface	Mechanical Port
Minimum Burst Factor	1.5	Wrap	Fiber: T-1000
Actual Rupture Pressure (psig)	8190 @ 200F		Resin: ARDE 31-43B
Weight (pounds)	55.0		Liner/Composite Bond=None
Qualification Basis Standard	MIL-STD 1522A	Environmental Vibration Load (He)	Component Qual
	AIAA-S081		Axial 16.47 g _{rms}
			Lateral 16.78 g _{rms}

Figure 10-3: ARDE 4293 tank RD[42]

The other equipment listed in the schematic is not listed separately here.

Due to the requirements for the Δv demands at begin of life and the corresponding requirements for the operational phase, corresponding mission timeline including the input values was used to simulate the system performance:

Manoeuvre	velocity increment [m/s]	propellant mass [kg]
Transfer Correction Manoeuvre 1 Part 1	32.79	78.10
Transfer Correction Manoeuvre 1 Part 2	18.81	43.08
Transfer Correction Manoeuvre 2	1.71	3.86
Transfer Correction Manoeuvre 3	0.67	1.51
Transfer Correction Manoeuvre delay allocation	18.42	40.86
Reaction Control manoeuvres for all TCM's	2.62	5.00
Summation TCM's	75.02	172.41
SK year 1	3.20	7.71
Science Mode year 1	3.25	7.80
SK year 2	3.20	7.63
Science Mode year 2	3.29	7.80
SK year 3	0.64	7.55
Science Mode year 3	0.667	7.80
Decomissioning	10.00	23.19
Summation SK + Science Mode	24.31	57.1

Table 10-2: Propulsion system timeline and input values

These values are based on a dry mass of the system of 1352.68 kg as updated after the IFP and adapted to the tank sizes as shown during the IFP. The values for year 3 of the mission (values should be similar to the values before) are multiplied with a factor (0.2) to calculate the mission lifetime fitting in the tank. With the overall values (for a mission lifetime of 3.5years) and the specific impulse values of the thruster, the volume of the tanks needed for the propellant mass as calculated above is higher than the implemented volume of the tanks, showing an overall mass deficit of around 49.6 l. Therefore, the tank configuration shown during the IFP and using the updated values of the IFP and afterwards lead to a potential mission lifetime of 2.2years.

Due to the impact of the mass change of the system which occurred during the IFP, an additional iteration only on the propellant subsystem was implemented. Due to the restriction of the tanks to keep the height of the tanks as they were during the IFP, additional check of tanks was performed. Since ARDE has as well developed a tank of the same height with a slight increase of volume and pressure, this tank was chosen to calculate the performance again. The best suited tank for this purpose is the ARDE 5016 tank RD[43]

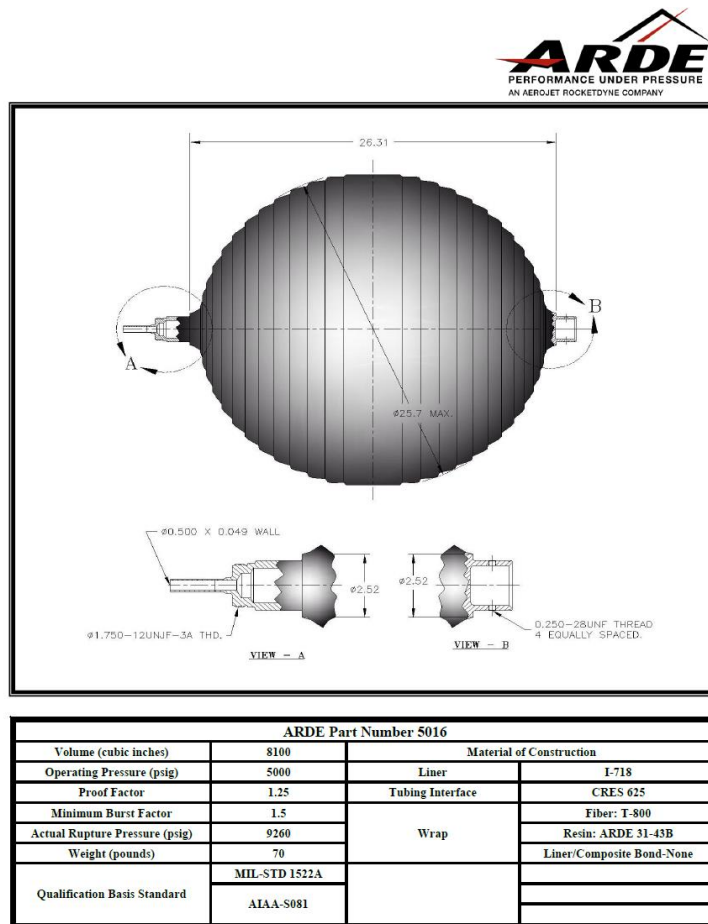


Figure 10-4: ARDE tank 5016

This tank has a slight increase to 132 l instead of 120 l. But the most important increase is the increase of pressure up to 344 bar, allowing the tank to be used for a higher pressure and therefore be able to accommodate more propellant mass. A system, consisting of the MT-Aerospace tank of 300 l and four of these tanks would then lead to a positive margin for the lifetime of three years of 36 l. The higher mass of the tank is then leading to a dry mass increase of the system (including the system margin of 30%) to 1389.81 kg. This is due to the change of the dry mass of the propulsion system from 208.58kg to 237.15kg. The propellant inside the tanks is then up to 257.1kg for all five tanks (propellant needed for all 3.5 years for the new dry mass is 252.1kg. This leaves a margin of 5kg (2%) of the propellants. The updated tank has not been taken into account in system design or any of the subsystems. This should be done in a next iteration.

10.4 List of Equipment

	mass (kg)	mass margin (%)	mass incl. margin (kg)	Number of items (-)	Total mass (kg)
SC (Spacecraft)	180.88	10.83	200.47		
SM (Service Module)	180.88	10.83	200.47		200.47
Cold_HP_Filter (Coldgas_HP_Filter)	0.11	5.00	0.12	1	0.12
Cold_HP_FVV (Coldgas_HP_FillVent_Valve)	0.25	5.00	0.26	1	0.26
Cold_HP_T (Coldgas_High_Pressure_Transducer)	0.23	5.00	0.24	2	0.48
Cold_HPLV (Coldgas_Latch_Valve_HP)	0.40	5.00	0.42	4	1.68
Cold_LP_Filter (Coldgas_LP_Filter)	0.18	5.00	0.19	4	0.76
Cold_LP_FVV_1 (Coldgas_LP_FillVent_Valve #)	0.25	5.00	0.26	4	1.04
Cold_LP_T(Coldgas_Low_Pressure_Transducer)	0.23	5.00	0.24	4	0.96
Cold_LPLV (Coldgas_Latch_Valve_LP)	0.34	5.00	0.36	2	0.72
Cold_Pipes (Coldgas_Pipes)	15.00	20.00	18.00	1	18.00
Cold_PR(Coldgas_Pressure_Regulator)	1.13	5.00	1.19	4	4.76
HT_CGT(HighThrust_Coldgas_Thruster)	0.12	5.00	0.12	16	1.92
LT_CGT (LowThrust_Coldgas_Thruster)	0.40	5.00	0.42	16	4.32
NO_PV_1 (NO_Pyro_Valve #1)	0.16	20.00	0.19	2	0.38
Prop_Tank (Central_Propellant Tank)	55.00	20.00	66.00	1	66.00
TCM_Prop_Tank(TCM Propellant Tank)	24.95	5.00	26.19	4	104.76
Grand Total	188.6	10.59	208.58		

Table 10-3: Propulsion system equipment list

10.5 Options

10.5.1 Hydrazine Propulsion System

Due to the high propellant mass of the system, an additional hydrazine propulsion system was investigated for the overall mission. For this, the current dry mass of all subsystems was used and the additional propulsion system was added as new baseline dry mass. The schematic of such a system is the following:

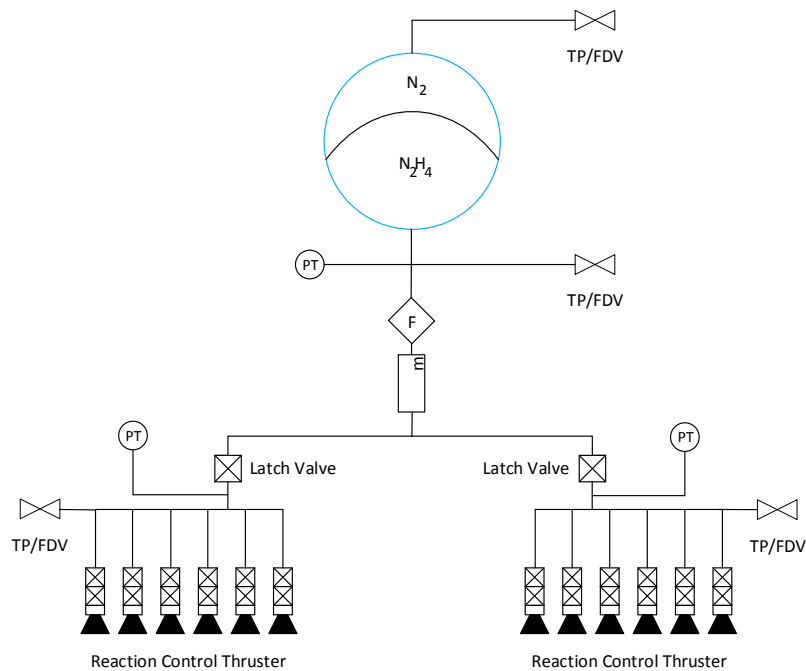


Figure 10-5: Hydrazine propulsion subsystem schematic

For the thruster, an unbalanced configuration leading to a higher Δv demand during the beginning of life manoeuvres was implemented. The thrusters are based on the Airbus 1 N thruster, the tank is manufactured by MT-Aerospace with a volume of 177 l. The propellant mass needed for the entire mission including an extension of two years is 90.5 kg, not including residuals of the propellant mass.

This hydrazine propulsion system is composed of the following equipment:

Equipment	Supplier	Amount	Mass per unit [kg]	Margin [%]	Mass incl. margin [kg]
Piping	Pipes	1	5	20%	6
Thruster	CHT-1N	12	0.29	5%	3.654
Tank	MTA PTD-177	1	15.5	5%	16.275
Pressure transducer	Moog Bradford - SAPT SAPT	3	0.23	5%	0.7245
Low pressure Fill & Vent valves	Nammo Cheltenham	4	0.09	5%	0.378
Low pressure filter	VACCO F1D10638-01	1	0.11	5%	0.1155
Mass flow meter	Bradford Ultrasonic Flow Meter	1	1.4	5%	1.47
Low pressure latch valve	MOOG	2	0.362	5%	0.7602
Total			22.982		29.3772

Table 10-4: Option of Hydrazine Propulsion System

10.5.2 Earth Trailing Option – Cold Gas System

An additional option investigated during this study was due to a different orbit, the Earth trailing orbit. In this orbit, the propulsion system is only used throughout the operational phase (station keeping and science mode), leading to a significant decrease of the Δv demand. For this, a corresponding cold gas system was chosen. The following schematic shows the system:

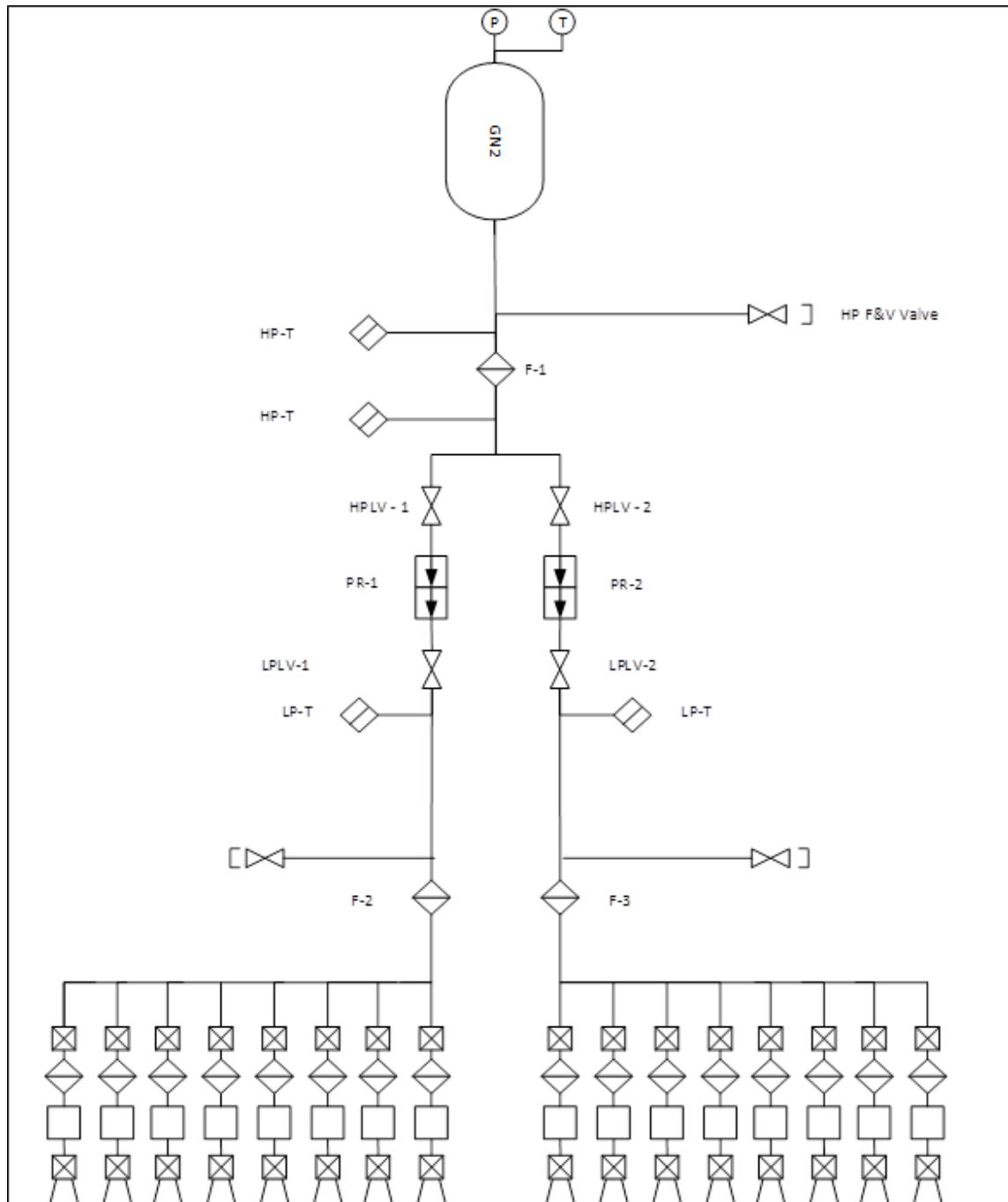


Figure 10-6: Trailing orbit cold gas system option

This system was originally studied but discarded in the middle of the study. Due to this, the system was not calculated by using the dry mass values mentioned above and this report therefore does not include the final propellant mass values nor the equipment list of this option.

10.5.3 Electric Propulsion

While the Δv requirements for the various manoeuvres do not necessarily imply a potential use of electric propulsion technology, the restrictions in terms of usable propellants and resulting high wet mass of the cold gas system as well as the AOCS requirements on fine-pointing and minimum impulse bits entail a trade-off with existing EP technologies.

For the lion's share of the Δv , i.e., TCM, stationkeeping, and decommissioning, a propulsion system based on Hall thruster technology (PPS-1350 from Snecma-Safran) is a likely candidate due to the relative higher thrust and flight heritage (e.g. on SMART-1). Since the required Δv is small for this technology, reducing the nominal operation point to about half the power input of 825 W is sufficient to require only about 10 kg of xenon propellant and about 40 kg of dry mass (depending on redundancy concept and eventual requirements). The electric power subsystem would increase in mass accordingly to be able to provide the 825 W during the manoeuvres. However, the nominal thrust of about 50 mN at this operation point is significantly lower than the required thrust of 1 N for the TCMs, and it was pointed out by Mission Analysis that such a low thrust might risk to lose the S/C. A chemical high-thrust option was therefore chosen for the TCMs. Since a hybrid solution of using chemical and electric propulsion architectures was deemed too complex and expensive, the trade-off was closed in favour of an all-chemical architecture (i.e. cold gas). For the Earth trailing option, since no TCM is required, an electric propulsion option might be able to reduce the system mass, but no detailed trade-off was performed during this study.

As for the fine-pointing thrusters, electric options like pulsed plasma thrusters (PPT), field-emission electric propulsion (FEED) and radio-frequency ion thrusters (μ RIT) can provide very accurate and miniscule impulse bits at much higher specific impulses than cold-gas thrusters, while also not using liquid propellants. The existing cold-gas chemical propulsion architecture for the main propulsive tasks, however, facilitates the addition of fine-pointing cold-gas thrusters, and therefore reduces their mass increase and complexity. Consequently, the trade-off closed in favour of the cold-gas option. Refined and/or changed requirements in later phases might, however, shift the trade-off towards an electric option, e.g., then with technologies like the PPTCUP (Mars Space) or the IFM Nano (Enpulsion).

10.6 Technology Requirements

The following technologies are required or would be beneficial to this domain:

Included in this table are:

- Technologies to be (further) developed
- Technologies available within European non-space sector(s)
- Technologies identified as coming from outside ESA member states.

Equipment and Text Reference	Technology	Suppliers and TRL Level	Technology from Non-Space Sectors	Additional Information
MT-A 300l tank	Development of the tank	MT-A		
NO Pyrovalves	Squibs for normally open pyrovalve without REACH restriction			

This Page Intentionally Blank

11 AOCS/DFACS

11.1 Requirements and Design Drivers

The payload/system requirements applicable to the AOCS/DFACS system are interpreted as follows:

SubSystem Requirements		
Req. ID	Statement	Parent ID
AOCS-010	The Spacecraft Position/Attitude during each measurement run (typically 40s) should be such that the Test Particle remains within 1mm of the release position in the optical bench rotating frame .	
AOCS-020	<p>The Spacecraft Position/Attitude evolution over a given set of measurement runs should be such that the repeatability of the Test Particle position at the end of each experiment remains within 14nm along the sensitive axis (x) in the optical bench rotating frame</p> <p>OR</p> <p>The test particle position due to spacecraft motion during each measurement run can be measured and corrected with higher accuracy than 14nm along the sensitive axis (x) in the optical bench rotating frame</p>	

These requirements could have been further apportioned into spacecraft attitude and position requirements. However, since the spacecraft position and attitude dynamics are highly coupled into the relative position of the particle in the rotating/translating spacecraft, it has been chosen to keep these requirements at optical bench level. Thus, full spacecraft-test mass dynamics are used for analysis of the test particle, leaving more room for trading-off spacecraft position and attitude requirements.

In addition, the second requirement AOCS-020 is a dual requirement. In order for the experiment to be successful, one of the two options must be fulfilled, but not necessarily both. Either the spacecraft must remain quiet enough to guarantee experiment success, without necessarily measuring the test particle; or a measurement system must be in place to guarantee that the test particle position can be known in the spacecraft frame and corrected for any spacecraft motion. Both options are explored since such a stringent requirement is at the edge of feasibility for currently known systems.

11.2 Assumptions

Assumptions	
1	Body Frame (BF) fixed to the spacecraft body, centred at the Centre of Mass (CoM)
2	Optical Bench Frame (OBF) fixed to BF, centred at the Test Particle (TP) release point
3	OBF is a rotating frame
4	The TP is released 1m below the CoM, with a 10mm offset along x (both + or – directions)

Assumptions	
	are considered to find the worst case)
5	The spacecraft Centre of Pressure (CoP) is 1m above the CoM, with a 10mm offset along x (both + or – directions are considered to find the worst case)

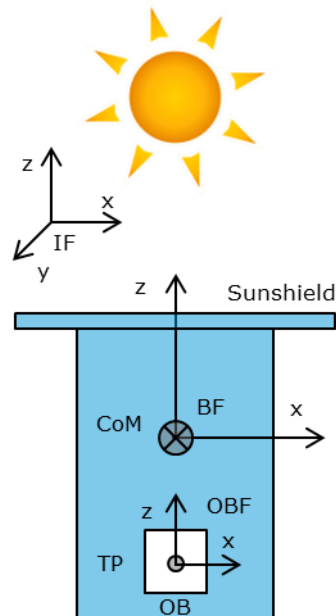


Figure 11-1: Reference Frame Definitions

Numerical Assumptions for Simulations	
S/C Mass [kg]	1000
Inertia [kg*m ²]	Diagonal [1000 1000 500]
Sunshield Area [m ²]	15
Sunshield Coefficient of Specular Reflection	0.6
Sunshield Coefficient of Diffuse Reflection	0.2
OBF Position in S/C frame [m]	[-0.01 0 -1]
Centre of Pressure [m]	[0.01 0 1]
Experiment Duration [s]	40
Initial S/C Angular Rates [as/s]	[0 0.1 0]'
Initial S/C Angles [as]	[0 10 0]

Table 11-1: Numerical Assumptions for Simulations

11.3 Trade-Offs/Options

As mentioned earlier, the TP position in the rotating frame is affected by both SC position and attitude. In order to ensure experiment repeatability, either the spacecraft motion (Optical Bench motion) relative to the TP must be below the experiment repeatability; or it must be measured and corrected for in post processing. Regardless of

the strategy, an appropriate sensor yielding better accuracy than the requirements during one measurement run is needed to ensure repeatability. In addition, there is also the option of ensuring repeatability implicitly without any measurements, by ensuring via analysis that the repeatability requirement is met. The options that might be feasible for QPPF, which are further explored below are as follows:

1. The use of off the shelf accelerometers for position sensing and/or control
2. The use of a dedicated ultra-high accuracy sensor such as the Lisa Pathfinder Inertial Sensor for position/attitude sensing and/or drag-free control
3. The use of high accuracy star trackers or gyros for attitude sensing/control
4. Ensuring repeatability implicitly via a free-drifting experiment both in attitude and/or position without the need for correction using sensors.

All these options are analysed further in the following sections.

11.3.1 Off the Shelf Accelerometers

Accelerometers can be used to propagate the spacecraft position from a given initial condition, which can then be used to correct the Test Particle position for spacecraft position drift. However, the test particle (TP) will drift with respect to the spacecraft due to internal forces not measurable by the accelerometer, such as spacecraft to TP self-gravity. Nevertheless, the effect of these internal forces might be repeatable and not affect the repeatability of the experiment.

The plot below shows the uncertainty in position resulting from the integration with a accelerometer of a given uncertainty over time. This plot shows that to achieve a $\sim 14\text{nm}$ measurement accuracy over a 40s experiment an accelerometer with an accuracy of $\sim 10^{-11} \text{ m/s}^2/\sqrt{\text{Hz}}$ is needed.

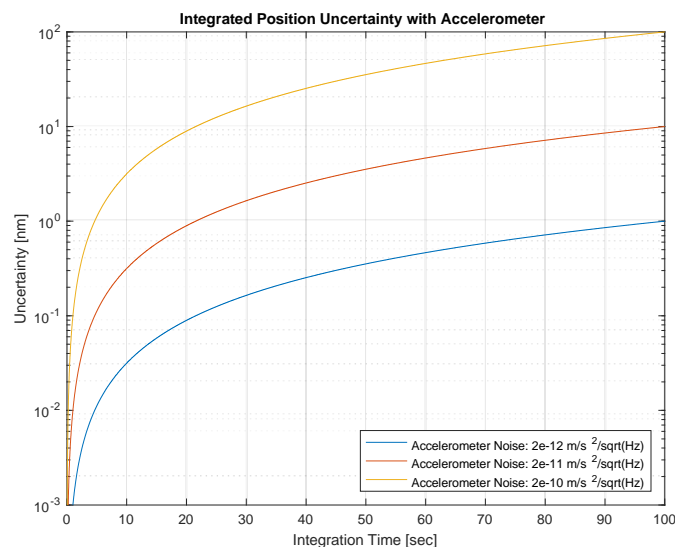


Figure 11-2: Accelerometer Position Uncertainty

However, the best available off the shelf accelerometer for space applications has an accuracy of about $\sim 10\mu\text{g}$ ($\sim 10^{-4} \text{ m/s}^2$), which is seven orders of magnitude worse.

Therefore, no off the shelf sensor, current nor in development, can meet the required performance for this mission.

11.3.2 Lisa Pathfinder Inertial Sensor as an Accelerometer

The alternative to off the shelf sensors is to explore the use of custom built sensors high accuracy sensors such as the Inertial Sensor flown in the Lisa Pathfinder (LPF) mission and their successors being developed for the Lisa mission.

In order to understand the measurement principle and published results of the LPF mission, the figure below shows the high accuracy measurements that were available, along with their accuracies.

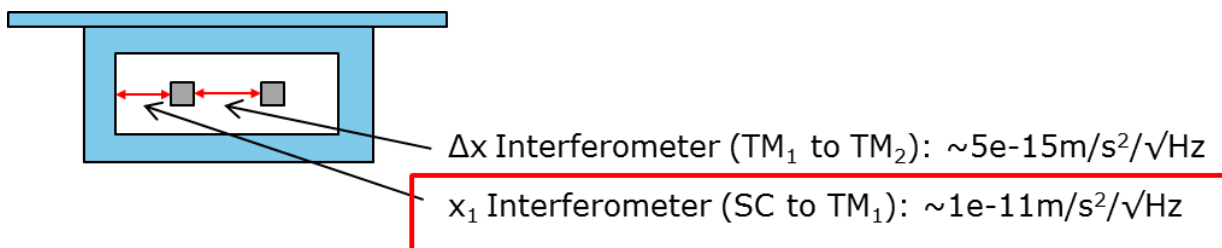


Figure 11-3: Lisa Pathfinder High Accuracy Measurements

In LPF, two Test Masses (TMs) were free floating inside the spacecraft. Along the sensitive axis, where the high accuracy measurements were available, TM2 (right) was controlled using an electrostatic suspension system to follow TM1 (left), while the spacecraft was controlled using its thrusters to follow TM1 in drag-free. The ultra-high accuracy differential acceleration noise achieved in LPF was the relative or differential acceleration (Δx) between the two test masses. The spacecraft jitter was thus common to the two test masses, and therefore not present in the high accuracy measurement.

Since in QPPF there is no direct measurement of the Test Particle, no differential acceleration measurement is possible. Therefore, if an LPF payload-like instrument is to be used in QPPF it would be employed as an accelerometer to measure spacecraft accelerations by measuring TM to spacecraft accelerations, equivalent to the x_1 measurement in LPF. This measurement had just enough accuracy in LPF to meet the 14nm requirement of QPPF.

The position control jitter of x_1 in LPF was about 10nm @ 10^{-2} Hz (100s). This implies that with a drag-free system equivalent to LPF, QPPF could achieve the 14nm performance requirement (AOCS-020) for experiment durations around 100s. However, the cost of such a sensor is currently estimated for the Lisa mission to be about 50MEUR per sensor head. QPPF would potentially require two heads in order to also correct for spacecraft attitude motion during the experiments, as the LPF sensor rotational measurements are based on electrostatics which have a lower accuracy. This option is not investigated further due to the fact that it may only provide marginal performance at a high cost and complexity.

11.3.3 Attitude Sensing/Control

The figure below provides a first approximation to analyse the impact of spacecraft attitude motion into test mass motion. Note that this analysis is applicable to both actual attitude motion (control errors), as well as attitude sensing errors when the angles are taken as the sensing uncertainties.

In the proposed QPPF configuration, the test mass will be at a distance (R) from the centre of mass, nominally along the axis pointing to the Sun (Z). Regardless of the orientation of this offset, the displacement of the test particle in the Optical Bench (OB) frame due to a small angular change in the spacecraft attitude can be represented as shown in the right side of this figure.

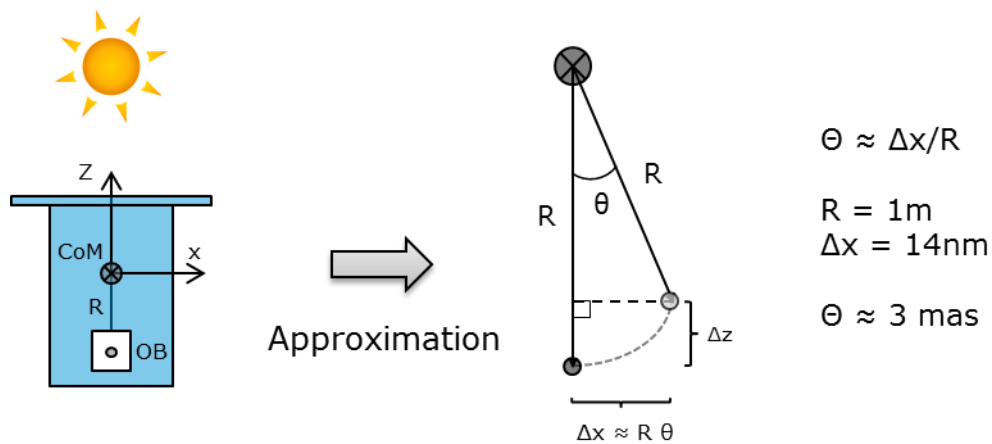


Figure 11-4: QPPF Attitude Couplings into Test Particle Position

This approximation shows that there will be two components to the displacement, one larger (Δx) and one smaller (Δz). Ideally, in order to minimise the couplings, the sensitive experiment axis should be placed along the smaller displacement direction (Δz). However, in the proposed QPPF configuration this is not possible due to the fact that the Solar Radiation Pressure (SRP) will produce an acceleration along this direction, which will be dominant. Therefore, with the proposed QPPF configuration the sensitive experiment axis is along the spacecraft X axis, which will be perpendicular to the offset (R).

With this configuration, the spacecraft attitude on test particle position along the sensitive experiment axis can be quantified as shown by the figure. Assuming a 1 meter offset as per the current QPPF system configuration, the 14nm requirement along the sensitive axis would be violated by an attitude error of about 3 milli-arc-seconds (mas). This translates into either an attitude determination error better than 3 mas if a sensor will be used for correction of the test particle position due to attitude errors; or a relative pointing error (RPE) control requirement better than 3 mas over the experiment duration (nominally 40s), to ensure the experiment repeatability requirement is met. This is currently not feasible even with the highest accuracy off the shelf sensors under development, being high accuracy star trackers or gyros.

11.3.4 Free-Drifting Experiment

Allowing the spacecraft to drift freely from an initial condition during one or several experiment runs might ensure that the repeatability requirements are met without the need for ultra-high accuracy measurements of the spacecraft position and attitude. In order to analyse this in detail, a simulator was set-up to implement the non-linear equations describing the motion of the Test Particle inside the 6-dof spacecraft system. Note that this simulator was needed to ensure a deeper understanding of this complex system, since initial assessments via back of the envelope calculations were too pessimistic and would have constrained the feasibility of the mission.

The simulator developed for the QPPF study is shown in the figure below and includes the following components:

- Spacecraft Dynamics and Kinematics (both rotational and translational effects)
- Test Particle Dynamics model in the spacecraft rotating frame (position/velocity)
- Solar Radiation Pressure (force/torque) model with specular & diffuse reflections
- Spacecraft Gravity Gradient torque due to the Sun
- Spacecraft-Test Particle Self Gravity accelerations

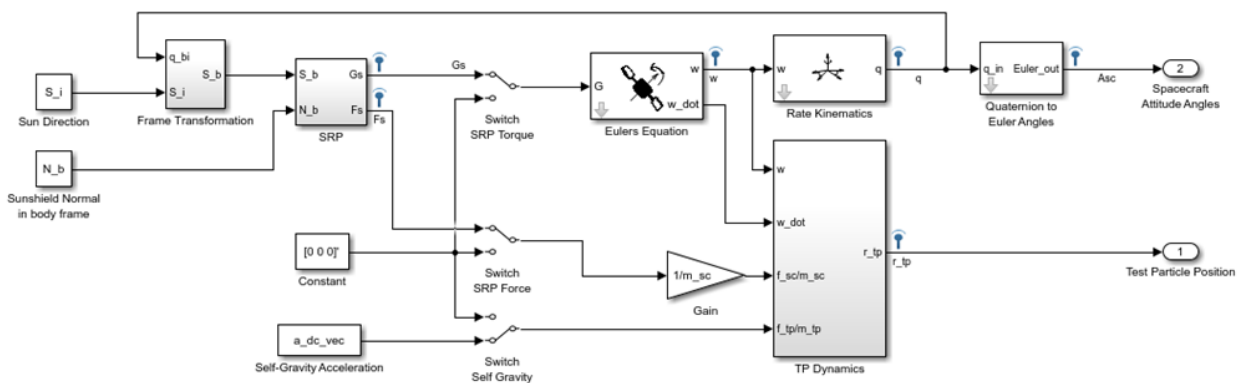


Figure 11-5: QPPF Dynamics Simulator

The dominating environmental disturbance affecting the absolute attitude and position of the QPPF spacecraft will be the Solar Radiation Pressure (SRP) forces and torques. Gravity gradient torque will be mainly from the Sun in the proposed QPPF orbits, and is almost negligible compared to the SRP. The gravity gradient force, or change in gravity field along the spacecraft orbit, will contribute to the repeatability of the TP position at longer time-scales in the order of days, affecting repeatability only between the long term experiment batches. For this reason, this disturbance is not taken into account in this simulator, which is focused on the short term effects of spacecraft attitude on the TP position.

The test case investigated is a long period of spacecraft attitude free-drift during which test particles are successively released one at a time with a waiting period in between corresponding to the experiment duration. During this time the TP is left free floating inside the spacecraft and their position relative to the optical bench is recorded. Repeatability is then computed as the difference in end position of each of these particles with respect to the rotating optical bench.

Several simulations were executed in order to find the timing parameters which provide the longest possible experiment time, where the particles remain inside the optical bench measurement range and the repeatability requirement is met. The following sections describe the results of the baseline timings found after testing several options during the complete simulation campaign.

11.3.4.1 Free Drifting Spacecraft Attitude Evolution

As mentioned before, SRP forces and torques are the dominating environmental disturbance on the proposed QPPF orbits. The figures below show the free-drifting spacecraft attitude evolution over time starting from an almost perfectly quiet and Sun pointing attitude. The initial rates and off-pointing angles, which are assumed to have been achieved by an attitude controller before the free-drifting phase, are shown in Table 11-1.

The plots below show the evolution of the spacecraft attitude and rates over time, as the spacecraft drifts freely under the effect of the environmental torques. The evolution of the main torque contributor (SRP), which depends mainly on the spacecraft geometry exposed to the Sun, is also shown below.

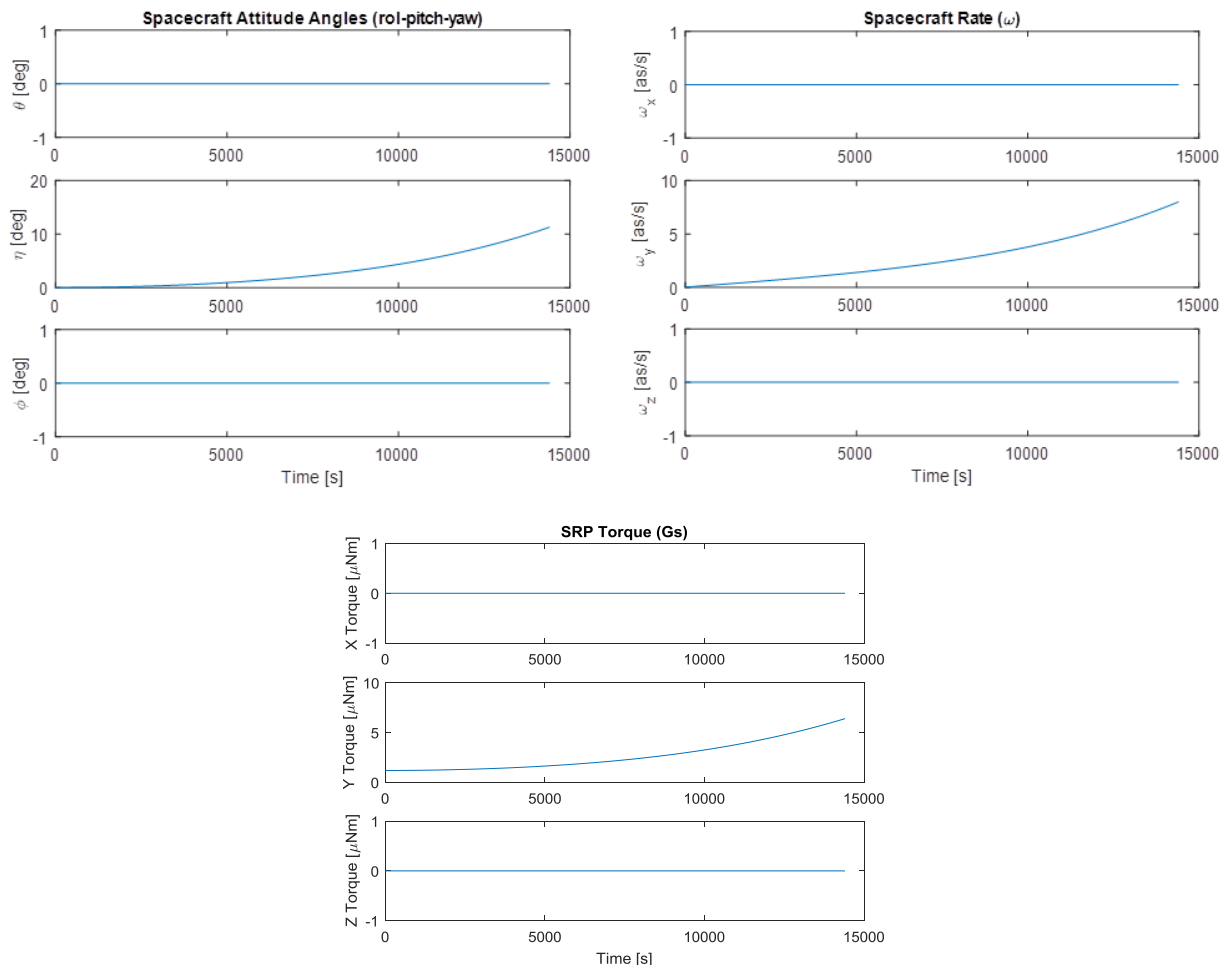


Figure 11-6: Free-Drifting Spacecraft Attitude Evolution

These figures show that the spacecraft attitude reaches about a 10 degree off-pointing to the Sun in about 4 hours of free drift. The final rates, which would have to be nulled by an attitude control system after the free-drifting phase, reach about 8 arcsec/s. These final conditions represent the limiting factor for a free-drifting phase, since the spacecraft geometry must be such that no part of the spacecraft other than the sunshield is exposed to the Sun with such an off-pointing; and an attitude control system with high enough accuracy to achieve the required free-drift initial conditions must also be able to recover these final conditions in a reasonable amount of time to resume the experiments. Note that in order to achieve low enough de-pointing angles at the end of the drift phase, the initial angular rates must be small. The shown results, with an initial rate of 0.1as/s are no longer achievable if the initial rates are in the order of 1as/s. In addition, even though the final de-pointing angle is not as sensitive to the initial angular off-pointing to the Sun (in the order of 10as for the shown simulations), the evolution of the SRP force is quite sensitive to this initial value. Therefore, if calibration using an SRP model is foreseen (see discussion in the next sections about repeatability), a good enough absolute angular attitude knowledge is required.

It is worth mentioning that simulations not presented here have shown that these results are highly sensitive to the chosen coefficients of specular and diffuse reflection and the geometry of the sunshield centre of pressure (CoP). The values assumed for these simulations were taken as to be a representative mix of solar cells and MLI at middle of life from RD[44]. However, for this reason, the results given here should be taken as an order of magnitude guideline for the design; or the sunshield coefficients should be optimised during the next phases of the design of this mission in order to obtain the longest possible experiment time.

11.3.4.2 Test Particle Position in Optical Bench (rotating) frame

During the free-drifting phase, test particles are successively released one at a time and left free floating inside the spacecraft for the duration of the experiment (nominally 40s). Their position relative to the rotating optical bench for the entire duration of the spacecraft free-drift period is shown on the left of Figure 11-7. The right of this figure shows a zoom in on the first few experiments, where the position of each test particle can be seen drifting for the duration of the experiment, with a new particle released at the end.

This figure shows that after 40 seconds of drift the particles still remain within 1mm of their release position in the rotating frame (AOCS-010 is met). This means that experiments could be much longer than 40 seconds without violating the AOCS-010 requirement. However, experiment repeatability must be analysed for longer durations, as it is affected by the duration of the experiments. Free fall is anyhow limited by other factors (e.g. acceptable collision rate).

Note that no experiment preparation time is considered in this analysis. However, a delay before the release of the next particle will not affect the position evolution of a particle that is released at the same time. Therefore, this analysis is also applicable if experiment preparation time or other delays are required in between each experiment, by simply ignoring the particles that would have been released during this time. This means that preparation time must be subtracted from the number of possible experiments that this analysis yields.

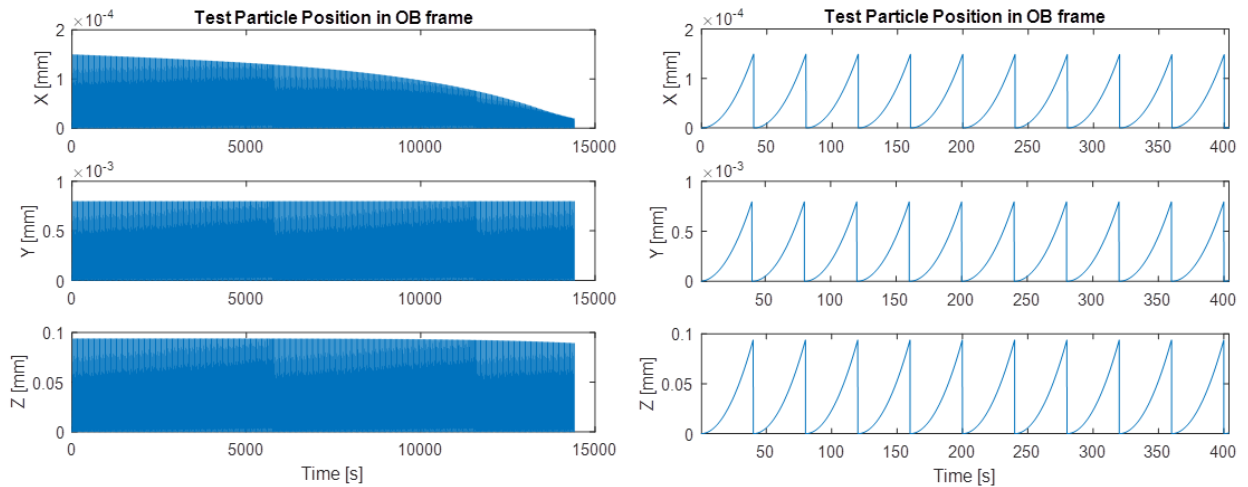


Figure 11-7: Position of the Test Particles Relative to the Rotating Optical Bench during the 4 hour spacecraft free-drift period (left) and zoom (right)

11.3.4.3 Experiment Repeatability

The experiment repeatability is computed as the difference in end position of each of these particles with respect to the rotating optical bench. The left side of the figure below shows the difference between the end position of each test particle and the end position of the test particle after the first experiment.

It can be seen from this figure that over the 4hour spacecraft free-drift period the experiment repeatability exceeds the 14nm requirement on the sensitive (x) axis (AOCS-o2o), reaching about 150nm. The right side of this figure shows a zoom where it can be seen that if the 14nm repeatability requirement along the x axis must be ensured implicitly, only about 150 experiments (without preparation time) can be performed successively. That is, the spacecraft can only be left free-drifting for about 100 minutes before experiment repeatability becomes compromised and the spacecraft attitude must be re-set.

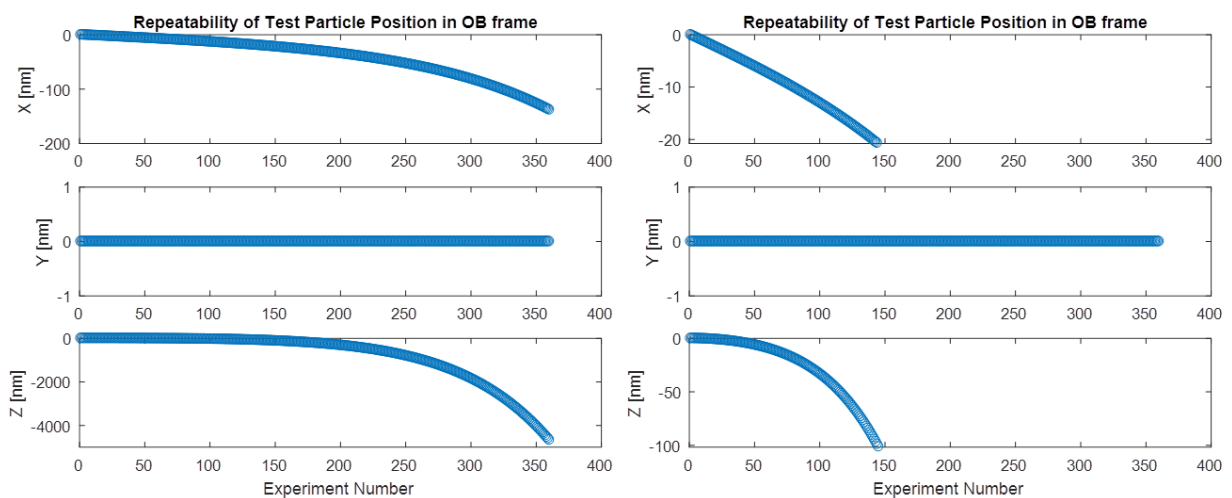


Figure 11-8: Repeatability of Test Particle end Position

However, since the test particles are still within the 1mm measurement range after 4 hours, the experiment batches could run longer if repeatability can be calibrated for using a model of the SRP disturbances. This is due to the fact that the evolution of the particle end positions shown in the figure above is deterministic and depends mainly on the SRP disturbances, which can be accurately modelled. An alternative calibration strategy foresees the use of regular “calibration runs” of the test particles (a particle released for the required experiment duration, measured by the CMOS+interferometer stage, would give the current “true” particle position deviation wrt release point, allowing to correct for the position of the subsequent particles (which will be subject to the matter-wave experiment), until the drift exceeds again the 14 nm requirement, which would be the time for a new calibration run. This latter calibration strategy is assumed as baseline for the CDF study.

It is worth mentioning that simulations not presented here have shown that taking into account the SRP forces and torques simultaneously in the analysis makes repeatability better in all cases with respect to an analysis splitting the position and attitude effects. For this reason, it is imperative to employ a 6-dof simulator to understand the couplings between spacecraft position and attitude on the test particle position.

11.4 Baseline Design

According to the analysis above the most promising and feasible option for the QPPF mission is a free-drifting spacecraft during the experiments, as analysed in Section 11.3.4. No known off the shelf sensors can yield the performance required to meet the QPPF requirements via direct measurement and/or control of the spacecraft states to guarantee TP position repeatability either directly or by post processing using those measurements. An LPF-like system may yield the required performance for QPPF, but at a great cost and complexity. Moreover, this option should be further analysed to established feasibility since it is not clear that the spacecraft attitude can be measured and/or controlled with sufficient accuracy with such a system, as there is no direct measurement of the TP to be used in the control loops as was done in LPF to achieve its quoted performance.

Note that a free-drifting system may be further improved with open-loop SRP compensation using a low noise micro-propulsion system. However, the analysis required to establish the feasibility of such an approach was out of the scope of this CDF study and may be analysed in the future. For now, the chosen baseline design consists of a purely free-drifting spacecraft during the experiment runs, with an attitude control system to re-set the spacecraft attitude after each experiment batch. The following sections describe the baseline design for the AOCS system.

11.4.1 Science Timeline Baseline

The science timeline with this free-drift + recovery system would be as follows:

1. Free-drifting spacecraft for about 4hours until spacecraft de-pointing to the Sun reaches 10deg. During this period no thrusters or other actuators are in use. Note that the repeatability requirement (AOCS-010) will be violated after about 1 hour of spacecraft free-drift. Therefore, a correction of the science data is required either by using an SRP model; or by interleaving science calibration runs with the

experiments where the TP position is measured throughout the drifting period and this information is used to calibrate the experiments.

2. Sun-pointing Attitude recovery phase to re-start experiments. According to the sensors and actuators chosen (details in the following sections), this phase will take about 90min with 1mN thrusters to recover the attitude from a 10deg de-pointing and a ~30min settling time will be required. This recovery time drives the propulsion system required maximum thrust. However, in order to achieve the fine pointing initial conditions required to re-start the experiments, the propulsion system minimum impulse bit (or minimum thrust for a throttle-able system) cannot be large. Simulations have shown that in order to ensure repeatability during the free-drift period, initial rates below 0.1uRad/s are required. For the mass and inertia characteristics of the QPPF spacecraft, thrusters with a resolution of 0.5uN are required to achieve this small enough initial rates for experiment. In addition, accurate attitude knowledge with respect to the Sun is required in order to ensure the initial Sun off-pointing is small enough to yield long drift times. For these reasons, a high accuracy star tracker or a lower accuracy star tracker plus a high accuracy gyro will be required to achieve the free-drift initial conditions.
3. The cycle repeats from Step 1.

The figure below summarises the spacecraft attitude over time during one science cycle. Note that the phase descriptions on the top of the graph only represent the phases of the slew manoeuvre the spacecraft needs to perform to recover, used to analyse the fuel consumption. The spacecraft will only be in two different modes during each cycle: Micro-propulsion Standby Mode (MSTB) and Micro-propulsion Sun Pointing Mode (MSPM). The AOCS controller will be completely off in MSTB, and there will only be one controller augmented with a slew guidance law that will seamlessly handle all the other phases of the recovery.

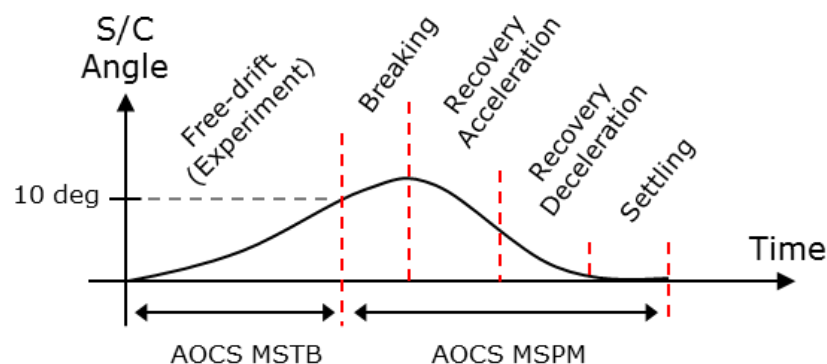


Figure 11-9: Spacecraft Angular Profile over a Science Batch Cycle

11.4.2 Sensor Selection for Drift-Recovery AOCS

As mentioned earlier, in order to achieve low enough de-pointing angles at the end of the drift phase, the initial angular rates must be extremely small, in the order of 0.1as/s. In addition, initial angular off-pointing to the Sun must be in the order of 10as and

accurate absolute attitude knowledge is required for any calibration of the experiment repeatability using the SRP model.

Taking into account the order of magnitude of the rates that is being considered, the traditional AOCS rule of thumb dictating that an order of magnitude better knowledge is required to achieve a given control accuracy does not hold. Instead, the spacecraft inertia plays a crucial role, filtering the attitude jitter even if the knowledge is worse than the required control accuracy. For this reason, it is considered that a rate knowledge in the order of the required control accuracy is sufficient. That is, a rate knowledge of roughly 0.1as/s is sufficient.

For these reasons, two options are considered to obtain the required attitude and knowledge:

1. A single ultra-high accuracy star tracker with an accuracy in the order of 0.1as , as the one currently under development by Jena Optronik. The rate estimation error that can be achieved with simple filtering of the derivatives of such a star tracker attitude solution would be in the order of 0.1as/s .
2. A high accuracy gyro (such as the Astrix 1120) combined with a medium accuracy off the shelf star tracker (such as the Jena Optronik ASTRO 10) in a gyro-stellar estimator to remove any gyro bias. Such a solution would provide an absolute attitude knowledge error of about 10as and a rate knowledge error of about 0.4as . With such an accuracy and a set of micro-propulsion thrusters with about $1\mu\text{N}$ resolution, an attitude controller for QPPF can be designed with a pointing error of about 15as and a residual rate error below 0.1as . For details please see the spreadsheet: [AOGNC Workbook Issue2.4 QPPF.xlsm](#).

The first proposed solution has the advantage that if high accuracy attitude knowledge is required for experiment calibration, this is directly provided by the proposed sensor. However, an additional gyro would also be required for the transfer phase, but this gyro can be of lower accuracy.

The second option provides a good solution that can meet the requirements of initial rates for the drift phase and it can also be used for the transfer phase AOCS. However, it might be marginal in terms of attitude knowledge for calibration of the experiment repeatability. Nevertheless, this option does not require development of any new technologies and can be achieved with off the shelf sensors. For this reason, this is the baseline selected for this CDF.

11.4.3 Fuel Consumption (Science)

Assuming the above timeline, the fuel consumption for the science phase can be computed by analysing each segment of Figure 11-9. The consumption is computed for both the case of a 1 hour and 4 hour drift for comparison, performing drift-recovery cycles continuously without interruptions. Antenna re-pointing and other non-science related activities can be performed during the recovery part of the cycle. Table 11-2 summarises the contributions of fuel per phase. For more details and assumptions please refer to the [AOCS QPPF Budgets.xlsx](#) spreadsheet.

Science Phase with Micro Propulsion System (MPS)			
		1 hour drift	4 hour drift
Fuel Consumption [g/day]			
Attitude Recovery		6.98	10.48
Settling time (10x min thrust)		5.42E-01	1.77E-01
Antenna re-pointing		4.25E-03	4.25E-03
Totals Per Year [kg]	Margin [%]		
Attitude recovery	100	5.1	7.7
Settling time	100	0.4	0.1
Antenna re-pointing	100	3.10E-03	3.10E-03
Total Per Year [kg]		5.5	7.8
Mission Total [kg]		16.5	23.4

Table 11-2: Science Phase Fuel Consumption

In summary, the science phase AOCS fuel consumption is about 23 kg over 3 years (7.8kg/year) using 1 mN thrusters (45s ISP) for recovery from a 4 hour drift. This recovery takes about 2 hours, yielding an overall cycle duration to about 6 hours: 4 hours of science with a free-drifting spacecraft + 2 hours of Sun pointing attitude recovery. Note that since safe modes are the same as the recovery from science if the FDIR is tuned to trigger below a 10deg Sun de-pointing, no fuel allocation is needed for this phase as it is equivalent as a recovery from a science drift phase.

11.4.4 Transfer Baseline Design

For the transfer phase of the mission, additional AOCS equipment and fuel is needed to support the LEOP and perform the transfer manoeuvres to the science orbit.

During the transfer a larger propulsion system is assumed with 1N Reaction Control System (RCS) thrusters in order to complete the manoeuvres in a reasonable amount of time. The Transfer AOCS system must perform the following functions:

- De-tumble & Sun Acquisition (SAM) after separation from launcher or safe mode
- Control attitude during Orbit Correction Manoeuvres (1 day total burn duration)
- Control attitude during transfer cruise (1.5 days total cruise time)

Table 11-3 summarises the fuel consumption contributors during this phase.

Transfer Fuel Budget [kg]	Margin [%]	RCS
De-tumbling / SAM	30	0.58
Control during OCM	30	4.88
Control during cruise	100	2.12E-03
Total Transfer AOCS Fuel [kg]		5

Table 11-3: Transfer Phase Fuel Consumption

The total propellant required for the transfer phase is 5kg, assuming thrusters with a specific impulse (ISP) of 60s.

11.4.5 Preliminary AOCS Modes List

The table below summarises the foreseen control system modes required for the entire mission. Note that the modes are separated by the mission phase (Transfer and Science) since a different set of thruster with different control authorities will be employed for each phase. This implies that the attitude controllers will be different for each phase, requiring different modes.

Mission Phase	Sub-Phase	MODE	MODE Description	Notes
LEOP / Transfer	Launch	RSTB	Standby	High-force Reaction Control System (RCS)
	De-tumble / Sun Acquisition	RSAM	Sun Acquisition Mode	
	Transfer	ROCM	Orbit Control Manoeuvre	
	Anomaly	RSAM	Safe Mode	
Science	Commissioning	MCSP	Coarse Sun Pointing Mode	Low-force Micro Propulsion System (MPS)
	Fine Sun Pointing / Free-Drift Recovery	MSPM	Sun Pointing Mode	
	Free-Drift (Science)	MSTB	Standby	
	Anomaly	MSAM	Safe Mode	

Table 11-4: Control system modes

Note that any required station keeping manoeuvre during the science phase will use the ROCM mode in order to take advantage of the larger thrusters available in this mode. However, no station keeping manoeuvres are foreseen in the fuel budget for the nominal mission orbit.

11.5 List of Equipment

This section summarises the equipment needed for the AOCS subsystem. Note that even though the thrusters are mentioned here for completeness, they are part of the propulsion system equipment list and corresponding budgets. The AOCS equipment needed for the complete mission is as follows:

- Sensors (in addition to payload):
 - 2x Star Trackers, hot redundant (both required for full performance)
 - 3x Sun Sensors, triple majority voting hot redundancy
 - 2x high accuracy gyros (also used for Transfer), cold redundant
- Actuators (in Propulsion Subsystem):

- 16 x 1mN RCS cold gas thrusters for Science (8 cold redundant)
- 16 x 1N RCS cold gas thrusters for de-tumbling & transfer (8 cold redundant)
- Propellant (for AOCS only, transfer delta-v not included):
 - 23kg of Cold Gas for Science (3 year mission, 100% margin)
 - 5 kg of Cold Gas for de-tumbling & transfer (including manoeuvres)
 - Total fuel (not accounting delta-v): 28 kg N₂ (3 years full margins)

Equipment details are given in the next sections.

11.5.1 Star Tracker

As explained in Section 11.4.2, a medium accuracy off the shelf star tracker can be used for QPPF in combination with a high accuracy gyro. The selected star tracker is the following:

ASTRO 10

Manufacturer: Jena Optronik

TRL: 9

Mass:

Optical Head < 1.2Kg

Baffle < 0.6Kg

Electronics Unit < 1.4Kg

Power:

Total 15W max

Optical Head < 5.5W

EU < 11W

Dimensions:

Optical Head + Baffle < 140 mm Ø x 264 mm

EU < 150 mm x 145 mm x 75 mm

Features:

Field of View: 16.7° x 12.5° [effective]

Attitude accuracy < 1.5 arcsec [1σ] xy-axes < 12 arcsec [1σ] z-axis

Attitude re-acquisition < 8 s

Slew rate: 1.0° s⁻¹ [full performance], 3.0° s⁻¹ [operational]

Sampling time: 125 ms

Sensitivity: SNR = 10 for 6.0 mi Go-ref. star

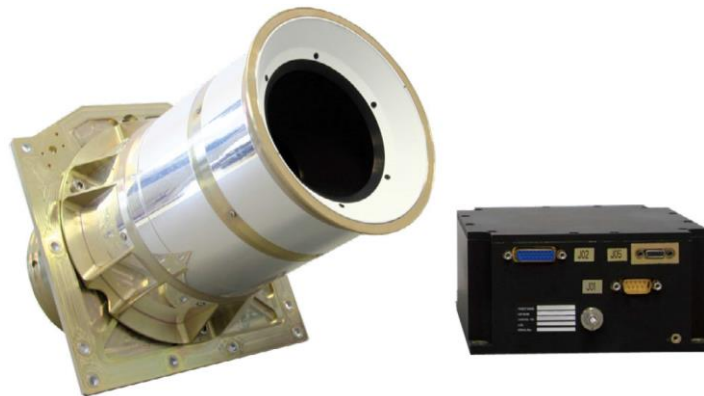


Figure 11-10: ASTRO 10 Star Tracker

11.5.2 Gyros

As explained in Section 11.4.2, a high accuracy gyro is needed in combination with an off the shelf star tracker for QPPF in order to achieve the required rate control for initial drift conditions. The selected gyro is the following:

Astrix 1120

Manufacturer: Airbus

TRL: 9

Mass: 4.5 kg

Power: 13.5 W

Range: +/- 20 deg/sec

Bias stability over 1 hour: <0.003 deg/hr

Angle Random walk: < 0.002 deg/sqrt(hr)

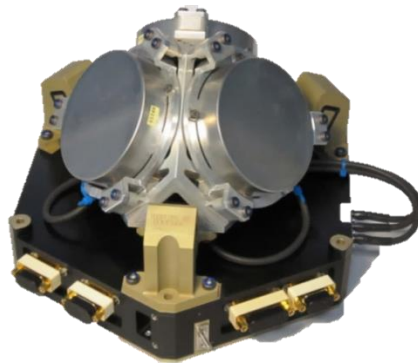


Figure 11-11: Astrix 1120 Gyro

11.5.3 Digital Sun Sensors

The Sun sensors are needed in QPPF for transfer and safe mode. They do not have the accuracy required for science, when the star tracker and gyro are used.

S3 – Smart Sun Sensor

Manufacturer: Leonardo

TRL: 9

Mass: 0.33 kg

Power: 1 W

FOV: 128 x 128 deg

Accuracy: (2σ) < 0.02 deg

Resolution: < 0.005 deg

Heritage: GOCE, LPF

Dimensions: 112 x 12 x 43 mm

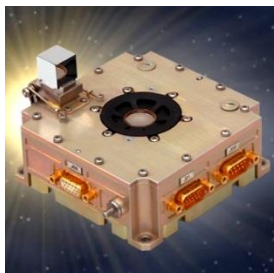


Figure 11-12: S3 – Smart Sun Sensor

11.6 Technology Needs

Technology Needs						
*	Equipment Name & Text Reference	Technology	Supplier (Country)	TRL	Funded by	Additional Information
*	ASTRO 10 Star Tracker	Available	Jena Optronik (DE)	9		
*	Astrix 1120 Gyro	Available	Airbus (FR)	9		
*	S3 – Smart Sun Sensor	Available	Leonardo (IT)	9		
	High Accuracy Star Tracker	In development	Jena Optronik (DE)	6	ESA	

* Tick if technology is baselined

11.7 Summary & Conclusions

The identified design for QPPF consists of a free-drifting attitude/position during each experiment batch with no control system actuation. This is necessary to achieve the repeatability requirement of particle position at the end of each experiment. The selected baseline consists of a 4 hour free drifting phase until the spacecraft Attitude reaches about 10deg. Recovery of the attitude to restart a new free-drifting cycle takes about 2 hours. Note that the experiment repeatability requirement of 14nm is exceeded after about 1h of free drift. Therefore, repeatability must be corrected by post-processing either using a solar radiation pressure model or other techniques (discussed in the science section of this report).

In order to ensure the drifting phases experiment repeatability without exceeding the Sun off-pointing constraint of 10deg, it is critical that the free-drift phase initial conditions are in the order of 10as and 0.1as/s. These are only feasible by employing a high accuracy star tracker or a high accuracy gyro in combination with a medium accuracy star tracker, and a micro propulsion system with 1 uN resolution and 1 mN maximum thrust. Low enough initial spacecraft rates are critical for the feasibility of the 4 hours of free-drift phase.

It might be possibility to start experiments with an initial rate in opposite direction of the free drift (after initial calibration) in order to extend the experiment batch time. This should be investigated further in future studies.

The proposed AOCS baseline design does not require any dedicated technology developments.

This Page Intentionally Blank

12 TELECOMMUNICATIONS

12.1 Requirements and Design Drivers

12.1.1 Requirements

Subsystem Requirements		
Req. ID	Statement	Parent ID
COM-010	<p>The telecommunication subsystem shall be able to perform the following functions regardless of the spacecraft's attitude, throughout all the mission phases:</p> <ul style="list-style-type: none"> Receive and demodulate the uplink signal from the ground segment and transmit the telecommand (TC) data stream to the data handling system as defined in RD[45] and RD[46] Receive a telemetry (TM) data stream from the data handling system and transmit this data to the ground segment as defined in RD[45] and RD[47] Receive, transpond, and re-transmit a ranging signal as defined in RD[48] 	
COM-020	Active (hot) redundancy shall be provided for telecommand (uplink) and passive (cold) redundancy for telemetry (downlink)	
COM-030	<p>The link budget margins shall be as defined in TBD</p> <ul style="list-style-type: none"> Nominal > 3 dB Mean 3*sigma > 0 dB RSS worst case > 0 dB 	

12.1.2 Design Drivers

The telecommunication subsystem design has various drivers. Primarily, the data volume to be transferred and the time available for this transfer is a strong driver, especially for the choice of suitable frequency allocations. The stringent requirements on the spacecraft surface uniformity and the necessary shadowing of the cryo-cooler restrict the antenna type and size. Requirements on spacecraft pointing, power consumption and operational constraints for the subsystem further narrow the design space.

12.2 Assumptions and Trade-Offs

Assumptions	
1	For every day of science observations, science data of 14.3 Gb is generated. This figure already includes possible data compression measures.
2	For every day of operation, housekeeping telemetry data of 0.5 Gb is generated. Real-time housekeeping telemetry is produced at 6kbit/s.
3	An additional overhead of 18% on the data volumes needs is required for the

	CCSDS data link layer.
4	An L2 orbit with Sun-Spacecraft-Earth angles varying between 10° and 35° is used during the mission.
5	The nominal duration of science phases is 22 days with an interruption of 7 days.
6	During the science phase, the communication subsystem cannot do antenna repointing.
7	During the science phase, the communication subsystem can turn on the transmitter, i.e. the thermal gradient caused by the transmitter warm-up does not interfere with the science performed (TBC in next study phases).

12.2.1 Bandwidth Trade-Off

For the general subsystem architecture, a suitable choice of frequency band is required. RD[45] specifies a bandwidth limitation of 6 MHz for transmissions in S-Band, which makes the transfer of high-volume science data unfeasible.

Typically, Lagrange point missions move to X- and K-Band with their higher bandwidth allocations (10 MHz for X-Band, no hard limitation for K-Band) for performing payload telemetry download (PDT). The drawback of using a K-Band PDT is that in practice, an additional X-Band subsystem is always required for TT&C, increasing the subsystem cost and complexity together with size, mass and power consumption.

Given recent technology developments towards higher order modulations for high data rate telemetry RD[49], an X-Band communications subsystem capable of transferring the required data volume while adhering to applicable restrictions is selected.

12.2.2 Antenna/Power Trade-Off

For a given link geometry, the data rate and modulation/coding combination require a specific amount of effective radiated power (EIRP). Therefore, it is possible to trade off antenna gain against transmitter output power. While higher antenna gain increases the antenna mass, size and pointing requirements, a higher transmitter output power requires more electrical input power.

Because of the less stringent pointing requirements and the reduced impact on size and mass budgets, a baseline design with relatively high transmitter output power and smaller antennas are selected.

12.2.3 Orbit Trade-Off

During the early study phases, alternative orbit selections were presented. While the L2 orbit was chosen as a baseline, the impact of a change to an Earth trailing or Earth leading heliocentric orbit was analysed. The presented baseline design is sized for an L2 orbit and the biggest design driver for other orbits is the increasing distance to Earth. With up to 50 million km Spacecraft-Earth distance at end of mission, the link budget can only be closed with more EIRP from the spacecraft. This can be achieved by resizing the TWT amplifier and by moving from an MGA to a high gain reflector antenna. While reflector antennas of around 60 cm diameter are sufficiently flight proven, their use has the drawback of tighter pointing requirements. Additionally, problems with accommodation on the spacecraft can be expected if the same restrictions on sunshield surface uniformity exist.

12.3 Baseline Design

Based on the requirements and assumptions given above a communications subsystem was designed and sized, considering that the science phase can last up to 22 days.

As baseline, an X-band architecture is proposed, its block diagram is shown in Figure 12-1.

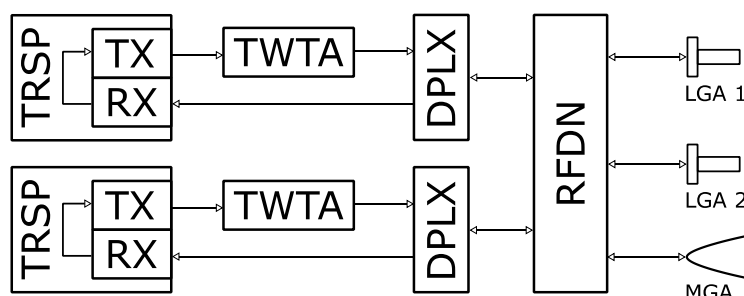


Figure 12-1: Communications subsystem overview

The design is based around the Thales Alenia Space Deep Space transponder and redundant TWTAs. A suitable distribution network connects these components to two low-gain antennas (LGAs) and one steerable medium-gain antenna (MGA). The communication strategy is twofold: During the long science phases, one daily contact is scheduled using the LGAs, which are used for housekeeping telemetry only. After the science phase, the MGA can be used to downlink all stored science data to Earth.

PARAMETER	VALUES	NOTES
RANGE [km]	1775253.6	
FREQUENCY [MHz]	8450	
BIT RATE [kbps]	8000.00	net bit rate, including overhead
TX EIRP [dBW]	35.62	MGA, including pointing losses
PATH LOSSES [dB]	235.96	calculated
ATMOSPHERE LOSS [dB]	0.00	
RX G/T [dB/K]	50.80	Cebreros 35m X-Band
DEMOD. LOSS [dB]	1.00	
REQUIRED OBO [dB]	0.29	
REQUIRED Eb/No [dB]	3.68	CER < 1e-4
MINIMUM MARGIN [dB]	5.06	

Table 12-1: Link budget for science downlink sessions

Using the presented baseline configuration, a daily ground station pass of 2-3 hours is used for telemetry downlink using the LGAs. Using the maximum data rate that can be achieved using the selected MGA+TWTA design, the science data can be transferred during 3-5 days with pass durations between five and three hours. These figures already include margin for dedicated ranging sessions, which are assumed to take place outside of the science phases.

To achieve the data rate of 6.8 Mbit/s available for science data, modulation and coding according to CCSDS 131.2 is adopted as baseline. The selected combination (MODCOD 8) uses 8PSK modulation and achieves a spectral efficiency of 1.1 bit/Hertz. Pointing losses of 1 dB were taken into consideration, which translate to pointing accuracy requirements of around 2°. For low gain antenna communications, MODCOD 1 was chosen, as occupied bandwidth is not an issue in these phases and less EIRP is required for successful reception. Consolidated link budgets for science and housekeeping downlink are shown in Table 12-1 and Table 12-2.

PARAMETER	VALUES	NOTES
RANGE [km]	1775253.6	
FREQUENCY [MHz]	8450	
BIT RATE [kbps]	32.00	net bit rate, including overhead
TX EIRP [dBW]	10.62	LGA, including pointing losses
PATH LOSSES [dB]	235.96	calculated
ATMOSPHERE LOSS [dB]	0.00	
RX G/T [dB/K]	50.80	Cebreros 35m X-Band
DEMOD. LOSS [dB]	1.00	
REQUIRED OBO [dB]	0.32	
REQUIRED Eb/No [dB]	1.57	CER < 1e-4
MINIMUM MARGIN [dB]	6.12	

Table 12-2: Link budget for housekeeping telemetry downlink

12.3.1 Transponder and Travelling-Wave Tube Amplifier

For the two transponders, the Thales Alenia Deep Space Transponders are considered for the baseline design. Their receivers operate in hot redundancy while the transmitters are cold redundant. The transponder is shown in Figure 12-2.



Figure 12-2: Deep space transponder

While the transponder design itself is mature and has heritage on various deep space mission, its use on the QPPF mission requires a technology development. It is foreseen to implement the CCSDS 131.2 “Flexible advanced coding and modulation scheme for high rate telemetry applications” standard. This coding and modulation scheme was established and standardized in 2012, and has been already implemented for a Payload Data Transmitter (PDT) in an activity with TESAT.

TWTAs for space applications are commercially available as off-the-shelf components. The baselined TWTA foresees an output power of 40 W. Data from Thales TH4604 amplifiers were used as the baseline design.

12.3.2 Radio Frequency Distribution Network (RFDN)

The RFDN is waveguide-based and contains switches, isolators and duplexers, all items with proven flight heritage and low failure probability. The link budgets presented in the design use a conservative approach for RFDN loss estimation, i.e. already include a reasonable number for RFDN losses. The RFDN design includes a spare port that can be used for an additional LGA as presented in 12.5.2 with only minor impact on complexity.

A schematic view of the devised RFDN can be seen in Figure 12-3.

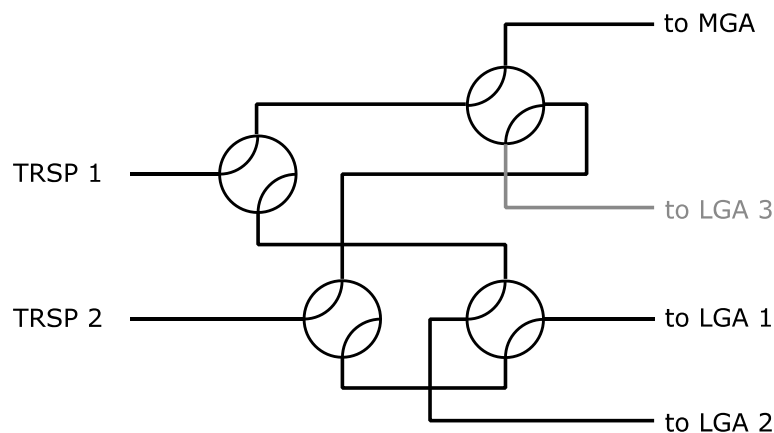


Figure 12-3: RFDN schematic

12.3.3 Low Gain Antennas (LGA)

Two X-Band LGAs are baselined for the communications subsystem. These need to be accommodated to ensure quasi-omnidirectional coverage so communications can be ensured during safe mode / emergency operations regardless of spacecraft attitude. This constraint restricts the placement of the LGAs on the outer circumference of the sun shield, opposite to each other. Shadowing by any other spacecraft parts can be minimised this way.

In addition to LEOP and safe mode operations, the LGAs will be used during the science phase to transfer real time housekeeping telemetry to ground on a daily basis. If larger volumes of housekeeping telemetry are required, refer to the option presented in 12.5.2.

For the link budget calculations, the radiation pattern data of the Bepicolombo X-Band LGA FM was used, which could also be adopted for this mission. The LGA and its corresponding radiation pattern are shown in Figure 12-4 and Figure 12-5.



Figure 12-4:
Bepicolombo LGA

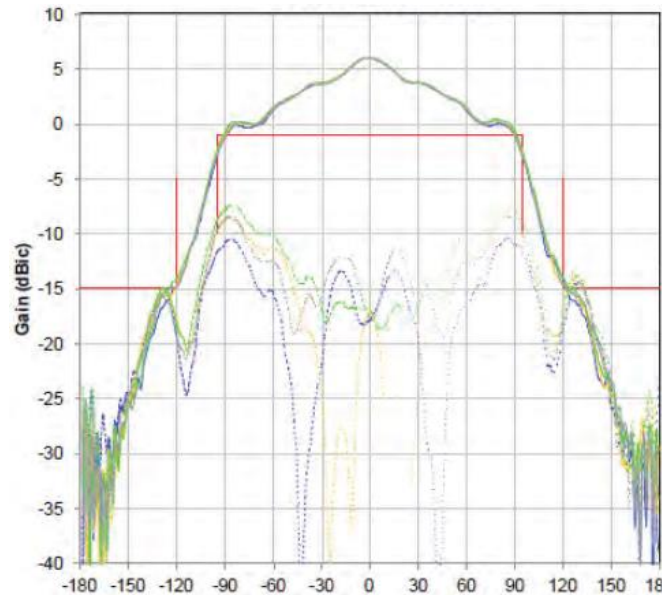


Figure 12-5: Bepicolombo LGA pattern

12.3.4 Medium Gain Antenna (MGA)

Between the science phases, there is a seven-day period for platform recycling and preparations, which can also be used for the science data transfer. For the medium gain antenna, the FM data from Bepicolombo was taken as a reference. This antenna design presents a small and lightweight solution, which is already flight-tested on a deployable two-degree-of-freedom mechanism.

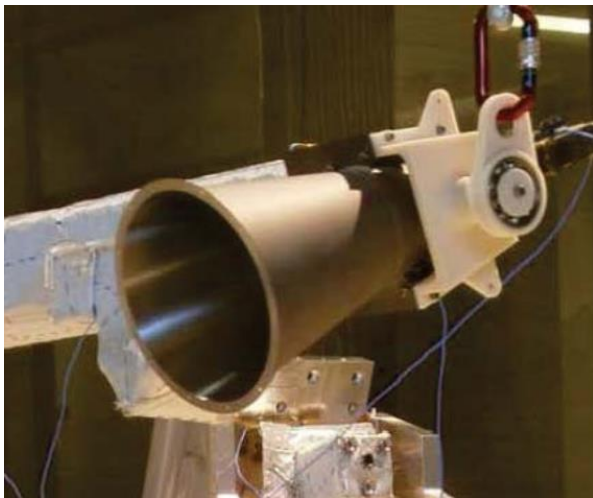
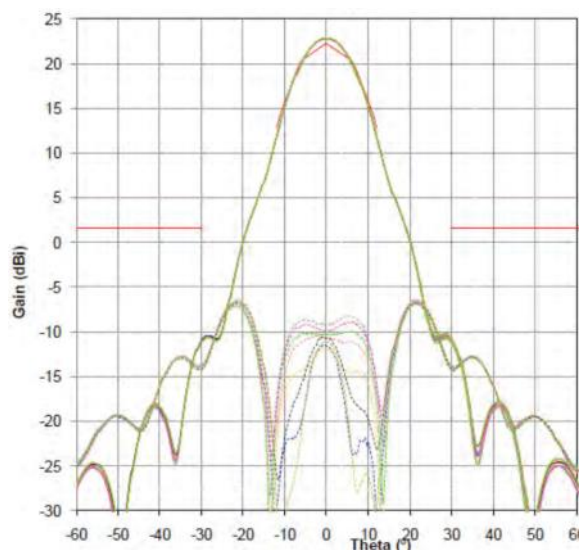


Figure 12-7: Bepicolombo MGA



**Figure 12-6: Bepicolombo MGA
pattern**

The antenna and its radiation pattern are shown in Figure 12-7 and Figure 12-6. While the antenna and its boom need to be retracted during the science phases to avoid disturbing the SRP forces acting on the spacecraft, it is deployed during these recycling phase and can be kept pointed to Earth by means of a pointing mechanism. One joint of this mechanism is located on the spacecraft body, while the other, orthogonal joint is placed close to the antenna at the end of the boom. Using this configuration, the antenna can be pointed towards Earth without requiring the spacecraft itself to reorient.

12.4 List of Equipment

	mass (kg)	mass margin (%)	mass incl. margin (kg)
SC (Spacecraft)	31.00	13.03	35.04
SM (Service Module)	31.00	13.03	35.04
DIP_1 (Diplexer #1)	0.40	10.00	0.44
DIP_2 (Diplexer #2)	0.40	10.00	0.44
HPA_TWTA_1 (High Power Amplifier (TWTA) #1)	2.30	5.00	2.42
HPA_TWTA_2 (High Power Amplifier (TWTA) #2)	2.30	5.00	2.42
LGA_1 (Low Gain Antenna #1)	1.00	10.00	1.10
LGA_2 (Low Gain Antenna #2)	1.00	10.00	1.10
MGA (Medium Gain Antenna)	2.00	10.00	2.20
RFDN (Radio Frequency Distribution Network)	5.00	20.00	6.00
XPND_1 (Transponder #1)	3.30	5.00	3.47
XPND_2 (Transponder #2)	3.30	5.00	3.47
MGAPM (Medium Gain Antenna Pointing Mechanism)	10.00	20.00	12.00
Grand Total	31.00	13.03	35.04

Table 12-3: Communications system mass budget

Power (W)	P_on	P_stby
SC (Spacecraft)	269.83	31.00
SM (Service Module)	269.83	31.00
DIP_1 (Diplexer #1)	0.00	0.00
DIP_2 (Diplexer #2)	0.00	0.00
HPA_TWTA_1 (High Power Amplifier (TWTA) #1)	69.92	13.00
HPA_TWTA_2 (High Power Amplifier (TWTA) #2)	69.92	13.00
LGA_1 (Low Gain Antenna #1)	0.00	0.00
LGA_2 (Low Gain Antenna #2)	0.00	0.00
MGA (Medium Gain Antenna)	0.00	0.00
RFDN (Radio Frequency Distribution Network)	0.00	0.00
XPND_1 (Transponder #1)	55.00	0.00
XPND_2 (Transponder #2)	55.00	0.00
MGAPM (Medium Gain Antenna Pointing Mechanism)	20.00	5.00
Grand Total	269.83	31.00

Table 12-4: Communications subsystem power budget

12.5 Options

12.5.1 Medium Gain Antenna accommodation options

In addition to the baseline accommodation option of the MGA assembly behind the sunshield, three other options were discussed during the study. These are graphically illustrated in Figure 12-8.

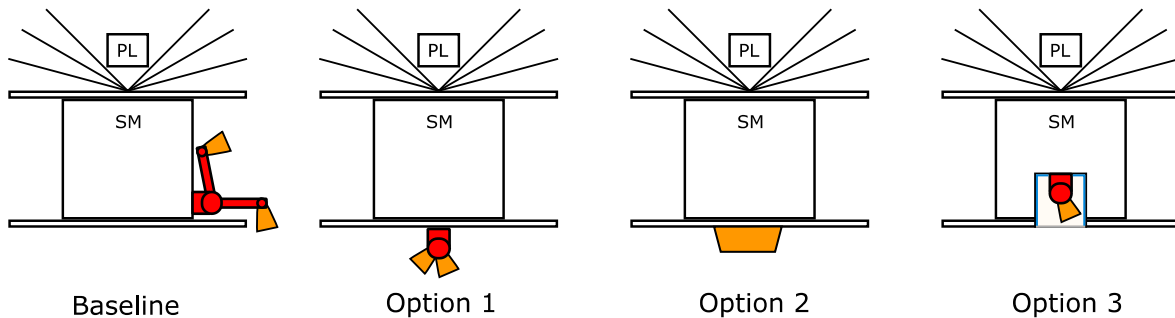


Figure 12-8: MGA accommodation options

12.5.1.1 Steerable MGA placed on spacecraft sunshield

While the problems with constraints with solar radiation pressure uniformity on the sunshield were mentioned before, the study was not able to produce a conclusive study on the free-fall time degradation caused by installing the antenna directly on the sunshield. An accommodation there likely would still require storing the antenna to a known position during science phases to minimise this free-fall time degradation. An advantage of this approach would be reduced torques on the spacecraft by antenna pointing plus a more compact and lightweight mechanism.

12.5.1.2 Phased Array Antenna placed on spacecraft sunshield

With the idea being close to the option presented in 12.5.1.1, a phased array antenna similar to the one used on the GAIA mission could be used on the sunshield. With its simple and uniform surface, it could simplify the analysis of the impact on solar radiation pressure uniformity. The downside of this option is the high associated cost of the unit.

12.5.1.3 Steerable MGA behind RF-transparent cover on sunshield

To avoid degrading the surface uniformity of the sunshield, the MGA with its associated pointing mechanism could be placed inside a box/cylinder, which can be recessed inside the spacecraft. The box is covered by an RF-transparent material while being reflective/opaque to the portions of spectrum relevant to solar radiation pressure. The other faces of the box could be clad with RF absorptive material to reduce the influence of reflections on the far field radiation pattern. This way, the advantage of sunshield surface uniformity is preserved, while the MGA could have constant visibility of the Earth and would not require a deployment mechanism.

The downside of this approach is that there is no flight heritage of such a design. The MGA and pointing mechanism could likely not be procured as individual items but would need to be procured together with the container box, to verify their performance before spacecraft integration.

12.5.2 Additional Low Gain Antenna option

The baseline design uses a conventional approach of using two LGAs for quasi-omnidirectional coverage. As the LGAs need to be mounted on opposite spacecraft sides and cannot be accommodated on the face containing the cryo-coolers, their most favourable radiation direction is pointing 90° off the Sun in nominal spacecraft attitude. This places the minima of the radiation patterns in the Sun/Earth direction. While this still gives sufficient coverage for emergency/safe mode operations, it is not possible to transfer the stored daily housekeeping telemetry in a reasonable ground pass time.

To remedy this shortcoming, a third LGA could be accommodated on the sun-pointing face of the spacecraft. The baselined RFDN contains an unused port for this antenna, so changes in the baseline design would be minimal. The addition of such a third LGA would enable downlink of stored HK TM during a daily 2h ground station pass (35 m ESTRACK station). In addition, it would make use of 15 m ground stations for real time telemetry downlink feasible.

12.6 Technology Needs

The modification on the deep space transponder presents the main technology development required. As the process of standardization for CCSDS 131.2 is finished and parts of the standard have already been implemented in activities, there is high confidence in technology readiness and availability until mission adoption.

Technology Needs						
*	Equipment Name & Text Reference	Technology	Supplier (Country)	TRL	Funded by	Additional Information
*	Deep Space Transponder	CCSDS 131.2 high order modulation and SCCC for TM, LDPC coding for TC	TAS (Italy)	6		Implemented with TESAT as TETra up to EQM level
	MGA Assembly	MGA & Pointing Mechanism integrated in box with RF transparent cover	-	3		One of the MGA accommodation options

* Is the baseline

This Page Intentionally Blank

13 DATA HANDLING

13.1 Requirements and Design Drivers

SubSystem Requirements		
Req. ID	Statement	Parent ID
DHS-010	DHS shall demodulate, decode, validate, distribute and execute time-tagged or Essential ground Telecommands (TC) allocated to spacecraft (S/C) or payload (P/L) units	
DHS -020	DHS shall collect S/C and P/L health telemetry (HTM) during all mission phases including transfer and science phases (100 temperature, 16 R-LCL, 16 analog)	
DHS -030	DHS shall be able to time-stamp the telemetry with respect to the On-Board Time	
DHS -040	DHS shall be able to distribute the OBT to the rest of equipment	
DHS -050	DHS shall support autonomous science operations and autonomous FDIR functions and transition to Safe Mode	
DHS -060	The DHS shall be able to cope in terms of on-board storage and download data rate with a real-time telemetry average data-rate of 6 kbit/s	
DHS -070	The DHS shall be able to cope in terms of on-board storage and download data rate with a Science data rate is of 300Gbit/contact	
DHS -080	The DHS shall be able to cope in terms of on-board storage and download data-rate with a ground contact worst-case for download once every 22 days	
DHS -090	The possibility to execute complex AOCS function (tens of MFLOPs) at about 10Hz has to be provisioned (although it has not yet been identified)	
DHS-110	The DHS shall be able to offer CFDP services for appropriate operations and on-board file management	
DHS -100	<p>The OBC shall be able to run software tasks estimated on 7-10 MIPs in a SPARC architecture with the following functions:</p> <ul style="list-style-type: none"> - Housekeeping collection - Memory management - Telecommand Manager - Telemetry Manager - PUS services - On-Board Time manager - Event actions 	

13.2 Assumptions and Trade-Offs

Assumptions	
1	The science data rates provided by the payload team are considered with compression already applied
2	HK data rates have been taken as a requirement but they have been recalculated during the study iterations
3	SpaceWire as command and data link with the payload equipment Conservative data storage requirements have been considered for the on-board data storage:
4	<ul style="list-style-type: none"> - 5% of file system overhead - 20% of ECC overhead - 10% of EoL degradation of the Flash devices - 50% free space Centralised: single box as star point for most of data harness and processing
5	Justification: less power consumption, easier to isolate thermally and optimised volume

13.2.1 On-Board Storage Calculation

One of the main requirements mentioned in Section 13.1 is the need for enough on-board data storage to overcome the current mission plan. Taking into account the fourth assumption present in Section 13.2, the on-board data storage requirement results in:

1.63002 Tbit

The selection of an appropriate equipment is based on this minimum capacity.

13.2.2 Housekeeping Real-Time Telemetry Check

Based on the estimation of 60 temperature measurement points for the thermal control, 10 pieces of equipment connected in the platform command and control network and 4 units connected via SpaceWire on the Payload Module command and control network, a draft calculation of the possible housekeeping telemetry data rate has been performed and presented in Table 13-1. Given the difficulty to properly estimate such values at this early stage, it is considered appropriate to use a 100% margin on this value. In this case that results in 5989 bps, which is very close to the DHS-060 requirement of 6 kbps.

In practice, the tuning of the final real-time telemetry will be done with the final available bandwidth of the data downlink, and the parameters that cannot be download in real-time will be downloaded with the science data when the spacecraft is repointed every twenty-two days.

HK parameter	Size [Byte]	Period [s]	N equipments	subTOTAL [bits/s]	
Temperatures	6	60	60	48	
SMU Secondary Voltages	2	1	10	160	
CAN-bus error counter	2	1	10	160	
SpW Error counter	2	1	4	64	
SMU Unit modes	2	1	10	160	
SMU Unit State	2	1	10	160	
SMU temperature control	20	60	1	2.666666667	
SMU Number TC Exec	2	1	1	16	
TM(1,1)	2	1	1	16	
TM(1,2)	2	1	1	16	
TM(1,7)	2	1	1	16	
TM(1,8)	2	1	1	16	
TM(5,1)	2	1	1	16	
TM(5,2)	2	1	1	16	
TM(5,3)	2	1	1	16	
TM(5,4)	2	1	1	16	
MTL	2	1	1	16	
PDU Acq List	128	1	1	1024	
PDU Acq List state	2	1	1	16	
Payload Module Acq List	128	1	1	1024	
Payload Module Acq List state	2	1	1	16	
				2994.666667 TOTAL [bits/s]	
				259 TOTAL [Mbit/day]	

Table 13-1: Housekeeping Telemetry calculation/check

13.2.3 Centralised vs. Distributed Architecture Trade-Off

It was taken as an assumption (number 5 in Section 13.2) that a single-box star topology for most of data harness and processing would be a more efficient solution than a distributed data collection one due to its inherent lower power consumption, mass and volume, which make it easier to isolate thermally and place it in a physical configuration. At the end of the study this has been re-evaluated and it is still considered a correct approach as the number of sensors and actuators to control and acquire by the on-board computer are still under 100.

If in further studies this situation changes dramatically (over 300 sensors and actuators) it would need to be re-evaluated to trade-off again the equipment mass with the harness on the two topologies.

13.3 Baseline Design

Following the overall functional requirements and in particular assumption number 5 of section 13.2, the most suitable piece of equipment for the baseline spacecraft has been considered the next generation Spacecraft Management Unit from RUAG Sweden.

The new SMU is an evolution of the current generation of avionics developed by RUAG Sweden and used in on-going programmes like JUICE, Small GEO, EarthCare, etc. The current architecture can be considered quite generic as it has already been adapted to be compatible to all those different kind of mission, and the evolution unit has benefit from that background, putting as a target the need for further integration in order to achieve better performance along with a significant reduction of mass and power.

The schedule of such evolution is fully compatible with QPPF requirement of TRL 6 achieved by all elements at the end of phase B1 (assumed in CDF study as 2024).

Key features that makes the next generation SMU a very good candidate with respect to the heritage unit from the functional perspective are:

- Updated TM/TC standards to support data relaying capability
- Higher CPU performance to allow the core computer to take responsibility of new tasks such as payload control
- Mass memory based on flash technology and supporting file management system for data transfer to/from ground
- Increased Essential TM supporting a higher number digital and analog parameter acquisition regardless the processor modules status
- Possibility to integrate in the same OBC box both RTU and Mass Memory functionalities.



Figure 13-1: Next generation RUAG SMU

13.3.1 Redundancy Concept

The redundancy and FDIR concept of the proposed design is different with respect to the existing OBC generation due to a lower number of boards and high integration of functionalities in ASICs. There will be a reduced number of converters, less cross-strapping and less circuitry.

FDIR management is simplified, and the system-level lower reliability due to fewer cross-strappings is balanced out at board-level by a reduced number of components due to the higher level of integration.

Going into the detail, we can say that all spacecraft management functions are integrated in a single ASIC called CREOLE while the discrete I/O concept is mainly unchanged.

The application processor is separated and all I/O functions are processed by a dedicated processor integrated in the CREOLE ASIC. This approach has a twofold benefit:

- To allow to handle future performance increase by replacing the application processor without changing the other core functions
- To allow an easier implementation of time and space partitioning SW architectures.

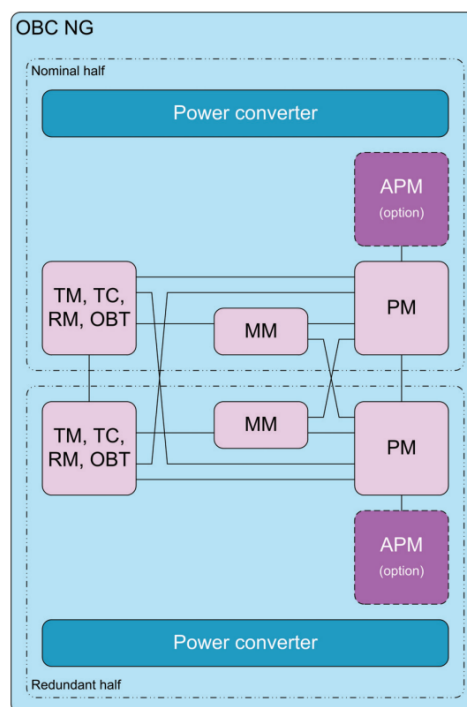


Figure 13-2: OBC redundancy concept

The proposed QPPF DHS is based on an all-in-one OBC+RTU+Mass Memory box with the following independent redundant modules:

- Two Computer Modules based on the SBCC (Single Board Computer Core) for the traditional OBC functions
- Two AOCS interface plus Standard I/O for the traditional RTU functions
- Two Mass Memory Module, which deals with the payload data only
- Two Power Converter module, to derive appropriate power rails.

Additional I/O modules could be accommodated with minimal design impact if new requirements appear in a later stage of the project that need so.

13.3.2 Computer Module: Single Board Computer Core

The OBC is based on the SBCC (Single Board Computer Core) RD[50] under development by RUAG Sweden. The SBCC functional architecture follows the SAVOIR

reference architecture RD[53] and the design is based on the CREOLE ASIC that integrated in a single device all spacecraft management functions (TC, TM, Reconfiguration, Safeguard Memory, OBT) previously split onto three different chips. It is based on LEON2-FT and features 110 DMIPS at 87.5 MHz. All I/O functions are processed by a dedicated processor integrated in the CREOLE ASIC.

The application processor is separated and the current development features the LEON based NGMP (Next Generation Multi Processor) based on 4-core LEON4 CPU and with performance up to 800 MIPS at 250 MHz.

The main I/O interfaces provided by the SBCC are:

- Two Controller Area Network bus (CAN)
- Two MIL-STD-1553B bus
- One OBDH bus
- Seven SpaceWire links externally available and a number of SpaceWire links for internal connections with the other modules.

The SBCC will have the same form factor and similar mechanics as the existing processor board used for example in JUICE mission (Figure 13-3).



Figure 13-3: JUICE processor board

13.3.3 I/O System With AOCS Interface

The RTU functions are integrated in the same unit of the SBCC and communicates internally via the OBDH bus. The design of the RTU side is based on the Advanced Flexible I/O (AFIO) RD[51] system developed by RUAG Sweden and it is based in two board types:

- Standard I/O board: thermistor acquisitions, analog measurements, relay acquisitions etc. The number of boards can be increased according to mission I/O's requirements
- AOCS I/O board: DC/DC converters, interfaces to propulsion, magnetorquers, magnetometers, etc.
 - A picture of the old version of the boards can be found in Figure 13-4.

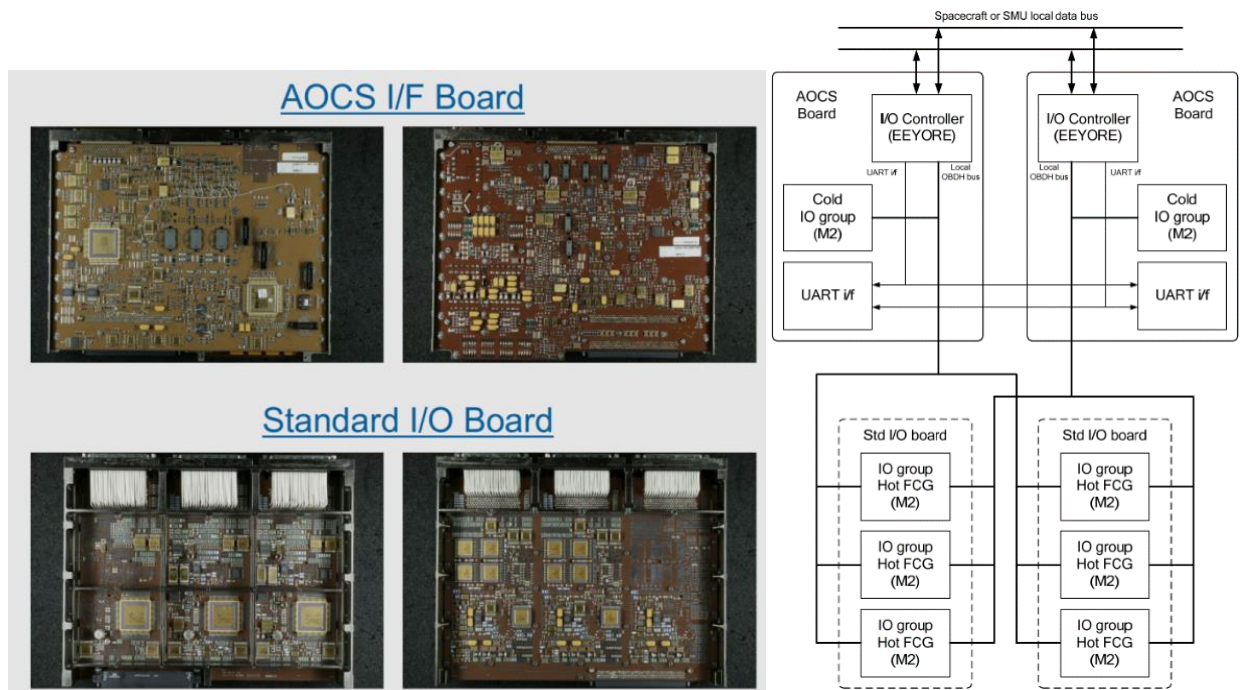


Figure 13-4: Old AOCS and Standard I/O boards (left) and new SMU architecture for the RTU part of the SMU (right)

13.3.4 Solid State Mass Memory

The design of the Solid State Mass Memory (SSMM) Module is based on the “OBC Mass Memories study” RD[52] performed by a project team consisting of RUAG Sweden, SCYSYS and DSI GmbH. The SSMM design has been conceived to be implemented in the same unit as the OBC or as a stand-alone physical unit. In case of integration in the OBC unit, two configurations are possible:

- *Flat Memory I/F*: In this configuration the processing function of the OBC is used for mass memory control and file system. The OBC PM is connected via internal SpaceWire links to the memory boards and flash access controller.
- *Packet Storage & File System I/F*: this configuration is similar to a self-standing mass memory unit but is integrated into the same physical unit as the OBC. The MM contains a dedicated processor board implementing mass memory control and file system and the memory boards including flash memories and flash access controller.

The baseline for QPPF is to integrate the mass memory in the same unit of the OBC and with the processor module implementing the controlling functions and the file system. The mass memory hardware is not file system dependant therefore different file systems can be used according to the requirements that will be defined for QPPF. For file transfer, the CFDP protocol is supported.

The mass memory supports multiple levels of redundancy. The first level is the physical redundancy of the mass memory itself. A complete redundant mass memory can be implemented by using two identical modules and using them in cold or warm redundancy depending on the QPPF mission needs. A second level of redundancy is the

capability to store critical data in more than one place. Another level of redundancy is the connection between mass memory and the QPPF payload where multiple SpaceWire connections can be used. This memory board can support up to 16 SpaceWire links.

In order to fulfil the QPPF requirement in terms data storage while using only one+one memory modules, the mass memory will use flash memory devices. By using 3D-Plus 128 Gbit NAND flash stacks, each memory board has a capacity storage of 2 Tbit, enough to allocate the baseline memory needs of 1.63 Tbit.

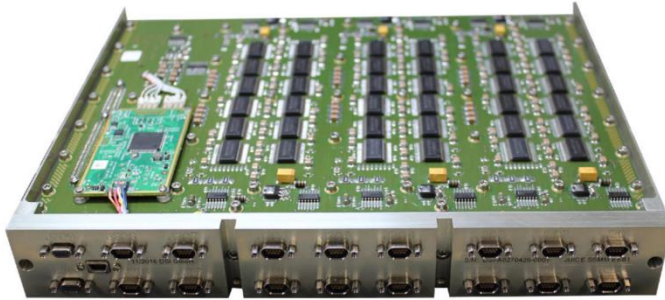


Figure 13-5: Flash based SMU mass memory board

13.3.5 Spacecraft Data Handling Architecture

The platform Command and Control network is based on CAN-bus. Though much platform equipment supports this command and control system, it is possible that at the time of QPPF there is still some units that have to be commanded through MIL-1553-bus or RS-422. The SMU is prepared to cope with such needs, although in such case the overhead will come in the heavier harness and power consumption of MIL-1553-bus with respect to CAN-bus. Other important features of the SMU for the global commanding are the time-triggered deterministic send list with timing information plus filtering of receive messages into multiple streams with arbitrary sized circular receive buffers with time mark.

Instead, the payload command and data network is based on SpaceWire. Thanks to the time-triggered deterministic send lists with timing information and receive lists with identification and time stamping of individual packets, the integration of the payload data-handling subsystem is very likely to be highly simplified. It is to be noted that nowadays thanks to programs like Bepicolombo, SpaceWire is a well-established payload command and data handling mechanism.

To facilitate operations and following DHS-110, the data storage for both platform and payload information is based on file system, and the transfer mechanism is based on CFDP.

13.4 List of Equipment

As it was explained in the previous section, a single piece of equipment is necessary to overcome the data handling subsystem task on the platform side, and that is the RUAG Sweden Next Generation Spacecraft Management Unit.

The most important information for the OCDT model can be found in Table 13-2.

	Unit mass [kg]	N_boards	Mass [kg]	Equipment Margin [%]	Mass including margin
Single Board Computer					
Core	1.2	2	2.4	10%	2.64
OBC Mass Memory Module	1	2	2	10%	2.2
AOCS/IO Board	1.3	2	2.6	10%	2.86
DC/DC converter board	1	2	2	10%	2.2
Motherboard and housing	1.9	1	1.9	10%	2.09
TOTAL			10.9	10%	11.99

Table 13-2: List of equipment, mass

	Power Operational [W]	Power Standby [W]	Width [mm]	Height [mm]	Length [mm]
Single Board Computer					
Core	7	6.47	36	277	242
OBC Mass Memory Module	6.6	3.5	36	277	242
AOCS/IO Board	6.5	4	36	277	242
DC/DC converter board	12.48	8.5	36	277	242
SUBTOTALS	32.58	22.47	288	277	242
Motherboard and housing	N/A	N/A	28.8	N/A	N/A
TOTAL	32.58	22.47	316.8	277	242

Table 13-3: List of equipment, power and size

13.5 Options

The most immediate fall-back option would be to use the current version of the RUAG Sweden Spacecraft Management Unit with companion Mass Memory Unit from Steel Electronique (France). This will count on TRL-9 equipment but would increase the mass, power and volume budgets by 50% at least, depending on the configuration of the RTU part.

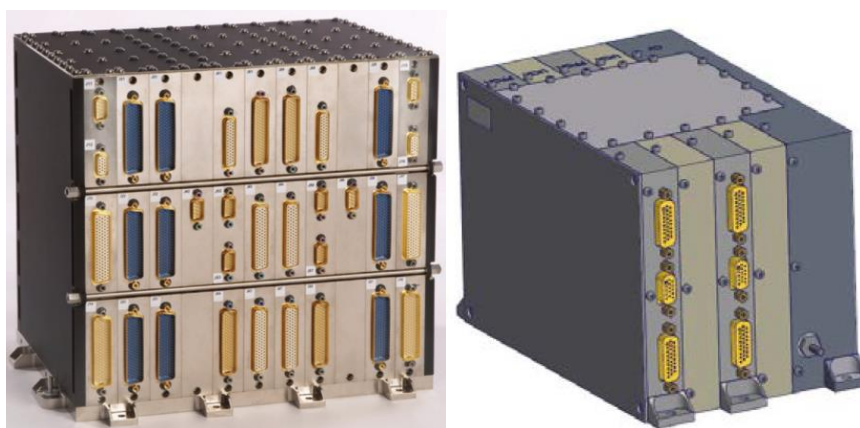


Figure 13-6: RUAG SMU (left) and Steel Electronique Mass Memory Unit (right)

On the other hand, if geo-return needs do not allow having such development in Sweden, the Airbus Defence and Space 250 Platform could also cope with the QPPF requirements and offer TRL-9 equipment. This is, instead, more a decentralised architecture based on separate on-board computer, remote terminal unit and mass memory unit.



Figure 13-7: OSCAR OBC (AirbusDS, left), AS250 RTU (AirbusDS, center) and AirbusDS MMU (right)

13.6 Technology Needs

There is currently no technology development needs, as the next generation RUAG SMU is already baselined for current programs in early phases.

14 POWER

14.1 Requirements and Design Drivers

SubSystem Requirements		
Req. ID	Statement	Parent ID
POW-010	The power subsystem of the spacecraft shall be able to generate, store, condition, distribute and monitor the electrical power used by the spacecraft throughout all mission phases in the presence of all environments actually encountered for the complete lifetime of the mission.	
POW-020	The design of the battery shall be compliant with the launch mode power consumption with a duration of 2 hours.	
POW-030	Solar array EOL dimensioning shall be done considering 3.5 years with additional mission extension of 2 years.	L3-MIS-211100
POW-040	The solar array configuration shall be body mounted.	

The analysis considered a launch in 2030 with 3.5 years of lifetime and additional mission extension of 2 years. There are no major differences for the power system in considering 3.5 years or 5.5 years (2 years extension), so for the purpose of sizing the power subsystem the worst option has been analysed.

The baseline assumption is that the spacecraft is located in L2, therefore no eclipses should be considered. This has some implications for the power system electronics, for instance the battery is only used during the launch mode. The solar array design and sizing must take in account the radiation-induced degradation in the solar cells and the maximum temperature. This is further discussed in §14.3.1.

QPPF shall be a three-axis stabilised spacecraft and it shall be kept Sun pointed with a off-pointing of 10deg.

14.2 Assumptions and Trade-Offs

Assumptions	
1	Maximum temperature of the solar array is 140°C based on Lisa Pathfinder mission
2	Factor degradation of the solar array are extracted of Lisa Pathfinder mission. This S/C has body mounted solar panels and is operating in L1 orbit
3	Sun pointing S/C with off-pointing of 10deg ± 2deg of error

The power subsystem consists of three main elements, solar array, rechargeable battery and a Power Conditioning and Distribution Unit (PCDU)

A trade-off for the power architecture implemented in the Power Conditioning and Distribution Unit is given in the next sections. For the Solar Array and Battery cells the most recently technology available, at the time of this study, has been selected.

14.2.1 MPPT vs S3R

A trade-off often performed is about the SAR converter, there are two different possibilities: MPPT or S3R. For the same output power the first is heavier and less efficient but is able to extract all the solar array power available under a large range of conditions (BoL, EoL, different SAA, etc.). The latter is simpler, lighter, cheaper and in general more efficient but is very rigid in the way power extraction is performed, in this case it is not possible to extract all the available power from the solar array and the size of the panel has to be oversized respect MPPT architecture, considering the same loss in the PCDU for both architectures. However, the lower power dissipation advantage is mitigated when the input power is of 28V instead of 50V and with low power level S/C. In QPPF due to the heritage of the units a power bus of 28V has been preferred and the level of the power is low.

Additional advantages of the MPPT versus S3R are the better behaviour from the EMC point of view and the negligible thermal gradient between strings.

For the QPPF spacecraft the maximum output current in both SAR cases is about 20Amps, so with this current the power dissipation in the S3R is around 20W and in the MPPT around 27W, so no high differences are found considering this aspect.

Therefore, considering that the solar array size can be optimised using MPPT and the low power consumption of QPPF and the heritage of Lisa Pathfinder S/C, this architecture has been selected for this spacecraft.

14.2.2 Regulated vs Unregulated Power Bus

Some trade-offs exist for deciding on the power systems architecture which type of bus is used. The most common is regulated vs unregulated bus. Adopting a regulated bus has a benefit on the power system because the solar cells works during all the mission at the same voltage, therefore it is possible to optimise the design of the Solar Array in terms of power generated.

With a regulated bus there is also a small impact on the battery size since inefficiencies linked to BCR and BDR. However the sizing of the complete subsystem is improved with a regulated bus when the power provided is considerable high.

In this case considering that the spacecraft orbit is L2, so no eclipses are considered, there will not be variations in the bus voltage during the normal operation, so a non-regulated bus has been selected in order eliminate from the design, the mass and cost of the BCR and BDR modules.

14.3 Baseline Design

The architecture proposed is showed in Figure 14-1, it is SAR based in MPPT with an unregulated power bus of 28V. Each element is explained in detail in next sections.

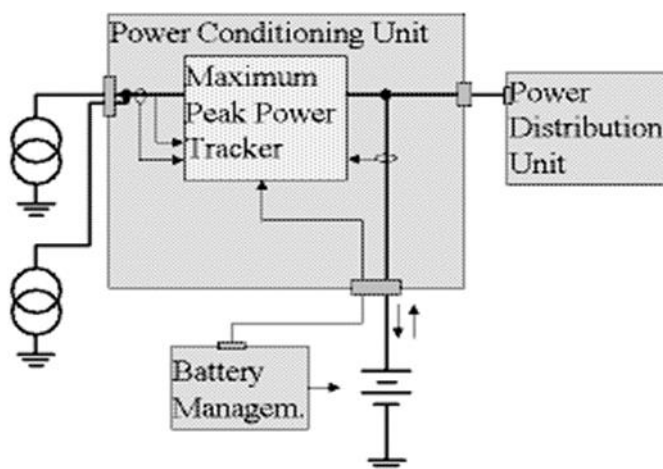


Figure 14-1: Power Subsystem architecture for QPPF

14.3.1 Solar Cell

The sizing of the solar array is fixed by the maximum power consumption during science mode.

The solar cell type proposed for the design is the Triple Junction GaAs Solar Cell 3G30C from Azurspace (30.18 cm², 30%).

Dimensions (ø x H)	30.18 cm ²
Weight	≤ 86 mg/cm ²
Open circuit voltage VOC (BOL)	2700 mV
Short circuit current ISC (BOL)	520.2 mA
Voltage at max. power VMP (BOL)	2411 mV
Current at max. power IMP (BOL)	504.4 mA
Efficiency (BOL)	29.5 %

Table 14-1: 3G30 characteristics (Values given @ 28°C)

For the solar array cells design, all the factor degradations given in Table 14-2 and the radiation degradation has been considered. The mission orbit and lifetime leads to high radiation fluence for the solar cells. The same values for the degradation factors in Lisa Pathfinder have been considered due to the similarities between the missions, even though Lisa is in a L1 orbit.

A cover glass of 150μ has been considered for radiation protection to reduce the effect of the radiation degradation in the solar array.

Parameters	Degrad. Factors
Sun Intensity (SI)	0.968
Contamination (CON)	0.99
UV& microm (UVM)	0.995
Random failure (RF)	1
Sun Angle (SA)	1
Coverg & ESD (COV)	0.982
Panel off-pointing (POP)	0.9848
Cell mismatch (MIS)	0.97
Calibration (CAL)	0.99
Random losses (RL)	1

Table 14-2: Degradation factors Solar Array

The curve of the Solar Array EoL at 140°C is given in Figure 14-2, blue curve shows the current-voltage characteristics and the red curve shows the power-voltage characteristics. The proposed architecture is going to extract the maximum power for the solar array in case that it is needed. So, the sizing of the solar array has been done to ensure that the maximum power consumption at the load + losses of the PCDU is provided for the solar array at EoL.

The maximum temperature for the solar cells is based on other projects operating in the same orbit with a body mounted solar array.

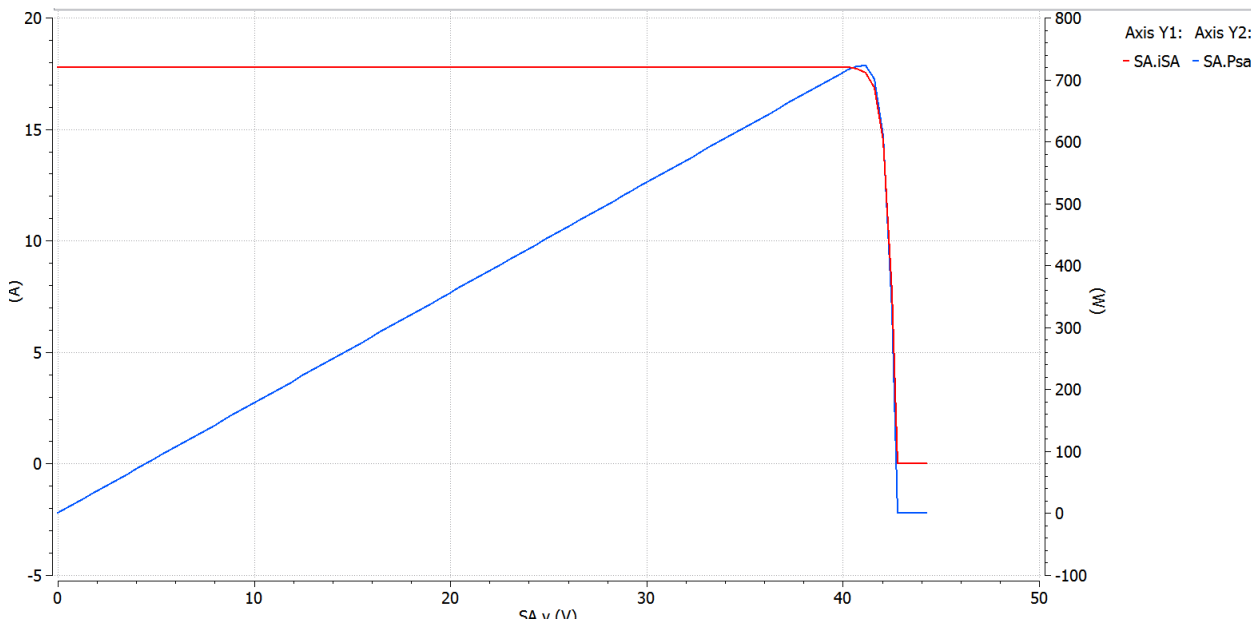


Figure 14-2: Solar Array curves @ Temp 140degC

For the solar array, just loss of one string has been considered in the analysis.

14.3.2 Battery

The battery is only used during launch mode, so the sizing of the battery is determined using the energy needed during launch mode and considering BoL parameters. A time of 2 hr is considered for this mode.

The battery cells proposed for QPPF power system are VES 16 Li-ion from SAFT.

The main characteristics of the cells are:

Dimensions (\varnothing x H)	33 x 60 mm (D-size)
Weight	≤ 114.4 g
Volume	0.051 dm^3
Voltage range	[2.7-4.1] V
Nominal capacity (C)	4.5Ah on 4.1 – 2.7V @ C/2, 20°C
Nominal energy	16Wh on 4.1-2.7V @ C/2, 20°C
Specific energy	$> 140 \text{ Wh/kg}$
Internal resistance	$\leq 35 \text{ m}\Omega$ @ 20% DoD
Operating temperature	[+10; +30] °C

Table 14-3: VES 16 cells main characteristics

During the launch mode, just PCDU and Data Handling module are switched ON.

As a result of the low energy required during launch mode, the size of the battery is very small.

High DoD of the battery can be considered due to the fact that it is almost only used during launch mode, the unique limitation for the design, as it is an unregulated bus, is that the bus voltage has enough level to ensure that units are not switched off due to an under-voltage.

14.3.3 Power Conditioning and Distribution Unit

The PCDU is connected directly to the solar array and battery, and distributes the power to the loads through LCL/R-LCL. Each load is connected to dedicated protected switches type LCL, except the On Board Computer which is supplied by a R-LCL.

As was discussed in §14.2, the architecture implemented in the PCDU is a MPPT with an unregulated bus of 28V. The bus voltage at the output of the PCDU is stable enough during the mission due to the lack of eclipses. Only during the launch mode the power bus decreases until 25.9V.

The design drivers for the PCDU and a detailed analysis shall be able to guarantee a Single Point Failure (SPF) free system, which shall eliminate by design any possible catastrophic results that might arise from a failure.

The MPPT is implemented with 3 DCDC converters in parallel, sharing the output current. Each regulator has a total output power capability of 350W, being two of them able to cope with 700W, which covers the actual maximum output power need.

Redundancy of the PCDU is implemented for the Latch Current Limiter which distributes the power to the loads, cold redundancy is implemented.

14.4 Simulations Results

The power subsystem was implemented in EcosimPro software using PEPS. Simulation has been done with the orbit of the mission using the orbit/geometry model implemented in PEPS.

For the sizing of the solar array a simple scenario considering constant flux has been carried out. For the battery the sizing considers only the launch mode.

The power consumption considering for this analysis is:

	LM	TM	SM	SAFE	PSM	COMMIS	COM
Service Module	57	151	167	135	167	172	256
Payload Module	0	60	188	0	60	60	60
Heaters	0	178	163	194	163	158	0
Losses in PCDU + harness	1	47	54	40	47	46	39
Total without margin	57	436	571	369	436	435	355
Margin 30%	17	131	171	111	131	131	107
Total w/ margin	74	567	742	480	567	566	462

Duration	2h	No eclipses
-----------------	----	-------------

Table 14-4: Modelling power consumption

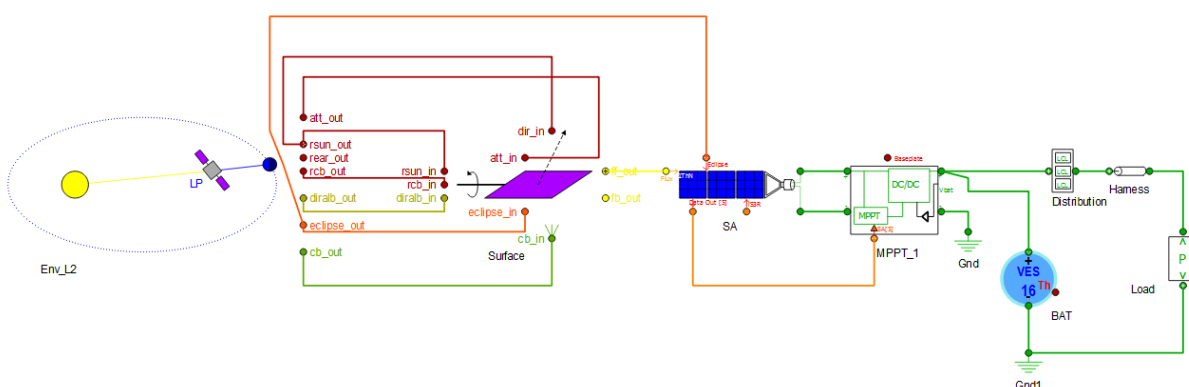


Figure 14-3: Simulation model EcosimPro

The following scenarios have been analysed in order to verify the compliance of the power system with the mission:

- A) Science mode without eclipses and sun pointing with off-pointing of 10deg considering 2deg of error for the dimensioning of the solar array

B) Launch mode for the dimensioning of the battery.

The results are given in next figures. Just the results for the battery are given due to the simplicity of the design in nominal operation.

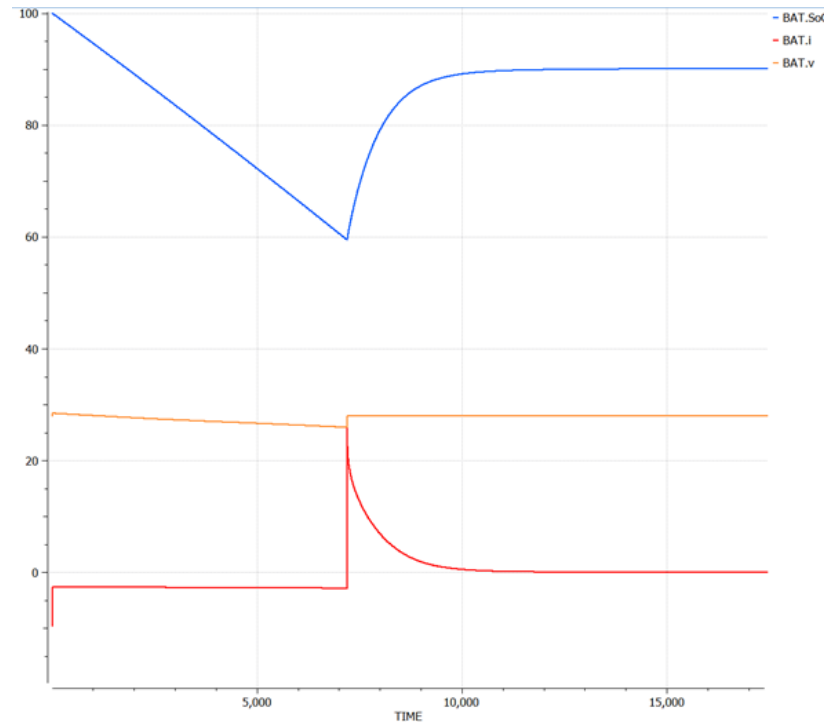


Figure 14-4: Battery waveforms during launch mode (red: current, blue: SoC, brown: voltage)

14.5 List of the Components

The design considering elements given in next sections is compliant with all the QPPF scenarios.

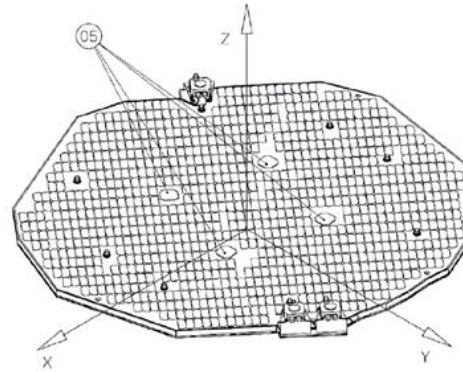
New design of the Solar Array and Battery shall be needed for QPPF, however all the components involved in these designs are already qualified in the frame of other projects. Therefore, just test to qualify the power subsystem under QPPF environment will be needed.

For the PCDU, the design of Lisa Pathfinder spacecraft can be proposed to be used in QPPF with minor modifications, if needed, to adapt them to the specific requirements of this mission.

14.5.1 Solar Array

The solar array main features are:

- Solar array body mounted with solar cells 30G30
- 24 strings series with 39 strings in parallel (24s39p)
- 3 sections of 6 strings and 3 sections of 7 strings. Total of 39 strings
- 1 blocking diodes per string
- Mass of $17.3\text{kg} \pm 20\%$
- Substrate with a surface of $3.4 \text{ m}^2 \pm 20\%$ and thickness between 31 and 34mm



14.5.2 Battery

The battery main features are:

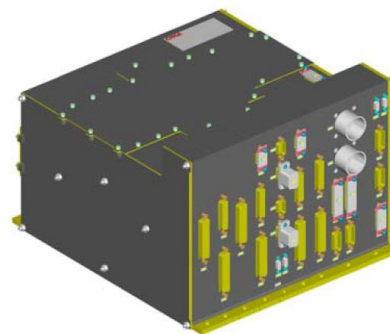
- 1 battery with 3 string in parallel and 7 cells in series type VES 16 (7s3p)
- Mass of $3.024\text{kg} \pm 20\%$
- Volume of $3402 \text{ cm}^3 \pm 20\%$ [280 x 135 x 90 mm³]



14.5.3 PCPU

The main features of the PCPU are:

- 28V unregulated bus
- MPPT modules, 3 DCDC converters of 300W
- TMTC and protections implemented in all modules
- Fix power dissipated: 30W
- Mass of $14.17\text{kg} \pm 5\%$
- Volume of $310 \times 345 \times 220 \text{ mm}^3 \pm 5\%$



	mass (kg)	mass margin (%)	mass incl. margin (kg)
SC (Spacecraft)	34.48	13.84	39.25
SM (Service Module)	34.48	13.84	39.25
BAT (Battery_Module)	3.02	20.00	3.63

	mass (kg)	mass margin (%)	mass incl. margin (kg)
PCDU (Power_Conditioning_Distribution_Unit)	14.17	5.00	14.88
SA (Solar_Array_Module)	17.29	20.00	20.75
Grand Total	34.48	13.84	39.25

Table 14-5: Power subsystem mass budget

Power (W)		
	P_on	P_stby
<input checked="" type="checkbox"/> SC (Spacecraft)	30.00	0.00
<input checked="" type="checkbox"/> SM (Service Module)	30.00	0.00
BAT (Battery_Module)	0.00	0.00
PCDU (Power_Conditioning_Distribution_Unit)	30.00	0.00
SA (Solar_Array_Module)	0.00	0.00
Grand Total	30.00	0.00

Table 14-6: Power subsystem power budget

14.6 Options

14.7 Technology Needs

Technology Needs						
*	Equipment Name & Text Reference	Technology	Supplier (Country)	TRL	Funded by	Additional Information
✓	PCDU	MPPT unregulated bus	Airbus Spain TERMA Thales Alenia Space Belgium	7		Based on the Lisa Pathfinder design
✓	Battery	Cells VES16	SAFT France	7		Based on the Lisa Pathfinder design
✓	Solar Array	Cells 3G30	LEONARDO Thales Alenia Space Airbus	7		Based on the Lisa Pathfinder design

* Tick if technology is baselined

This Page Intentionally Blank

15 THERMAL and VACUUM

15.1 Requirements and Design Drivers

SubSystem Requirements		
Req. ID	Statement	Parent ID
THE-010	The TCS of the PLM shall provide a cryogenic temperature of 20K	
THE-020	The TCS shall not produce any mechanical vibrations (e.g. no mechanical coolers)	
THE-030	The Optical Bench shall have a temperature stability of +/- 5 mK during a period of 1 week.	
THE-040	The TCS shall be designed in order to be compatible with a vacuum of 10^{-11} Pa	
THE-050	The TCS shall allow nominal operation with a solar aspect angle of +/- 10°	
THE-060	The TCS shall allow operation of the optical bench at 20 K, 50 K, and 80 K – NOT COMPLIANT	

15.2 Assumptions and Trade-Offs

Assumptions	
1	Parts within the optical bench and V-Groove structural materials are compatible with vacuum firing and extensive bake-out procedures, with outgassing values sufficiently low to ensure 10^{-11} Pa, or 10^{-13} mbar
2	V-Groove conductive heat loads assumed to be the same as used for the LiteBIRD CDF Study
3	Non-Evaporable Getters based on TiZrV thin films provide their nominal outgassing capacities at 20 K and in a space environment
4	[For SVM] Radiator and heater power sizing is based upon equipment dissipations listed in the OCDT model
5	[For SVM] Radiator coating emissivity assumed to be 0.8 at EOL
6	[For SVM] A 10°C margin is considered on top of operating and non-operating temperatures of units for radiator sizing. A margin of 20% is considered for heater power sizing.

15.3 Baseline Design

The Spacecraft Payload Module is passively cooled to 50 K, using a V-Groove type structure with 3 staged radiators, similar to Planck and Ariel type arrangement. An additional cooling stage down to 20 K of the Optical Bench is provided with a H₂ Sorption Cooler.

The Service Module is composed of a sunshield, which also includes the solar arrays, the SVM main body which houses the SVM sub-systems and also some payload equipment,

and on top the intermediate shield, which serves as an interface from the SVM to the PLM.

The spacecraft design allows for a Solar Aspect Angle of $\pm 10^\circ$, in such a way that there is no solar heat flux impinging on any of the V-Grooves. Solar heat flux impingement on the V-grooves in any phase of the mission is strictly forbidden given the V-grooves high specular reflectivity there is a chance of light trapping in small cavities, concentrating the light and creating local heating phenomena that are potentially damaging for vital equipment such as instrument harness.

Due to fairing dimension constraints, a relative angle between sunshield and intermediate shield is not feasible in order to avoid solar heat flux impinging on the intermediate shield from below. This side of the intermediate shield shall be covered in MLI with a low absorptance, reflecting in a diffuse manner. Thus some solar heat flux can be reflected onto the SVM main body enclosure.

This heat flux hasn't been assessed during the CDF studies but it is considered to be non-critical given the large area available for additional radiator on the panels forming the SVM enclosure. However, once a more detailed SVM design is considered, the layout of the radiators in the SVM can be made in a way that limits the solar heat flux reaching them.

The Service Module employs a passive thermal control, with most components mounted on structural shear panels thermally coupled to the radiators, which form part of the SVM enclosure, or directly mounted on the inner side of the radiators. The SVM enclosure Thermal control shall be done with either passive cooling or heaters.

No two-phase heat transport hardware is allowed due to the possibility of liquid sloshing perturbing the position of the centre of mass which needs to be known at nanometer-scale precision.

The temperature stability requirement of ± 5 mK over 1 week for the Optical Bench is a challenging design driver, which is addressed in the following manner. The Sorption H₂ Cooler can ensure a temperature stability of about 1 mK, provided that there is a constant heat load and a closed-loop PID temperature control on the cold tip. Heat load variations on the optical bench need to be smoothed out with a compensation heater.

An additional source of temperature instability in the PLM is seasonal temperature variations on the SVM, rippling out to the Optical Bench. These are addressed by on one hand reducing the conductive and radiative couplings between PLM and SVM, and on the other hand by employing a closed loop thermal control on the V-groove struts interface on the SVM side. The radiative coupling is minimised thanks to the intermediate shield that has MLI on the PLM side, and the conductive coupling might require a hold-down release mechanism to achieve the required thermal decoupling.

An initial requirement of performing experiments at 20 K, 50 K and 80 K is not possible to achieve due to the following main reasons:

- Above 20 K it is highly unlikely that the target pressure of 10^{-13} mbar is reached
- Temperature stability would not be reachable at such higher temperatures because the H₂ Sorption Cooler would be non-operating and the optical bench

would be subjected to the V-Groove temperature variations, which are likely to be much higher than the requirement of ± 5 mK

- A heat switch would have to be employed in order for VG-3 not to be warmed up to 80 K, desorbing a large part of the gas molecules it had previously adsorbed.

The Optical detector sits outside the optical bench on VG-3 at 50 K, it must be noted that the temperature stability on VG-3 is not nearly as good as in the optical bench. Data from Planck show 0.2-0.3 K intraseasonal variations RD[57].

In this view the thermal architecture is set to a constant optical bench temperature of 20K. A schematic of the thermal architecture is shown below.

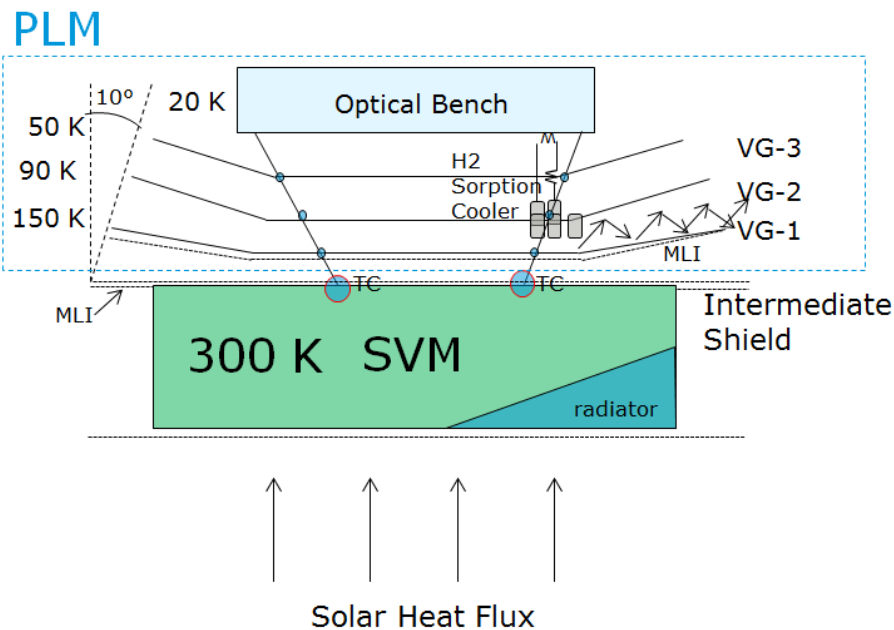


Figure 15-1: QPPF Thermal architecture of PLM and SVM

15.3.1 H₂ Sorption Cooler Dimensioning

The H₂ Sorption Cooler considered for QPPF is based on the development carried out at University Twente with also the participation of Airbus D&S Netherlands, where a TRL₅ was successfully reached for the cold tip temperature of 26 K and a cooling power of 25 mW.

Rev. Sci. Instrum. 78, 065102 (2007)

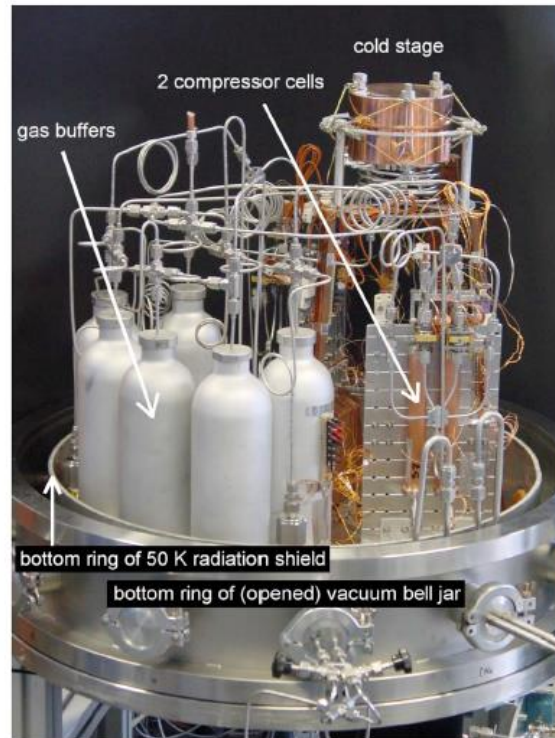


Figure 15-2: 4.5K H₂ sorption cooler

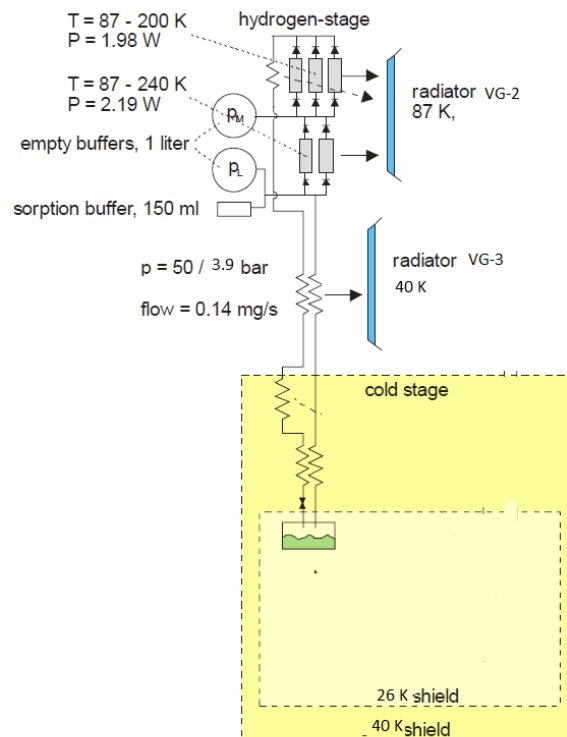


Figure 15-3: Schematic layout of H₂ sorption cooler

The H₂ Sorption Cooler uses activated charcoal pumps, known as Sorption Cells, to circulate the H₂ in a Joule-Thomson cooling loop. The main difference with the Planck H₂ Sorption Cooler is the sorbent material and the temperatures applied at the sorption cells.

The sorption cells have to be cycled between 90 K and 250 K, so in the thermal architecture each is coupled via its respective heat switch (the heat switch is an integrating part of the sorption cell) to the V-Groove 2 (VG-2). The Sorption Pumps cycling will be the most dimensioning heat load of the V-Groove Radiators.

The heat load in the cold finger is grossly estimated as composed of the following parts:

Optical Bench Dissipation	21.7	mW
duty cycles included	1.2	mW
compensation heater	1	mW
Parasitics struts	0.2	mW/K
Parasitics Harness	0.5	mW/K
Parasitics Radiation	0.3	mW/K
Total Parasitics (50K-20K)	30	mW
Total Heat Load (mW)	32.2	mW
Margin (50%)	16.1	mW
Cooling Power Required	48.3	mW

Table 15-1: Gross estimate of heat load at cold finger

Given a high uncertainty surrounds these values a conservative cryogenic systems margin of 50% in the total cryogenic heat load is applied, giving a total required cooling power of 50 mW at 20 K.

The cooler developed at UTwente provided 25 mW at 26K with a 40 K last pre-cooling stage.

In the current case a 50 K last pre-cooling stage is employed, with a 20 K cold tip temperature and a higher heat load of 50 mW. The impacts on the sizing of the cooler are the following:

- The change from pre-cooling from 40 K to 50 K is dramatic and results in a 60% decrease in available enthalpy of H₂, which results in an increase of the required mass flow and consequently the number of sorption cells and the heat load at the last pre-cooling stage, VG-3.
- The change from 26 K to 20 K, requires a change in pressure on the low pressure side from 3.21 bar to 1 bar, requiring a low pressure flat-on-flat check valve which is still TRL3 and needs further work in order to keep its leak tightness after mechanical environment testing.
- A lower pressure is also not so beneficial for the sorption pump efficiency as for the typical charcoal isotherm, the adsorbed amount per sorbent volume drops with decreasing pressure.
- The higher cooling power required has an impact on the required mass flow, which in turn impacts the number of sorption cells and the heat load at the last pre-cooling stage, VG-3.

Considering the extrapolation performed by U. Twente for the EChO case, a similar extrapolation at 26 K from 25 mW to 100 mW results in 5 sorption cells in total, with a sorption cell heat load of 6.2 W and a mass flow 0.23 mg/s, which results in a heat load of 1.5 W at 50 K pre-cooling stage.

Considering the degradation caused by the pre-cooling stage moving from 40 K to 50 K and the lower required temperature of 20 K, the 50 mW shall be obtained with the same number of cells and heat load as for the above mentioned case.

The main impact of this scaling is on the VG-2 heat load, and on the VG-3 heat load, which depends mostly on the mass flow.

For a higher fidelity thermal model, a more thorough scaling of the cryocooler involving simulation or even maybe testing will be required, since the heat load on VG-2 is the main driving parameter for the total size of the V-Grooves.

The following heat loads are applied into the sizing of the V-Grooves:

Stage	Sorption Cell Heat Load (W)	Remarks
VG-1	0	The Sorption Cooler is considered to be decoupled from VG-1.
VG-2	6.2	
VG-3	1.5	

Table 15-2: V groove heat load sizing

An additional way to limit the heat load on VG-2 is to use VG-1 to help the recycling of the sorption cells by providing cooling to 150 K on the way down to 90 K, this involves at least an additional heat switch per sorption cell and an efficient heat transport system.

Further improvements on the sorbent adsorption performance and packing methods may also have a reducing impact on the heat loads on VG-2.

The following assumptions were used for the V-Groove sizing:

- The same conductive couplings between V-Grooves are taken as for LiteBIRD study
- No solar heat flux impinges on the V-Grooves at any time
- Interface temperature of the intermediate shield at 300 K.

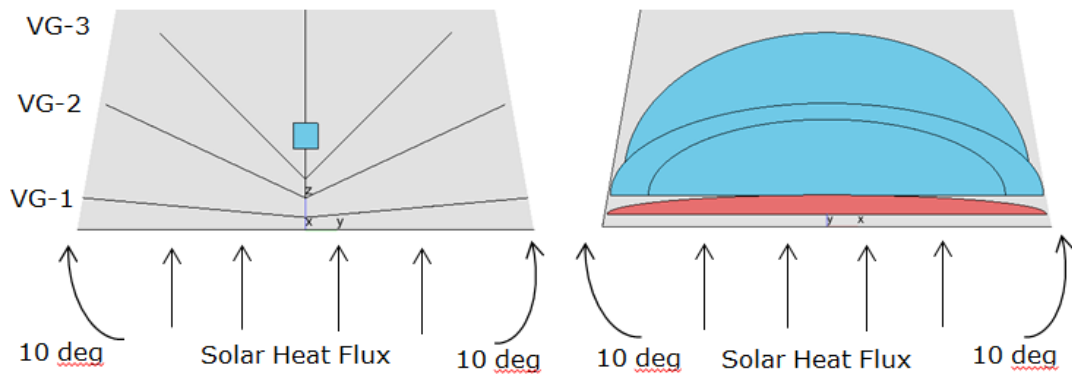


Figure 15-4: V-groove sizing assumptions

	Conductive Coupling [W / K]	Remarks
SVM, VG-1	0.0128	
VG-1, VG-2	0.00811	
VG-2, VG-3	0.003713	
VG-3, Optical Bench	0.000425	
VG-1, VG-3	0.000116	

Table 15-3: V-groove conductive coupling assumptions from the LiteBIRD CDF study

The V-Groove radiators are composed of 3 radiators:

- VG-1, with a 5° tilt, MLI on the under side facing the Intermediate Shield, and a highly specular low-emissivity VDA coating on the upper side facing VG-2
- VG-2, with a 20° tilt relative to VG-1, VDA coated on the bottom side facing VG-1, and partially VDA-coated on the upper side facing VG-3, with a high emissivity white paint on an outer rim of the radiator
- VG-3, with a 20° tilt relative to VG-2, VDA coating on the lower side facing VG-2, and a high emissivity white paint on the upper side, facing deep space.

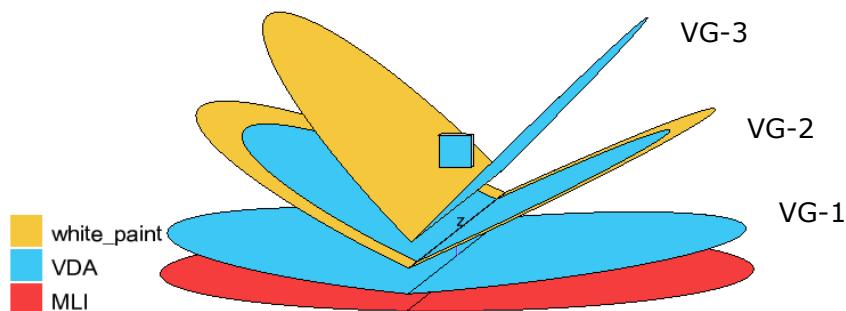


Figure 15-5: V-groove layout

Given the high heat load on VG-2, the choice to use a high-emissivity outer rim is tied to the fact that the specular highly reflective surfaces required for the multi-reflections to reject the heat are more and more critical at inner parts of the V-Grooves, on the outer part this effect is less critical and a high emissivity coating on a sufficiently large outer rim can bring a net positive effect on the heat rejection capacity. This was verified by analysis as will be shown further.

The optical bench is mounted on top of VG-3, which is at 20 K provided by the H₂ Sorption Cooler, a total parasitic heat loss of 11 mW is found coming from VG-3 into the Optical Bench.

In order to account for modelling uncertainties and the dependence on some parameters, a sensitivity analysis was performed. The parameters that were studied are the following:

Parameter	Variation
No. Rays Nominal	1000-100 000
VDA specular reflectivity	0.7-0.95
VDA emissivity	+/- 50%
MLI emissivity	+/-50%
White paint emissivity	+/-0.1
Conductive Couplings	+/- 50%
V-Groove angle	10-30°
Outer rim width	+/- 50%
Heat Loads	+/- 20%

Table 15-4: Thermal modelling parameters

The results are the following:

	Sunshield	optical bench	VG1 MLI	VG1 VDA	VG2 VDA	VG2 rim	VG3
Case	Temperature [C]						
nominal	26.85	-225.63	-57.38	-172.16	-183.00	-183.32	-223.82
V-groove angles 10	26.85	-226.96	-58.66	-172.19	-181.63	-181.96	-224.87
V-groove angles 30	26.85	-221.13	-59.80	-170.85	-183.54	-183.86	-219.83
MLI emissivity -50%	26.85	-225.63	-85.45	-172.18	-183.00	-183.32	-223.82
MLI emissivity +50%	26.85	-225.63	-44.62	-172.14	-183.00	-183.32	-223.82
Rim width -50%	26.85	-225.51	-59.25	-171.64	-177.77	-178.00	-223.83
Rim width +50%	26.85	-225.53	-59.26	-172.52	-186.67	-187.03	-223.86
VDA emissivity -50%	26.85	-224.82	-59.26	-157.44	-176.38	-176.83	-223.76
VDA emissivity +50%	26.85	-226.18	-59.25	-179.84	-187.48	-187.73	-223.81
VDA specular reflectivity 0.7	26.85	-225.53	-59.25	-171.90	-182.85	-183.17	-223.71
VDA specular reflectivity 0.8	26.85	-225.56	-59.25	-172.02	-182.90	-183.22	-223.74
VDA specular reflectivity 0.9	26.85	-225.61	-59.25	-172.13	-182.98	-183.31	-223.80
White paint emissivity 0.65	26.85	-224.72	-59.00	-172.03	-181.65	-181.94	-222.53
White paint emissivity 0.85	26.85	-226.44	-59.26	-172.29	-184.25	-184.60	-224.94
GL +50%	26.85	-224.60	-59.07	-163.66	-182.64	-182.86	-223.31
GL -50%	26.85	-226.94	-59.07	-185.26	-183.18	-183.80	-224.41
QI +20%	26.85	-223.63	-59.07	-171.69	-178.96	-179.34	-221.71
QI -20%	26.85	-227.76	-59.07	-172.57	-187.70	-187.96	-226.34
No. Rays Normal 1000	26.85	-225.54	-58.52	-172.20	-183.02	-183.35	-223.85
No. Rays Normal 100000	26.85	-225.59	-59.08	-172.19	-183.11	-183.44	-223.92
			- increase in temperature over the nominal case				

Table 15-5: Sensitivity analysis results

So a high dependence is found on the VDA emissivity and also its specularity, and the VG-2 outer white paint rim. Taking into account the total quadratic sum of the temperature deviations, a new sizing of the V-Grooves is taken, yielding the following heat load budget:

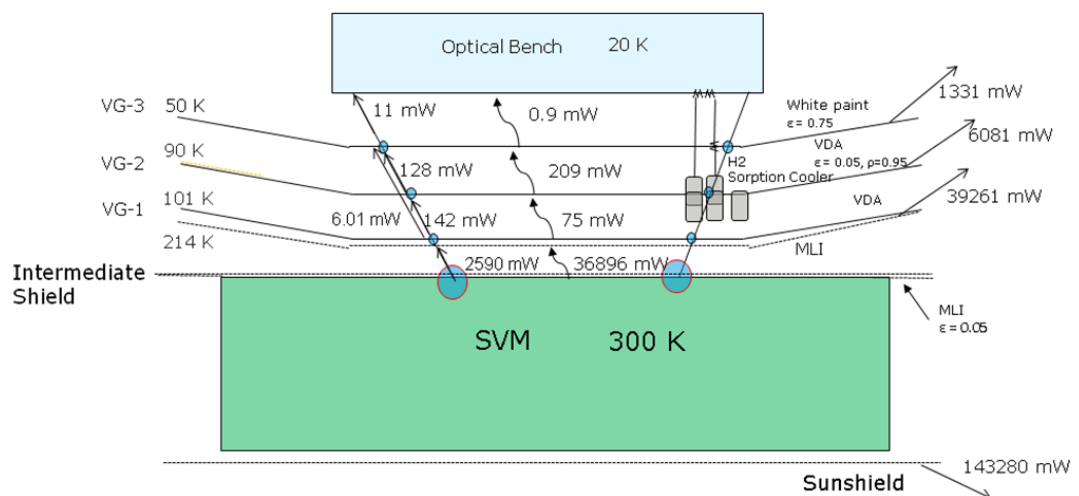


Figure 15-6: Refined thermal design and heat load budget

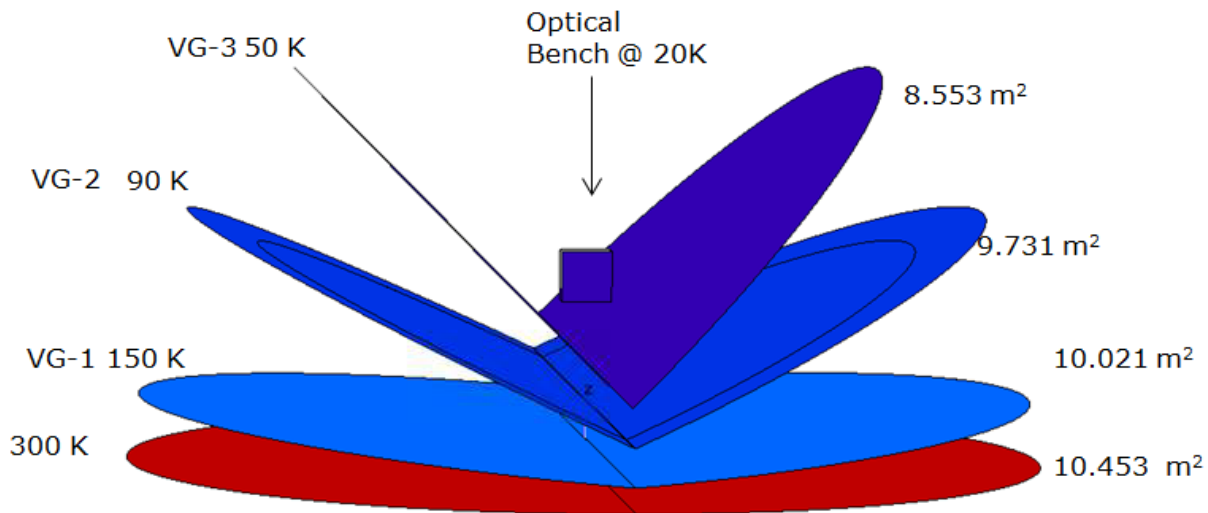


Figure 15-7: Refined V-groove layout

15.3.2 SVM Thermal Architecture

The Service Module employs a passive thermal control, with most components mounted on structural shear panels thermally coupled to the radiators, which form part of the SVM enclosure, or directly mounted on the inner side of the radiators. The SVM enclosure Thermal control shall be done with either passive cooling or heaters.

Further design aspects include:

- The internal cavity is painted black to promote temperature uniformity within the SVM, kept at around room temperature, -20 C to +20 C.
- Thermal doublers or spreaders are employed in case of high heat flux density units
- Thermal fillers are employed to promote conductive coupling to radiator panel
- MLI on parts of the SVM enclosure which are not radiator
- Possibly a closed loop temperature control at the SVM-PLM interfaces
- Heat is removed via external radiating surfaces with high emissivity finishes
- Heaters and thermistors installed near the unit's Temperature Reference Points (TRP's).

The sizing of the radiators and heaters is done according to the power dissipation modes, as shown below:

	Sizing of the radiator									
	Target Temp.	Target Temp.	Target Rad. Temp.	T space	σ	Rad. EPS	Rad. Eff.	Int. Heat Load	Rad. Area	Rad. Area (incl. margin)
	(°C)	(K)	(K)	(K)	(W/m ² K ⁴)	(-)	(-)	(W)	(m ²)	(m ²)
Mode	Radiator (Cold Case)				black paint					20%
SM	-15	258	248	4	5.67E-08	0.8	0.9	266.65	1.7	2.1
	Heater sizing (cold case)									
	Target Temp.	Target Temp.	Target Rad. Temp.	T space	σ	Rad. EPS	Rad. Area	Rad. Eff.	Int. Heat Load	Heater demand
	(°C)	(K)	(K)	(K)	(W/m ² K ⁴)	(-)	(m ²)	(-)	(W)	(W)
Mode	Heater sizing (cold case)				black paint					
LM	-30	243	233	4	5.67E-08	0.99	2.1	1	56.5	286.3
TM	-30	243	233	4	5.67E-08	0.99	2.1	1	148.65	194.2
SM	-30	243	233	4	5.67E-08	0.99	2.1	1	228.17	114.6
SAFE	-30	243	233	4	5.67E-08	0.99	2.1	1	99	243.8
PSM	-30	243	233	4	5.67E-08	0.99	2.1	1	138.65	204.2
COMMIS	-30	243	233	4	5.67E-08	0.99	2.1	1	138.65	204.2

Table 15-6: Radiator and heater sizing

The radiator is sized for SM Mode, at 2.1 m². The Heater power budget is sized for SAFE mode, at -30C, 244 W.

15.3.3 Vacuum Aspects

The initial requirement of 10⁻¹⁵ mbar is not compliant, mainly because the state-of-the-art measurement techniques are limited to higher pressures, which won't allow for an end-to-end verification on ground of the instruments' capacities.

Even though deep space vacuum is estimated at around 10⁻¹⁹ mbar, the vacuum surrounding a spacecraft is typically several orders of magnitude lower. The following typical pressures are expected:

- Deep space, estimated 1x10⁻¹⁹ mbar
- Inside Spacecraft bus, 1x10⁻⁶ mbar
- Sun-shaded part, 1x10⁻⁸ mbar
- V-groove cryopumping 1x10⁻⁹ mbar
- Wake Shield facility 1x10⁻¹² mbar

The Science goals were adapted according to an ultimate pressure of 10⁻¹³ mbar, which is within reach of the Extremely High Vacuum measurement techniques, allowing on-ground verification.

In order to reach such a low pressure or extremely high vacuum, a design relying mainly on physisorption and chemical sorption, providing cryopumping is employed:

- V-Grooves provide cryopumping at 150 K, 90 K and down to 50 K.
- H₂ Sorption Cooler provides cryopumping at 20 K.
- The Optical Bench inner walls are coated with a Non-evaporable Getter, metal hydride type material, thin-film based off of TiZrV specially designed for chemisorption of H₂ at extremely high vacuum.
- Materials present at the PLM and specifically at the optical bench have to be screened for hydrogen outgassing (e.g. no honeycomb type panels for the V-

Grooves) are subjected to extensive bakeout and vacuum firing procedures, in order to reduce hydrogen outgassing to acceptable values in order to reach the 10^{-13} mbar.

- Optical Bench is equipped with a venting door, in order to release non-condensable gases that might saturate the NEG coating
- Cool-down performed in phased sequence where optical bench is venting during the whole time and NEG coated walls are kept at a temperature higher than VG-3.

Using the wake effect, as used in the Wake Shield facility could in principle achieve the same vacuum, however, the wake effect is not very predictable and verifiable on-ground.

Regarding the cryopumping at 20 K, a lower temperature such as 4 K would be more beneficial for the vacuum. However, such a temperature would require either a mechanical cooler or an additional sorption cooler using 4-He which requires too much heat load in order to size a V-Groove radiator that fits in the Ariane 64 large fairing. Also, such a cooler would have a finite leak of 4-He, which would be an additional gas that wouldn't be cryopumped in any surface of the payload and thus would saturate the NEG's.

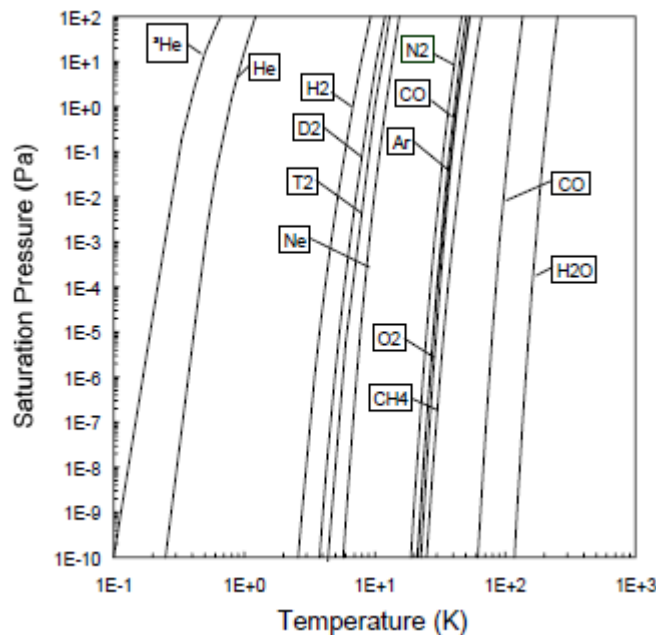


Figure 15-8: Cryo-coolers saturation vs temperature

The Non-Evaporable getters developed at CERN, thin films of TiZrV perform at 20 K to reach 1×10^{-13} mbar, provided species other than H_2 are pumped alternatively. Strong evidence backs this RD[58] RD[59], but no unequivocal measurement at 20 K relying only on cryopumping have been found.

The venting door on the Optical Bench, to allow for initial venting and NEG desaturation and activation, has to be actuated several times over lifetime and be suitable for cryogenic temperatures (low power dissipation) and survive high temperatures (at least 180°C).

V-groove light panel structure must rely on an innovative ALM technique or an uncommon welding technique to allow such a light structure without resorting to adhesives or other species that might outgas H₂ in large quantities.

Table 5
Some measured outgassing rates at room temperature suitable for XHV

Material	Surface treatment	Outgassing rate (Pa m s ⁻¹)	Reference
Stainless steel	Glass bead blasted + vacuum fired at 550°C /3 days + baked at 250°C/24 h.	1.6×10^{-13} [H ₂]	[59]
Stainless steel (304L)	Air fired at 400°C/38h + baked at 150°C/7 days.	1×10^{-12} [H ₂]	[54]
	Air fired 390°C/100 h + baked at 150°C.	5×10^{-12} [H ₂]	[53]
Stainless steel	Vacuum fired at 960°C/25 h +baked at 180°C /6 h.	1×10^{-12} [H ₂]	[60]
Aluminium	Vacuum fired at 960°C/25 h +baked at 180°C /6 .	9×10^{-13} [N ₂]	[58]
Copper (OFHC)	Vacuum fired at 550°C/3 days + baked 250°C/24 h	6×10^{-14} [H ₂]	[59]
Copper (OFHC)	Baked at 525°C	2×10^{-13} [N ₂]	[58]
TiN on stainless steel.	Vacuum fired at 430°C/100 h and 500°C/ 100 h.	1×10^{-13} [H ₂]	[61]
Aluminosilicate glass	Baked at 500°C/18 h + 600°C/2 h + 700°C/2 h/500°C/10 h.	2.5×10^{-13} [N ₂]	[62]

Table 15-7: Material outgassing rates

During pump-down, until 20 K is reached, NEG must be kept warmer than vicinities, in order to avoid monolayer formation (CO₂, N₂, CO, any other) and subsequent activation. E.g. monolayer time at 1E-6 mbar is 1s.

If NEG activation is required, NEG must be warmed up to 180C, while keeping the coldfinger at 20K. This means a heater on optical bench and heat switch at 20K must be employed, otherwise contaminants will form a monolayer, saturating the NEG.

This last aspect might become critical, given many components in the optical bench will not withstand such high temperatures.

In order to assess the NEG's effectiveness in a relevant environment, as well as the true necessity of activation over lifetime, and the required temperature, a development activity with an optical bench STM at 20 K, having undergone proper bake-out procedures would mitigate many risks foreseen with this considered approach to reach 10⁻¹³ mbar.

15.4 List of Equipment

SVM:

- Heaters for thermal control of separate units
- Heaters for closed loop thermal control at interface

- Thermal spreaders
- 20-layer MLI with solar diffusive reflective outer layer, like SSM
- Black Paint for Radiator parts
- Thermistors
- Intermediate shield with MLI on both sides

PLM:

- V-Groove 3-stage radiators
- H₂ Sorption Cooler
- High resolution temperature measurement sensor, at most 0.1 mK
- Compensation Heater in closed loop for temperature stability
- Thin Film Non-Evaporable Getters coating the inner walls of the optical bench

	mass (kg)	mass margin (%)	mass incl. margin (kg)
SC (Spacecraft)	135.09	19.99	162.10
PLM (Payload Module)	8.02	19.98	9.62
CDE_SORPH2 (Drive_Electronics_SorptionH2)	2.00	20.00	2.40
SORP_H2 (Sorption_H2_cryocooler)	6.00	20.00	7.20
CryoHT_01 - 20 (CryogenicHeaters)	0.02	10.00	0.02
SM (Service Module)	127.07	19.99	152.47
VG (VGrooves)	111.01	20.00	133.21
HT_01 - 40 (Heaters)	0.05	5.00	0.05
RAD (Radiator)	16.00	20.00	19.20
Therms_01 - 60 (Thermistors)	0.01	5.00	0.01
Grand Total	135.09	19.99	162.10

Table 15-8: PLM and SVM Thermal System Mass Budget

	P_on	P_stby	Total P_on
SC (Spacecraft)		0.00	467.80
PLM (Payload Module)		0.00	80.00
SORP_H2 (Sorption_H2_cryocooler)	50.00	0.00	1 50.00
CDE_SORPH2 (Drive_Electronics_SorptionH2)	10.00	0.00	1 10.00
CryoHT_01 (CryogenicHeaters)	1.00	0.00	20 20.00
SM (Service Module)		0.00	387.80
HT_01 (Heaters)	9.70	0.00	40 388
Grand Total		0.00	467.80

Table 15-9: PLM and SVM Thermal System Power Budget

15.5 Options

- Hold-Down Release Mechanism on Interface between Intermediate Shield and V-Groove Struts (Structural/Mechanisms Item, but required for thermal purposes)
- Venting latch door on optical bench
- Heat switch on 20K cold finger, to allow NEG activation at higher temperatures

15.6 Technology Needs

Technology Needs						
*	Equipment Name & Text Reference	Technology	Supplier (Country)	TRL	Funded by	Additional Information
	NEG	NEG operation in space representative environment	CERN	3		
	H ₂ Sorption Cooler	Flat-On-Flat Check Valve qualification	NL	3		
	Cryogenic Thermal Sensor	High Resolution Cryogenic Thermal Sensor	-	3		

This Page Intentionally Blank

16 ENVIRONMENT

16.1 Requirements and Design Drivers

Performing quantum physics experiments in space is a big challenge from a space environment point of view. The vacuum of space offers the necessary cool and low pressure environment but also includes plasma, radiation and micrometeoroid hazards which could limit the required sensitivity of the measurements. The effects of space environment hazards can be split in two parts: one concerning the disturbances due to the space environment on the measurement itself, the other concerning the space environment hazards on the overall S/C system during the mission lifetime. The requirements for proper spacecraft are detailed here, the requirements for scientific payload operation follow the defined mission requirements.

16.1.1 Requirements on Scientific Payload

The requirements on the scientific payload are the most stringent due to the high level of sensitivity needed to perform the quantum decoherence measurements. The science objective of testing for deviations from quantum physics can only be met if the test particle is not subjected to known decoherence effects that would otherwise mask these deviations. Since the measurement principle is based on an accurate position measurement of a nanoparticle, any mechanism that couples the centre-of-mass motion of the physical system to the space environment needs to be investigated. The relevant requirements that need to be met are L2-SCI-111000, L3-MIS-121200 and L4-MIS-115120.

- **Plasma:** Interplanetary space is not vacuum but filled with plasma composed of ionized atoms and electrons coming from the Earth's atmosphere and the Sun. The parameters describing the plasma environment are the particle's temperature and the overall density. These determine the flux of particles incident on a surface which in turn will determine the surface equilibrium potential RD[63]. In case of the scientific payload the flux of particles incident on the nanoparticle surface needs to be low enough so the nanoparticle doesn't charge and cannot interact with any electric field surrounding the optical bench.
- **Radiation:** Energetic radiation from solar particle events and cosmic rays have enough energy to transfer a considerable amount of momentum to the nanoparticle, disturbing the measurement. When the radiation energy is high enough (as for galactic cosmic rays) the particles can penetrate deeply into the spacecraft and cause displacement damage. This is of particular concern for the storage of the nanoparticles which are subject to this type of radiation for the entire mission lifetime. The radiation damage can cause individual atoms inside the nanoparticles to change position inside the lattice or charge up as a side-effect of radiation penetrating into matter. This effect may degrade the test particles in storage through the mission lifetime.
- **Micrometeoroids:** Interplanetary space is filled with micrometeoroid particles. During a measurement, when a microparticle hits the spacecraft the spacecraft and optical bench will change in position with respect to the nanoparticle itself, causing a displacement of the test bench with respect to the free floating test

particle and as a result potentially a degradation of the interference pattern measured.

16.1.2 Requirements on S/C System

The mission duration is several years including mission extensions. This means that the S/C components need to be robust enough to survive for this amount of time in space. The main spacecraft hazard mitigation requirements are listed below.

- **Plasma:** Depending on the spacecraft surface materials, the equilibrium potential of these different surfaces may differ significantly. When this potential difference is high enough there is a risk of electrostatic discharges (ESD).
- **Radiation:** Radiation damage to the spacecraft entails degradation of S/C materials like for example the solar arrays, diminishing the power produced over the mission lifetime, as well as single event effects (SEE) impacting the performance of electronic components on the S/C.
- **Micrometeoroids:** Impacts of micrometeoroid particles cannot be avoided but the risk of failure needs to be assessed when a more detailed configuration of the S/C is available.

16.2 Assumptions

The space environment the S/C encounters is mainly determined by its intended orbit. This study initially considered a highly elliptical Earth orbit (HEO), L1, L2, Earth leading and Earth trailing orbits. In this section, the differences and similarities between the different orbits are listed here for each of the space environment hazards.

16.2.1 Plasma Environment

The orbits named above encounter essentially only two different plasma environments which can be categorised as inside and outside of the magnetosphere. Inside the magnetosphere, the variability of plasma parameters is much higher than outside due to its complicated structure. Outside of the magnetosphere the S/C resides in the solar wind environment which is essentially the same for L1, L2, Earth leading and trailing orbits RD[64]. The variation in plasma environment for each of these orbits is smaller than the variation of the solar wind parameters itself so a single solar wind plasma environment is adopted with the exception of L2 where a magnetotail environment can be encountered. The plasma environment parameters are listed in Table 16-1 along with the expected ambient current density to the S/C surface.

	Electron density [m ⁻³]	Electron temperature[eV]	Ion Density[m ⁻³]	Ion temperature[eV]
<i>L1/L2 solar wind</i>	1 ± 0.5E7	15	1 ± 0.5E7	10
<i>L2 magnetotail/sheath</i>	<1E7	180	<1E7	600
<i>Earth leading/trailing</i>	1 ± 0.5E7	15	1 ± 0.5E7	10
<i>HEO inner magnetosphere</i>	<2.5E9	2	<2E7	2

	Electron density [m ⁻³]	Electron temperature[eV]	Ion Density[m ⁻³]	Ion temperature[eV]
<i>HEO magnetosheath</i>	<1.5E8	25	<1.5E8	150
<i>HEO solar wind</i>	1 ± 0.5E7	15	1 ± 0.5E7	10

Table 16-1: Plasma parameters (temperature and density) for the considered orbits

16.2.2 Radiation Environment

For the orbits under consideration the same distinction as for the plasma environment can be made: in- and outside of the magnetosphere. Only for a HEO orbit the spacecraft encounters the radiation belts inside the magnetosphere where the solar wind and galactic cosmic rays are shielded. The HEO orbit under consideration (7000 km perigee and 114000 km apogee) will ensure the spacecraft will pass through the outer Van Allen radiation belt fast and will take it through the regions where the solar wind particles are deflected by the Earth's magnetic field. The near-Earth interplanetary orbits - L1, L2, Earth-leading and Earth-trailing – all reside fully in the solar wind and therefore the radiation environment is fully determined by it. From here the radiation analyses will address the near-Earth interplanetary environment and therefore no distinction will be made between the different orbits anymore.

Assuming a radiation environment near Earth includes taking into account the two most pronounced sources of radiation: particles originating from the Sun and galactic cosmic rays. Both are modulated by the solar cycle in the sense that high solar activity will entail a higher prevalence of solar energetic particle events but it also means the galactic cosmic rays are more effectively shielded by the Sun's magnetosphere. To analyse the implications of radiation on the payload and the spacecraft a worst-case radiation environment is assumed: a solar particle flux corresponding to solar maximum activity and including observed worst-case particle event fluxes and a worst-case galactic cosmic ray flux spectrum corresponding to solar minimum.

The solar particle flux is given by the SAPPHERE (Solar Accumulated and Peak Proton and Heavy Ion Radiation Environment) RD[65] model which covers all SEP environment time scales across all relevant ion species in a consistent probabilistic manner. A worst event fluence with a 95% confidence level using ions in a mass range from H to U is and there is no magnetic shielding implied. The galactic cosmic ray flux is given by the ISO 15390 model RD[66] which is a semi-empirical GCR model taking into account solar activity variations and including ions in a mass range from H to U. Also for this a worst-case fluence with a 95% confidence level is assumed corresponding to solar minimum data from May 1996. The worst case fluences are shown in Figure 16-1.

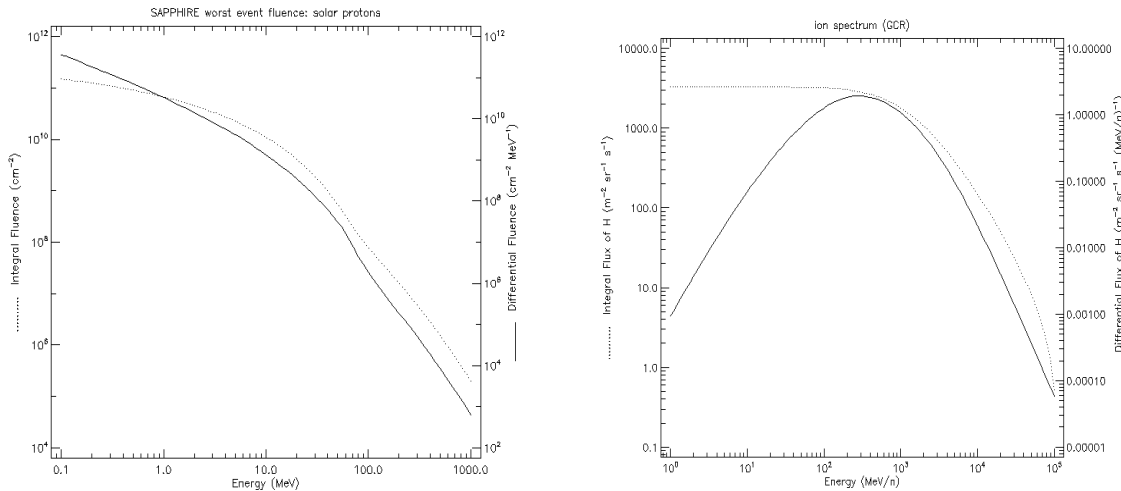


Figure 16-1: Worst case fluences for solar particles (SAPHIRE model, left) and galactic cosmic rays (ISO 15390, right)

16.2.3 Micrometeoroid & Debris Environment

The micrometeoroid environment of the spacecraft is for most of the orbits under consideration fairly uniform with the exception of the HEO orbit. To model this the Grün meteoroid flux model is used which is also implied in the ECSS space environment standard (E-ST-10-04C) RD[67]. The model gives the number of particles per square meter per year, equal to or larger than a given mass. The isotropic integral flux is calculated using a mass range between 1E-18 g up to 1 g. For information a particle of mass 1E-18 g is assumed to have a diameter of 9.8E-7m and a density of 2 g/cm³. The integral fluxes for the different orbits are listed in Table 16-2 and the Grün meteoroid flux is shown in Figure 16-2. The fluxes for the HEO orbits are higher because of gravitational focusing by the Earth.

Any form of risk concerning collisions with debris object is considered to be negligible since 90 % of all debris is located below 1200km altitude.

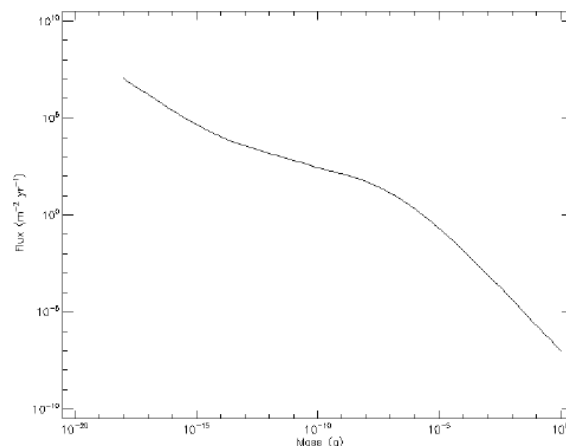


Figure 16-2: The Grün meteoroid flux model

	Grün meteoroid flux [m ⁻² yr ⁻¹]
HEO perigee	1.15E7
HEO apogee	8.74E6
L1/L2/Earth leading/trailing	8.30E6

Table 16-2: Grün meteoroid fluxes for the orbits under consideration

16.2.4 Summary

The environment assumptions made above will be used for the analyses of the radiation, plasma and micrometeoroid hazards to the payload and spacecraft and are listed here in Table 16-3. Since the baseline orbit of the mission will be located in near-Earth interplanetary space this will also be the assumed environment for the analyses carried out further on. Distinctions with regards to a HEO orbit will be made when needed.

Assumptions	
1	The baseline plasma environment in which the spacecraft resides is a general solar wind environment with parameters $T_e = 15$, $N_e = 1E7 \text{ m}^{-3}$, $T_i = 10$, $N_i = 1E7 \text{ m}^{-3}$.
2	The baseline radiation environment constitutes a worst-case combination of solar particle event fluxes (given by the SAPHIRE model) corresponding to solar maximum and galactic cosmic ray fluxes (given by the ISO 15390 model) corresponding to solar minimum.
3	The micrometeoroid flux is given by the Grün meteoroid flux model, corresponding to an isotropic integral flux of $8E6 \text{ particles m}^{-2} \text{ yr}^{-1}$ in near-Earth interplanetary space.

Table 16-3: Assumptions on environment for simulations

16.3 Trade-Offs

The main trade-off concerning the scientific payload level for space environment is the question of exposing the measurement unit (an optical bench) to space or shielding it by enclosing it in a cover. Exposing the optical bench to space meets the necessary cooling and pressure requirements but also means it will be subject to plasma, energetic radiation and micrometeoroid fluxes which could disturb the measurement. The open or closed cover design trade-off for the optical bench is detailed here for each of these hazards.

- **Plasma:** In an open design the fluxes of charged particles and electric fields built up are entirely subject to the properties and variability of the plasma, in a closed cover design the plasma can be shielded off to exclude the possibility of charging the nanoparticles.
- **Radiation:** For an open cover design, radiation can easily access the optical bench, a closed cover design can shield the particles preventing them from disturbing the measurement.

- **Micrometeoroids:** A closed cover design evidently shields the optical bench from microparticles.

16.4 Analysis Results

In this section the results from analyses focused on the scientific payload of QPPF are presented. For each environment hazard (plasma, radiation and micrometeoroids) the trade-off of having an open or closed cover design (as detailed in Section 16.3) will be discussed. The results only detail simulations performed for a near-Earth interplanetary environment as discussed in Section 16.2 if not specified otherwise. Simulations for the entire spacecraft are not discussed here because of the need for a much more detailed spacecraft model. However some recommendations for doing these simulations in the future are discussed in Section 16.5.

When discussing the impact probabilities of particles or radiation impacting the nanospheres in the scientific payload Poisson statistics are always assumed, where the probability P of having exactly m impacts or collisions is set by

$$P(m) = \frac{N^m}{m!} e^{-N}$$

with $N = \gamma t$ the average number of collisions, γ the collision rate and t the measurement time. To ensure that decoherence effects are not masked less than 2 impacts during the given measurement time are required.

16.4.1 Plasma Environment

The near-Earth plasma environment is determined by the properties of the solar wind. All spacecraft interact with the plasma by collecting or emitting currents from its surface. In a steady state, the surface attains an equilibrium potential or voltage at which the net current to the surface is zero. Depending on the plasma temperature and density (which determines the current density to a S/C surface) and also the material properties, surfaces could charge to a different potential posing the risk of electrostatic discharges. Due to the much smaller mass of electrons with respect to ions the thermal velocity (commonly given by $v = \sqrt{kT/m}$ with kT the thermal energy and m the mass RD[64]) is much higher which causes the current density of electrons to any surface in space to be much higher than the ion current density. The most important other current is caused by photoemission, by which electrons get released from the surfaces due to solar illumination. In this sense the photoemission current discharges a negatively charged S/C surface. Illuminated surfaces tend to charge even to several volts positive whereas surfaces in eclipse tend to charge to negative voltages.

The solar wind has a drift velocity of the order of several hundreds of kilometres per second which causes a so-called wake effect: the high thermal velocity of the electrons will ensure that the electron current can reach all surfaces of the spacecraft whereas in the anti-sunward direction there is a significant depletion in ion density due to its lower thermal velocity. This is also confirmed by a simulation done using SPIS (Spacecraft Plasma Interaction Software RD[68]), a dedicated S/C charging software tool. A 1.5m diameter disk (mimicking the S/C sun shield) in the plasma environment detailed in Assumption 1 and including a drift velocity of 500 km/s was simulated, the results are

shown in Figure 16-3 where the density of electrons and ions are shown in log scale. The electrons are indeed distributed isotropically around the disk whereas the ions form a wake behind the spacecraft.

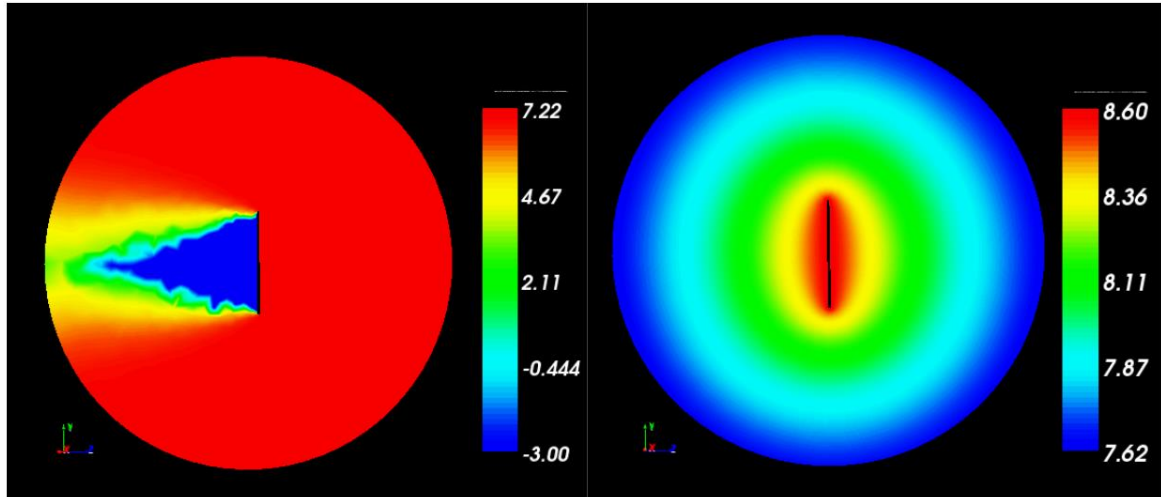


Figure 16-3: Plots extracted from SPIS of the ion (left) and electron (right) density surrounding a 1.5m diameter disk. A wake develops behind the anti-sun facing surface where the ion density is depleted and the surfaces charge negatively

The effect of the plasma environment on the scientific payload in the case of an open design is considerable: the surfaces surrounding and on the payload charge to a certain voltage causing the presence of electric fields and the nanoparticles can charge up to a certain voltage, producing an undesirable electromagnetic interaction between the measurement system and the nanoparticle. To estimate the charging of the nanoparticle the collision rate can be calculated and from this the time it takes to charge to a certain potential. This was done for the plasma environments detailed in Table 16-1, including the HEO orbits and the resulting values of current densities, collision rates and charging times up to 1 mV are listed in Table 16-4. The current densities listed correspond to the electron current densities since the ion current densities are many orders of magnitude lower, especially in the wake of the spacecraft where the payload is located.

	Ambient current density [A/m ²]	Collision rate [s ⁻¹]	Charging time to 1 mV [s]
<i>L1/L2 solar wind</i>	1E-6	~ 0.05	0.7
<i>L2 magnetotail/sheath</i>	<3.5E-6	~ 0.2	0.2
<i>Earth leading/trailing</i>	1E-6	~ 0.05	0.7
<i>HEO inner magnetosphere</i>	<9.5E-5	~ 4.5	0.007
<i>HEO magnetosheath</i>	<2.0E-5	~ 1	0.03
<i>HEO solar wind</i>	1E-6	~ 0.05	0.7

Table 16-4: Ambient current densities, collision rates and charging times to 1 mV for the plasma environment parameters given in Table 16-1

It can be seen from the calculated values that the nanoparticles charge to 1 mV in all environments in less than one second which is already much above the requirement of having non-charged test particles. Hence the density of the plasma in the solar wind is too high to allow for an open cover design of the payload module. In combination with the inevitable charging of the surrounding surfaces when exposed to the plasma this is a sufficient driver to close the payload design and shield the test particles and measurement system from the plasma.

16.4.2 Radiation Environment

The radiation models for the solar particles and Galactic Cosmic Rays, SAPPHIRE and ISO 15390 are implemented in SPENVIS (Space ENVironment Information System) which was used to analyse the radiation effects on spacecraft and payload in particular. The outputs in SPENVIS are given as particle fluences, defined as the amount of particles dN incident on a sphere of cross-sectional area dA RD[69]. By using a sphere, the area perpendicular to the direction of each particle is accounted for so that all particles passing through this volume of space are included (as illustrated in Figure 16-4). The fluences given as outputs in SPENVIS are binned in energy intervals which is in fact a differential energy fluence spectrum giving information on the energy distribution of the incident particles. A fluence is measured over a certain amount of time, in the analysis performed here one day of collecting particles is assumed to have good statistics, this is later converted to a fluence over the measurement or freefall time of the test particle. In the same way the fluence over one square meter can be converted to the fluence over the 100 nm diameter particle cross sectional area which is equal to $7.85E-15 \text{ m}^2$.

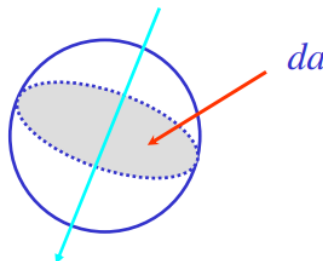


Figure 16-4: Definition of the (perpendicular) cross-sectional area dA used to calculate the particle fluence

To assess the need of having a closed or opened payload design the fluences are analysed with and without a layer of shielding which has a spherical geometry of 20 cm radius, roughly the size of the optical bench. The material was chosen to be aluminium and different amounts of thickness were assumed, ranging between 1 and 20 mm to analyse the effectiveness of the shielding.

16.4.2.1 Solar particles

As discussed above the solar particle events are modelled according to the SAPPHIRE model corresponding to a worst case event fluence over one day. The differential fluence spectrum without any shielding (so the fluence spectrum present in interplanetary space at roughly 1AU) is shown in Figure 16-5(a). Since collision probabilities is of interest this

can be integrated over the energies of the particles to calculate the total amount of particles. The integral fluence over one day amounts to $3\text{E}17$ solar particles/ m^2 . The fluences can be converted to an expected amount of particles impacting the nanoparticle over a certain measurement time and are listed in Table 16-5(a). Assuming Poisson statistics also the probabilities of having less than two impacts are given here. It can be seen that the chances of having less than two impacts as required by L2-SCI-111000 is already lower than 50% for a measurement time of 100 s. In addition to the arguments to shield the payload from the plasma particles, also this is a sufficient argument to close the payload design.

It can also be seen that the solar particle fluence spectrum is affected a lot by having simply 1 mm of Aluminium shielding. This is shown in Figure 16-5(b) from which also the integral fluence can be calculated. This is reduced to $1\text{E}14$ particles/ m^2 in one day with respect to the unshielded case, resulting in the calculated number of collisions and probabilities listed in Table 16-5(b). It can be seen than the probability of having less than two collisions is nearly 100% in all cases, offering another argument to shield the payload with a minimum amount of material.

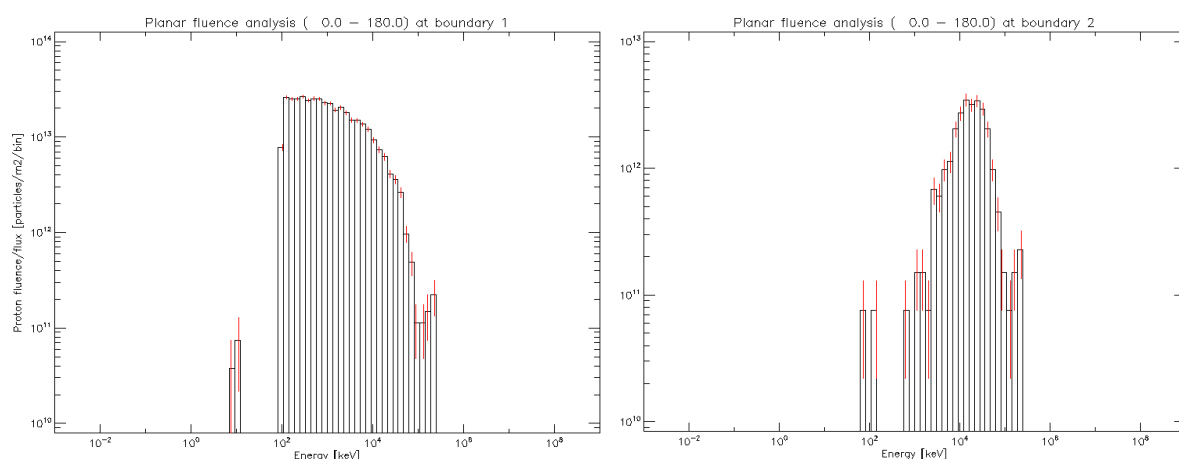


Figure 16-5: (a, left) Solar proton differential fluence spectrum without any shielding and (b, right) Solar proton differential fluence spectrum behind 1mm Al shielding

t	100 s	200 s	1000 s	t	100 s	200 s	1000 s
N	0.0009	0.0018	0.009	N	2.73	5.45	27.27
P(N, <2)	0.999	0.999	0.999	P(N, <2)	0.49	0.09	5.7E-10

Table 16-5: (a, left) Open cover design number of expected collisions of solar particles with the test particle over a designated measurement time and probabilities of having less than two impacts and (b, right) Closed cover design number of expected collisions of solar particles with the test particle over a designated measurement time and probabilities of having less than two impacts

16.4.2.2 Galactic cosmic rays

The cosmic ray spectrum in interplanetary space is much different from the solar particle spectrum in the sense that they are much more energetic and can thus penetrate more deeply into matter, creating secondary particle radiation along its path. The question of shielding the payload design is therefore less simple than in the solar particle analysis: more shielding also means more secondary particles can be created along its path. The primary radiation is attenuated in energy but for this analysis the only interest is in the total amount of particles reaching the test particle so it suffices to integrate the differential fluence spectrum as was done for the solar particles. The fluence spectra for protons, gamma rays, electrons and neutrons are shown in Figure 16-6. The integral fluence spectrum of all species over one day amounts to $1.2E15$ particles/m², unshielded. As done for the solar particles we can calculate the expected number of collisions with the test particle during the measurement time, these are listed in Table 16-6. It can be seen that the probability of having less than 2 impacts is near 100% for all measurement time spans for an unshielded design. The same analysis was carried out using different thicknesses and materials for the shielding layer but in each case the total integral fluence remained around the same value due to the large amount of secondary particles created. An important remark needs to be made here: although the total amount of particles does not vary very much for which ever type and amount of shielding, the particles energies are attenuated and may end up as charges being deposited on the test bench, causing undesirable internal charging. See also comments in Section 16.5.

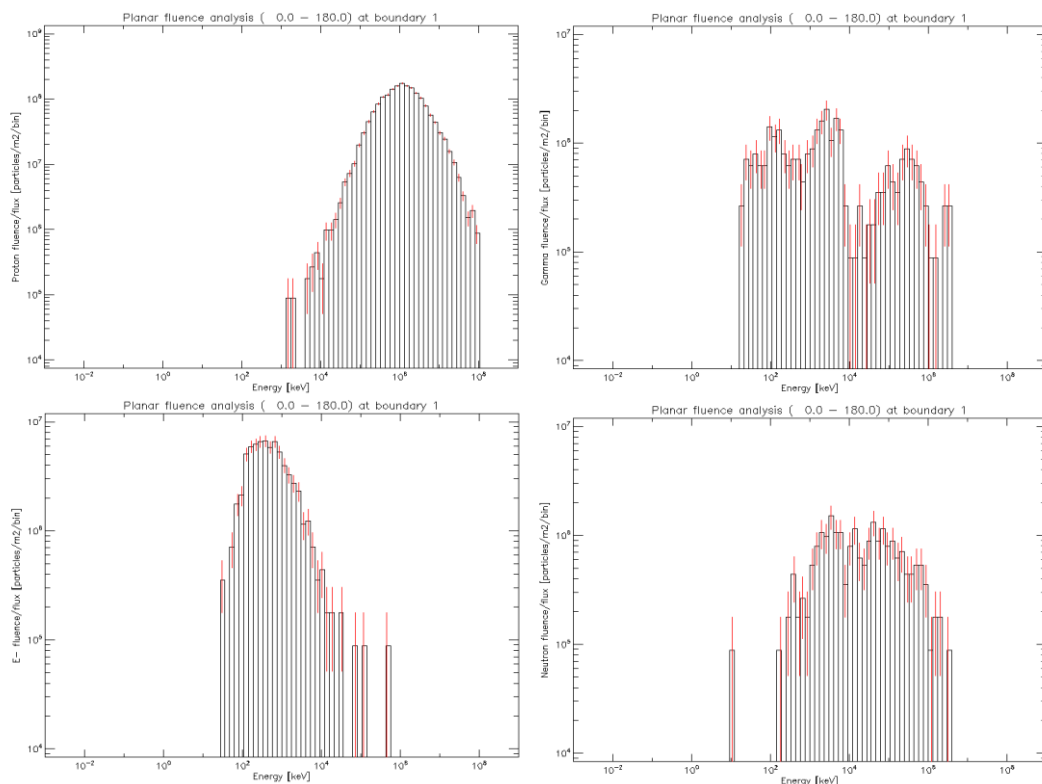


Figure 16-6: Differential fluence spectra for protons (top left), gamma rays (top right), electrons (bottom left) and neutrons (bottom right), all constituents of the galactic cosmic ray spectrum

t	100 s	200 s	1000 s
N	0.011	0.022	0.22
P(N, <2)	0.999	0.999	0.998

Table 16-6: Open cover design number of expected collisions of cosmic rays with the test particle over a designated measurement time and probabilities of having less than two impacts

16.4.3 Micrometeoroids

The Grün meteoroid flux detailed in Section 16.2.3 is given in number of particles per m² per year which can be converted to number of particles impacting a 100 nm sized particles over a 100 s long measurement time. The results, including those for a HEO orbit are listed in Table 16-7. We can see that even for an unshielded payload design the number of impacts is extremely low and will evidently be reduced to zero when the payload cover is closed.

	Number of impacts (using Grün model)
HEO perigee	2.9E-13
HEO apogee	2.1E-13
L1/L2/Earth leading/trailing	2.0E-13

Table 16-7: Number of expected impacts according to the Grün model on a 100 nm sphere during 100s

The risk associated with meteoroid impacts on the S/C itself were not analysed here but it is necessary to assess the effect of momentum transfer in a collision with a meteoroid during a measurement since it disturbs the pointing and drift of the spacecraft as detailed in requirements L3-MIS-121200 and L4-MIS-115120. To assess this a detailed S/C geometry model is required.

16.4.3.1 Total ionising dose

Typically, from a S/C design standpoint, these worst-case particle event fluxes are used to compute short timescale effects of radiations: SEE rates on components and systems. At the other side of the scale, long terms effects of radiations are assessed using the total ionising dose (TID). Given the phase of the mission development, the TID had been computed for a representative spherical Al shielding and isotropic radiation sources. The mission duration was assumed to be 4 years, with a short transfer orbit through the Earth radiation belts toward the interplanetary environment at 1AU (which is valid for L1, L2, and ET/EL). The TID and its contributions, computed in SPENVIS with the SHIELDOSE-2 model RD[70] are shown in Figure 16-7.

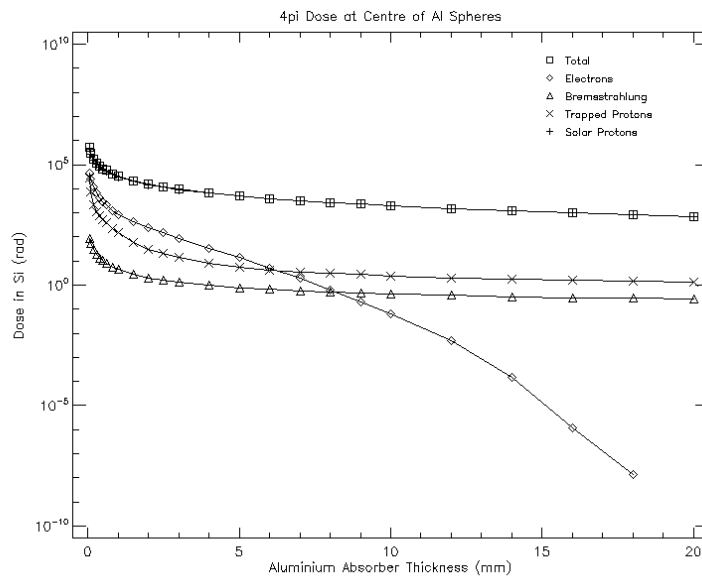


Figure 16-7: Total ionising dose (and contribution from the various sources) for various equivalent Al shielding thicknesses from the SHIELDOSE-2 model

16.4.3.2 Non-ionising dose/displacement damage

Typical damage caused by energetic particles mentioned above come from deposition or ionisation energy along the path of the particle; But in some materials (Silicium and more generally semi-conductors) the damage is produced by kinetic energy transfer to atoms nuclei, causing a displacement of atoms in the crystalline lattice. This displacement creates defects in semi-conductors is responsible, notably, for degradation in image sensors and solar arrays, changing the sensitivity of sensor pixels and yield of solar cells. This non-ionizing energy loss (NIEL) is typically given in $\text{MeV.cm}^2/\text{g}$ or as an equivalent n MeV fluence for a specific material thickness. The 1MeV equivalent fluence for typical triple junction solar cells, obtained with the EQ-FLUX model RD[71], is shown in Figure 16-8. The power degradation on the same solar cell over 4 years caused by the NIEL, estimated with the MC-SCREAM model RD[72] is expected to be around 4%.

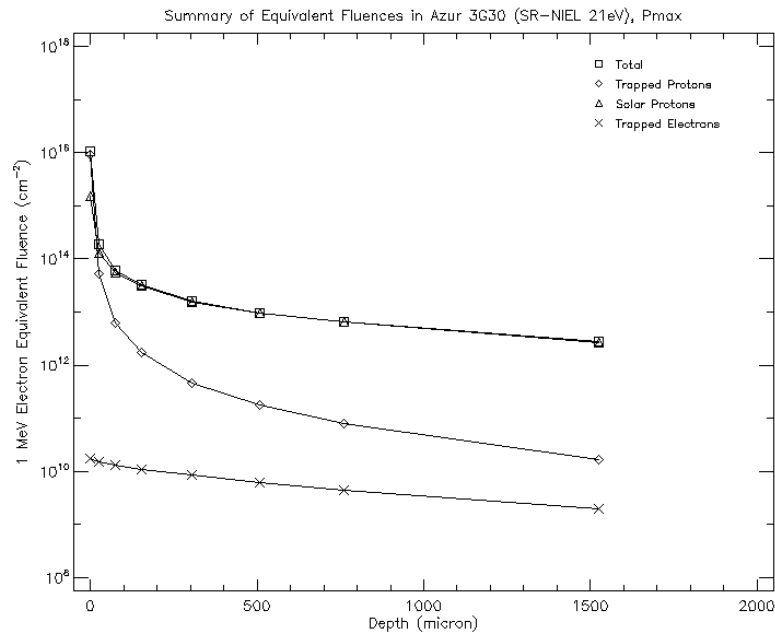


Figure 16-8: 1MeV equivalent fluence (total and contributions) for a triple junction solar cell (Azur 3G30) as a function of coverglass thickness (from the EQ-FLUX model)

Nevertheless, the displacement damage does not only matters for S/C platform radiation effects assessment detailed above. Indeed, during the study, the fate of the test particles, stored in the spacecraft and waiting to be used for the experiment was questioned. Indeed, the lattice damage observed in silicium and other crystalline structures might also affect these particles.

At this stage of the study, general values can only be derived with SPENVIS from the Messenger model RD[72] and are shown Figure 16-9. The damage equivalent dose applies to Silicon only and is computed for various shielding thicknesses in a simplified spherical geometry, similarly to the TID (see 16.2.2). These values could be used and refined in a future study - according to the test particles composition and geometry, S/C structure, container structure and duration of mission – in order to assess the damage on the test particles.

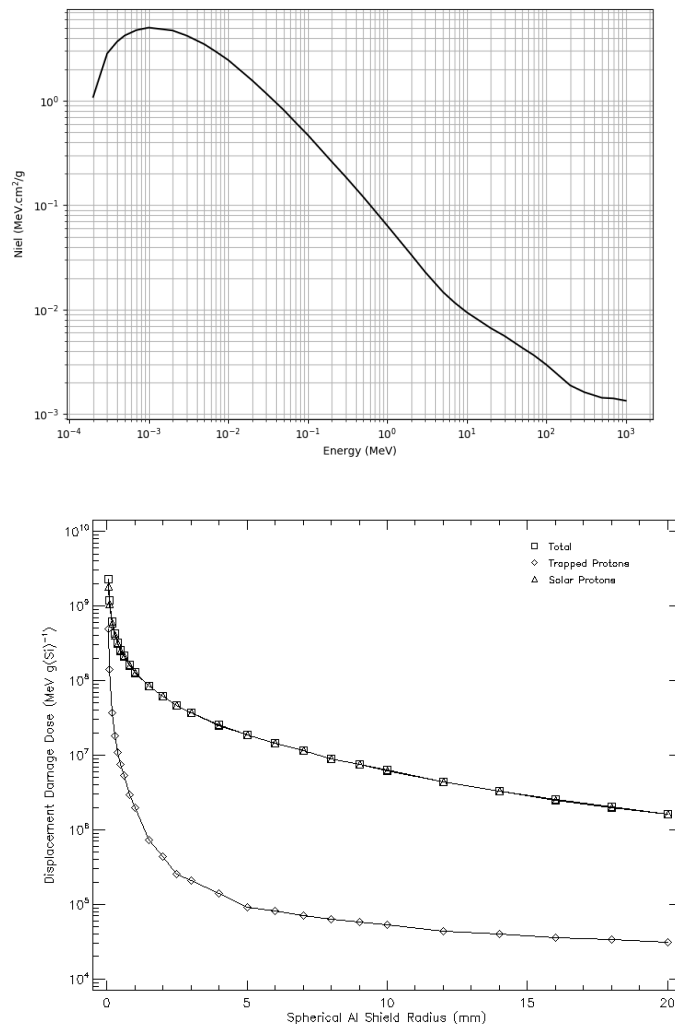


Figure 16-9: Niel (top) and damage equivalent dose (bottom) for Silicon, from the Messenger model RD[72]

16.5 Summary & Recommendations

The necessary requirements on the scientific payload were tested against the environmental models assumed in a near-Earth interplanetary orbit and HEO orbit. A basic solar wind plasma environment was assumed and a worst-case radiation environment including solar particles and cosmic rays was chosen. Under these conditions the clear conclusion is that the payload design needs to be closed to shield the particles from impacting and/or charging the test particles and payload during the measurement. When a minimal amount of shielding is present there is almost no risk of plasma or radiation disturbing the measurements. To meet the pressure requirements in the scientific payload a vent in the cover is needed to connect it to space and allow gas particles to be released. This vent needs a labyrinth type of structure to inhibit charged particles to reach the optical bench inside the payload but also a direct opening to enable venting of the particles in the free molecular flow regime. Surface charging to

negative voltages (due to its location in the wake of the spacecraft) on the outside of the cover will inhibit electrons to enter the vent since they will be repelled but the labyrinth structure needs to absorb the ions that are attracted by the negative surface charging in an efficient way. This is a technology development that requires further attention.

More detailed analyses are required to analyse the internal charging due to particles released and deposited as result of the interaction of energetic radiation with matter. More accurately, the variation of internal charging needs to be analysed since a steady amount of internal charging may not have a big impact on the measurement itself since the nanoparticle is required to be uncharged during its freefall. Next to this, the impact of continuously impacting radiation on the nanoparticles may cause significant displacement damage. Also the necessity of analysing the magnetic field and variations of the magnetic field needs to be investigated. Most importantly the effect of micrometeoroid impacts causing attitude disturbances needs to be determined using a detailed S/C geometric model.

In this study all the effects of the space environment on the S/C system itself were not analysed but for future studies on the QPPF platform it would be necessary to analyse the spacecraft charging due to plasma to limit the ESD risk, analyse more thoroughly the impact of radiation causing material degradation and SEE effects in electronic components, and analyse the risk of loss of measurement due to micrometeoroids.

This Page Intentionally Blank

17 GS&OPS

17.1 Assumptions and Constraints

Assumptions	
1	22 days of Science operations followed by 7 days of stored data downlink using MGA.
2	No use or repointing of MGA during the science operations period. (22 days)
3	The Science operations period of 22 days is composed of 6 hour windows split into 4 hours of science and 2 hours of slew correction and settling time, to correct for drift.
4	Slew correction burns are automatically calculated on board (depends on the drift acquired during the 4 hour science period).
5	The X-Band transmitter has to be OFF during the 4 hour Science window.
6	During the two hour slew correction window the X-Band transmitter can be switched ON and can be used for communications using LGA (no MGA).
7	L2 orbit station keeping burns are estimated (in worse case) twice per week.
8	L2 orbit station keeping burn parameters to be determined and uplinked from ground.
9	14.3 Gbit of Science data generated per day.
10	Real time HKTM data generation rate of 6kbps

17.2 LEOP and Transfer Phase

The choice of a target L2 orbit allows extensive re-use of tried and tested operations approaches as used in L2 for existing (GAIA, Herschel, Planck) and upcoming future missions (Plato, ATHENA, ARIEL).

The primary time critical operations during the Launch and Early Orbit phase (LEOP) are the execution of the Trajectory Correction Manoeuvres (TCM) burns. To ensure the mission has sufficient orbit knowledge, gathered through ground-based Range and Doppler measurements, and sufficient visibility of the mission to execute the required platform operations, ground station coverage and Flight controls teams will be on console for the first critical phase 24/7. This critical LEOP phase nominally ends after completion of the TCM burn 1. After this burn the spacecraft enters into Transfer phase.

Transfer Phase may last up to ~30days where the additional Transfer Correction burns are executed resulting in acquisition of the operational orbit at L2. During this phase the operational teams and ground station passes from the 35m antennas are nominally reduced to 8 hours per day and 7 days per week. Additional back-up support from a second ground station around the TCMs and critical platform activities would be provided.

The Commissioning phase nominally starts during the Transfer phase with initial platform commissioning. Payload commissioning can only be executed in full after completion of the payload cool down. The commissioning phase, dependent of platform

and payload design, can take from 3 to 6 months. After execution of the In Orbit Commissioning Review the Routine phase can start.

17.3 Routine Phase Operability

The routine phase platform and payload operations has been split into 22 days of Science operations followed by a number of days of platform operations to allow for use of the MGA and downlink of the Science data to ground. This cycle is repeated throughout the routine operations phase for each test batch.

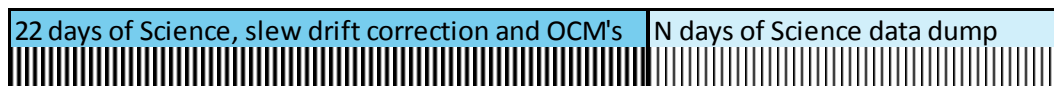


Table 17-1: Routine operations Test Batch

The Science operations period of 22 days is composed of 6 hour windows split into 4 hours of science and 2 hours of slew correction and settling time, to correct for any pointing drift experienced during the Science period (due to Solar radiation pressure etc.).

The 6 hour repeatable operations window will require a high level of automation from the on board systems for both payload operations and control and slew correction. The slew correction, following free drift period, to correct depointing involves thruster firing and settling period post attitude correction. To maximise automation and minimise the interaction from ground these slew correction burns would be automatically calculated on board and autonomously executed during the 2 hour slew period window. During the two hour slew correction window the X-Band transmitter may be switched ON and can be used for communications using LGA. There is no use of MGA during the complete 22 day Science window.

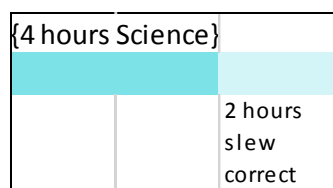


Table 17-2: Six hour repeatable operations window

After completion of the 22 days of Science operations, 7 days of Platform Operations are executed. This period of platform operations allows for high rate science data dump of the ~300Gb of stored science and stored HK data via the high speed downlink at 6.8 Mbps utilising the accurately pointed MGA. The possible ground station pass profiles could be;

- 5 days for 3hours/day of G/S download
- 4 days for 4 hours/day
- 3 days for 5 hours/day

The preferred option would be for the latter 3 days for 5 hours per day to optimise the allocation of the 35m ground station usage shared capability and to minimise the time away from Science data takes.

The Platform operations period would also be used for uplink of new mission timelines for the following payload operation period and any routine maintenance operations which need to be carried out.

17.3.1 HKTM Downlink Strategy Operational Approach

Since the MGA cannot be used during the 22 day Science phase, only the LGA antenna will be available for routine TT&C during this period. The use of LGA very much restricts the downlink data rates achievable and the amount of data which can be dumped to ground. The HKTM Downlink strategy proposed during Science phase is as outlined below.

During the 22 day science period the X-Band transmitter can only be switched on during the 2 hour post science operations windows. This 2 hour post science operations window can be used periodically (e.g. once every 24 hours) for TT&C to transmit the real time HK data at a rate of 32 kbps, TC uplink as needed and for any ranging needs. During this 2 hour window real time HKTM at 32 kbps can be received on ground, HKTM System Logs containing high resolution event data can be downlinked and with an optimised use of e.g. PUS Service 4 parameter statistics reporting, operators would be able to establish confirmation of the general health of satellite and successful execution of platform and payload activities outside of coverage periods. If anomalous data found, additional ground station passes can be scheduled to downlink any stored HKTM data using LGA. This would require about 6 hours of collated (split into two hour periods) ground station time to dump 24 hours of stored HKTM.

The complete backlog of stored HKTM data will be dumped after the ~22 day science period using the high speed data link via HGA together with the science data.

{4 hours Science}		
		2 hours slew correct
		X-Band On
		Real time HKTM/TC Ranging

Table 17-3: Real time HKTM access windows

17.3.2 Orbit Determination, Ranging and Station Keeping

Based on the proposed propulsion subsystem (cold-gas micro thrusters) Station Keeping Manoeuvres to maintain the L2 orbit are estimated to be executed twice per week with a burn duration of approximately four hours per SKM burn. This is significantly more than a hydrazine propelled L2 mission which would nominally execute SKM approximately once every 30 days.

The SKM burns do not need to be executed during ground station coverage, however sufficient ranging data needs to be collected prior to the burns which subsequently drives the ground station pass requirement. Approximately six hours of ranging data would be needed in the days before SKM. (e.g. 3 passes of 2 hours each) to provide enough ranging data to enable sufficient orbit determination to be executed on ground. Orbit determination is carried out on ground by the mission control centre and the resulting station keeping burn parameters are uplinked from ground.

The resulting operational profile is therefore as proposed in the following diagram combining the HKTM spacecraft health check passes with the needs for SKM ranging data collection and manoeuvre uploads. This results in approx. 26 hours of ground station usage per week.








Day 1 24 hours	Day 2 24 hours	Day 3 24 hours	Day 4 24 hours	Day 5 24 hours	Day 6 24 hours	Day 7 24 hours
						
Ranging	Routine	SKM Burn	Routine	Ranging	Routine	SKM Burn
3 TT&C passes for ranging data collection	1 TT&C pass. Orbit determination and burn calculation.	2 TT&C passes. SKM burn parameters	1 TT&C pass	3 TT&C passes for ranging data collection	1 TT&C pass. Orbit determination and burn calculation.	2 TT&C passes. SKM burn parameters uplinked.

Table 17-4: One week routine operations overview

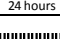
24 hours								24 hours	24 hours							
(4 hours Science)	(4 hours Science)	(4 hours Science)	(4 hours Science)	(4 hours Science)	(4 hours Science)	(4 hours Science)	(4 hours Science)		(4 hours Science)	(4 hours Science)	(4 hours Science)	(4 hours Science)	(4 hours Science)	(4 hours Science)	(4 hours Science)	SKM Burn execution
2 hours slow correct	2 hours slow correct	2 hours slow correct	2 hours slow correct	2 hours slow correct	2 hours slow correct	2 hours slow correct	2 hours slow correct		2 hours slow correct	2 hours slow correct	2 hours slow correct	2 hours slow correct	2 hours slow correct	2 hours slow correct	2 hours slow correct	
X-Band On	X-Band On	X-Band On	X-Band On	X-Band On	X-Band On	X-Band On	X-Band On	Orbit determination and burn calculation	X-Band On	X-Band On	X-Band On	X-Band On	X-Band On	X-Band On	X-Band On	SKM Burn uplinked
Ranging	Ranging	Ranging	Ranging	Ranging	Ranging	Ranging	Ranging		Ranging	Ranging	Ranging	Ranging	Ranging	Ranging	Ranging	

Table 17-5: Orbit determination, Ranging and Station Keeping profile

17.3.3 Data Management, Storage, Operability

The on board data storage areas need to provide enough on board storage capacity to allow for the infrequent downlink of the Science data. In addition the storage area needs to provide a large enough system log area enabling a high enough granularity of the events to be stored for regular (daily) downlink and large enough storage area for mission timeline commands to cover the 22 day science period. The mission timeline could also be uplinked via the LGA in a piece meal approach, however use of the MGA and uplink of complete Batch time line would be the preferred approach.

Due to the limited period of science downlink a high preference for use of file based storage supporting the use of CFDP protocols in the space to ground link would be recommended to ensure completeness of dumped data with minimum re-dump operational overhead.

17.4 List of Equipment

The ground stations foreseen for use by such an L2 QPPF mission would include the following;

For LEOP and Routine use of the ESTRACK 35 m antennas would be envisaged. All three 35m antennas support X-Band uplink (7145-7235 MHz range) and downlink capability (8400-8500 MHz) at the data rates currently foreseen. This would include the Cebreros, Malargüe and New Norcia-1 ground station antennas.

Additional antennas could be foreseen to provide additional TT&C support during early phases of LEOP for first acquisition and during TCMs. These antennas could include, New Norcia-2 (4.5m), Kourou, Maspalomas and / or Malindi antennas.

Use of the Kourou (15m) could possibly be made during routine phase in support of the low rate real time TT&C passes although the link budget is marginal.

17.5 Options

When considering the Earth trailing or Earth leading orbits:

- The operational profile would be significantly simplified due to the simplified LEOP with nominally no transfer phase, no manoeuvres and no orbit correction.
- During routine phase there would be no need to execute SKMs.
- The complexity arises in achieving the link budget as the mission extends over the mission lifetime.

This Page Intentionally Blank

18 PROGRAMMATICS/AIV

18.1 Requirements and Design Drivers

No specific requirements for AIV and programmatics have been given as input to the study.

The main goal of programmatics within the QPPF study is to compile an overview of the technology developments required for the baseline design and discuss their impact on the schedule and the development approach. The schedule shall be compliant to the typical approach for Science M-class missions.

18.2 Technology Requirements

The Technology Readiness Levels (TRL) present a systematic measure supporting the assessments of the maturity of a technology of interest and enabling a consistent comparison in terms of development status between different technologies.

The TRL definitions from RD[73] are shown in Table 18-1:

TRL	ISO Definition	Associated Model
1	Basic principles observed and reported	Not applicable
2	Technology concept and/or application formulated	Not applicable
3	Analytical and experimental critical function and/or characteristic proof-of concept	Mathematical models, supported e.g. by sample tests
4	Component and/or breadboard validation in laboratory environment	Breadboard
5	Component and/or breadboard critical function verification in a relevant environment	Scaled EM for the critical functions
6	Model demonstrating the critical functions of the element in a relevant environment	Full scale EM, representative for critical functions
7	Model demonstrating the element performance for the operational environment	QM
8	Actual system completed and “flight qualified” through test and demonstration	FM acceptance tested, integrated in the final system
9	Actual system completed and accepted for flight (“flight qualified”)	FM, flight proven

Table 18-1: TRL scale

Although a general statement is made that only technology sufficiently advanced (TRL) to start the Implementation Phase will be proposed, there are TRLs as low as 3, 4 and 5 identified.

In the following paragraphs, the overall technology statuses of the SVM as well as the PLM are outlined.

The product tree for the SVM, as established at the end of the QPPF study, is shown in Table 18-2. It identifies for each subsystem the associated equipment, sometimes components, their TRL as well as references related to suppliers, previous missions, or other remarks related to their development.

Subsystem	Equipment	TRL	Reference
AOGNC	Sun Sensors	6	GOCE, Lisa Pathfinder
	Star Tracker	4	JenOptik, CDR completed 2016 (in development)
	IMU	6	Airbus
COMMS	TWTA (power conditioning + TWT)	9	Extensive heritage
	RF Distribution Network	9	Extensive heritage
	LGA	9	Extensive heritage
	MGA	6	Herschel Planck
	MGA Pointing mechanism	9	Solar Orbiter
	Transponder	6	TAS-I X2PND
PROP	1N thrusters cold gas	6	
	Small tanks	9	US supplier
	Pyro Valve	4	Under development
	Other components	9	Extensive
	Large tank	4	300l tank under qualification
DHS	Processing unit for PL		
	SMU	5	EQM expected 2019
	Mass memory	6	Euclid
	Interface board	6	
PWR	Battery	6	MTG, Cheops, Euclid
	Solar Cells	6	Proba 3, Biomass, Euclid, Cheops
	PCDU	6	Lisa Pathfinder, Earthcare, Sentinel 2, SWARM, Exomars
STRU	Primary Structure	6	
	V-grooves	4	
TCS	MLI	9	Extensive EO, NAV, TIA, SCI
	Heaters	9	Extensive EO, NAV, TIA, SCI
	Cryo-cooler	3	
	Non-evaporable getters	4	
	Thermistors	9	Extensive EO, NAV, TIA, SCI
	High precision low temperature sensors	4	
	Thermal doubler	9	Extensive EO, NAV, TIA, SCI

Table 18-2: overview TRL's for SVM

The pyro valves for propulsion as well as the SMU for the data handling system are both presently under development. It is expected that they can reach a TRL of 6 within 3 respectively 1 year.

The technologically least mature elements for the SVM are the V-grooves of the structures subsystem and the cryo-cooler, the non-evaporable getters and the high precision low temperature sensor for the thermal subsystem. The thermal subsystems are expected to require predevelopment times of approximately 3 years each, while the pre-development of the V-grooves may require 3-4 years, depending on the finally chosen solution. These times are based on the technical development times, they have to be increased by any additional times needed to initiate the activity, which depend on the respective programs under which the development will be funded.

The product tree for the PLM is shown in Table 18-3. It groups the different functions of the experiment/payload as discussed with the experts and identifies for each “subsystem” of each function the associated equipment, sometimes components and their TRLs.

Subsystem	Equipment	TRL	Remark
Particle handling	Particle steering	2	European Space Technology Master Plan (ESTMP) generic
	Particle selection wheel	4	
	Particle Storage Container and ejection	2	
	Paul Trap Driving Electronics	4	
	Paul Trap Electrodes	4	
	UV LED assembly for particle Desorption and Charging	4	
Optical bench	High-finesse cavities	4	
	Interferometric position of test-particle	3	
	Baseplate optical bench (SiC)	5	
	GHz Electro-Optical Modulators	4	
	Acousto-Optical Modulators	6	Lisa Pathfinder
	NIR laser	5	
	Deep UV laser and grating	4	
	Cooling test particles	4	
	Cooling with multiple cavity modes	2	
	Spatial mode multiplexers	4	

Subsystem	Equipment	TRL	Remark
	Temperature tunable narrow-band fiber Bragg filters	3-4	
	Low-noise fiber amplifiers	4	Being developed for LISA
	Homodyne detection	4	
	Cavity housing incl. particle disposal	4	
	Cavity venting opening mechanism	4	

Table 18-3: overview TRLs for PLM

Table 18-4 shows an indication of the development time depending on the current TRL. According to the European Space Technology Master Plan (ESTMP), to prepare the contractual basis for multi-annual programs it takes about 18 months to reach political agreement on financial ceiling. This has also been included in the table.

TRL	Duration
5-6	4 years + 1.5 year
4-5	6 years + 1.5 year
3-4	8 years + 1.5 year
2-3	10 years + 1.5 year
1-2	12 years + 1.5 year

Table 18-4: TRL – development duration

Assuming, that the development of technology at TRL lower than 6 is already approved and on-going, it can expect that another 2 years is needed before the implementation phase can start for technologies at TRL 4 and another 4 years for technologies at TRL 3 unless very special effort is made to speed up the development.

Based on Table 18-4, the estimated pre-development times for the PLM subsystems and functions range from 3.5 years up to approximately 11.5 years. Only two subsystems (the acousto-optical modulator and the low-noise fibre amplifiers) are either existing or are already being developed so that they can be considered as TRL6 for the start of the implementation phase.

18.3 Model Philosophy

For the SVM, the following model philosophy is proposed:

- Development models: V-grooves, Cryocooler
- E(Q)M for at least DHS, PWR
- CQM
- Software Validation Facility & Avionics Test Bench (ATB)
- Any E(Q)M shall be subsequently used in the ATB if possible

- STM
- PFM

The STM/PFM approach is chosen due to the technological maturity of a large number of subsystems. It is supported by dedicated development models. Due to the criticality of thermal and structural performance of the SVM for fulfilling the science requirements, special effort needs to be done here.

For the PLM, a QM/FM approach needs to be chosen since almost all equipment and subsystems are newly designed. The following model philosophy is proposed for the PLM:

- Development models for pre-development
- E(Q)M at subsystem level
- Software Validation Facility & Avionics Test Bench (ATB)
- Any E(Q)M shall be subsequently used in the ATB if possible
- QM
- FM

18.4 System Level Verification Aspects

A split at the PLM/SVM level has been assumed within the QPPF study, following the common approach of separating the development of the payload from the system bus. The present design assumes that the SVM will be built around the PLM. Due to the stringent performance requirements for the PLM, special attention needs to be given to the verification of these requirements on the SVM before the final mating of PLM and SVM.

Due to the stringency of some of the requirements it is very important that the design of the SVM and PLM will be taking into account the suitability of existing or to be developed verification methods for verifying these requirements already during the preliminary and the detailed design phases for SVM as well as PLM.

The following aspects have been identified in the course of the study as having a special impact on the system level design and verification requirements:

- Micro-vibration during the measurement phases
- Thermal stability
- Positional stability during the measurement phases
- Pressure environment:
 - Outgassing control / material choice, ground handling
- Radiation shielding towards PLM
- Magnetic fields from and towards PLM

18.5 Development Approach

For the SVM, most proposed systems have a relatively high TRL so that they can be further developed or delta developed within the nominal project phases. Table 18-4

shows an overview. Special attention has to be given to the structural thermal model and the aluminium foam sandwich panels, which have never before been used as spacecraft structural elements in these dimensions and under the stringent thermal requirements as for QPPF.

For the PLM, as the maturity of almost all parts of the system is very low, various predevelopment activities need to be performed. Due to the amount of necessary predevelopment, at different TRL levels, and the nature of the topic (fundamental quantum research), it is likely that the funding for the activities may be realised via a multitude of funding organizations and programmes within and without the space sector. Examples of the space sector include different ESA technology programmes and studies, funding via national space agencies (programmes and special activities), EU Horizon 2020 (and successor).

The technology pre-developments for the PLM are, programmatically, the main driver for mission feasibility and schedule. During the CDF study, the required pre-developments have only been analysed at a preliminary level. In order to get a more detailed understanding of the efforts and durations involved, it is recommended to perform a dedicated technology readiness assessment for the elements of the PLM to identify the required activities in detail, their technical and programmatic interconnections, and to evaluate those in light of different potential funding sources.

Due to the low TRL for many of the PLM technologies it is possible that specifications and requirements as known today have to be updated as outcome of the technology development activities. This needs to be considered as input to Phase 0 of the SVM as well as any related technology readiness assessment for the SVM.

18.6 Schedule

The schedule has been set up to be compatible with the typical durations and decision milestones for Science M-class missions. The aim when creating the schedule was to evaluate possible launch dates taking into account the technology developments for all items listed in section 18.2.

The following assumptions have been used for the synthesis of the schedule:

- Review durations: 30days
- ITT 6 months each at start of Phase A/B1 and Phase B2/C1/C2/D
- Overall contingency: 6 months
- Launch campaign duration: 3 months
- TRL6 at start of Phase B2
- SVM: Phase C split in C1/C2: allows earlier start of subsystem QM and STM
- SVM: SVF/ATB started after PDR
- SVM: PFM starts before end of STM
- PLM: development parallel to SVM until PLM PDR
- PLM: TRL developments based on ESTMP assumed durations including 1.5 years for reaching financial agreements.

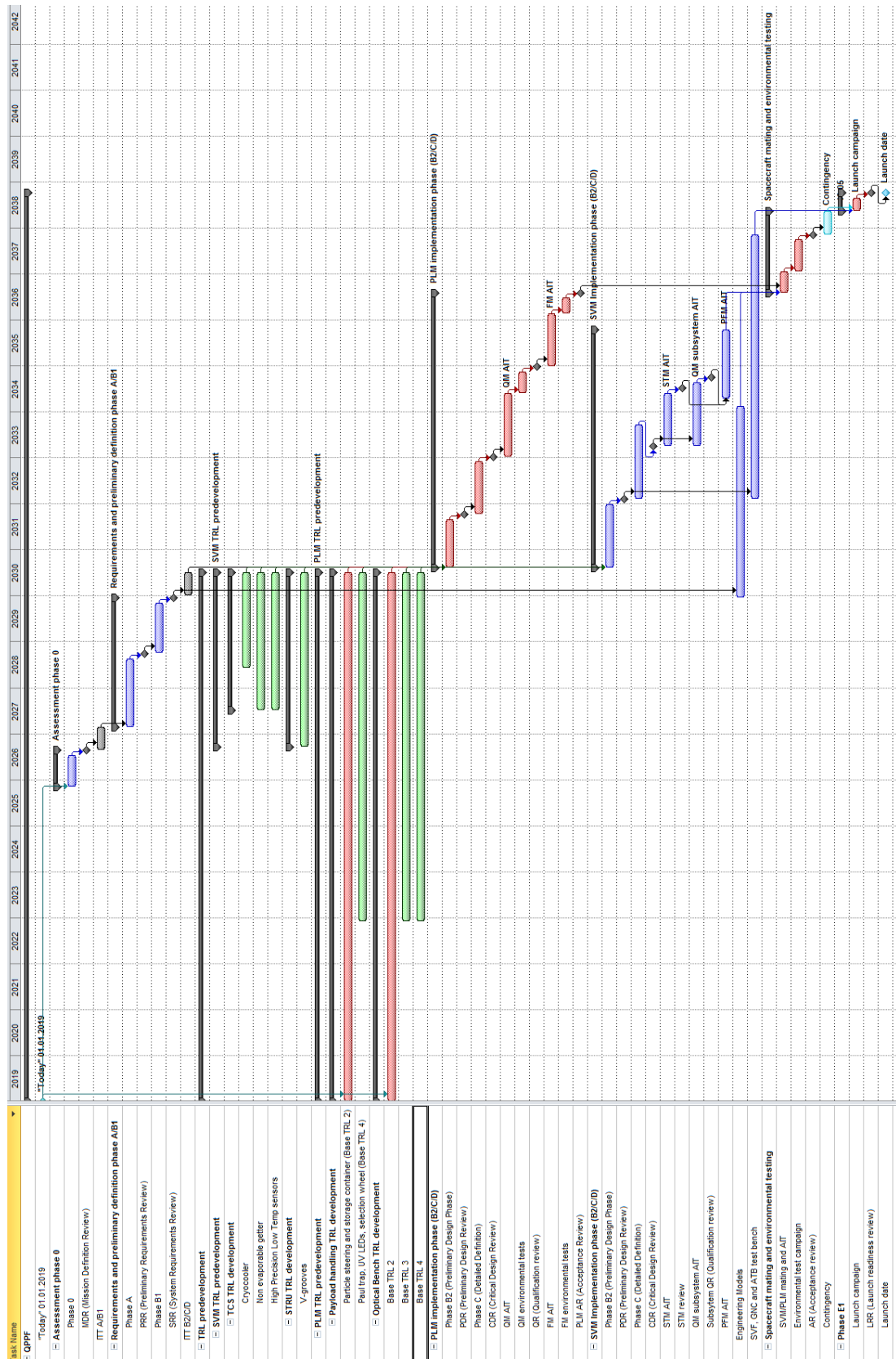


Figure 18-1: Scenario 1 - Baseline schedule for QPPF based on ESTMP

Figure 18-1 shows the overall baseline schedule for QPPF (“Scenario 1”). It can be seen that the main driver for the schedule are the necessary pre-development activities for the PLM. The resulting launch date is 2038. In this case, the start of Phase 0 would begin mid 2025, and the start of the implementation phase (B2/C/D) would be mid 2030.

The schedule has a one year margin between SVM and PLM, which is mainly due to the QM/FM approach for the PLM. Any SVM technology pre-developments do not need to be started before 2026. This is of particular interest as it may be possible that in the meantime some of the proposed technology developments for the SVM may have been performed in the frame of other activities, so that they do not need to be included in the technology development plan for the SVM anymore.

Looking at the baseline schedule above and the list of technology pre-developments for the PLM, it can be seen that there are 3 out of 8 areas that have a very low level of maturity (TRL 2 in Table 18-3). A second schedule (“Scenario 2”) was now created under the assumption that an increased effort is done to “boost” these 3 technology areas so that they can come in line with the majority of the other technology developments. This approach results in a possible launch date in late 2034 (Figure 18-2). This also has a direct effect on the starting date of phase 0, which is moved forward to late 2021. Correspondingly, the start of the implementation phase (B2/C/D) would be mid 2026.

As with the first scenario, the schedule provides a one year margin between SVM and PLM, which is mainly due to the QM/FM approach for the PLM. In the second scenario, SVM technology pre-developments could be started in late 2022 for all technologies that have not yet reached a sufficient maturity level by then.

This second scenario is the earliest expected launch date assuming investments in additional efforts for technology pre-development. Any even earlier launch date can be expected to non-linearly increase predevelopment costs and increase the risk to the schedule since a much larger number of technology developments have to be accelerated.

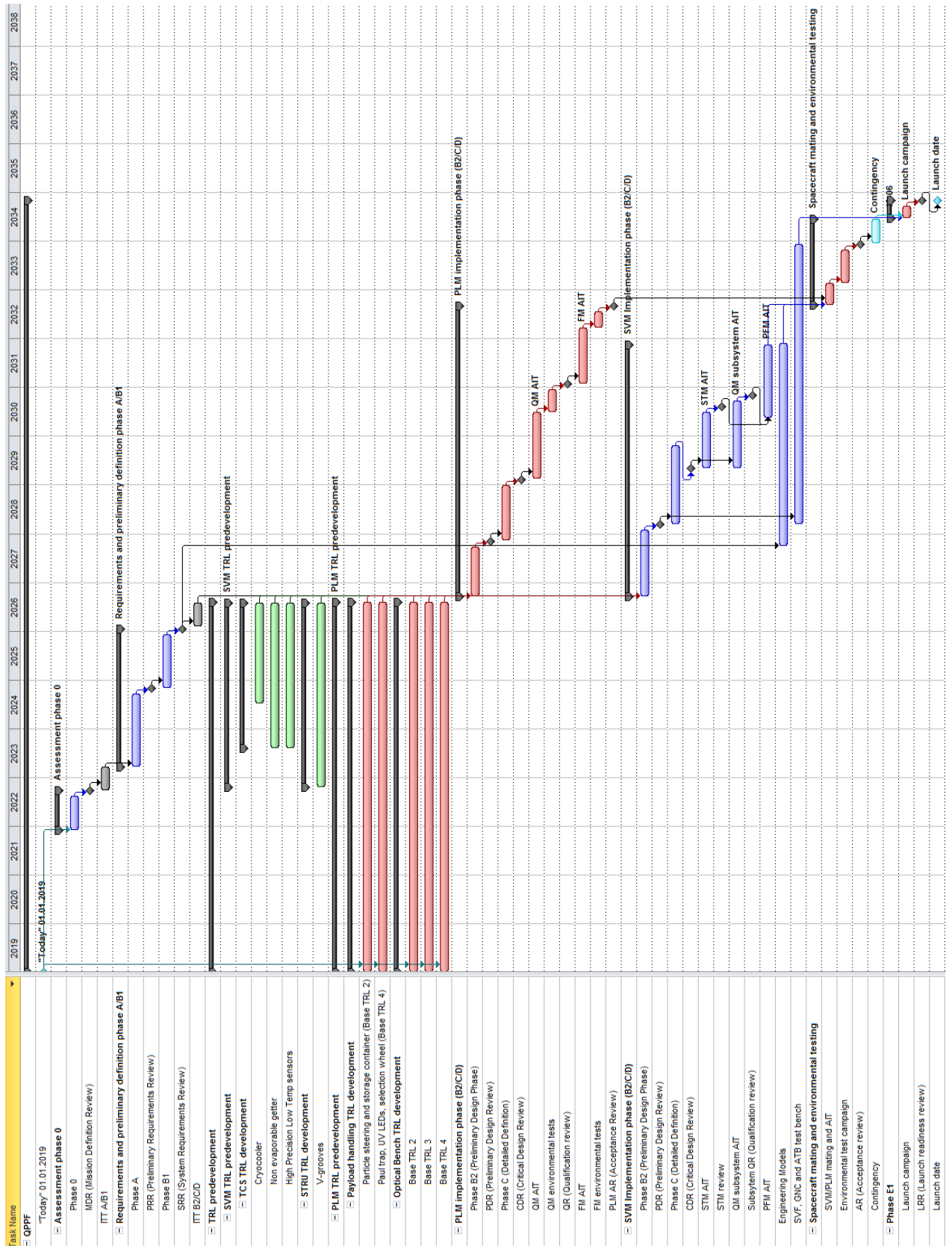


Figure 18-2: Scenario 2 – “accelerated PLM technology developments”

18.7 Summary and Recommendations

The low TRL of the PLM technologies are the main driver for the QPPF schedule. The expected launch date is 2038. In case additional efforts are made to decrease the development times of a limited number of technology developments, the launch date could be anticipated to as early as 2034.

In both evaluated schedule scenarios, the launch dates are based on preliminary assessments of the required technology developments for the PLM. It is recommended to create a dedicated Technology Roadmap / Technology Readiness Assessment for the PLM to come to a more detailed understanding on the efforts and durations of these technology developments and to evaluate their impact on mission feasibility. An assessment of the results of the TRA should be performed before Phase 0 and before the start of any technology activity for the SVM in order to take into account any changed specifications and requirements due to the PLM technology predevelopment activities.

Some of the requirements that need to be fulfilled for are very stringent and will pose a challenge for current verification methods. This means that feasibility of verification methods will need to be specifically evaluated already early in the design process and be included in system level tradeoffs.

19 TECHNICAL RISK ASSESSMENT

19.1 Reliability and Fault Management Requirements

The following reliability and fault management requirements were proposed for the QPPF study/ mission.

ID	Requirement
REQ-01	The overall reliability of the mission shall be $\geq 85\%$ at end of life (loss of S/C).
REQ-02	The lifetime* of S/C shall be compatible with the mission requirement.
REQ-03	Single-point failures with a severity of catastrophic or critical (as defined in ECSS-Q-ST-30C/40C) shall be eliminated or prevented by design.
REQ-04	Single-point failures (other than catastrophic or critical) shall be avoided in the design of the mission units.
REQ-05	Retention in the design of single-point failures of any severity rating is subject to formal approval by ESA on a case-by-case basis with a detailed retention rationale. Multiple failures, which result from common-cause or common-mode failure mechanisms, shall be analysed as single failures for determining failure tolerance.
REQ-06	A failure of one component (unit level) shall not cause failure of, or damage to, another component or subsystem within and between mission units.
REQ-07	The failure of an instrument shall not lead to a safe mode of the mission units.
REQ-08	The design shall allow the identification of on-board failures and their recovery by autonomously switching to a redundant functional path. Where this can be accomplished without risk to spacecraft and instrument safety, such switching shall enable the continuity of the mission timeline and performance.
REQ-09	Where redundancy is employed, the design shall allow operation and verification of the redundant item/function, independent of nominal use.
REQ-10	The design and its operation shall be compliant with applicable Space Debris rule** in all phases of its lifecycle. (e.g. ESA/ADMIN/IPOL Space Debris Mitigation for Agency Projects)
REQ-11	The S/C design and its operation shall be compliant with applicable launch requirements in all phases of its lifecycle. (e.g. CSG Safety Regulations)

* see applicable mission criteria's **Table 19-2**

** depending on the responsible launch authority and/ or launch operator

Table 19-1: Reliability and Fault Management Requirements

The requirements were reviewed during the course of the study and found to be adequate for the QPPF mission.

19.2 Risk Management Process and Scope of Risk Assessment

Risk management is an organised, systematic decision making process that efficiently identifies, analyses, plans, tracks, controls, communicates, and documents risk in order to increase the likelihood of achieving the project/ study goals. The procedure comprises four fundamental steps:

- **Step 1:** Definition of the risk management policy which includes the project success criteria, the severity & likelihood categorisations, and the actions to be taken on risks
- **Step 2:** Identification and assessment of risks in terms of likelihood and severity
- **Step 3:** Decision and action (risk acceptance or implementation of mitigating actions for the risk reduction)
- **Step 4:** Monitoring, Communication and documentation and risk acceptance

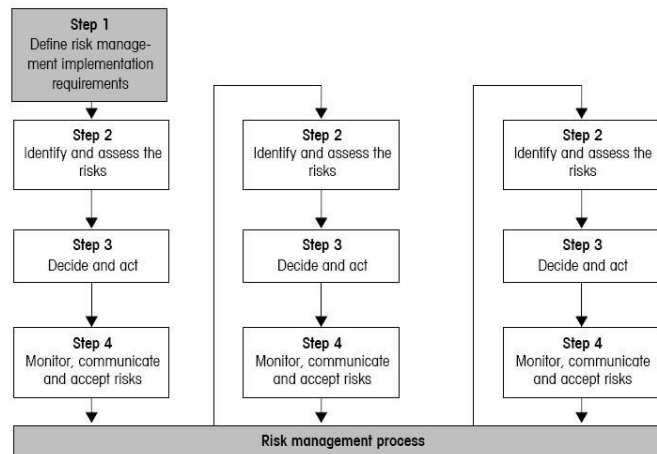


Figure 19-1: ECSS-M-ST-80C, 2008 Risk Management Process

The QPPF CDF-Study is a pre-phase A feasibility assessment and results of all 4 steps have to be seen as preliminary. The full documentation of the Risk assessment is premature. Nevertheless, one of the major study objectives (see in PRO1/2 in Table 19-2) is to identify future development needs. Therefore risk related to the maturity of the payload equipment had to be assessed differently – the risk index was adjusted accordingly (see chap. 19.3.3).

The basis for the preliminary risk assessment is the kick-off documentation/presentation of the study. Changes in the kick-off baseline which are caused by identified risks were already seen as mitigation measures.

The scope of the preliminary risk assessment was clearly defined at the beginning and during the study. The risk assessment comprises all mission phases and mission elements.

The preliminary risk assessment for QPPF study considered risk during the following Mission phases

- Mission realisation (project phase)
- Launch preparation and launch
- Cruise to/ around L2
- Science phase
- S/C disposal

19.2.1 Approach for the Risk Identification and Risk Reduction

The assessment of the specific risks presented in section 19.5 based on the overall approach for the hazard description visualised in Figure 19-2.

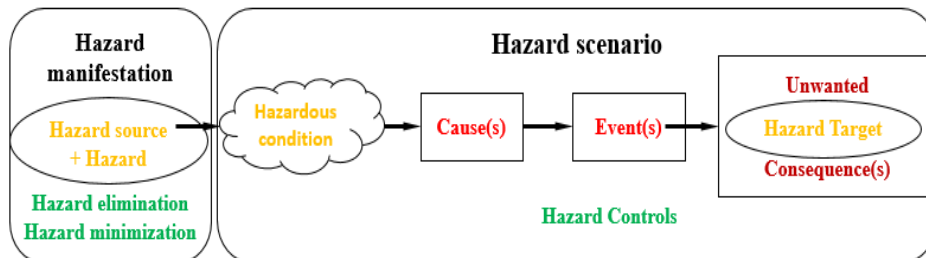


Figure 19-2: Risk identification and risk reduction

The assessment started with the definition of the ‘Hazard Source’, the ‘Hazard’ and the ‘Hazard Target’.

In the next step the ‘primary Hazardous Condition’ which is inherently connected to the Hazard Source, the Hazard and the Hazard Target will be identified including the expected ‘Unwanted Consequences’.

Finally, the ‘Cause’ (e.g. the root cause failure mode) which is triggering the ‘Event’ and originating the Unwanted Consequence will be recognised. The occurrence of the Cause, its transition to an Event (or Event Chain) and the realisation of the Unwanted Consequence is often influenced by circumstances summarised as ‘secondary Hazardous Conditions’.

Based on this information the likelihood of the occurrence of the Unwanted Consequences can be judged as point estimate which applies in general to the ‘worst case’ Severity category.

In case the risk is not acceptable in terms of the used Risk Index (see section 19.3.3) Risk Reductions via Mitigation Measures has to be defined to bring the risk in an acceptable area of the Risk Index. Such mitigation measures like hazard elimination, hazard minimisation and hazard controls are beyond the baseline. They have to be considered in a delta study or in the project/ mission phase.

An initial risk for one hazard target can be connected or lead to a new/ additional risks for the same or another hazard targets as a consequence of its reduction e.g. the mitigation of dependability risks (e.g. increase of the redundancy) can lead to an impact on other hazard targets like programmatic (e.g. possible overrun of the mass budget) and/or cost and/ or schedule. Such risk propagation is visualised in Figure 19-3 hereafter.

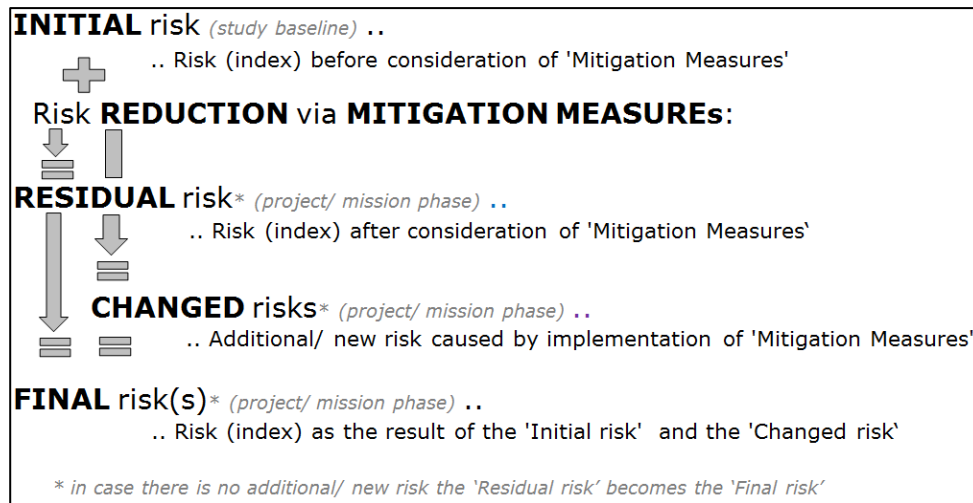


Figure 19-3: Risk propagation

The terms used in connection with the risk identification are defined as:

Hazard ¹ [H]	Existing or potential property/ state ² of a Hazard Source that can result in a mishap for the Hazard Target
Hazard Source [HS] ³	An item/ entity of the CDF study and/ or space mission
Hazard Target [HT]	An item/ entity/ person which could get affected by the mishap like performance (science, services, ..)/safety (harm, damage)/ cost/ schedule
Hazardous Condition ² [HC]	Hazardous conditions are levels/ borders capacities or situation/ circumstances which can initiate a 'Hazard scenario' and can be associated . * . with physical, chemical or biological capacity of a 'Hazard source' (primary condition [HCp]) – intrinsic property but also with the technology, design, manufacturing, organisation (secondary conditions [HCs]) – functional/ physical state
Hazard Manifestation	The Hazard Source with its potential Hazards and Hazardous Conditions becomes part of the study baseline/ future mission
Hazard Scenario	The combination of 'Cause(s)' and 'Event(s)', which results into a specific Unwanted Consequence
Cause	Root Cause which is the origin of a Hazard Scenario
(final) Event	Final physically event or status which is directly leading to the Unwanted Consequence under the given Hazardous Conditions
Event Chain	Between the Cause and the Event several intermediate events might occur
Unwanted Condition	Is a/are potential result(s) of a Hazard Scenario which specified the negative effect for the Hazard TARGET[HT] in the frame of the CDF study the Unwanted Conditions has to be specified based on the Study/ Mission Success Criteria's (see chap. 1.3.1)
Hazard Elimination ⁴	The Hazard will be fully eliminated mostly by elimination of the Hazard Source
Hazard Minimisation ⁴	The Unwanted Consequences (Severity category) will be downgraded

	mostly via changes in the primary Hazardous Condition
Hazard Control ^{4, 5}	Engineering or administrative measurements

Remarks:

- 1/3 *Hazards are NOT events (neither accidents nor incidents) but potential threats to the Hazard Target;*
- 2 *Property or state which can be associated with the design, manufacturing, operation, organisation, application or environment, an intrinsic property of an item/ entity, e.g. unstable isotopes/ radiation, Hardware/ sharp edges, a functional/physical state of an item/ entity e.g. Medium/ high pressure in a vessel; Hardware/ high temperature of a surface, ...*
- 3 *Prerequisite(s) for the occurrence of 'Hazard scenarios' with their negative effects ('Unwanted Consequences') on 'Hazard Target(s)'*
- 4 *basic strategies/ Mitigation Measures for the Risk Reduction*
- 5 *e.g. - Design selection (failure tolerance, ..)*
 - *Design to minimum risk (Safety margins/factors)*
 - *Automatic safety device, design to contain,*
 - *Warning device, crew escape/ safe haven,*
 - *Dedicated procedures, regulations, standard's, programmes, ...*

19.3 Risk Management Policy

The CDF risk management policy for QPPF aims at handling risks which may cause serious programmatic/ cost/ schedule/ technological, performance (science or services)/ technical and safety/ protection* impact on the future project.

Nevertheless, one of the major study objectives (see in PRO2.1/2.2 in Table 19-2) is to identify future development needs. Therefore, risk related to the maturity of the payload equipment had to be assessed differently – the risk index was adjusted accordingly (see chap. 19.3.3).

* 'Safety' related to the human life and health(harm) has a higher priority and importance than 'Safety' related to property and environment (damage). To have a clear split between both safety aspects in the report the term

- 's - safety' is used exclusively for risks related to human life and health on ground and in space
- 'p - protection' is used exclusively for risks related to equipment, property, and planetary environments (terrestrial, space and specific solar objects)

19.3.1 Success Criteria

The success criteria with respect to the program, science, technical, safety/ protection safety, schedule, and cost objectives are presented in Table 19-2:

Study/ Risk Domain	Success Criteria
Programmatic	<p>PRO1: <i>(for mission)</i> To provide a reference feasible design for a 'Quantum physics' mission to test the quantum superposition principle</p> <p>PRO2.1: <i>(for study)</i> To refine and mature the payload design (especially related to the nanoparticles feeding concept)</p> <p>PRO2.2: <i>(for study)</i> To identify technology development activities. To estimate the</p>

Study/ Risk Domain	Success Criteria
	cost class of the mission, its development time, and the associated risks
Performance (Science/ Services) Technical	TEC1: The SC operates successfully over the designated mission lifetime of 3.5years (0.5 years mission commissioning and 3 years nominal operation) TEC2: A reliability of >85% (loss of S/C) at the end of mission/ program
Safety & Protection	SAF1: Catastrophic hazard (2 Failure/Error Tolerance), critical hazard (1 Failure/Error Tolerance) incl. undesired incl. human performance (human related error/failure) SAF2: No SPF can lead to catastrophic hazards; No performance degradation owing to SPF, and no failure propagation. PRT1: Mission shall be compliant with ESA policy for space debris mitigation ESA/ADMIN/IPOL(2014)2 PRT2: Mission shall be compliant with applicable 'Launch Requirements' (e.g. CSG Safety Regulations)
Schedule	SCH1: All architecture elements are available and their FRR successful for the launch (NLT 2030)* SCH2: The contributions from international partners are available at the relevant milestones of the development schedule SCH3: TRL > 5** for all components at the time of mission adoption SCH4: Low development risk during Phase B2/C/D <i>* the launch date was seen as orientation to complete the study but not as a fixed launch date for the expected mission ** ISO scale 2016</i>
Cost	COS1: CaC for ESA ≤ ???M€ (2015 EC) -> ?? Class Mission(20?? e.c).

Table 19-2: Success Criteria

19.3.2 Severity and Likelihood Categorisations

For the QPPF CDF-study a preliminary assessment of the risks in all Hazard Targets like programmatic(pr) in terms of e.g. cost(c), schedule(sh), technological readiness (tr), performance(dp)* / technical(dt) and safety(s)/ protection(p) was performed as described in 19.2.

** 'Performance' is standing for e.g. 'science' incl. 'technological tests' or 'services' (e.g. telecommunication, navigation , cargo)*

The severity of the risk scenarios are classified (based on the study baseline) according to their Hazard Target of impact. The consequential severity category of the risks scenarios is defined according to the worst case potential effect with respect to programmatic and science / performance objectives, technical and safety/ protection objectives, schedule objectives and/or cost objectives (see Table 19-2).

In addition, identified risks that may jeopardise and/or compromise the QPPF study/ mission will be ranked in terms of likelihood of occurrence and severity of unwanted consequence (shortened as 'severity of consequence') as well for the study baseline as under consideration of possible mitigation actions.

The scoring scheme with respect to the severity of consequence on a scale of 1 to 5 is established in Table 19-3, and the likelihood of occurrence is normalised on a scale of A to E in Table 19-4 and based on recommendations given for the risk assessment in ECSS-M-ST-80C.

Score	Severity	Dependability Performance(Science - dp) & Technical (Dependability) (dt)	Safety & Protection (s/p)	Schedule (pr/ sh) incl. technological readiness (pr/ tr)	Cost (pr/ c)
5	Catastrophic	<u>Performance:</u> * Failure leading to the impossibility of fulfilling the mission's performance <u>Technical:</u> failure propagation: * from lower system level to highest system level * from mission to constellation/ campaign level * leading to loss of safety-related barriers	<u>Safety:</u> * Loss of life, life-threatening or permanently disabling injury or occupational illness; * Loss of an interfacing manned flight system <u>Protection:</u> * Loss of the system (e.g. S/C)** * Severe detrimental environmental effects * Loss of launch site facilities.	Delay results in project cancellation	Cost increase result in project cancellation
4	Critical	<u>Performance:</u> * Failure resulting in a major reduction (70-90%) in overall performance according mission objective * <u>Technical:</u> * Major damage to flight systems	<u>Safety:</u> * Temporarily disabling but not life- threatening injury, or temporary occupational illness; <u>Protection:</u> * Major detrimental environmental effects. * Major damage to or ground facilities. * Major damage to public or private property	Critical launch delay (24-48 months)	Critical increase in estimated cost (20 -50%)
3	Major	<u>Performance:</u> * Failure resulting in a major reduction (30- 70%) in overall performance <u>Technical:</u> * Major degradation of the flight system	<u>Safety:</u> * Minor injury, minor disability, minor occupational illness. <u>Protection:</u> * Minor system or environmental damage	Major launch delay (6-24 months)	Major increase in estimated cost (10 -20%)
2	Significant	<u>Performance:</u> * Failure resulting in a substantial reduction (10-30%) in overall performance <u>Technical:</u> * Minor degradation of system (e.g.: system is still able to control the consequences)	<u>Safety:</u> * Impact less than consequences defined for severity level '3- Major'	Significant launch delay (3-6 months)	Significant increase in estimated cost (5 – 10%)
1	Minimum	<u>Performance:</u> * No/minimal consequences (0 - 10%) in overall performance <u>Technical:</u> * No/ minimal consequences	<u>Safety:</u> * No/ minimal consequences * Space Debris Mitigation: casualty risk <10E-4	No/ minimal consequences (1-3 month delay)	No/ minimal consequences (<5%)
0	No	Initial risk fully eliminated	Initial risk fully eliminated	Initial risk fully eliminated	Initial risk fully eliminated

* 'mission' stands for a '.. set of tasks, duties ..' ECSS-S-ST-00-01C; para. 2.3.139

** 'system' stands for a '..set of interrelated or interacting functions constituted to achieve a specified (mission) objective..' ECSS-S-ST-00-01C; para. 2.3.212

Table 19-3: Severity Categorisation

Score	Likelihood	Definition
E	Maximum	Certain to occur, will occur once or more times per project.
D	High	Will occur frequently , about 1 in 10 projects
C	Medium	Will occur sometimes , about 1 in 100 projects
B	Low	Will occur seldom , about 1 in 1000 projects
A	Minimum	Will almost never occur, 1 in 10000 projects

Table 19-4: Likelihood Categorisation

19.3.3 Risk Index & Acceptance Policy

The risk index is the combination of the likelihood of occurrence and the severity of consequences of a given risk item.

Risk ratings of low risk (green), medium risk (yellow), high risk (red), and very high risk (dark red) were assigned based on the criteria ‘Severity’ and ‘Likelihood’ of the risk index scheme (see Table 19-5).

The level of criticality of a risk item is denoted by the analysis of the adapted risk index. By policy medium, high and very high risks are not acceptable and must be reduced via Mitigation Measures (see Table 19-6) as e.g. proposed in Table 19-8.

The standard risk index for CDF studies was adjusted (see Table 19-6) according the study objectives (PRO 1.1/2.; see Table 19-2). Therefore, risk related to the maturity of the payload equipment were seen as acceptable for higher risk level as far as it is not related to ‘safety’ and ‘protection’.

Standard Risk Index

Severity					
5 (catastr.)	A5-s(<10E-4)	B5-s	C5-s	D5-s	E5-s
	A5-p	B5-p	C5-p	D5-p	E5-p
4 (critical)	A4	B4	C4	D4	E4
3 (major)	A3	B3	C3	D3	E3
2 (signif.)	A2	B2	C2	D2	E2
1 (minor)	A1	B1	C1	D1	E1
0	no risk				
	A (min.) ≤ 1/10000 (10 ⁻⁴) almost never	B (low) ≤ 1/1000 (10 ⁻³).. seldom	C (medi.) ≤ 1/100 (10 ⁻²).. sometimes	D (high) ≤ 1/10 (10 ⁻¹).. frequent	E (max.) ≤ 1.. certain
					Likelihood

pr - programmatic/ dt - dep.(tech.) / dp - dep.(perform.) / p - protection / s -safety/ sh - schedule/ c - cost

Table 19-5: generic Risk Index

Adjusted Risk Index

Severity						
5 (catastr.)	A5-s(<10E-4)*	B5-s	C5-s		D5-s	E5-s
	A5-p	B5-p	other	C5-p	D5-p	E5-p
4 (critical)	A4	B4	other	C5-p	D4-s/p	E4- s/p
					other	other
3 (major)	A3	B3	C3	D3-s/p	E3-s/p	
				other	other	
2 (signif.)	A2	B2	C2	D2	E2-s/p	
					other	
1 (minor)	A1	B1	C1		D1	E1
0	no risk					
	A (min.) ≤ 1/10000 (10 ⁻⁴) almost never	B (low) ≤ 1/1000 (10 ⁻³).. seldom	C (medi.) ≤ 1/100 (10 ⁻²) .. sometimes		D (high) ≤ 1/10 (10 ⁻¹).. frequent	E (max.) ≤ 1 .. certain
pr - programmatic/ dt - dep.(tech.) / do - dep.(perform.) p - protection / s - safety/ sh - schedule/ c - cost						Likelihood

pr - programmatic/ dt - dep.(tech.) / dp - dep.(perform.)/ p - protection / s -safety/ sh - schedule/ c - cost

* Safety related (e.g. the 'casualty risk' for controlled re-entry shall be less than 1 in 10000 projects)

Table 19-6: generic Risk Index (adjusted)

Risk Magnitude	Proposed Actions (during project/ mission phase)
Very High Risk	Unacceptable risk: implement mitigation action(s) - either likelihood reduction or severity reduction through new baseline with appropriate party
High Risk	Unacceptable risk: see above
Medium Risk	Acceptable risk for study however unacceptable for project: therefore implement further reduction action(s) with responsible party/ project partners
Low Risk	Acceptable risk: control, monitor; during project seek responsible work package management attention.
Very Low (‘0’ - no) Risk	Acceptable risk/ no risk: see above; ‘0’ - no actions to be taken e.g. in case the risk is eliminated

Table 19-7: Proposed Mitigation Actions

19.4 Risk Drivers

The following risk drivers have been considered in the identification of specific risk items:

- New technologies (TRL)
- Design challenges (configuration, mass, volume, power, lifetime, mission/ ground operation, communication, ...)
- Dependability (Reliability, Availability and Maintainability in terms of the performance of science operation)
- Safety (harm), and Protection (damage - Environmental & Property factors)
- Functional/ technical and dependability issues (Reliability, Availability and Maintainability in terms of the performance of ... science/ service , single point failures (SPFs))
- Major mission events
- Programmatic factors.

19.5 Top Risk Log (preliminary)

Top risk items have been preliminary identified at the mission (ESA) levels. Please refer to Table 19-8 for a complete list of preliminary identified top risks and their corresponding suggested mitigating actions.

The Risk Index results reflecting the initial risk assessment are summarised in Table 19-9a and reflecting the final assessment in Table 1-9b considering mitigation measures as described in Table 19-8.





The risks are sorted and marked* according the study/ mission timeline:

- Study/ Mission Design + realisation
- Launch (preparation) + LEOP & IOT (S/C deployment)
- Cruise * Mission deployment
- Mission performance + Space Debris (SD) + Planetary Protection (PP)
- Other risks
- Overall Cost (OC) + Overall Schedule (OS)




* the underlined abbreviations are used in Table 19-8 as the beginning initials of the Risk no..





The risk numbering (1st column of Table 19-8) is associated to the study internal risk allocation and does not give a ranking according their importancy or any other numerical order.



Risk no. - Risk Title	Risk Classification	Risk Context	Risk Scenario	1. Mitigation Measure	2. Mitigation Measure	3. Mitigation Measure
	- Initial Risk Index	Hazard Source [HS], Hazard [H], Hazardous Condition [HC] .. could endanger .. Hazard Target [HT]	Cause [C] .. could cause .. Event [E] .. resulting finally in .. Unwanted consequences[UC]	Residual Risk / Residual/ Final Risk Index	Residual Risk / Residual/ Final Risk Index	Residual Risk / Residual/ Final Risk Index
				Changed Risk: / Final Risk Index	Changed Risk: / Final Risk Index	Changed Risk: / Final Risk Index
Design & mission realisation						
DII - TRL	Programmatic - shedule (pr/sh) DII_pr/sh ----- - 3E(adj.) <div></div>	HS .. Components/ subsystems H .. TRL (Technological Readiness Level) HC* .. New technology (even for terrestrial use); technology first time used in space technology; uniquely used for this mission .. could endanger .. HT .. CDF study (acceptance from programmatic viewpoint)	C .. TRLs for the subsystems* lower than required (<5) .. could cause .. E1 .. unforeseen long qualification time and/ or E2 .. re-design during the project phase .. resulting finally in .. UC ..Study rejection or Project/ mission schedule (delay) Remark: * all PL equipment e.g. - particle storage container	<u>Mitigation Measure:</u> a) consideration of low TRL equipment in CTP**, GSTP*** <u>Risk Reduction via:</u> Likelihood <u>Remaining risk:</u> Programmatic DI_pr 2E(adj.) <div></div> Remark: ** CTP – Science Core Technology Programme		




Risk no. - Risk Title	Risk Classification - Initial Risk Index	Risk Context	Risk Scenario	1. Mitigation Measure	2. Mitigation Measure	3. Mitigation Measure
		Hazard Source [HS], Hazard [H], Hazardous Condition [HC] .. could endanger .. Hazard [HT] Target	Cause [C] .. could cause .. Event [E] .. resulting finally in .. Unwanted consequences[UC]	Residual Risk / Residual/ Final Risk Index Changed Risk: / Final Risk Index	Residual Risk / Residual/ Final Risk Index Changed Risk: / Final Risk Index	Residual Risk / Residual/ Final Risk Index Changed Risk: / Final Risk Index
		Remark: * Study objective: PRO2.2: (for study) to identify technology development activities	TRL=1 - particle Desorption & Charging TRL=3 - Laser unit TRL=3 - Optical bench TRL=2 - Optical structure and detectors TRL=3 - for many other PL components/ subsystem the TRLs were not available in the frame of the study	*** GSTP – General Support Technology Programme		
DIII - Mass, volume budget	Programmatic (pr) DIII_pr ----- - 5C (adj.)* 	HS .. S/C (design) H .. S/C mass HC .. Final mass budget could not take into account e.g. the latest configuration of the propulsion system * .. could endanger .. HT .. CDF study (acceptance from programmatic viewpoint) Remark: * 159kg for TCM + 65kg SK+Sc. Mode => 3rd tank needed which is not cons in baseline	C .. Changed propulsion configuration including increase of wet mass for propulsion (e.g. for the mission operation like orbit maintenance)/ dry mass of propulsion system (e.g. an additional tank) .. could cause .. E .. S/C design not suitable in terms of H3 launch mass .. and/ or .. E2 .. S/C redesign .. resulting finally in .. UC .. project delay (or even study rejection)	<u>Mitigation Measure:</u> a) adoption of science program <u>Risk Reduction via:</u> <i>Risk eliminated</i> <u>Residual risk:</u> - DIII_pr elim.  ----- <u>Changed risk:</u> Dependability (science return) DIII^_dp 2C 	<u>Mitigation Measure:</u> b) delta study based on alternative S/C (re)design <u>Risk Reduction via:</u> Severity <u>Residual risk:</u> programmatic – DIII_pr 3C 	



ESA UNCLASSIFIED – Releasable to the Public

Risk no. - Risk Title	Risk Classification - Initial Risk Index	Risk Context Hazard Source [HS], Hazard [H], Hazardous Condition [HC] .. could endanger .. Hazard Target [HT]	Risk Scenario Cause [C] .. could cause .. Event [E] .. resulting finally in .. Unwanted consequences [UC]	1. Mitigation Measure	2. Mitigation Measure	3. Mitigation Measure
				Residual Risk / Residual/ Final Risk Index	Residual Risk / Residual/ Final Risk Index	Residual Risk / Residual/ Final Risk Index
		explosively ** HC2 (H1/2) .. handling of laser/ hydrogen on ground during S/C deployment/ testing .. could endanger .. HT .. Ground personal <i>Remark:</i> * 350mW optical power ** cooler contains some gram of H2 ()	impact on a ground personal* .. resulting finally in .. UC .. Disabling injury or occupational illness <i>Remark:</i> * H2+O => 571kJ/mol; 1gH2 -> 0.5mol => 280kJ (1J will accel. 2kg of mass on 1m/s)	<u>Remaining risk:</u> LI_s 5A	<i>Risk remains the same with lower likelihood</i> 	
Cruise and Mission deployment						
CI - Cruise / operation to/ in L2	safety risk - damage (p) CI_p ----- -- 5C 	HS .. S/C and ground operation + operational location L2 H .. Mission conditions (trajectory precision over long distance) HC .. Limited communication possibilities in terms of com. sequence and distance* .. could endanger .. HT .. S/C <i>Remark:</i> * autonomous cruise with limited operation capacity.	C .. Onboard anomalies/ failures demanding immediate correction .. could cause .. E1 .. Uncompensable trajectory deviations .. resulting finally in .. UC .. Loss of S/C <i>Remark:</i> *so far all ESA missions operating in L2 were successful; however the statistic basis is even not big enough to verify a lower likelihood than 'sometimes' of the possible loss of the S/C	<u>Reduction:</u> a) adequate S/C autonomy & FDIR concept <u>Risk Reduction via:</u> <u>Remaining risk:</u> CI_p 5B	<u>Reduction:</u> b) intermediate S/C health checks during cruise <u>Likelihood</u> <i>risk remains unchanged</i> 	
Mission performance + Space Debris						

Risk no. - Risk Title	Risk Classification - Initial Risk Index	Risk Context Hazard Source [HS], Hazard [H], Hazardous Condition [HC] .. could endanger .. Hazard Target [HT]	Risk Scenario Cause [C] .. could cause .. Event [E] .. resulting finally in .. Unwanted consequences [UC]	1. Mitigation Measure	2. Mitigation Measure	3. Mitigation Measure
				Residual Risk / Residual/ Final Risk Index	Residual Risk / Residual/ Final Risk Index	Residual Risk / Residual/ Final Risk Index
MIII - S/C deployment	safety risk - damage (p) MIII_p ----- 5C 	HS .. S/C (release mechanism)* H .. Release function HC1 .. Launch load (vibration, shock, change of temperature and pressure, ..) HC2 .. Release mech. are often SPF sources .. could endanger .. HT .. Science return Remark: * - mechanism needed for deployment of antenna, solar array or to fix e.g. payload parts during launch (truss mechanism); - mechanism have to be seen as sensitive components in terms of impact on the functionality of S/C and payload	C .. Unspecified vibration/ shock/ depressurization .. could cause .. E .. No activation possible, blockage .. resulting finally in .. UC(HC1) .. Loss of S/C* UC(HC2) .. Major reduction in science return ** Remark: * is seen as the leading consequence (worst case) for final risk assessment ** e.g. the failure in the release of one of the antenna might be compensated by use of other antenna however with impact on the science operation concept	Mitigation Measure: a) use of ESSB-HB-E-014 HB Safety Critical Mechanism Risk Reduction via: Residual risk: MIII_p 5B	Mitigation Measure: b) intensive PA process, e.g. due to tracing of SPF sources via CIL* (ECSS-Q-..-10-04) Likelihood unchanged  Remark: * Critical item list	
MIV - Out-gassing	dependability – performance (dp) MIV_dp ----- 4D(adj.) 	HS .. S/C structure and materials H .. Volatile media and its release into the S/C surrounding HC1.1 .. Space environment (thermal load, pressure change/ level) HC1.2 .. Science experiment with extreme accuracy/ stability requirements* HC1.3 .. Limited cleaning possibilities after launch	C(HC1) .. Outgassing in PL coverage C(HC2) .. Coating concept in PL not suitable .. could cause .. E(HC1/3) .. Contamination of optical PL parts like mirrors E(HC2) .. Change of coating concept .. resulting finally in .. UC(HC1) .. Critical reduction in science return UC(HC2) .. Minor delay in project/	Mitigation Measure: HC1 .. a) ECSS-Q-T-70-02C Thermal vacuum outgassing test Risk Reduction via: Residual risk: MIV_dp(adj.) 4C	Mitigation Measure: HC2 .. b) preferred use of metallic materials Likelihood unchanged 	Mitigation Measure: HC2 a) thermal analysis for PL comp./ re-design of PL Risk Reduction via: Severity/ Likelihood Remaining risk: unchanged MIV_dp

Risk no. - Risk Title	Risk Classification ----- Initial Risk Index	Risk Context Hazard Source [HS], Hazard [H], Hazardous Condition [HC] .. could endanger .. Hazard Target [HT]	Risk Scenario Cause [C] .. could cause .. Event [E] .. resulting finally in .. Unwanted consequences[UC]	1. Mitigation Measure	2. Mitigation Measure	3. Mitigation Measure
				Residual Risk / Residual/ Final Risk Index	Residual Risk / Residual/ Final Risk Index	Residual Risk / Residual/ Final Risk Index
				Changed Risk: / Final Risk Index	Changed Risk: / Final Risk Index	Changed Risk: / Final Risk Index
		<p>HC2 .. Coating in PL area -> relatively high heat-up to guarantee cleanliness conditions in PL after launch</p> <p>.. could endanger ..</p> <p>HT(HC1) .. Science return</p> <p>HT(HC2) .. Project schedule</p> <p><i>Remark:</i> * e.g. 10nm measurement/ calibration Accuracy; 20K vacuum conditions with extreme low pressure</p>	<p>mission</p> <p><i>Remark:</i> *UC(HC1) is seen as the leading aspect for the risk assessment</p>			
<p>MV a/b - Space environment (Radiation + micro meteoroids)</p>	<p>a - safety risk - damage (p) *</p> <p>b - dependability risk - performance (dp) **</p> <p>MVa/b_p/dp</p> <p>-----</p> <p>5C </p> <p><i>Remark:</i> * safety risk is seen here as the dominating one</p>	<p>HS .. Space environment</p> <p>H .. Radiation + micro meteoroids</p> <p>HC1.1 .. Exposure dose(energy) and ionised particles (radiation)*</p> <p>HC1.2 .. Radiation sensitive S/C components*/ materials</p> <p>HC1.3 .. Long exposure time,</p> <p>HC2 .. Impact energy - impulse + damage (micro meteorites)</p> <p>HC3 .. Extreme requirements on experiment accuracy/ instrument quality</p> <p>.. could endanger ..</p> <p>HT .. Science return</p> <p><i>Remark:</i> * - LEO radiation - van Allen belt</p>	<p>C (HC1/3) .. High energetic and ionised particles, penetrating S/C surface*</p> <p>C(HC2/3) .. Micro meteoroids colliding with S/C</p> <p>.. could cause ..</p> <p>E(HC1/3) .. Radiation effects including generation of particle shower in radiation shielding*</p> <p>E(HC2/3) .. Impulse transfer from micro meteoroids to S/C/ PL</p> <p>.. resulting finally in ..</p> <p>a:</p> <p>UC(HC1) .. Loss of S/C</p> <p>b:</p> <p>UC(HC1+2/3) .. Major reduction of science return</p>	<p><u>Mitigation Measure:</u> a) ECSS-E-HB-10-12A .. Radiation.. Margin policy HB</p> <p><u>Risk Reduction via:</u></p> <p>Residual risk: MVa/b_p_5B </p>	<p><u>Mitigation Measure:</u> b) adequate Failure tolerance requirements</p> <p><u>Likelihood</u></p> <p>unchanged</p>	

Risk no. - Risk Title	Risk Classification - Initial Risk Index	Risk Context Hazard Source [HS], Hazard [H], Hazardous Condition [HC] .. could endanger .. Hazard Target [HT]	Risk Scenario Cause [C] .. could cause .. Event [E] .. resulting finally in .. Unwanted consequences [UC]	1. Mitigation Measure	2. Mitigation Measure	3. Mitigation Measure
				Residual Risk / Residual/ Final Risk Index	Residual Risk / Residual/ Final Risk Index	Residual Risk / Residual/ Final Risk Index
	because severity level (dependability risk is subject of MVIa,b,c)	radiation - Galactic radiation	Remark: * - interaction with experiment particles/ equipment, e.g. collision requirement (21.5% having NO collisions with any particle) - short term (e.g. SEE) - long term (e.g. derating)			
MVI a/b - Experimental continuity + repeat ability	Dependability risk – performance (dp) MVIa/b, ..dp ----- - 4D(adj.) 	HS .. Test bench + supporting equipment H .. Instability of experimental conditions + particle HC1 .. Required science return need a continuous and undisturbed operation of : - particle storage/ selection/ steering - test equipment (e.g. detectors, test bench, ...) HC2 .. 20K vacuum conditions for PL HC3 .. Science Mode timeline (144 tests/ phase; 60s* test-prep. + 40s free fall) .. could endanger .. HT .. Science return(quantity) Remark: * TbC	C1 .. Failure/ errors in test bench and supporting equipment C2 .. Unspecified deviations from specified experimental conditions .. could cause .. E1 .. Instabilities in the experiments performance .. resulting finally in .. UC .. Critical performance degradation in terms of quantity of science return Remark: * - the experimental conditions are specified so far based on science need but not on the details which consider the technical realisation, e.g. is the physical/ technical concept of the particle transport which requires also the change of the particle direction on the test bench even not solved on a technological	<u>Mitigation Measure:</u> a) timely consideration in CTP, GSTP or other suitable European technology development programs <u>Risk Reduction via:</u> Residual risk: MVIa/b 3C 	<u>Mitigation Measure:</u> b) delta study based on more detailed Likelihood/ Severity unchanged 	

Risk no. - Risk Title	Risk Classification - Initial Risk Index	Risk Context Hazard Source [HS], Hazard [H], Hazardous Condition [HC] .. could endanger .. Hazard [HT] Target	Risk Scenario Cause [C] .. could cause .. Event [E] .. resulting finally in .. Unwanted consequences[UC] level	1. Mitigation Measure	2. Mitigation Measure	3. Mitigation Measure
				Residual Risk / Residual/ Final Risk Index Changed Risk: / Final Risk Index	Residual Risk / Residual/ Final Risk Index Changed Risk: / Final Risk Index	Residual Risk / Residual/ Final Risk Index Changed Risk: / Final Risk Index
MV1c – Measurement accuracy	Dependability risk – performance (dp) MV1c_p r ----- - 4D(adj.) 	HS .. S/C + Test bench H .. Experimental inaccuracy + particle quality HC1.1 .. - High sensitivity of test bench/ test particle against outside influences * HC1.2 .. Extreme measurement-precision is needed for specified science return (e.g. S/C momentums) * HC2 .. 20% having NO collision with any particles (particle cross section)** .. could endanger .. HT .. Science return Remark: * impulse by S/C equipment (vibration) and radiation and micro meteoroids; thermal impact **interaction between radiation (products) <-> particles and; - No more than 2 collisions in average over Tff (free fall time) with a “good” probability - assumed for the CDF that 80% is “good” enough (initially was	C .. Radiation, S/C movement, micro meteorites, micro vibration .. could cause .. E1 .. Uncertainties/ inaccuracies in experiment results .. resulting finally in .. UC .. Critical performance degradation in terms of quality of science return Remark: *	<u>Mitigation Measure:</u> a) timely consideration in CTP, GSTP or other suitable European technology development programs <u>Risk Reduction via:</u> <u>Residual risk:</u> MV1a/b 3C	<u>Mitigation Measure:</u> b) delta study based on more detailed <u>Likelihood/Severity</u> unchanged 	



Risk no. - Risk Title	Risk Classification - Initial Risk Index	Risk Context Hazard Source [HS], Hazard [H], Hazardous Condition [HC] .. could endanger .. Hazard Target [HT]	Risk Scenario Cause [C] .. could cause .. Event [E] .. resulting finally in .. Unwanted consequences[UC]	1. Mitigation Measure	2. Mitigation Measure	3. Mitigation Measure
				Residual Risk / Residual/ Final Risk Index	Residual Risk / Residual/ Final Risk Index	Residual Risk / Residual/ Final Risk Index
		>99%);		Changed Risk: / Final Risk Index	Changed Risk: / Final Risk Index	Changed Risk: / Final Risk Index
SDII – Space debris – limitation of in-orbit time	Protection risk (p) SDII_p 4D 	<p>HS .. S/C</p> <p>H .. Crossing of LEO & GEO</p> <p>HC1 .. Limitation of unreliability for passivation*</p> <p>HC2 .. On-going performance manoeuvres to maintain L2** and Sun/ Earth acquisition</p> <p>.. could endanger ..</p> <p>HT .. GEO (keep out for 100a) & LEO (stay not longer than 25a)</p> <p>Remark: * Number of space debris has to be limited in GEO/ LEO by limitation of its 'remaining' time in GEO/ LEO ** instable orbit -> return to LEO/ GEO possible</p>	<p>C .. Anomalies after separation from dispenser or during orbit maintenance and Earth-link manoeuvres incl. loss of S/C control*</p> <p>.. could cause ..</p> <p>E .. A faulty orbit crossing LEO/ GEO</p> <p>.. resulting finally in ..</p> <p>UC .. Crossing of GEO/ LEO for more than 100a/ 25a</p> <p>Remark: * e.g. propulsion ignition at a wrong point of time or impulse incl. uncontrolled release of propellant</p>	<p>Reduction: a) mandatory applicability of ESA Space Debris regulation</p> <p>Risk Reduction via: Likelihood</p> <p>Remaining risk: unchanged with lower likelihood</p> <p>SDII_p 5A_p </p>		

Table 19-8: Risk Log

Initial Risk Assessment

Severity					
5 (catastr.)			DIII_pr; CI_p; MIII_p; MVa/b_p	LI_s	
4 (critical)				SDII_p; MIV_dp; MVla,b_dp; MVlc_dp	
3 (major)					DII_pr/sh; DVIIIb_dp
2 (signif.)					MI_p
1 (minor)					MII_p
0 (no)	DIII_pr				
	A (min.) ≤ 1/10000 (10 ⁻⁴) almost never	B (low) ≤ 1/1000 (10 ⁻³).. seldom	C (medi.) ≤ 1/100 (10 ⁻²) .. sometimes	D (high) ≤ 1/10 (10 ⁻¹).. frequent	E (max.) ≤ 1 .. certain
					Likelihood

pr - programmatic/ dt - dep.(tech.) / dp - dep.(perform.) / p - protection / s - safety/ sh - schedule/ c - cost

Table 19-9: Top Risk Index – Initial Risk Assessment

Initial adjusted Risk Assessment

Severity					
5 (catastr.)			DIII_pr	CI_p; MIII_p; MVa/b_p	LI_s
4 (critical)				SDII_p	
3 (major)				MIV_dp; MVla,b_dp; MVlc_dp;	
2 (signif.)					DII_pr/sh; DVIIIb_dp
1 (minor)					MI_p
0 (no)	no risk				
	A (min.) ≤ 1/10000 (10 ⁻⁴) almost never	B (low) ≤ 1/1000 (10 ⁻³).. seldom	C (medi.) ≤ 1/100 (10 ⁻²) .. sometimes	D (high) ≤ 1/10 (10 ⁻¹).. frequent	E (max.) ≤ 1 .. certain
					Likelihood

pr - programmatic/ dt - dep.(tech.) / dp - dep.(perform.) / p - protection / s - safety/ sh - schedule/ c - cost

Table 19-10.: Top Risk Index – Initial adjusted Risk Assessment

Final adjusted Risk Assessment

Severity					
5 (catastr.)	LI_s	CI_p; MIII_p; MVa/b_p			
4 (critical)	SDII_p		MIV_dp		
3 (major)			MVla,b_dp; MVlc_dp; DIII_pr	DVIIIb_dp	
2 (signif.)			DIII^_dp or		MI_p
1 (minor)					DII_pr/sh; MII_p
0 (no)	DIV_pr/dp; DII_pr				
	A (min.) ≤ 1/10000 (10 ⁻⁴) almost never	B (low) ≤ 1/1000 (10 ⁻³).. seldom	C (medi.) ≤ 1/100 (10 ⁻²) .. sometimes	D (high) ≤ 1/10 (10 ⁻¹).. frequent	E (max.) ≤ 1 .. certain
					Likelihood

pr - programmatic/ dt - dep.(tech.) / dp - dep.(perform.) / p - protection / s - safety/ sh - schedule/ c - cost

Table 19-11: Top Risk Index – Final adjusted Risk Assessment

19.5.1 Risk Log General Conclusions

- Very high risks and high risks are typical of a Phase A project. Areas with lack of definition or little previous experience pose a priori more risk to the mission and therefore are the ones with more risk reduction potential
- Experience shows that all risk items with a critical risk index (red, orange area) must be analysed and proposals for risk treatment actions elaborated
- In the end, ideally all risk items should achieve a level of justifiable acceptance (yellow, green)
- The risk management process should be further developed during the project definition phase in order to refine the risk identification/analysis and provide evidence that all the risks have been effectively controlled.

19.6 Risk Log Specific Conclusions and Recommendations

The scientific objectives of the QPPF study:

- To provide a reference feasible design for a 'Quantum physics' mission to test the quantum superposition principle.

This requires extremely stable/ undisturbed experimental conditions and high precision instruments design operating over a relatively long lifetime. Such ambitious studies contain naturally a high risk potential (see Table 19-8 and Table 19-11).

Furthermore this mission can not be built up and benefit from comprehensive practical ESA-internal experiences in the area of quantum physics performed under conditions of the space domain. Therefore one of the major study objectives was:

- To refine and mature the payload design (especially related to the nanoparticles feeding concept) and
- To identify technology development activities, and to estimate the cost class of the mission, its development time, and the associated risks.

The study itself can be seen as a Risk mitigation measure related to the technology readiness of the experimental technology (see study objectives PRO 2.1/.2 in Table 19-2). Therefore it lays in the nature of this pre-study that several of the initially identified risks justified as 'very high', 'high' and 'medium' could not be mitigated (see Table 19-8 and Table 19-9) sufficiently based on the standard Risk index (Table 19-5) during the study. Consequently, the Risk Index was adjusted accordingly (Table 19-7/ Table 19-11).

However this study still contains a high risk potential in the payload area from technological viewpoint in terms of maturity for a start of the project phase. Risks that are seen as acceptable for this pre-study like **MV1a/b/c** won't be acceptable for a pre-project study. A further assessment and maybe mitigation in follow-up studies is needed. For example there was no full technological solution presented for the particle redirection from the storage container to the test bed. The suitability of particle storage, which works well under terrestrial conditions, has still to be demonstrated under launch/ space conditions. E.g it was assumed that the cohesion forces are strong enough to keep the test particles at the surface of the particle container during launch. Nevertheless, final evidence has to be provided that shows that e.g. the vibration

(including resonances in the container) during launch does not lead to a major loss of test particles. Furthermore, the evidence that the ‘mass budget’ limit which was just reached during the pre-study might not be overstepped by further detailing of the payload (see **DVIIIb**) and platform (e.g. is the amount of propellant/ number of propellant tanks sufficient for the expected science mode).

The following risk could not be mitigated to an acceptable risk area (yellow/ green – see Table 19-10 in the frame of this study. All this risks are related to protection (safety – damage) and can be reduced to an acceptable level anyway first in the project phase by applying and following adequate standards and procedures or control it via the Critical Items List and its connected specific Product Assurance approach.

- S/C deployment – SPF in release mechanism (**MIII_p**)
- Space environment (Radiation + micro meteoroids) (**MVa/b_p/dp**)
- Cruise/operation to/ in L2 (**CI_p**)

The risk related to Radiation/ micro meteoroids (MVa/b_p/dp) needs specific attention because of

- The possible impact of particle shows cause by the cosmic radiation in the shielding on the test particles (see **MVIc**) – this means simple increase of the thickness of the shielding might not lead the expected risk reduction and
- The impact of the ‘micro meteoroid’-impuls on the S/C / payload components which might contribute remarkable to the risk **MVIa/b** in terms of disturbance of the science mode

The risk related to the cruise/ operation to/in L2 (**CI_p**) is still seen as a medium risk because neither the control of the S/C during the cruise nor the level of S/C autonomy in the frame of a FDIR concept nor a final redundancy concept could be sufficiently detailed during this pre-study. However, ESA has comprehensive experiences in this areas and its reduction to an acceptable risk level will be reached for sure in the project phase.

The risk assessment shows that the QPPF pre-study has an acceptable risk level (Table 19-11). However, before the results of the QPPF pre-study can be used for the design of a mission in the frame of a project it is recommended to push forward the PL development and its technical detailing and specification. Consequently, a delta CDF study is recommended to perform a risk re-assessment especially for the payload area.

.

This Page Intentionally Blank

20 COST

This chapter not included in this public version of the report.

This Page Intentionally Blank

21 CONCLUSIONS

21.1 Satisfaction of Study Objectives

The study objectives, as modified throughout the study, have been satisfied.

OBJ 1. To provide a reference feasible design for a Quantum physics mission to test the quantum superposition principle, with a set of consistent requirements, iterated and agreed with the science community. Some of the original requirements of the science community have been changed over the course of the study due to unfeasibility. These changes have been agreed with the science community and a clear reason for the change has been provided. The final iterated requirements have been agreed by the community and the CDF team.

OBJ 2. To refine and mature the payload design (especially related to the nanoparticles feeding concept). The instrument has been kept the same as originally proposed. The payload sequence has been looked into and a baseline sequence, which fits in the mission lifetime has been proposed. The nanoparticle transportation and storage concept has been investigated in detail. It became clear over the course of the study that this system has a very low TRL and required dedicated technology developments.







OBJ 3. To provide a justified reference orbit for the mission. A complete orbit trade-off has been performed. The L2, earth trailing and, earth leading orbits have been identified as feasible orbits. Due to time limitations only the L2 orbit has been studied in detail, and a feasible design solution has been identified for this orbit.

OBJ 4. To identify technology development activities. Many Technology developments identified by the experts are elaborated in their respective chapter.

OBJ 5. To estimate the cost class of the mission, its development time, and the associated risks. The risk, cost, and schedule have been estimated by the experts. Their results are in line with the expected/hoped for results.

21.2 Satisfaction of Mission Requirements

ID	Requirement	Comments
L3-MIS-000100	Mission Lifetime The total mission duration shall not exceed 3.5 years (TBC) including Transfer and Commissioning phases.	✓

ID	Requirement	Comments
L3-MIS-211200	Total Number of Measurements <i>The mission shall support a minimum of 15 batches of measurements, consisting of 12500 particles in each batch, with a free fall duration tFF of 40s (goal : 1000s), consisting measurement runs between: 1e8amu - 2e9amu (goal : 1e11 amu)</i>	 <i>the goal of 1e11 amu(1000s free fall) can not be reached with existing design, the maximum reachable mass is around 5e9 amu with current assumptions, and with a test particle in Hafnium dioxide ; 2e9 with fused silica particle. Current limiting factor is the achievable pressure level.</i>
L4-MIS-000110	Science Availability <i>The mission shall provide a science availability of at least 50% (goal of 75%) over nominal science mission duration.</i>	 <i>Approximately 60% of the time the satellite will be in science mode (see Science Mode Timeline) Approximately 50% of the science mode will be dedicated to science the remaining part will be for</i> <ul style="list-style-type: none"> • Orbit maintenance • Repositioning of the satellite in between measurements • Downlinking of the data
L3-MIS-111100	Pressure <i>The pressure in the optical bench shall be below 10⁻¹¹ Pa TBC.</i>	 <i>The lowest pressure possible is 10⁻¹¹ Pa. This reduces the free-fall time to 40s which is sufficient to meet the science requirements</i>
L3-MIS-112100	Temperature Range <i>The temperature within the optical testbench during a measurement shall remain at 20K during the measurement duration.</i>	
L3-121100	Temperature Stability <i>The stability of the test bench temperature shall be better than 5 mK over the whole duration of a measurement run ((N*tFF TBC, so ~2 weeks for 10⁴ tests of 100s).</i>	
L3-MIS-115100	Spacecraft Control During Measurement Run <i>The S/C motion during each measurement run (typically 40s) shall be such that the particle remains within 1mm (TBC) of the nominal detection area, with a confidence level of 99.7% (TBC) (with the ensemble interpretation).</i>	

ID	Requirement	Comments
L3-MIS-121000	Spacecraft PDE – Measurement Accuracy Error The Spacecraft to Test-Particle Relative Position Drift Error (PDE) during a measurement (typically 40s) shall be much smaller OR known better than 20 nm, with a 99.7% confidence assuming the ensemble interpretation.	<input checked="" type="checkbox"/> Achieved with a combination of free drifting attitude concept (14 nm) and calibration runs with dedicated test particles (10 nm)
L4-MIS-115100	Spacecraft PDE – Particle Position Error The S/C motion during each measurement run shall be such that the particle remains within 1mm (TBC) of the nominal detection area, with a confidence level of 99.7% (TBC) (with the ensemble interpretation)	<input checked="" type="checkbox"/>

21.3 Further Study Areas

The following areas for further study have been identified.

- The current baseline is 10-11 Pa at 20K for the payload instead of the 10-13 Pa as per the original science requirements. 10-11 is feasible, assuming the use of Non Evaporable Getter (NEG) coating. However the NEG that coats the inner wall of the optical bench may need 180°C to be activated. This may have major system impact. A solution for this potential problem has not been proposed in the study and should be investigated since the getter is an important contributor to the high vacuum. A de-risking activity assessing the NEG (activation needs and system impact) **is a pre-requisite to confirm mission feasibility** (mission-enabling).
- The particle storage and transportation system, and method have to be investigated and developed. The degradation of the particles over the duration of the mission while they are in the storage container and the effect this will have on the mission will have to be investigated and any mitigation actions required flown down to the particle storage and transportation system design. **A de-risking activity on the particle storage and transportation is a pre-requisite to confirm mission feasibility (mission-enabling).**
- Further investigation needs to be done on the derivation of the high vacuum requirement and the number of particle hits that the experiment allows. Currently the requirement is derived by assuming that the probability of less than (or equal to) 2 collision is higher than 80%. It has to be analysed how the number of collisions in 1 run impact the science results, and derive based on that a consolidated system requirement (vacuum level, free fall time). **A consolidation**

of the acceptable collision probability is required by the science community to consolidate the system choices and confirm mission feasibility.

- What is the exact temperature stability of the optical bench and can this be reached with the small peak heat loads of the instrument.
- The current baseline assumes that the CMOS detector on the payload is capable of operating at 20K. This assumption has to be investigated and a technology development might be required.
- A preliminary design of the closed optical bench design has been performed during the study. The design of the cover has to be further elaborated mainly on the material and thickness of the cover to ensure the experiment will not be degraded due to radiation. The venting path of the cover has to be investigated. No detailed analysis has been done to ensure that the cover can vent correctly to the required pressure at which point the H₂ sorption coolers can reduce the pressure even more.
- The behaviour of the spacecraft is a major driver for the science efficiency, propellant budget during science mode and the propellant budget during the safe mode. Over the course of the study it has been analysed using some optimistic assumptions. More in depth analysis is required since the science efficiency is a major driver for the mission.

21.4 Final Considerations

Overall the QPPF CDF study was successful. The mission and science requirements have been iterated to a set of challenging yet feasible requirements. Based on these requirements the team managed to provide a baseline design solution that would be able to provide useful science data. Due to the limited time of a CDF study several options have been documented but left open for further investigation in the future.

22 REFERENCES

22.1.1.1 Chapter 3 Science Objectives References

- RD[1] QPPF Mission Requirements document, Issue 1 Revision 3, 23/08/2018, Reference ESA-QPP-EST-MIS-RS-001
- RD[2] QPPF CDF Inputs – version 12

22.1.1.2 Chapter 5 Mission Analysis References

- RD[3] Euclid, Consolidated Report on Mission Analysis, Florian Renk, MAS Working Paper No. 596, EUCL-ESOC-TN-5-001, issue 2.2, 24th October 2017

22.1.1.3 Chapter 6 Systems References

- RD[4] Quantum Physics Platform (QPPF), CDF input, Rainer Kaltenbaek et al., Issue 11, 2018-05-11
- RD[5] Quantum Physics Platform, Mission Requirements Document, ESA-QPP-EST-MIS-RS-001, Thomas Voirin, Issue 1 – draft, 2018-05-11
- RD[6] Macroscopic Quantum Resonators (MAQRO), M4 Proposal, Rainer Kaltenbaek et al., January 2015

22.1.1.4 Chapter 8 Structures References

- RD[7] Thales Alenia Space, *Planck PFM Dynamic Analysis & Sine Test Prediction Report*, H-P-3-ASP-AN-1405, Issue 2, 26-Nov-2017
- RD[8] Peter Spittle, *Gas turbine technology*, Rolls-Royce plc, Nov-2003, <http://users.encs.concordia.ca/~kadem/Rolls%20Royce.pdf>
- RD[9] William L. Ko, *Superplastically formed diffusion bonded metallic structure*, NASA, US Patent No 4,292,375 A, 29-Sep-1981, <https://patents.google.com/patent/US4292375>
- RD[10] Daniel G. Sanders, *Diffusion bonded multisheet SPF structure*, Boeing Co, US Patent No 6,820,796 B2, 26-Sep-1996, <https://patents.google.com/patent/US6820796>
- RD[11] Graham A. Cooper, Ian E. Bottomley, *Diffusion Bonding of Aluminum and Aluminum Alloys*, British Aerospace plc, US Patent No 5,224,645, 06-Jul-1993, <http://www.freepatentsonline.com/5224645.html>
- RD[12] EOS, *The additive manufacturing system for industrial production of high-quality large metal parts*, Nov-2017 https://www.eos.info/systems_solutions/metal/systems_equipment/eos_m_400
- RD[13] Dirk Schwingel, Hans-Wolfgang Seeliger, Claude Vecchionacci, Detlef Alwes, Jürgen Dittrich, *Aluminium foam sandwich structures for space applications*, Acta Astronautica 61, pp 326 – 330, 26-Mar-2007 <https://www.sciencedirect.com/science/article/pii/S0094576507000513>

- RD[14] John Banhart, Hans-Wolfgang Seeliger, *Aluminium Foam Sandwich Panels: Manufacture, Metallurgy and Applications*, Advanced Engineering Materials 10(9), 793–802, 2008
https://www.helmholtz-berlin.de/media/media/spezial/people/banhart/html/A-Journals/open/postprint/a120_banhart2008.pdf

22.1.1.5 Chapter 9 Nano Particle Handling References

- RD[15] M. Yamashita and J. B. Fenn, “Electrospray ion source. Another variation on the free-jet theme,” *J. Phys. Chem.*, vol. 88, no. 20, pp. 4451–4459, 1984.
- RD[16] M. D. Summers, D. R. Burnham, and D. McGloin, “Trapping solid aerosols with optical tweezers: A comparison between gas and liquid phase optical traps,” *Opt. Express*, vol. 16, no. 11, p. 7739, 2008.
- RD[17] D. Grass, J. Fesel, S. G. Hofer, N. Kiesel, and M. Aspelmeyer, “Optical trapping and control of nanoparticles inside evacuated hollow core photonic crystal fibers,” *Appl. Phys. Lett.*, vol. 108, no. 22, 2016.
- RD[18] P. Mestres, J. Berthelot, M. Spasenović, J. Gieseler, L. Novotny, and R. Quidant, “Cooling and manipulation of a levitated nanoparticle with an optical fiber trap,” *Appl. Phys. Lett.*, vol. 107, no. 15, 2015.
- RD[19] P. Asenbaum, S. Kuhn, S. Nimmrichter, U. Sezer, and M. Arndt, “Cavity cooling of free silicon nanoparticles in high vacuum,” *Nat. Commun.*, vol. 4, pp. 1–7, 2013.
- RD[20] D. Guo, G. Xie, and J. Luo, “Mechanical properties of nanoparticles: Basics and applications,” *J. Phys. D. Appl. Phys.*, vol. 47, no. 1, 2014.
- RD[21] “Intermolecular and Surface Forces,” 2011. [Online]. Available: http://courses.washington.edu/overney/course_material/surface_forces.pdf.
- RD[22] Y. I. Rabinovich, J. J. Adler, M. S. Esayanur, A. Ata, R. K. Singh, and B. M. Moudgil, “Capillary forces between surfaces with nanoscale roughness,” *Adv. Colloid Interface Sci.*, vol. 96, no. 1–3, pp. 213–230, 2002.
- RD[23] J. Dejeu, M. Bechelany, L. Philippe, P. Rougeot, J. Michler, and M. Gauthier, “Reducing the adhesion between surfaces using surface structuring with PS latex particle,” *ACS Appl. Mater. Interfaces*, vol. 2, no. 6, pp. 1630–1636, 2010.
- RD[24] F. Arai, D. Andou, and T. Fukuda, “Adhesion forces reduction for micro manipulation based on micro physics,” *Micro Electro Mech. Syst. 1996, MEMS '96, Proceedings. 'An Investig. Micro Struct. Sensors, Actuators, Mach. Syst. IEEE, Ninth Annu. Int. Work.*, pp. 354–359, 1996.
- RD[25] A. D. McLachlan, “Retarded dispersion forces in dielectrics at finite temperatures,” *Proc. R. Soc. A Math. Phys. Eng. Sci.*, vol. 274, no. 1356, pp. 80–90, 1963.
- RD[26] I. W. Lenggoro, H. M. Lee, and K. Okuyama, “Nanoparticle assembly on patterned ‘plus/minus’ surfaces from electrospray of colloidal dispersion,” *J. Colloid Interface Sci.*, vol. 303, no. 1, pp. 124–130, 2006.

- RD[27] J. Millen, P. Z. G. Fonseca, T. Mavrogordatos, T. S. Monteiro, and P. F. Barker, "Cavity cooling a single charged levitated nanosphere," *Phys. Rev. Lett.*, vol. 114, no. 12, pp. 1–5, 2015.
- RD[28] D. Goldwater and J. Millen, "Levitated electromechanics: all-electrical cooling of levitated nano- and micro-particles," 2018.
- RD[29] C. Marxer *et al.*, "Reflective duplexer based on silicon micromechanics for fiber-optic communication," *J. Light. Technol.*, vol. 17, no. 1, pp. 115–122, 1999.
- RD[30] W. C. Young, R. G. Budynas, and A. M. Sadegh, *Roark's formulas for stress and strain; 8th ed.* New York, NY: McGraw Hill, 2012.
- RD[31] M. Frimmer, K. Luszcz, S. Ferreira, V. Jain, E. Hebestreit, and L. Novotny, "Controlling the net charge on a nanoparticle optically levitated in vacuum," *Phys. Rev. A*, vol. 95, no. 6, 2017.
- RD[32] J. D. Sivers, L. R. Simkins, S. Weidt, and W. K. Hensinger, "On the application of radio frequency voltages to ion traps via helical resonators," *Appl. Phys. B Lasers Opt.*, vol. 107, no. 4, pp. 921–934, 2012.
- RD[33] J. C. Schwartz, M. W. Senko, and J. E. P. Syka, "A two-dimensional quadrupole ion trap mass spectrometer," *J. Am. Soc. Mass Spectrom.*, vol. 13, no. 6, pp. 659–669, 2002.
- RD[34] P. Wieburg, "A Linear Paul Trap for Ytterbium Ions," *Masters Thesis*, 2014.
- RD[35] I. Alda, J. Berthelot, R. A. Rica, and R. Quidant, "Trapping and manipulation of individual nanoparticles in a planar Paul trap," *Appl. Phys. Lett.*, vol. 109, no. 16, pp. 1–5, 2016.
- RD[36] D. T. Meyer, "Design of Superconducting Transmission Line Integrated Surface-Electrode Ion-Traps," 2011.
- RD[37] M. Roland, "Ion-trap design for magnetic-field-driven quantum information processing," 2004.
- RD[38] D. Scharl, "High temperature superconducting ion traps," 2016.
- RD[39] C. J. Foot, *Atomic Physics*. OUP Oxford, 2004.

22.1.1.6 Chapter 10 Propulsion References

- RD[40] Moog 1N thrusters
http://www.google.com/url?sa=t&rct=j&q=&esrc=s&source=web&cd=1&ved=0ahUKEwiRu8Sy_4fcAhXRL1AKHXCFc9IQFggoMAA&url=http%3A%2F%2Fwww.moog.com%2Fcontent%2Fdam%2Fmoog%2Fliterature%2Fspace_defense%2Ftechnical_bulletins%2Fcold_gas_thruster-technical-summary.docx&usq=AOvVaw1p03amPu-Wb36YF-TgqfPB
- RD[41] MT-A 300l tank https://www.mt-aerospace.de/files/mta/tankkatalog/Datenblatt_M-XTA-120-300-Family.pdf
- RD[42] ARDE 4293 tank (<http://www.ardeinc.com/sketches/copy/4293.pdf>)
- RD[43] ARDE 5016 tank (<http://www.ardeinc.com/sketches/copy/5016.pdf>)

22.1.1.7 Chapter 11 AOCS/DFACS References

- RD[44] Modelling of Solar Radiation Pressure Effects: Parameter Analysis for the MICROSCOPE Mission, International Journal of Aerospace Engineering, Volume 2015, Article ID 928206, <http://dx.doi.org/10.1155/2015/928206>.

22.1.1.8 Chapter 12 Telecomms References

- RD[45] ECSS-E-ST-50-05C Rev. 2, *Radio Frequency and Modulation*, 4 October 2011, complemented with CCSDS 131.2-B.1, *Flexible advanced coding and modulation scheme for high rate telemetry applications*, March 2012.
- RD[46] ECSS-E-ST-50-04C, *Telecommand protocols synchronization and channel coding*, 31 July 2008 complemented with CCSDS 231.B-3, *TC synchronization and channel coding*, September 2017.
- RD[47] ECSS-E-ST-50-01C, *Telemetry synchronization and channel coding*, 31 July 2008.
- RD[48] ECSS-E-ST-50-02C, *Ranging and Doppler Tracking*, 31 July 2007, complemented with CCSDS 4.1.4-B-2, *Pseudo-Noise (PN) Ranging Systems*.
- RD[49] CCSDS 131.2-B-1, *Flexible advanced coding and modulation scheme for high rate telemetry applications*, March 2012.

22.1.1.9 Chapter 13 Data Handling References

- RD[50] "Single Board Computer", Final Report phase 2, P-SBCC-REP-1150016-RSE issue 1, RUAG Space AB, 2015-06-26
- RD[51] "Advanced Flexible I/O", Final Report, P-AFI-REP-00025-RSE issue 2, RUAG Space AB, 2011-06-17
- RD[52] "Mass Memory for OBC", Final Report, P-MMOBC-REP-1178785-RSE issue 1, RUAG Space AB, 2016-11-28
- RD[53] "SAVOIR generic OBC specification", TEC-SW/12-536/JLT issue 6, ESA ASRA study team, 31/03/2014

22.1.1.10 Chapter 14 Power References

- RD[54] LISA Pathfinder. Power Conditioning and Distribution Unit (PCDU). Design Report & Performance Analysis. Ref. S2-CRS-RP-2002 . 21/08/2009. Crisa
- RD[55] LISA Pathfinder Solar Array. Design report SA-AAS-F-RP-2001. Ref. 2002473117C. 16/11/07. Thales Alenia Space.
- RD[56] LISA Pathfinder. Solar Array Sizing Technical Note. Ref. S2.ASu.TN.2106. 19/01/2016. EADS Astrium

22.1.1.11 Chapter 15 Thermal References

- RD[57] Planck Collaboration: Planck Early Results. II. The thermal performance of Planck, Astronomy & Astrophysics manuscript no. Planck 2011-1. 3 c, January 4, 2012
- RD[58] J. Burger et al, Review of Scientific Instruments, 78, 065102 (2007)

- RD[59] Vacuum properties of TiZrV non-evaporable getter films, C. Benvenuti et al
RD[60] Non-evaporable Getters: From pumping strips to thin film coatings
RD[61] Extreme High Vacuum, PA Redhead, National Research Council, Ottawa, CA
RD[62] Basics and Applications of cryopumps, C. Day, Forschungszentrum Karlsruhe

22.1.1.12 Chapter 16 Environment References

- RD[63] Lai, S. T., *Fundamentals of Spacecraft Charging*, Princeton University Press, 2011
RD[64] Fitzpatrick, F., *Plasma Physics : An Introduction*, CRC press, 2015
RD[65] Jiggins, P. et al, *Defining the SEP environment for specifications using the SAPHIRE model*, 16th European Conference on Radiation and Its Effects on Components and Systems (RADECS), 2016
RD[66] SPENVIS – Space Environment Information System,
<http://www.spervis.oma.be/spervis/>
RD[67] ECSS-E-ST-10-04C Space Environment Standard, version linked to software tools is available at www.spervis.oma.be/spervis/
RD[68] SPIS – Spacecraft-Plasma Interaction Software,
<http://dev.spis.org/projects/spine/home/>
RD[69] Sabol, J., Weng, B., *Introduction to Radiation Dosimetry*, World Scientific, 1995
RD[70] Seltzer, S. M., “Updated calculations for routine space-shielding radiation dose estimates: SHIELDOSE-2”, NIST Publication NISTIR 5477, Gaithersburg, MD., December 1994.
RD[71] Marvin, D. C., Assessment of Multijunction Solar Cell Performance in Radiation Environments, Aerospace Report No. TOR-2000(1210)-1, 2000.
RD[72] Messenger, S.R., Walters, R.J., Warner, J.H., Evans, H., Taylor, S.J., Baur, C. and Heynderickx, D., Status of Implementation of Displacement Damage Dose Method for Space Solar Cell Degradation Analyses, , 2008.

22.1.1.13 Chapter 18 Programmatics References

- RD[73] ECSS-E-AS-11C

22.1.1.14 Chapter 19 Technical Risk References

- RD[74] Space Project Management, Risk Management, ECSS-M-ST-80C, 31 July 2008.

22.1.1.15 Chapter 20 Cost References

- RD[75] ESA Cost Engineering Charter of Services, Issue 4, TEC-SYC/12/2009/GRE/HJ
RD[76] TEC-SYC Cost Risk Procedure, TEC-SYC/5/2010/PRO/HJ, February 2010
RD[77] ECSS-E-AS-11C Adoption Notice of ISO 16290, Space Systems – Definition of the Technology Readiness Levels (TRLs) and their Criteria of Assessment, dated 1 October 2014. To be supersede by EN16603-11.

This Page Intentionally Blank

23 ACRONYMS

Acronym	Definition
μ RIT	Radio-frequency Ion Thruster
AFIO	Advanced Flexible Input/Output
AFM	Atomic Force Microscope
AFS	Aluminium Foam Sandwich
AIT/V	Assembly, Integration and Test/Verification
AKE	Attitude Knowledge Error
Amu	Atomic Mass Unit, corresponding to the mass of a nucleon, or approx. $1.66e-27$ kg
ALM	Additive Layer Manufacturing
AOCS	Attitude and Orbital Control System (LEOP and Transfer)
AOM	Acousto-Optic Modulator
APE	Absolute Pointing Error
as	Arc-seconds
ASIC	Application Specific Integrated Circuit
ATB	Avionics Test Bench
AU	Astronomical Unit
au	Atomic unit of mass
BCR	Battery Charge Regulator
BDR	Battery Discharge Regulator
BF	Body Frame
BoL	Beginning of Life
CaC	Cost at Completion
CAN	Controller Area Network
CFDP	CCSDS File Delivery Protocol
CFRP	Carbon Fibre Reinforced Polymer
CMA	Cost Model Accuracy
CoM	Centre of Mass
CoP	Center of Pressure
CPU	Central Processing Unit

Acronym	Definition
CQM	Cryogenic qualification model
DB	Diffusion Bonding
DFACS	Drag-Free Attitude Control System
DHS	Data Handling System
DMM	Design Maturity Margin
DOA	Degree of Adequacy of the cost model
DoD	Depth of Discharge
DSN	Deep Space Network
DUV	Deep UV
E(Q)M	Engineering (Qualification) Module
EB	Electron Beam
ECSS	European Cooperation for Space Standardisation (Standards)
EIRP	Effective Isotropically Radiated Power
ELO	Earth-Leading Orbit
EM	Engineering Model
EoL	End Of Life
EOM	Electro Optic Modulator
EPE	External Project Events
EQM	Engineering Qualification Model
ESD	Electrostatic Discharge
ESI	Electrospray ionisation
ESTMP	European Space Technology Master Plan
ETO	Earth-Trailing Orbit
eV	Electron-volt, 1 eV equals 11605 kelvin
FDIR	Failure, Detection, Isolation and Recovery
FEPP	Field-Emission Electric Propulsion
FM	Flight Model
FSW	Friction Stir Welding
GCR	Galactic Cosmic Ray
GSE	Ground Support Equipment
HEO	High Earth Orbit

Acronym	Definition
HEO	Highly Elliptical Orbit
HK	Housekeeping
HKTM	Housekeeping Telemetry
Imp	Maximum Power Point Current (Solar Cell)
IQM	Inherent Quality of the cost Model
IR	Infra Red
Isc	Short Circuit Current (Solar Cell)
L1/L2	Lagrange points 1/2
LCL	Latched Current Limiter
LEOP	Launch and Early Orbit Phase
LGA	Low Gain Antenna
LS	Laser Sintering
mas	Mili-arc-seconds
MEMS	Microelectromechanical systems
MGA	Medium Gain Antenna
MLI	Multi-Layer Insulation
MOC	Mission Operations Centre
MPPT	Maximum Power Point Tracker (Tracking)
NEG	Non-Evaporable Getter
NIEL	<i>Non-Ionizing</i> Energy Loss
NIR	Near Infra-Red
OBC	On-Board Computer
OBF	Optical Bench Frame
OBT	On-Board Time
PCDU	Power Conditioning and Distribution Unit
PDE	Position Drift Error
PFM	Proto-Flight Model
PLA	Payload Adapter Ring
PLM	Payload Module
POE	Project Owned Events
PPT	Pulsed Plasma Thrusters

Acronym	Definition
QIV	Quality of the Input Values
QM	Qualification Model
QPPF	Quantum Physics Platform
REQ	Requirement
RF	Radio Frequency
RFDN	Radio Frequency Distribution Network
RKE	Rate Knowledge Error
R-LCL	Retriggerable Latch Current Limiter
RPE	Relative Pointing Error
RTU	Remote Terminal Unit
S/C	Spacecraft
S3R	Sequential Switching Shunt Regulator
SA	Solar Array
SAPPHIRE	Solar Accumulated and Peak Proton and Heavy Ion Radiation Environment
SAR	Solar Array Regulator
SBCC	Single Board Computer Core
SEE	Single Event Effect
SEP	Solar Electric Propulsion
SEP	Solar Energetic Particle (event)
SKM	Station Keeping Manoeuvre
SMU	Spacecraft Management Unit
SoC	State of Charge
SOC	Science Operations Centre
SPENVIS	Space ENVironment Information System
SPF	Single Point Failure
SPF	Superplastic Forming
SPIS	Spacecraft-Plasma Interaction Software
SRP	Solar Radiation Pressure
SSM	Secondary-Surface Mirror
SSMM	Solid State Mass Memory
STM	Structural Thermal Model

Acronym	Definition
SVF	Software Verification Facility
SVM	Service Module
TC	Telecommand
TCM	Trajectory Correction Manoeuvre
TEM	Transverse ElectroMagnetic
TID	Total Ionising Dose
TIG	Tungsten Inert Gas
TM	Telemetry
TMs	Test Masses (of Lisa Pathfinder)
TP	Test Particle
TRA	Technology Readiness Assessment
TRL	Technology Readiness Level
TT&C	Telemetry, Tracking and Command
VDA	Vapor-Deposited Aluminium
vdW	van der Waals
Vmp	Maximum Power Point Voltage (Solar Cell)
Voc	Open Circuit Voltage (Solar Cell)